Southeast Regional Carbon Sequestration Partnership

Report Type:	Report and documentation of milestone completion
Report number :	Phase III 3.1.1 b
Report title:	**Risk Assessment using Certification Framework**
Completion Date:	May 2011
Report Issue Date:	September 30, 2011
DOE Award Number:	DE-FC26-05NT42590

Jean-Philippe Nicot[1], James E. Houseworth[2], Curtis M. Oldenburg[2], Jong-Won Choi[1], HamidReza Lashgari[1], Stuart Coleman[1], Timothy A. Meckel[1], Preston Jordan[2], Alberto Mazzoldi[2]

[1]Bureau of Economic Geology,
University of Texas,
University Station, Box X
Austin, Texas 78713-8924

[2]Lawrence Berkeley National Laboratory,
Earth Sciences Division, 90-1116
Berkeley CA 94720

Introduction and Results

The RCSP requires a risk assessment. However, the EOR flood and associated down-dip injection that supported the SECARB HiVIT test are conducted at a commercial EOR site. The site operator has conducted their own proprietary assessment of business risk and designed the operation to be compliant with State regulation. It is therefore important that the risk assessment conducted as part of the RCSP program not be considered an assessment of the commercial activities either business risk or leakage risk, as such assessment might be construed as improper intrusion on the commercial project.

An initial minimal approach to risk assessment via use of the Quintessa list of Features, Events, and Processes (FEPS) was therefore proposed. However, the separately funded methodology known as the Certification Framework (CF) desired to test that method in development at an EOR site. The SECARB project was able to serve as CF Case Study V. The report from this case study is appended to this report as Appendix A.

Appendix A

Certification Framework Demonstration of Leakage Risk Assessment for and EOR site. Case Study V
SECARB Phase III
CO_2 Storage Project at a Mississippi EOR Site

Jean-Philippe Nicot[1], James E. Houseworth[2], Curtis M. Oldenburg[2], Jong-Won Choi[1], HamidReza Lashgari[1], Stuart Coleman[1], Timothy A. Meckel[1], Preston Jordan[2], Alberto Mazzoldi[2]

[1]Bureau of Economic Geology,
University of Texas,
University Station, Box X
Austin, Texas 78713-8924

[2]Lawrence Berkeley National Laboratory,
Earth Sciences Division, 90-1116
Berkeley CA 94720

April 2011
Rev. for SECARB September, 2011 SDH

Acknowledgments: This work was supported by the Assistant Secretary for Fossil Energy, Office of Sequestration, Hydrogen, and Clean Coal Fuels, National Energy Technology Laboratory (NETL), and by Lawrence Berkeley National Laboratory under Department of Energy Contract No. DE-AC02-05CH11231. Additional support comes from the Bureau of Economic Geology at the University of Texas at Austin and the SECARB project, managed by the Southern States Energy Board and funded by the U.S. Department of Energy, NETL, as part of the Regional Carbon Sequestration Partnerships program under contract number DE-FC26-05NT42590. We are also grateful to Denbury Onshore LLC, the operator of the CO_2-EOR project, for field access and sharing of data. In addition, we thank IHS Energy for free access to the Enerdeq well database and PETRA software, and the Computer Modeling Group, Calgary, Alberta for free access to the compositional multiphase flow code CMG-GEM and related modules. Finally, we thank the following individuals for significant input: Carlos Puerta and Silvia Solano, both at BEG, for useful comments on the CBL log interpretation, and Susan Hovorka, Changbing Yang, and Katherine Romanak, researchers at BEG, for general input and discussion of the general approach to leakage risk assessment.

This page left intentionally blank

DISCLAIMER

THE APPROACH PRESENTED IN THIS DOCUMENT IS AN APPLICATION OF THE "CERTIFICATION FRAMEWORK" IN AN ENHANCED OIL RECOVERY SETTING. IT IS NOT AN ASSESSMENT OF ENHANCED OIL RECOVERY AND IT DOES NOT REPRESENT THE RISK ANALYSIS PERFORMED BY THE OPERATOR THAT STAYS CONFIDENTIAL.

This page left intentionally blank

Executive Summary

Introduction

The Southeast Regional Carbon Sequestration Partnership (SECARB) Phase III 1.5 million tonne CO_2 sequestration project is taking place on the eastern side of an oilfield in southwestern Mississippi in the so-called High Volume Injection Test area (HiVIT). The source of CO_2 for the project is the natural CO_2 reservoir at Jackson Dome, Mississippi. We apply the Certification Framework (CF) approach to assess the risk of CO_2 and brine leakage from the deep reservoir to various compartments where impacts could occur. The large depth (~10,000 ft, 3,050 m) of the Tuscaloosa Formation reservoir, presence of extensive thick marine mudstone confining zone, and well-known geology, among other factors, tend to minimize the likelihood of leakage. On the other hand, the large number of plugged and abandoned (P&A) wells provides potential flow paths for leakage upward to potable aquifers and potentially to the ground surface. A review of site characteristics relevant to leakage risk, simulation of the CO_2 injection, and modeling of performance of P&A wells is presented to demonstrate the application of the Certification Framework (CF) for leakage risk assessment in the context of an enhance Oil Recovery (EOR) project.

Site Background

The CF demonstration area is a gas and oil reservoir discovered in 1943. The structure is a near-circular four-way anticline 4 mi (6.4 km) in diameter created by a deep-seated salt dome. The field was depleted by 1965, but is once again producing oil as a result of CO_2-EOR. At the same time, CO_2 is being injected in the water leg at the eastern edge of the field below the oil-water contact to study deep aquifer storage as part of SECARB's geologic sequestration Phase III project. This geologic carbon sequestration research program aimed at better understanding of CO_2 storage capacity, pressurization, seal performance, and monitoring is led by the Texas Bureau of Economic Geology at the University of Texas at Austin.

Site Description

The SECARB Phase III site is in a rural, moderately hilly and heavily wooded area 15 mi (25 km) east of the Mississippi River. There are no critical habitats or wildlife refuges in the area. Land use is limited to agriculture, recreation, timber harvest, and oil and gas production. Annual rainfall averages 62 in, with gentle winds averaging less than 10 mph most commonly from the south. There are numerous small artificial ponds in the area, remnants of past oil and gas production, and the larger Lake Natchez 1.2 mi (2 km) from the operator lease boundary.

The SECARB Phase III site resides in the Mississippi salt basin, which is a part of the Gulf Coast sedimentary wedge running along the Gulf of Mexico from south of the Mexican Border to the Florida state line. The base of the sedimentary sequence consists of thick and extensive salt layers of Jurassic age. The deformation of the salt caused by loading by Cretaceous sediments led to the development of salt diapirs penetrating the overlying sediments. Transgressive-regressive cycles of sediment deposition occurred during the Cretaceous. The upper Cretaceous Tuscaloosa Formation was deposited during a transgressive-regressive cycle and is bounded by unconformities at the base and top of the formation that represent erosion surfaces. Within this cycle, the fluvial deposits of the lower Tuscaloosa Formation were slowly transgressed by the sea and deposition of the middle Tuscaloosa marine mudstone occurred, providing a valuable section of the confining system. The top seal for potential geologic CO_2 storage reservoirs consists of multiple upper Cretaceous mudstones (Eagle Ford, Austin, Taylor, Navarro and equivalents).

The eastern fault of a NW-SE trending crestal graben offsets the Tuscaloosa reservoir in the area of the Phase III injection. Throw on the fault decreases upward and no structure is expressed at the surface. Salt tectonics has ceased and the fault is inactive. The fault is not horizontally transmissive as evidenced by variance in oil-water contact elevation on either side of the fault at the time of field discovery, non-propagation of pressure during CO_2 injection, and well-breakout observations suggesting that the current maximum horizontal stress tends to close the fault.

The SECARB Phase III site lies on the Mississippi uplands of the alluvial margin and, from the ground surface down to the base of the Vicksburg-Jackson group, is within the coastal lowland aquifer system. Regional ground-water flow was directed southward to the coast with groundwater discharged by diffuse upward leakage to major rivers, low-lying coastal marsh areas, and to the ocean as seabed seepage in shallow nearshore areas. Groundwater pumping has altered this pattern in the Natchez area, but groundwater flow has remained southwards at the site. The area is blanketed by loess, a fine grained material that may limit recharge and confines the underlying aquifers. Three water-bearing sands at approximately 400, 600, and 1,000 ft (122, 180, and 300 m) have good water quality and are valuable water resources in the area. Groundwater with TDS higher than 10,000 mg/L is encountered at a depth of approximately 1,500 ft (460 m).

Oil and gas resources are abundant in the area. The first reservoir exploited at the site location was in the Wilcox Group, a 3,000 ft (900 m) thick accumulation of interbedded sandstone units encountered at a depth of approximately 4,000 ft (1,200 m). Today, the Wilcox is underpressured due to earlier and continuing hydrocarbon extraction. The Tuscaloosa, encountered at a depth of approximately 10,000 ft (3,000 m), is under production and pressurization by CO_2 injection. There are 287 documented wells, most of which are P&A and are over 70 years old. The operator's practice during EOR is to drill new injections wells and to reenter selected P&A wells to rework them as producers in patterns. Some P&A wells are not reused and remain plugged. Fourteen Cement Bond Logs (CBL's) from the field were located and used for this risk assessment study. The present quality of the cement bond ranges from excellent to poor.

Reservoir Simulation

Three-dimensional reservoir simulations of the HiVIT area of the oilfield were undertaken using CMG-GEM. The static model was created based on both seismic data and well logs using the Petrel software. In order to account for the lack of interwell data (as typical) and the limitations in quantifying permeability distribution in the horizontal direction in heterogeneous rocks, we generated five realizations of the permeability and porosity fields. The top and bottom boundary of the model are assumed not to allow flow and the injection formation is vertically bounded by low-permeability layers. The fault on the western side of the model domain is sealing and this boundary is modeled as a no-flow boundary. The boundary on the eastern side of the domain is an open boundary with constant pressure set at hydrostatic to model an infinite-acting system. We modeled five years of injection even though the Phase III project is limited to the first 1.5 years with injection at a rate of 1 million tonnes per year. Injection wells were assigned injection rates based on a simplified schedule of the actual measured rates or projections based on actual rates depending on whether the simulated time was before or after the present. Production was modeled at wells beginning when the CO_2-rich oil can self-lift to the surface consistent with the field production strategy.

Results for breakthrough of CO_2 and maximum pressure at the P&A wells for the five realizations show that CO_2 and over pressured brine will intersect P&A wells for all five realizations. Simulated breakthrough times range from less than a month after start of injection to beyond five years while the pressure rise ranges from less than 400 psi to over 1,500 psi (2.7–10.2 Mpa) depending on location of the P&A wells and permeability field realization. These simulated pressures tend to over predict conditions relative to well leakage that could actually occur in the oilfield and are higher than may occur during operations, because the model does not consider the optimization of the flood by the operator who will adjust injection and production rates in response to pressure measurements.

CF Leakage Risk Assessment

We specify the CO_2 storage region for the purposes of defining CO_2 and brine leakage as the Tuscaloosa Formation above the Washita-Fredericksburg group and below the regional seal of the middle Tuscaloosa. The non-transmissive fault on the west side is the updip boundary of the storage region, while the down-dip (water leg) lateral boundary is assumed to be an arbitrary 10 mi (16 km) from the lease boundary.

The only potential leakage pathway for CO_2 or brine upward out of the storage region is through P&A wells that reach the lower Tuscaloosa. Simulation results suggest that CO_2 and displaced brine at elevated pressures will encounter multiple P&A wells during the Phase III project. This means that the likelihood of intersection of CO_2 and brine at elevated pressure with P&A wells is 100%. Therefore, the calculation of leakage risk in

the CF reduces to a calculation of consequences or impacts of leakage along hypothetical flow paths provided by P&A wells. All wells are assumed to be properly plugged and abandoned at the end of oilfield and carbon sequestration operations such that their leakage risk is de minimis in the post-operational period.

A simple 1D single-phase model for flow up a P&A well with degraded cement or poor cement bond was developed and run for a range of assumed effective permeabilities representing a statistical sampling of well properties from 14 cement bond logs available from the oilfield. The bottom pressure is fixed and set equal to results from the 3D reservoir simulation. Flow in the well is allowed to move into adjacent formation as controlled by local rock properties. Results show that overpressure from CO_2 injection is rapidly dissipated in the upper Tuscaloosa and can be further reduced in the under-pressured Wilcox Group. But for CO_2, the buoyancy effect allows a residual leakage flux to continue up the well resulting in the possibility of non-negligible CO_2 leakage fluxes for wells with poor quality cement. For brine, the lack of buoyancy renders brine leakage fluxes negligible as overpressure dissipates into the upper Tuscaloosa and Wilcox.

A total of seven unaltered P&A wells and ten P&A wells retrofitted for production were evaluated as potential leakage pathways within the Phase III area. Statistical estimates of properties for these 17 wells used in the simplified model suggest that at most two (and possibly none) could be capable of conveying a total 1.8 tonnes CO_2 per year either to USDW or to the ground surface, with the remaining 15 wells effectively sealed. Overall, the well leakage rate is seen to be approximately 0.0002% of the annual injection rate. Given the large volumes of the potable aquifers and dissipative processes present above ground, fluxes of CO_2 of this magnitude are expected to have negligible impact on the USDW, ECA, and HS compartments.

If the leakage flux discharged in the shallow subsurface, it is possible that CO_2 concentrations could build up in the root zone to levels that could cause plant stress that would potentially be recognizable in the leaves and needles of the vegetation. Nevertheless, the risk to this NSE compartment is considered low because it will be localized around wells and potentially noticeable to workers and therefore subject to mitigation.

In summary, the CF approach was successfully applied to the SECARB Phase III CO_2 injection site. Conclusions of the test is that CO_2 leakage risk is low, and that brine leakage risk is de minimis. We note that the current regulatory environment and commercial field operator concur that well management is a focus area of proper field management. surveillance well management, mitigation and remediation if necessary are current best practices.

Table of Contents

Executive Summary i
Introduction i
Site Background i
Site Description i
Reservoir Simulation iii
CF Leakage Risk Assessment iii
Table of Contents v
Figures vii
Tables ix
Acronyms x
Acronyms x
1 Introduction 1
2 Site Background 2
2.1 Location and History 2
2.2 Current Research Activities 3
2.3 Data Sources for Leakage Risk Assessment 3
3 Site Description 10
3.1 Terrain, Land Use and Climate 10
3.2 Surface Water 11
3.3 Subsurface 11
3.3.1 Regional Geology 11
3.3.2 Regional Subsurface Hydrology 13
3.3.3 Shallow Subsurface and Aquifer Systems 13
3.3.4 Natural and Hydrocarbon Resources 15
3.3.5 Wells 15
4 Reservoir Simulation 46
4.1 Storage Reservoir 47
4.1.1 Static Model and Flow Parameters 47
4.1.2 Boundary and Initial Conditions 48
4.1.3 Injection Schedule 48
4.2 Modeling Results 48
5 CF Leakage Risk Assessment 65
5.1 Introduction 65
5.2 Storage Region 65
5.3 Terminology for Degree of Likelihood, Impact, and Risk 65
5.4 Likelihood of CO_2 and Brine Encountering Leakage Pathways 66
5.5 Upward CO_2 Leakage 66
5.5.1 Model for Leakage up P&A Wells 66
5.5.2 Leakage through Active Producers 69
5.6 Brine Leakage 69
5.6.1 Analysis of Upward Brine Leakage 70
5.6.2 Along-Dip Leakage of CO_2 and Brine 70
5.7 Impact to Compartments 70
5.8 Overall CO_2 and Brine Leakage Risk 71

6 References 77
7 Appendix A. Certification Framework Concepts and Definitions 82
7.1 Overview 82
7.2 Definitions 82
7.3 Compartments and Conduits 82
7.4 Risk and Flow Chart 82
8 Appendix B. Flow Induced in P&A Wells by CO_2 Injection Pressure 86
9 Appendix C. Pressure history at P&A well locations 93
10 Appendix D. Saturation history at P&A well locations 113
11 Appendix E: List of wells 167

Figures

Figure 1. Regional map of the site. 5
Figure 2. Location map of the field straddling Adams and Franklin counties in southwestern Mississippi. 5
Figure 3. Structure contoured on Basal Tuscaloosa sand of the reservoir. 6
Figure 4. Reservoir pressure, oil production, water production and injection during historical period. 7
Figure 5. Reservoir pressure, gas production, water production and injection during historical period. 7
Figure 6. Site map showing footprint of oil ring and gas cap and Phase II and Phase III numerical model domains as well as subdomain the Phase III model with focus on the DAS 8
Figure 7. Site map showing relationship between numerical model domains and SECARB operations: Phase II and focus on monitoring of pressure in the so-called EOR domain and Phase III and focus on the HiVIT and DAS domains. Red dots represent historical wells. 9
Figure 8. Photographs representative of the site showing wooded areas and clearings incised (10-20 ft) by a few streams 21
Figure 9. Physiographic districts and drainage basins in Adams County 22
Figure 10. Depth Contours for Natchez Lake and Relationship to the site 23
Figure 11. Wind rose showing principal wind directions of wind at Natchez, MS. 24
Figure 12. Structural Features of Mississippi 25
Figure 13. North-South Cross-Section 20 km East of the site Showing the Mississippi Embayment Aquifer System to Base of the Tertiary and the Coastal Lowland Aquifer System. 26
Figure 14. Stratigraphy at the site illustrating the basic lithology and TDS for each formation from the CO_2 injection interval to the surface. 27
Figure 15. Footprint of Mississippi Embayment Aquifer System 28
Figure 16. Transgressive-Regressive Depositional Cycles for the Tuscaloosa Formation (not necessarily entirely valid at the site) 29
Figure 17. Type log in the study area showing the basal massive sands of the injection interval overlaid by more fluvial deposits including the local seal of the reservoir and a thick marine mudstone. A likely marine sand overlays the marine mudstone and is monitored at the site for pressure changes. 30
Figure 18. Simplified hydrostratigraphic column with water quality 31
Figure 19. Depth to the base of: (a) fresh water (<1,000 mg/L); (b) slightly brackish water (<3,000 mg/L); and brackish water (<10,000 mg/L) 32
Figure 20. Cartoon demonstrating construction method of Figure 19. 33
Figure 21. Base of the fresh water in Adams County 34
Figure 22. Piper plot of groundwater chemistry of the shallow aquifer at the site 35
Figure 23. Location of known water wells. 36
Figure 24. Map of mineral resources in the vicinity of the site 37
Figure 25. Monthly production data from the Wilcox formation at the site since 1977 37
Figure 26. Cumulative production from the Wilcox formation since 1977 (oil and water) 38

Figure 27. Cumulative production from the Wilcox formation since 1977 (gas and liquids) 38
Figure 28. Location map showing wells drilled to the Wilcox Fm. at the injection site 39
Figure 29. Location map showing historical and recent wells drilled to the Tuscaloosa Fm. at the site 40
Figure 30. Location map showing wells drilled deeper than the Tuscaloosa Fm. (>11,000 ft) at the site 41
Figure 31. Annual well count for (a) all wells; (b) Wilcox wells; and (c) Tuscaloosa wells 42
Figure 32. Produced water volume from the Tuscaloosa interval per well: (a) uncorrected and (b) corrected 43
Figure 33. Site map illustrating the location and quality of each CBL log 44
Figure 34. Cross-section illustrating cemented intervals of each well with a CBL log. 45
Figure 35. The model domain covers the portion of the northeast section of the field that isnortheast of a non-transmissive fault (HiVIT domain) 55
Figure 36. Kx permeability distribution (layer 1, realization 1): (a) 3D view and (b) plan view. 56
Figure 37. Porosity (a) and permeability (md) (b) with nugget of 0.14 on 50 x 50 x 8 ft (realization 1) 57
Figure 38. Porosity (a), Kx (b), Ky (c) and Kz (d) with nugget of 0.14, upscaled 200x200x8 gt field (realization 1) 58
Figure 39. Relative permeability curves (oil/water and liquid/gas) 59
Figure 40. Injection Schedule (historical and future) 59
Figure 41. Cumulative injection in HiVIT wells. 60
Figure 42. Well location in the HiVIT domain. 61
Figure 43. Comparison of excess pressure at the seven P&A wells for the five realizations 62
Figure 44. Comparison of CO_2 breakthrough times at the seven P&A wells for the five realizations 63
Figure 45. Footprint of CO_2 plume in Layer 8: (a) on 12/1/2011 and (b) on 12/1/2013 64
Figure 46. Results for Flow in P&A Wells at the site 75
Figure 47. Wellbore Permeability Distribution for Wells without 100% Cement Bonds 76
Figure 48. CO_2 Mass Leakage Rate Distribution for Wells without 100% Cement Bond 76
Figure A-1. Generic schematic of compartments and conduits in the CF. 83
Figure A-2. CO_2 leakage risk schematic. 83
Figure A-3. Flow chart of CF process showing logic and inputs and outputs. 84
Figure B-1. Comparison of Analytical and Numerical Results for Single-Layer Test Case 88
Figure B-2. Comparison of Analytical and Numerical Results for Two-Layer Test Case 90

Tables

Table 1. Hydrocarbon summary production 17
Table 2. List of CBLs used for evaluation of the Tuscaloosa reservoir 18
Table 3. First indication of questionable cement bond above top of lower Tuscaloosa 19
Table 4. Wells used to generate the static model 50
Table 5. Geostatistical parameter used to generate flow parameter fields 52
Table 6. Flow parameters for the reservoir rock in the model 52
Table 7. Location of P&A wells (East of fault) 52
Table 8. Pressure (psi) at P&A wells 53
Table 9. Excess pressure (psi) at P&A wells 53
Table 10. CO_2 maximum mole fraction, maximum mole fraction time, and CO_2 breakthrough time at P&A well locations 54
Table 11. CO_2 breakthrough times at P&A well locations 54
Table 12. Likelihood terminology 73
Table 13. Impact terminology 73
Table 14. Risk terminology 73
Table 15. Well leakage base case hydrostratigraphy 73
Table 16. Well leakage base case parameters (for definitions of parameters, see Appendix B) 74
Table B-1. Single-Layer Test Case Parameters 87
Table B-2. Two-Layer Test Case Parameters 89

Acronyms

BCF	Billion Cubic Feet
bgs	Below Ground Surface
BI	Bond Index
BEG	Bureau of Economic Geology
CBL	Cement Bond Log
CF	Certification Framework
CLR	CO_2 Leakage Risk
CMG-GEM	Compositional multiphase flow numerical model
DAS	Detailed Area of Study
ECA	Emissions Credits and Atmosphere
EOR	Enhanced Oil Recovery
EPA	Environmental Protection Agency
GC	Gulf Coast
GEM	Compositional multiphase flow numerical model
GIP	Gas In Place
gpm	gallon per minute
HiVIT	High Volume Injection Test
HMR	Hydrocarbon and Mineral Resources
HS	Health and Safety
MDEQ	Mississippi Department of Environmental Quality
MGD	Million Gallons of water per Day
Mt	million tons
NEE	Net Ecosystem Exchange
P&A	Plugged and Abandoned
RA	Risk Assessment
RRC	Railroad Commission (of Texas)
SECARB	Southeast Regional Carbon Sequestration Partnership
SGR	Saturation of Gas at Residual (saturation)
TDS	Total Dissolved Solids
USDW	Underground Source of Drinking Water
USGS	United States Geological Survey

1 Introduction

This report presents a test of the certification framework (CF) (Oldenburg et al., 2009). methodology applied to assessment of and EOR and brine storage test site. CF assesses the risk of CO_2 and brine leakage. The test site is the U.S. Department of Energy's SECARB (Southeast Regional Carbon Sequestration Partnership) Phase III geologic carbon dioxide (CO_2) sequestration project taking place in the eastern side of an oilfield in southwestern Mississippi, operated by Denbury Onshore LLC. The SECARB Phase III project goal is to monitor injection of 1.5 million tonnes of CO_2 over 1.5 years through several injection wells during the so-called high-volume injection test (HiVIT). However, SECARB's research focus centers on a well located in the so-called Detailed Area of Study (DAS) located on the eastern side of the field. The source of CO_2 for the project is the natural CO_2 reservoir at Jackson Dome, Mississippi. In the CF, the leakage of concern is from the deep subsurface rather than from pipelines or other surface infrastructure. The CF leakage risk assessment is carried out by evaluating the likelihood and consequences of CO_2 or brine leakage to various compartments that could be impacted, e.g., underground sources of drinking water (USDW), near-surface environment (NSE) plants and animals, and health and safety (HS) of residents and workers. The leakage risk evaluated by the CF is entirely a technical risk as opposed to economic or business risk, as the potential consequences are CO_2 and brine leakage fluxes into the various compartments. The CF approach simplifies complex systems into a framework amenable to simple analyses, as summarized in Appendix A.

Several aspects of SECARB's Phase III project serve to minimize leakage risk, including (1) the large depth (~10,000 ft, 3,050 m) of injection in the Tuscaloosa Formation, (2) the presence of several seals including marine mudstones which are typically more extensive and uniform than those deposited in deltaic or fluvial environments, (3) a pressure sink owing to shallower oil and gas production from the overlying Wilcox Formation, (4) a thick vadose zone, (5) low natural seismicity in the area, (6) well-known geology because of the long history of oil and gas exploration and production, (7) CO_2 miscibility in the oil, in essence immobilizing it, and (8) low population density, (9) active management by a responsible operator. On the other hand, there are some obvious risk factors that must be considered including (1) many historic wells that could potentially provide leakage pathways, (2) variable topography that includes steep valleys that could potentially pond CO_2 accumulations if surface leakage were to occur, and (3) thick fresh-water aquifers and a deep transition from potable to unpotable groundwater. However, the most important aspect of the project relative to leakage risk is that the site is operated and actively managed by a private company with field technicians who actively control pressure via balancing the flood and perform daily site inspection. In addition, two dedicated above-zone observations wells monitor pressure and any deviation from the expected stable reading (Meckel and Hovorka, 2010). The ultimate liability of the site residing with the oil-producing company also justifies the short period of time (5 years) of interest to this study. At the end of the SECARB project, the two observation wells drilled for the sole purpose of the project will be plugged and abandoned and the oilfield will revert to its purely commercial nature.

Following a review of the SECARB Phase III site characteristics relevant to leakage risk assessment, this report presents results of modeling studies to demonstrate the value of the methodology to providing potential ranges of CO_2 saturation and pressure elevation that could

drive CO_2 or brine leakage up improperly constructed P&A wells. These reservoir simulation results feed into models of well leakage that are used to further quantify the potential leakage fluxes that are used as proxy consequences in the CF. Model results show that CO_2 and elevated pressure will encounter wells, we assume that any of these is potentially capable of conveying CO_2 or brine upward to USDW and higher. Therefore, the CF risk assessment focuses on the potential impacts or consequences of CO_2 and brine leakage up P&A wells as presented in Section 5. We emphasize the risk assessment tested here is for the SECARB Phase III injection of 1.5 million tonnes of CO_2, and not a larger geologic carbon sequestration project that could theoretically be carried out at the site sometime in the future.

2 Site Background

2.1 Location and History

The field is a depleted gas and oil reservoir in southwestern Mississippi near the Louisiana border (Figure 1, Figure 2). The closest city to the Phase III site is Natchez, about 15 mi (25 km) west of the field and located on a bluff above the Mississippi River. The Gulf of Mexico lies about 140 mi (230 km) south of the site. The original oil discovery was made in 1943 by a predecessor of Chevron and has produced >37 MMbbl oil and >672 BSCF gas from 1944 to 1965 (MOGB, 1966). The field is a near-circular four-way anticline (Figure 3) with a diameter of ~4 miles (6.4 km). The original resource consisted of a large gas cap surrounded by an oil ring at a depth of more than 10,000 ft (3,050 m) (Hovorka et al., 2009). The structure was created by a deep-seated salt dome that crests far below the field.

The field was unitized early in its life allowing consistent production and abandonment. Oil was recovered using recycled gas drive until the water cut became too high. The gas cap at the top of the structure was then blown down, removing the drive for oil production. The oil and gas production history is shown on Figure 4 and Figure 5. Even though the production voided a significant percentage of the pore space in the field, there is a strong water drive that restored pressure in the reservoir to near initial levels in the decades following production despite the deep pressure drop following gas blow down. Denbury Onshore, LLC from Plano, TX (Denbury) is the current field operator. After a hiatus of several decades, Denbury started to prepare the field for an Enhanced Oil Recovery (EOR) operation in 2006. The area has been under CO_2 flood since mid-July 2008 to sweep bypassed and residual oil (Hovorka et al., 2009).

The CO_2 used for enhanced recovery and sequestration research is provided by pipeline from the natural CO_2 accumulation of the Jackson Dome (Studlick et al., 1990) in Central Mississippi (Figure 1). The Jackson Dome CO_2 reservoir is a 24 mi- (40 km-) wide feature created by igneous activity during the Late Cretaceous (Huber et al., 1999). It is believed that the CO_2 contained in this feature was emplaced at about the same time, also as a result of igneous activity (IEA, 2005). In addition to CO_2, the reservoir gas also contains trace amounts of noble gases. The $^3He/^4He$ and $^4He/^{40}Ar$ ratios in the gas are indicative of a mantle source (Zhou et al., 2007; Stevens, 2005). These may be used to distinguish the injected CO_2 from an atmospheric source and are being used by researchers from the University of Edinburgh, Scotland, to trace the injected CO_2 at the site.

2.2 Current Research Activities

The SECARB program is funded by the U.S. DOE through the National Energy Technologies Laboratory (NETL) and managed by the Southern States Energy Board (SSEB). Specific SECARB-related operations at the oilfield are managed by the Gulf Coast Carbon Center (GCCC), headed by Susan Hovorka at the Bureau of Economic Geology (BEG) at the University of Texas at Austin. The goals of the SECARB Phase II project at the site were to (1) investigate CO_2-EOR effectiveness in retaining CO_2, especially considering the impact of well penetrations, (2) help in assessing the CO_2 storage capacity below and down-dip of the reservoirs, and (3) investigate whether pressure response in the near and far field is understood quantitatively well enough to safely move to large volume injection.

The SECARB Phase III project goal is to monitor the injection of 1.5 million tonnes CO_2 over 1.5 years in the HiVIT area. The Phase II and Phase III numerical model domains are shown in Figure 6 and HiVIT and DAS domains are displayed in Figure 7. The modeling and monitoring R&D objectives for the Phase III project are to (1) assess reservoir phase-transfer efficiency for the large volumes of CO_2 injected to better quantify CO_2 storage capacity (dissolution), (2) quantify pressure effects and brine movement though a heterogeneous rock volume to better understand the significance of these on storage capacity and ability to monitor pressure and brine migration, (3) quantify inter-well interactions as large plumes develop, focusing on interaction of pressure, heterogeneity, and gravity as controls on migration, (4) better understand the performance of pressure and capillary seals, (5) develop and assess the effectiveness of existing and novel monitoring tools, and (6) assess how monitoring tools can be used efficiently, effectively, and hierarchically in a long-term monitoring environment.

2.3 Data Sources for Leakage Risk Assessment

Relative to the oilfield itself, historical data is available and consists of (1) published information in a summary report by the Mississippi Oil and Gas Board (MOGB, 1966), (2) geophysical open hole well logs dating from the historical period (1944 to ~1967), and (3) historical production data from the IHS database (a private vendor collecting information from the oil and gas industry). Additional data only indirectly useful to this risk assessment and modeling work have also been retrieved from old cores in storage in Jackson, MS and through informal discussion with experts at Denbury. The MOGB (1966) summary report includes information on annual overall oil and gas production, water cut, permeability and relative permeability, oil and gas composition, and operational history. Earlier reports, published in trade journals and peer-reviewed literature (e.g., Hines, 1950) also provide additional information on historical operational issues. A variety of data presented in this report were acquired directly through field work and extracted from progress reports to SSEB and DOE but additional information was obtained from the following sources:

Federal

USGS programs such as the Regional Aquifer-System Analysis (RASA); all reports available at http://ms.water.usgs.gov/

The EPA web site provided information on sole source aquifers (http://cfpub.epa.gov/safewater/sourcewater/sourcewater.cfm?action=SSA).

State
MDEQ website. MDEQ includes the State Geological Survey (Office of Geology - http://www.deq.state.ms.us/MDEQ.nsf/page/Geology_home?OpenDocument) and (Office of Land and Water Resources - http://www.deq.state.ms.us/MDEQ.nsf/page/L&W_Home?OpenDocument)

MDEQ has a searchable dataset "Oil and Gas Online Search" (http://library.geology.deq.state.ms.us/) but it does not seem to include wells more recent than 1996 or to allow bulk download of well information.

Mississippi Oil and Gas Board (http://www.ogb.state.ms.us/)

Private Sector
IHS Energy, a private vendor of energy-related information and prospective (http://www.ihs.com/)

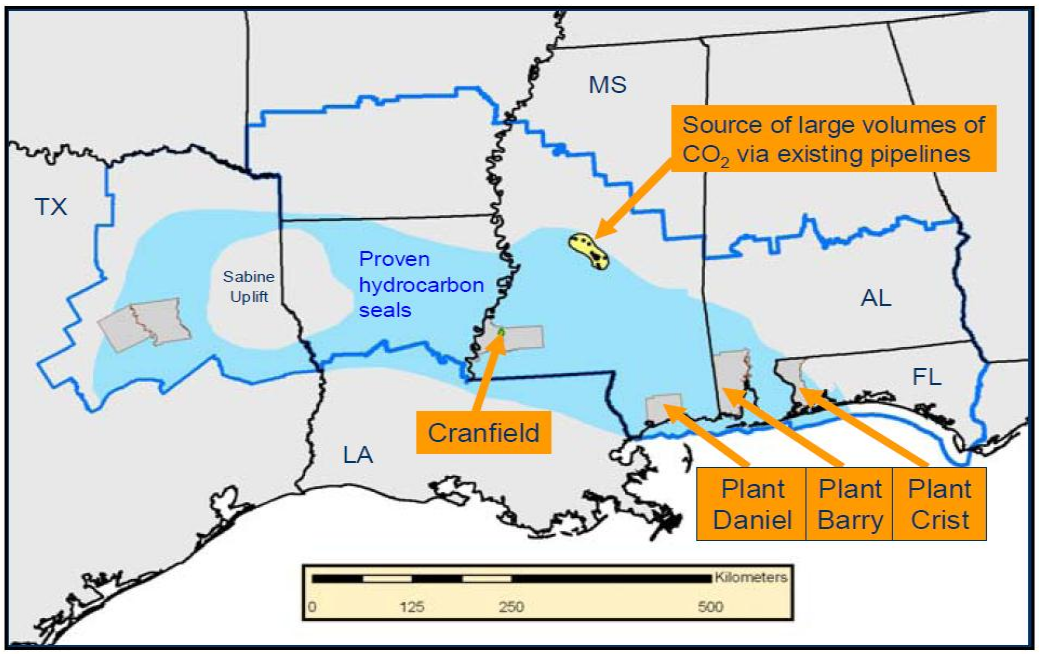

Figure 1. Regional map of the site.
(Source: SSEB/SECARB website)

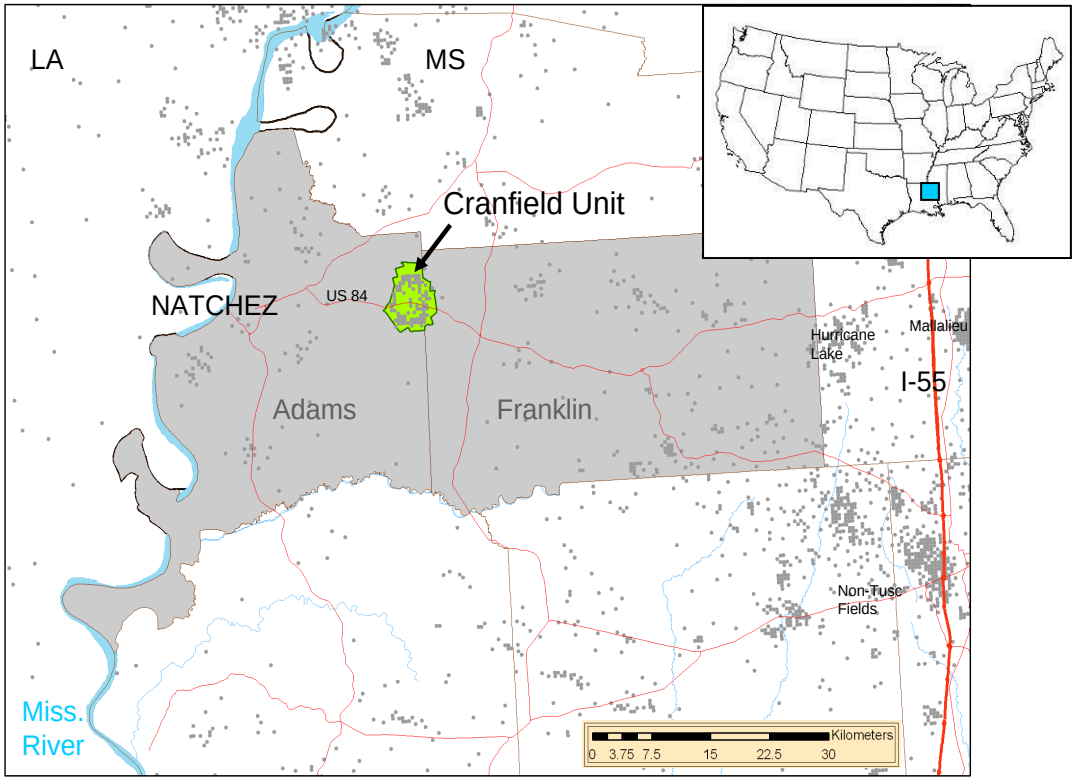

Figure 2. Location map of the field straddling Adams and Franklin counties in southwestern Mississippi.

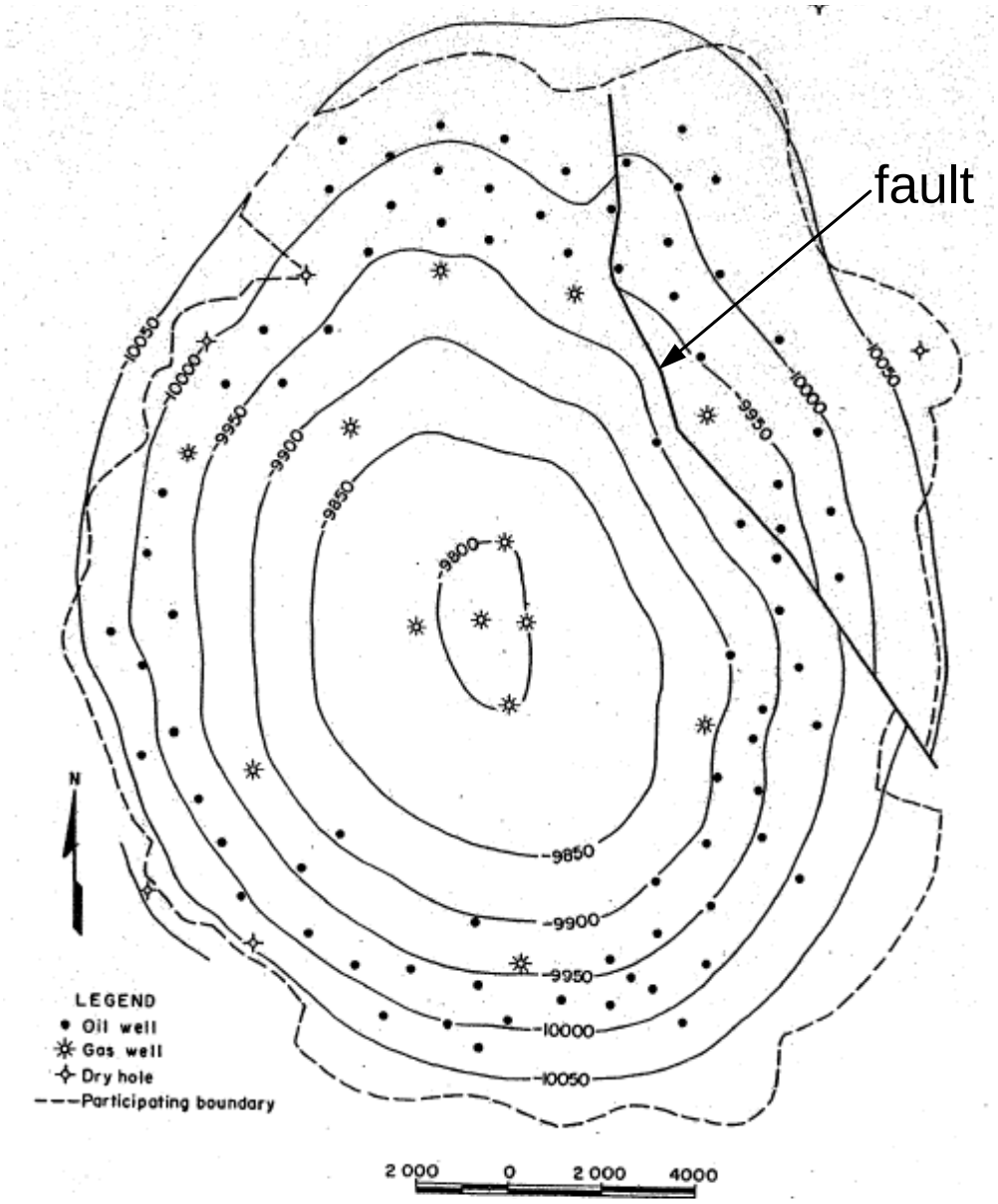

Figure 3. Structure contoured on Basal Tuscaloosa sand of the reservoir.
(Source: MOGB (1966)) Note: The gas cap is clearly visible at the center of the structure and shown by the distribution of gas wells.

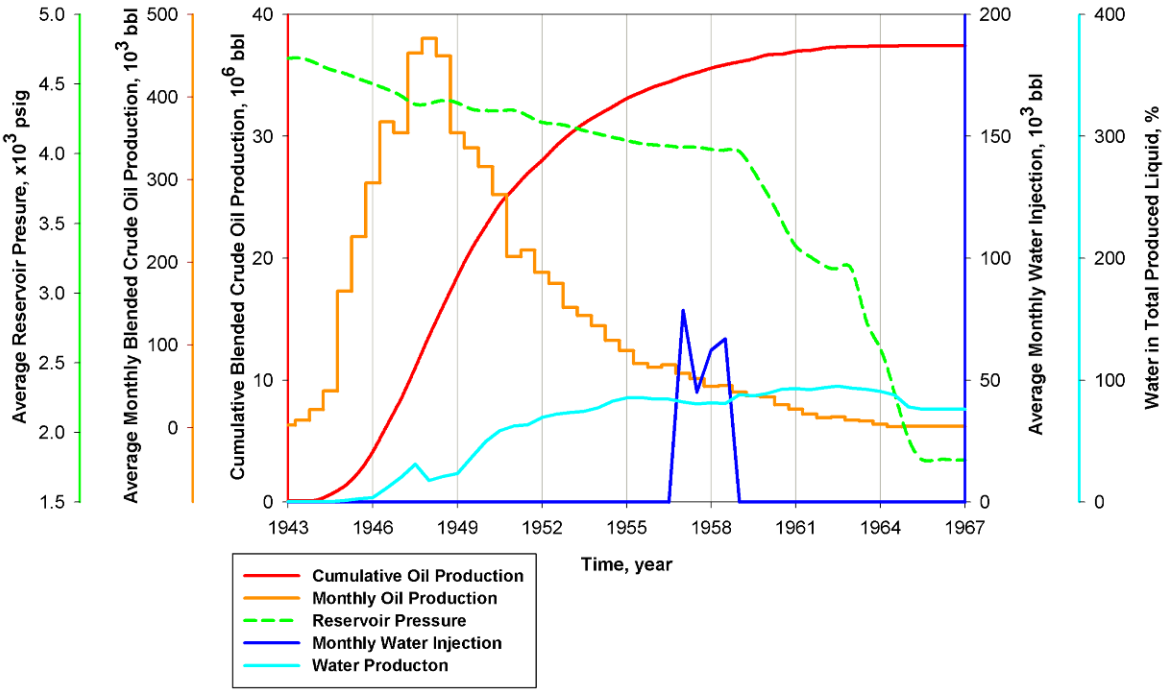

Figure 4. Reservoir pressure, oil production, water production and injection during historical period.
(Source: modified from MOGB (1966))

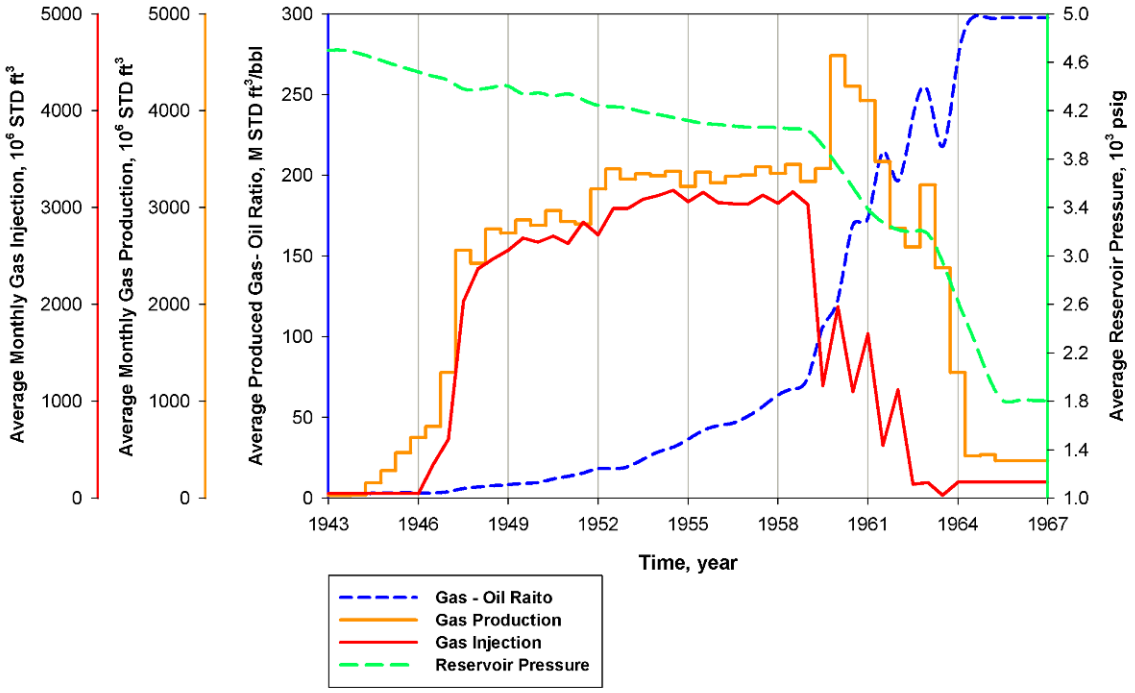

Figure 5. Reservoir pressure, gas production, water production and injection during historical period.
(Source: modified from MOGB (1966))

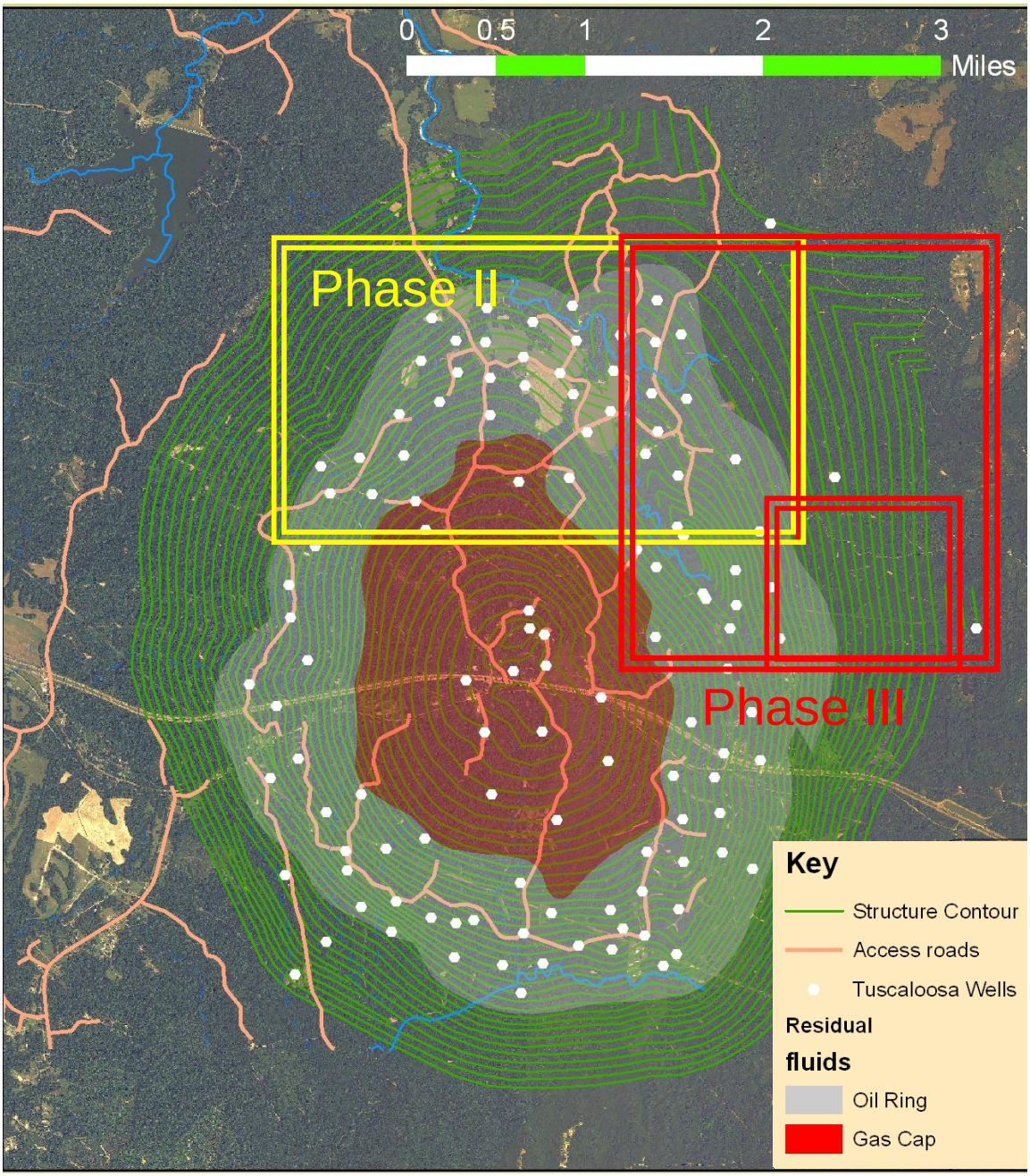

Figure 6. Site map showing footprint of oil ring and gas cap and Phase II and Phase III numerical model domains as well as subdomain the Phase III model with focus on the DAS

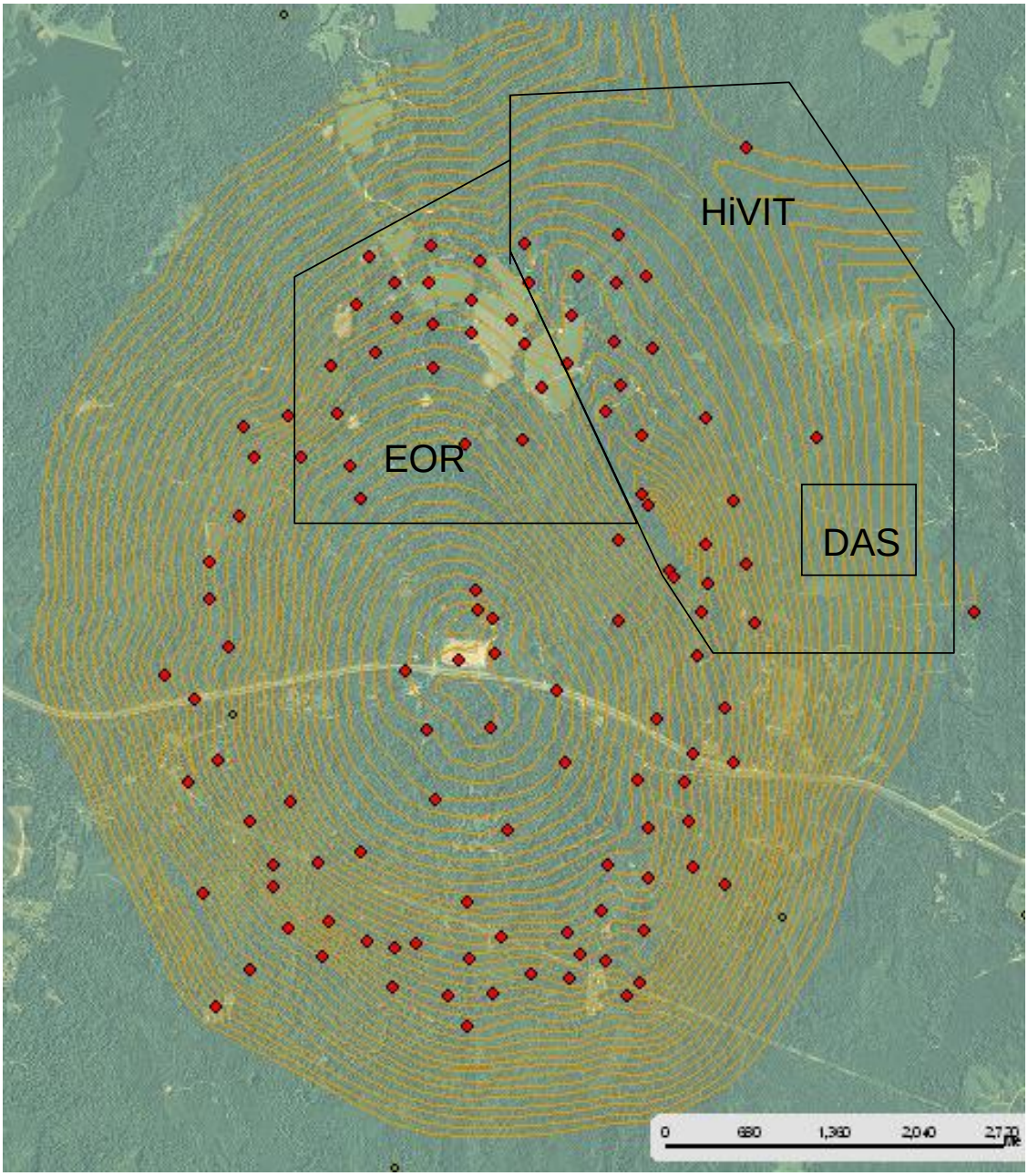

Figure 7. Site map showing relationship between numerical model domains and SECARB operations: Phase II and focus on monitoring of pressure in the so-called EOR domain and Phase III and focus on the HiVIT and DAS domains. Red dots represent historical wells.

3 Site Description

3.1 Terrain, Land Use and Climate

The oilfield is located in a rural area of southwestern Mississippi (31º32'39''N and 91º12'22''W). The area is heavily wooded with clearings and is moderately hilly with flat terrace areas near streams (Figure 8); elevations range from 60 to 120 m (200 to 400 ft). Towards the south and west topographical features are gentler and never exceed the elevation of the site. No wetlands are present in the area. Surface drainage is provided by the South Coles and Homochitto Creeks. The oilfield sits mostly within the Homochitto River watershed. Physiographic districts have been defined between the Mississippi River and the site (Figure 9). Renken (1985, Fig. 3) shows two provinces: Mississippi Alluvial Plain province, closely following the Mississippi River Valley on its eastern boundary in Mississippi, and East Gulf Coastal Plain province. At a more local scale, the latter is divided up in Adams and Franklin counties into at least three districts: (1) Mississippi Alluvial Plain located along the Mississippi River west of the oilfield; (2) the Loess or Bluff Hills, which includes the western part of the oilfield; and (3) the Southern Pine Hills, which includes the eastern part of the oilfield.

Land use in the vicinity of the site is mostly rural with economic uses based on natural resource production including timber production, gravel quarrying, rangeland and oil and gas production. U.S. Route 61 and U.S. Route 84 provide easy highway access to the area. A network of county and private gravel roads provides access to the well sites.

Critical habitats or wildlife refuges for listed species of plants or wildlife do not exist in the vicinity of the site. The St. Catherine Creek National Wildlife Refuge is located approximately 20 miles southwest of the project area on the east bank of the Mississippi River 10 miles south of the city of Natchez. the site lies east of Natchez State Park, with the western lease boundary nearly coincident with the eastern boundary of Natchez State Park. The site lies north of Homochitto National Forest, with the southern lease boundary approximately coincident with the northern boundary of the western limb of the forest (Figure 10). The closest large population center is Natchez (~18,000 inhabitants) 15 mi (25 km) to the west, but there are isolated residences spread out over the area along with oil and gas workers present around the site.

Because of the lack of a long series of weather data for the site (BEG recently installed a meteorological station), we assume data for the nearby city of Natchez are valid for the site (http://www.city-data.com/city/Natchez-Mississippi.html). Temperatures range from an average of about 10° C (50° F) in the winter to about 27° C (80° F) in the summer. Annual rainfall averages about 160 cm (62 in) (US Climate Data). Monthly precipitation averages 4.5 and 1.5 in (11.4 and 3.8 cm) in the summer and winter months, respectively. Snowfall is very rare. Relative humidity is variable during the day, from ~90% in the morning to ~65% in the afternoon throughout the year. Wind speed is the highest in March with average values reaching 9 mph (4 m/s) and lowest in the summer, averaging 6 mph (2.7 m/s). Although spatial variability is expected to result in somewhat different values at site, the wind speed records from other meteorological stations in the region (Jackson, MS; Baton Rouge, LA; and Shreveport, LA) indicate a spatial variability on the order of 1 mph. Wind directions are quite variable during the

year (Figure 11). Approximately 40% of the time the wind is blowing from south and southeast and ~17 % from the North.

3.2 Surface Water

The site straddles two drainage basins: (1) most of the field area drains to the Homochitto River about 12 mi (20 km) south of the site (Figure 9) and (2) its northernmost portion drains to the north in Coles Creek Basin into the South Fork Coles Creek which flows north towards a tributary of the Mississippi River. The Homochitto River flows west and southwest until joining the Mississippi River about 100 mi (60 km) southwest of the site. The Mississippi River and the associated alluvial flood plain lie about 12 mi (20 km) west of the site and are separated from the site by hilly terrain of the Loess (Bluff) Hills.

There are numerous manmade small ponds remaining from past oilfield practices at the site. Most of these bodies of water have maximum linear dimensions less than 250 m. The main exception is Natchez Lake in Natchez State Park, which lies about 1.2 mi (2 km) west of the lease boundary (Figure 10). The lake has a maximum linear dimension of about 0.9 mi (1.5 km), a surface area of about 250 acres (1 km^2), maximum depth of about 43 ft (13 m) and an average depth of about 20 ft (6 m). There are also two water bodies about 13 mi (8 km) south of the site with maximum linear dimensions of about 1,600 ft (500 m).

3.3 Subsurface

3.3.1 Regional Geology

The oilfield area is part of the Gulf Coast province running along the Gulf of Mexico from south of the Mexican Border to the Florida state line (for example, Williamson and Grubb, 2001). The Mississippi structural trough, a southward plunging syncline, is approximately traced out at the ground surface by the Mississippi River. The syncline has been subsiding since the end of the Paleozoic Era (Cushing et al., 1964). The base of the sedimentary sequence in the Gulf Coast Basin consists of thick and extensive salt layers of Jurassic age. The Mississippi salt basin (Figure 12) has accumulated a thick sequence of Mesozoic and Cenozoic sediments (for example, Cushing et al., 1964). The deformation of the salt caused by loading by Cretaceous sediments led to the development of salt diapirs penetrating the overlying sediments. The site lies on the southern border of the Mississippi Interior Salt Basin (Figure 12), which controlled Mesozoic deposition. The thick Jurassic salt layers of regional extent were found at ~20,000 ft (6,000 m) in a deep well at the site. Regional faults systems of the Mississippi salt basin do not intersect the structure at the site (Figure 12).

At the ground surface, the site is located on the coastal lowlands aquifer system as shown in Figure 13, a north-south cross-section that is about 12 mi (20 km) east of the site. The coastal lowlands aquifer system is a Gulf-ward-thickening, heterogeneous, unconsolidated to poorly consolidated wedge of discontinuous beds of sand, silt, and clay that range in age from Oligocene to Holocene. The base of the coastal lowlands aquifer system is the Vicksburg-Jackson confining unit that separates the coastal lowlands aquifer system from the underlying Mississippi embayment aquifer system. The reservoir targeted for CO_2 sequestration lies at a depth of about 10,000 ft (3,000 m) (Figure 14) and is therefore within the footprint of the Mississippi embayment aquifer system (Figure 13 and Figure 14). The Mississippi embayment consists of poorly consolidated rocks of late Cretaceous to middle Eocene age. Transgressive-

regressive cycles of sediment deposition during the Cretaceous period were controlled by global changes in sea level and subsidence of the Gulf Coast Basin. Subsequent sedimentation starting in the Tertiary period was deposited during progradational cycles of alluvial and deltaic infilling (Renken, 1998). Sedimentary rocks of Cretaceous to early Tertiary age crop out mostly in off-lapping bands that parallel the perimeter of the embayment and dip gently toward its axis. From a landward-outcropping edge, the entire sequence thickens greatly toward the axis of the Mississippi Embayment and the Gulf Coast.

The upper Cretaceous Tuscaloosa Formation was deposited during a transgressive-regressive cycle and is bounded by unconformities at the base and top of the formation that represent erosion surfaces (Figure 16). Regionally, the lower sandstone beds of the Tuscaloosa Formation are fluvial-deltaic sediments interpreted as deposited in a semiarid climate characterized by aggradational deposition (Chasteen, 1983; Mancini et al., 1987). The oil-producing interval of field is hosted by basal sandstones and conglomerates overlain by local fluvial mudrocks capping the reservoir. Additional mostly non-productive alternating sandstones and mudrocks complete the lower Tuscaloosa (Figure 17). A fine-grained marine sandstone overlies the massive sandstone. The fine-grained marine sandstone is overlain by dark marine mudstones of the middle Tuscaloosa Formation (Lu et al., 2011). With a reduction in accommodation and an increase in siliciclastic sediment supply, fluvial and marine reworked sandstone deposits of the upper Tuscaloosa Formation ended this depositional cycle (Mancini and Puckett 2005). The Tuscaloosa Formation is overlain by the thick carbonate mudstones of the upper Cretaceous.

3.3.1.1 Faults

The complex deep structure at the top of salt layers is reduced to a crestal graben in the Tuscaloosa interval at the depth of the oilfield. The boundary faults trend NW-SE, one cutting through the northeast section of the oilfield with the southeast compartment being the downthrown, the other just southwest of the oilfield with the downthrown compartment northeast of the fault. The relevant fault for this study is the one that bounds the study area in the northeastern portion of the field: its throw is ~25 m (80 ft) or approximately equivalent to the injection layer thickness (a subset of the lower Tuscaloosa). This puts the reservoir sands of the downthrown compartment against a thick underlying shale whereas the reservoir sands of the upthrown compartment abut the fluvial low-permeability material overlying the reservoir.

Both of the graben-bounding faults appear to be genetically related to the growth of the underlying salt dome. Salt dome growth is quiescent in the Mississippi salt basin and the faults are therefore not active. Major time of salt dome growth occurred during the late Jurassic and continued into the early Cretaceous with lesser movement in the late Cretaceous and early Cenozoic (Mancini, 2005, p.126). The northeast fault can be traced ~300 m (~1,000 ft) into the overlying strata to where it becomes undetectable in the available seismic data in the mudrocks of the Midway Group (Meckel, unpublished data). This is below where the fault would intersect the permeable Wilcox sands. In addition, the faults imaged on seismic have a limited lateral extent.

Several arguments can be made to support the contention that the faults are not horizontally transmissive: (1) the elevations of the oil-water contact on either side of the northeast fault were different at discovery; (2) current observations (Meckel and Hovorka, 2009) show that there is

no pressure response from CO_2 injection in the northeast section of the reservoir observed across the fault; and (3) well break-out observations suggest that the current maximum horizontal stress closes the fault (Meckel, unpublished data).

3.3.2 Regional Subsurface Hydrology

The Gulf Coast water-bearing formations from Texas to Alabama can be divided into three main systems: (1) a coastal Lowlands aquifer system of Miocene and younger age overlying the Vicksburg-Jackson mostly confining units; (2) Mississippi Embayment System aquifer system (Sparta, Carrizo, Wilcox sands) overlying the mostly confining Midway group; and then (3) the Cretaceous aquifers, sometimes also attached to the Mississippi embayment system.

The site lies on the Mississippi alluvial margin and, from the ground surface down to the base of the Vicksburg-Jackson group (Figure 13), is within of the coastal lowland aquifer system. The formations below this point belong to the Mississippi embayment aquifer system, including the oil reservoir in the Tuscaloosa Formation. In the coastal lowland aquifer system and upper portions of the Mississippi embayment aquifer, the natural flow pattern was convergent toward the axis of the Mississippi embayment syncline. Recharge to the coastal lowlands aquifer system is greatest in the topographically high areas east (area of the site) and west of the Mississippi River and along the landward margin of the aquifer. Regional ground-water flow was directed southward to the coast with ground water discharged by diffuse upward leakage to major rivers, low-lying coastal marsh areas, and to the ocean as seabed seepage in shallow near-shore areas.

Large ground-water withdrawals in southern Arkansas and northern Louisiana have caused declines of the potentiometric surface and some changes in direction of regional predevelopment flow in the Tertiary Sparta Sand of the Claiborne unit (Figure 14). The pumping has induced downward leakage of water into the Sparta Sand aquifer from the upper Claiborne and the Mississippi River Valley alluvial aquifers (Renken, 1998). Groundwater pumping from the coastal lowland aquifer has altered the pre-development groundwater flow pattern a large portion of southern Louisiana as well as in the area of Natchez where the natural upward flow in the coastal lowland aquifer system has become downward flow (Renken, 1998, Figures 56 and 57). However, the flow pattern at the site has not been affected by pumping and has remained downwards as in historical times.

3.3.3 Shallow Subsurface and Aquifer Systems

3.3.3.1 Aquifer Description and Water Quality

The city of Natchez derives most of its water from the coastal lowlands aquifer system that overlies the Mississippi embayment aquifer system. Specifically, water is taken mainly from the Holocene alluvial aquifer and from the Miocene Catahoula Formation (Strom et al., 1995). The alluvial aquifer consists of sand, gravel, silt and clay and has a maximum thickness of about 200 ft in the area of Natchez (Boswell and Bednar, 1985). Abundant, but discontinuous, fine-grained beds of local extent act as confining units for the alluvial aquifer, but cannot be traced over an area larger than several counties. The Catahoula is a confined aquifer system and has three main sand intervals called the 400-ft, 600-ft, and 1,000-ft sands. The total dissolved solids contents of these aquifers shows little change with depth and range from about 300 to 500 mg/L (Boswell and Bednar, 1985). Hydraulic conductivity of the aquifer is high. In the Natchez area, pump tests determined that conductivities were in the range of 36 to 150 ft/day and storage coefficients in the 0.0001-0.0004 range for a thickness of 60-65 ft (Marble, 1976b, Table 12).

Depictions of hydrostratigraphy and water quality are presented in Figure 14 and Figure 22. The semi-saline aquifers of the Claiborne group lie beneath the Vicksburg-Jackson confining unit but above the Wilcox Group. Any water producing zones within the Vicksburg-Jackson group are minor. A north-south cross-section that is about 20 km east of the site is given in Figure 13, showing the 10,000 mg/L boundaries within the Claiborne aquifers. The three Claiborne aquifers have total dissolved solids levels close to 10,000 mg/L in the vicinity of the site. Local Tuscaloosa brines have a TDS of ~180,000 mg/L whereas Wilcox brines are somewhat less saline varying from <100,000 to 150,000 mg/L. Both are Na-Cl brines with no sulfate and with non-negligible Ca in the Tuscaloosa.

Figure 19 shows contour lines for maximum depth of different salinity levels from Gandl (1982). The construction method used for Figure 19 is presented in Figure 20. The maps representing the area around the field (Adams and Franklin Counties) are extracted from maps giving the same information across the state of Mississippi. They display the maximum depth below which no lower salinity waters than the selected threshold occur, but some shallower strata may locally contain water with a higher salinity. The contour lines are not indicative of specific formations but simply track a salinity level. For example, in the field area, fresh-water bearing formations are all of Miocene age. Further north they do not exist and the Sparta Formation. is the fresh water-bearing aquifer.

The depth at which salinity of 1,000 mg/L occurs varies between 600 to 800 ft below ground surface (bgs) at the site (Figure 19a). Another source (Marble, 1976a) that is more detailed but restricted to Adams County (Figure 21) is overall consistent with the information presented in Figure 15a, but suggests that the base of fresh water can be as deep as 1,000 ft bgs.

Transition to a salinity >3,000 mg/L occurs at depths ranging from 1,200 to 1,400 feet bgs in the site area according to Figure 19b. This is still within formations of Miocene age (Figure 19b). Figure 19c illustrates that transition to salinity >10,000 mg/L occurs at a depth ranging from 1,400 to 1,800 feet bgs in the site area.

3.3.3.2 Shallow Subsurface

The area is blanketed by loess, fine-grained material that limits recharge and confines the underlying aquifers. Boswell and Bednar (1985) described the Mississippi River alluvial aquifer and three water-bearing sands in the shallow subsurface. In the Natchez area, the alluvial aquifer lies from the surface down to 200 feet and the three water-bearing sands are designed as the 400-, 600-, and 1,000-foot sands and correspond to the upper, middle, and lower Catahoula Formation sands. At the site, groundwater chemistry of the shallow alluvial aquifer (200-300 ft below surface) is mainly of the Ca-Mg-HCO3-Cl type according to SECARB chemical analyses (Figure 22). Some heavy metals including As, Cr, Mo, and Se are non-detectable. Boswell and Bednar (1985, Table 3) also provides chemical analyses of the Catahoula Sands.

SEM and XRD results of the sediment samples taken from a water well located within the footprint of the oilfield (UM-1) indicate that the aquifer is free of carbonate minerals (Lu, unpublished data). Saturation indexes for selected minerals show that calcite, dolomite and

gypsum are under-saturated in all groundwater samples (Yang et al., 2009), corroborating the petrographic analyses of cores from the same well.

3.3.4 Natural and Hydrocarbon Resources

The economic mineral map of the State of Mississippi last published in 2009 by MDEQ shows only hydrocarbons and shallow deposits of gravels and sands as resources in the v (Figure 24). Hydrocarbon accumulations exist both above and below the Tuscaloosa interval (Table 1). The Wilcox oilfield above the reservoir of interest was discovered before the Tuscaloosa and is still producing through two stripper wells according to IHS. Production from the Wilcox has been overall steadily declining for the past 40 years (Figure 25) with an increasing water cut (>90%) as displayed on Figure 26 and Figure 27. Those are large volumes of fluid retrieved from the subsurface. Gas accumulations also exist in underlying formations in the Washita-Fredericksburg and in the Paluxy (Childress, 1976, Table 5).

3.3.5 Wells

3.3.5.1 Water Wells

The MDEQ website states that 93% of the drinking water supply in Mississippi originates from aquifers. Only three public surface water systems presently operate in the state. Jackson, the state capital and largest city in Mississippi, uses a combination of surface and ground water. EPA has designated eastern Louisiana and southwestern Mississippi as a Sole Source Aquifer area (http://www.epa.gov/region04/water/groundwater/r4ssa.html#shills). SSA status draws attention to the vulnerability of the region's water resources but mostly triggers additional scrutiny for federally-funded projects of sufficient size to potentially impact the aquifer such as highway improvements, waste water treatment plants, or agricultural projects.

MDEQ (2009) lists all active municipal and public water supply wells, providing information on depth and yield. The closest municipal well field is that serving the City of Natchez, which consists of three wells. These wells are located a few miles east, northeast, and southeast from the city at a distance of over 10 mi (16 km) from the oilfield. Older USGS reports (Boswell and Bednar, 1985; Strom et al., 1995) provide more information. Strom et al. state that 24 wells withdraw water from three different levels from the Catahoula Sands at a rate of 9.2 MDG (in March 1995), that is, ~6340 gpm. Some shallow domestic wells as well as water supply wells to support oil field activities (<300 ft) exist in the area (Figure 23).

3.3.5.2 Oil and Gas Wells

Hydrocarbon wells at the site are shown in Figure 28, Figure 29, and Figure 30. Most of the wells in the Wilcox and Tuscaloosa were drilled in the 1950's (Figure 31) but the Wilcox reservoirs were revived twice (in the 1960's and 1970's), presumably with wells of increasing quality. The Wilcox was the early oil production target at the site, but the availability of well tests and pressure data is limited. The Wilcox Group is a thick ~3,000 ft (900 m) accumulation of interbedded sandstone units. Because Wilcox wells date back over 70 years and are currently operated as stripper wells, there is very limited availability of well tests and pressure data to determine if the Wilcox reservoirs are under pressurized and therefore a likely sink for potential upwarded migrating fluids, such as along a poorly cemented well. Only one well from the Wilcox data had reservoir pressure data. That well had a final shut-in pressure of 2,235 psi (15.2 Mpa), which is ~200 psi (1.4 Mpa) below the hydrostatic gradient of 0.433 psi/ft at a depth of

5,540 ft (1,700 m). This further suggests the Wilcox is under-pressured due to extensive production. According to IHS, there are approximately 150 wells in the Tuscaloosa (~10,000 ft deep) and approximately 100 in the Wilcox (~6,000 ft deep). More recent tertiary production has come from the Tuscaloosa Formation. Thanks to a single operator during most of its history, unrecorded wells do not seem to be an issue, although some well locations are poorly surveyed.

A conservative assessment of the quality of well cementing was performed using cement bond logs (CBL). The CBL logs used for this assessment were acquired from the private vendor IHS and the Mississippi Oil & Gas Board. A CBL is used to analyze the integrity of bonding between the cement and well casing. A lack of adequate cement in the annular space between casing and formation could create a preferential conduit for CO_2 migration along the well bore. A total of 14 CBL logs were acquired for this risk assessment, with the oldest log from 1961 and most recent from 2010. Five CBL logs were from wells drilled to the Wilcox Formation (symbols with thick black outlines on Figure 33). While CBLs for only 14 wells out of a total of 287 at the oilfield is a relatively small sample, it does provide some perspective on the range in cement bond integrity at the site. Some wells also had qualitative well cement logs like variable density logs and sonic profile logs, but they had limited implications relative to the quantitative assessment using the CBL logs. In general, CBL log findings were observed by BEG and operator consistent with actual state of the well when later reentered, increasing the confidence in the appropriateness of CBL in this RA. Additional suites of cement bond logs were collected for newly drilled wells however these were not used because they are not representative of the older well completions.

The analysis of CBL logs used cutoffs, established by Schlumberger, to evaluate zones of questionable cement, good cement, and 100% cement bonds along the casing. The CBL cutoffs are dictated by casing size and cement type for each well. Most wells had 7 in. casing with Class "H" cement, but a few wells had smaller casing or used POZ mix cement. Table 2 shows the CBL data obtained from well logs and well reports, along with the numeric interpretation of CBL cutoffs. The cement bond zones were established similar to picking net sand, where zones of good cement had a CBL reading below the established good bond cutoff. In agreement with the Schlumberger manual (Schlumberger, 2009), we assumed that both 100% cement bond index (BI) (that is, near-perfect bond between casing and cement) and good cement BI (that is, some non-connected areas with poor bond defined as BI>80%) translate into no flow along the well given that the good-cement interval is long enough.

Maps and cross-sections showing the CBL results were developed in the Petra software to allow identification of the wells with the greatest risk towards leakage. The cross-sections, such as Figure 34, illustrate the numerous geologic formations that separate the injection interval from the surface and protected aquifers relative to the CBL results (note the scaling difference between Table 2 and Figure 34, where the cement is evaluated on one foot intervals in the table, while each 100 foot interval of cement was characterized for Figure 34). It is critical to have good cement bonds through units with low permeability to maintain confinement.

From the data in Figure 33, Figure 34, Table 2, and Table 3, it can be determined that AM Ratcliffe LSE 1 #7 (API# 23001002490001) and CFU #1 (API# 23037000480001) are the wells of highest concern in terms of cement bond quality. These wells do not have an adequate segment of "good" cement across the confining middle Tuscaloosa, hence, there is significant

potential of CO_2 migration along the well bore, While CBL results are only available for a small portion of the wells, they indicate that a fraction of the wells could allow leakage. Even though some of the older wells have been worked over and recompleted to prepare them as producers for enhanced oil recovery operations, behind-casing leakage risk remains because cement bond is not typically remediated during this operation.

Table 1. Hydrocarbon summary production

Formation	Cumulative Oil Prod (bbl)	Cumulative Gas Prod (MSF)	Cumulative Water Prod (bbl)*	Number of Prod. Wells	Total Number of Wells	Average TD Depth (ft)
Wilcox	11,709,753	3,065,579	255,417,720 / 82,000,000	48	108	~5,800
Tuscaloosa*	35,885,662	617,046,280	111,342,522 / 62,500,000	92	147	~10,400
Washita-Fred.	0	3,058,756	20,475	2	9	~11,500
Paluxy	994,903	37,849,893	1,542,244	4	8	~12,300
Sligo	488	810,692	6,808	1	1	~15,000
Other	0	0	0	1	14	

(Source: IHS)

*: uncorrected, taking IHS data at face value / corrected (assuming typos in very high water producers) – see Figure 32

Note: Tuscaloosa well category includes recent Denbury wells; some older wells are not counted as producing but they may simply lack data

Table 2. List of CBLs used for evaluation of the Tuscaloosa reservoir

Well	Log Year	Total Depth	East of Fault	Casing Size	Casing Weight	Top of Cement	Bottom of Cement	Cement Interval Thickness	Cement	100% Cement Cutoff	Good Bond Cutoff	CBL Interpretation		
												ft Below Cutoff	ft Above Cutoff	ft @ 100%
API			Y/N	inches	lbs./ft	feet	feet	feet	Type	mV	mV			
23001001490000	1961	5,857	Y	7	26.0	3,873	4,671	798	POZMIX	3.4	12.1	163.6	490.1	144.3
23001001780001	2008	10,328	N	7	26.0	10,115	10,328	213	Class "H"	1.8	7.8	98.8	46.5	67.7
23001001940000	2007	10,358	N	7	29.0	10,125	10,329	204	Class "H"	2.5	9.4	94.8	74.2	35.0
23001002490001	2010	12,300	N	7	29.0	9,468	10,999	1,531	Class "H"	2.5	9.4	257.6	1219.3	54.1
23001002550000	1962	5,630	N	7 5/8	n/a	2,770	5,498	2,728	POZMIX	2.3	8.7	2477.6	28.9	221.5
23001209890000	1998	20,190	N	9 5/8	40.0	11,395	11,823	428	Class "H"	2.7	9.1	119.2	295.7	13.1
23001216050000	1978	6,110	Y	5 1/2	15.5	2,790	4,000	348	Class "H"	0.7	4.7	160.0	149.5	38.5
23001218550000	1979	4,524	N	5 1/2	15.5	3,300	4,459	1,159	Class "H"	0.7	4.7	399.7	326.2	433.1
23001224880000	1983	10,500	N	5 1/2	17.0	8,835	10,347	1,512	Class "H"	1.0	6.1	233.0	206.5	1072.5
23001226220000	1998	11,147	N	5 1/2	17.0	9,770	11,147	1,377	Class "H"	1.0	6.1	630.2	529.3	217.5
23001232910000	2005	11,700	Y	4 1/2	n/a	8,615	11,111	2,496	Class "H"	0.6	5.0	1662.4	483.6	350.0
23001233420000	2007	10,500	N	5 1/2	17.0	9,258	10,500	1,242	Class "H"	1.0	6.1	567.3	613.1	61.6
23001233650000	2008	11,073	Y	5 1/2	17.0	8,735	10,999	2,264	Class "H"	1.0	6.1	785.6	1454.6	23.8
23037000480001	2009	10,410	Y	7	29.0	9,540	10,401	861	Class "H"	2.5	9.4	51.3	805.0	4.7

Note: The CBL interpretation columns represent the cumulative lengths of cement below the threshold cutoff (questionable bond), above cutoff (good bond), and 100% bond. Wells east of the main fault through the Tuscaloosa reservoir are wells of focus in terms of leakage risk; mV=millivolt reading on the well log; color codes are identical to those used in Figure 34

Table 3. First indication of questionable cement bond above top of lower Tuscaloosa

Well	CBL Interpretation			Good Cement Thickness above top of lower Tuscaloosa before first sign of questionable cement bond	Comments
API	% Below Cutoff	% Above Cutoff	% @ 100%		
23001001490000	20.5%	61.4%	18.1%	n/a	23/26/29 lbs/ft casing wt.
23001001780001	46.4%	21.8%	31.8%	52 ft	casing wt. derived from transit time
23001001940000	46.5%	36.4%	17.2%	24 ft	
23001002490001	16.8%	79.6%	3.5%	31 ft	
23001002550000	90.8%	1.1%	8.1%	n/a	Avg. cutoffs used from casing size
23001209890000	27.9%	69.1%	3.1%	n/a	casing wt. derived from transit time. 2 cemented intervals, top interval is logged & evaluated
23001216050000	45.7%	42.7%	11.0%	n/a	log missing from 2,840 ft. – 3,700 ft. (% given for intervals logged)
23001218550000	34.5%	28.1%	37.4%	n/a	
23001224880000	15.4%	13.7%	70.9%	24 ft	
23001226220000	45.8%	38.4%	15.8%	12 ft	
23001232910000	66.6%	19.4%	14.0%	20 ft	Avg. cutoffs used from casing size
23001233420000	45.7%	49.4%	5.0%	2 ft	
23001233650000	34.7%	64.2%	1.1%	18 ft	
23037000480001	6.0%	93.5%	0.5%	5 ft	23/29 casing wt., 29lbs/ft casing wt. used for cutoffs

Note: color codes are identical to those used in Figure 34

Figure 8. Photographs representative of the site showing wooded areas and clearings incised (10-20 ft) by a few streams

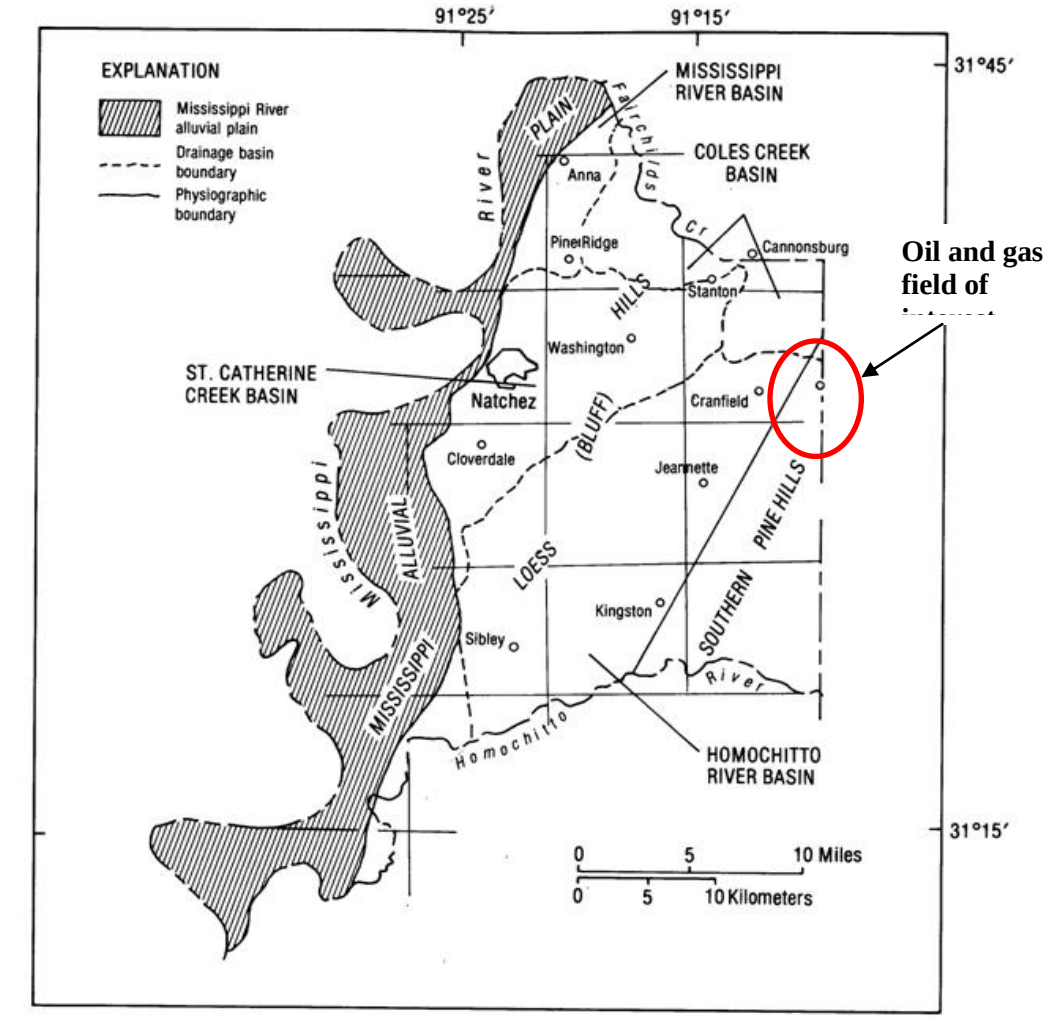

Figure 2.—Physiographic districts and drainage basins in Adams County.

Figure 9. Physiographic districts and drainage basins in Adams County
(Source: Boswell and Bednar, 1985, Figure A)

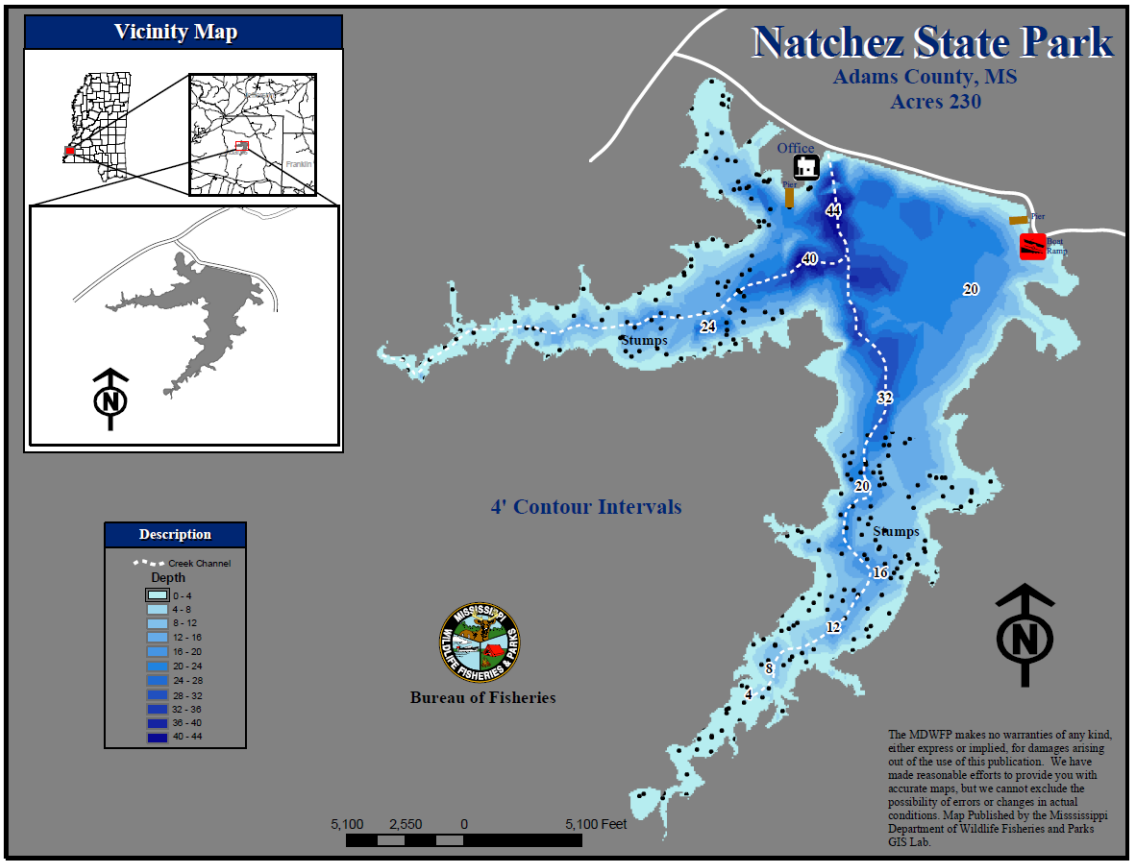

(a)

(b)

Figure 10. Depth Contours for Natchez Lake and Relationship to the site

(a) Depth contours (Source: Mississippi Wildlife Fisheries & Parks, Bureau of Fisheries, http://home.mdwfp.com/pdfgallery.aspx?Albumid=84&Page=2)

(b) Relationship of site location to Natchez Lake and Homochitto National Forest

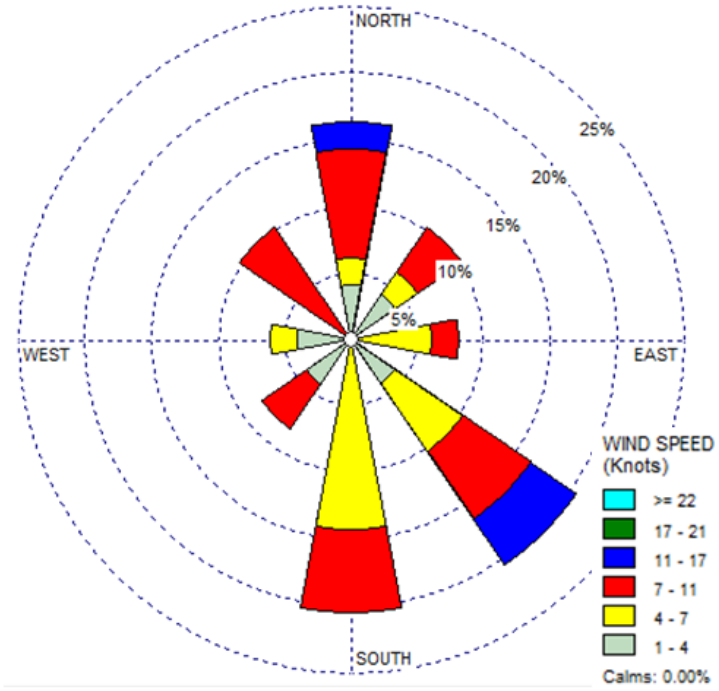

Figure 11. Wind rose showing principal wind directions of wind at Natchez, MS.

(Sources: http://www.wcc.nrcs.usda.gov/ftpref/downloads/climate/windrose/mississippi/ and http://www.city-data.com/city/Natchez-Mississippi.html)

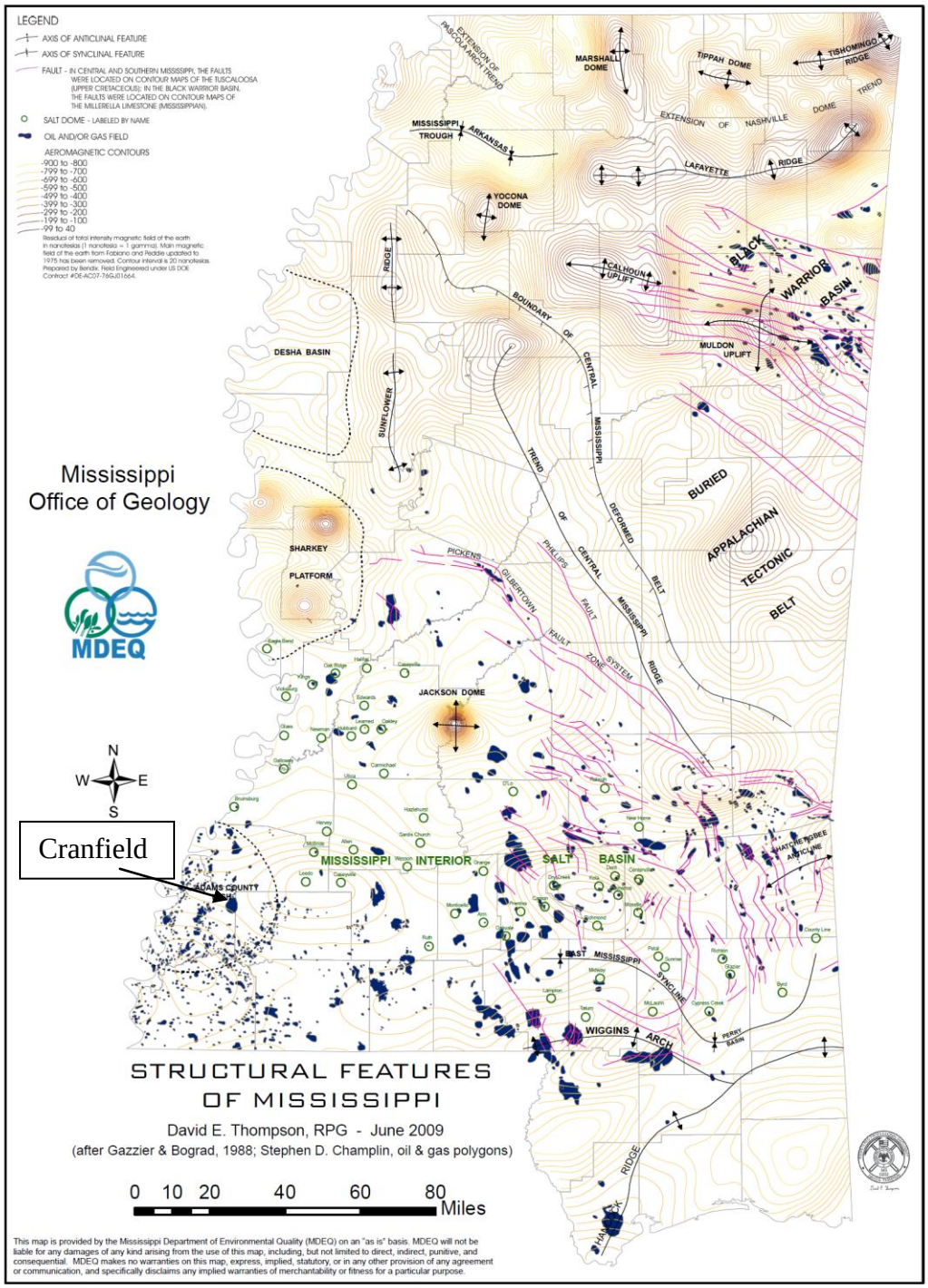

Figure 12. Structural Features of Mississippi
(Source: MDEQ website)

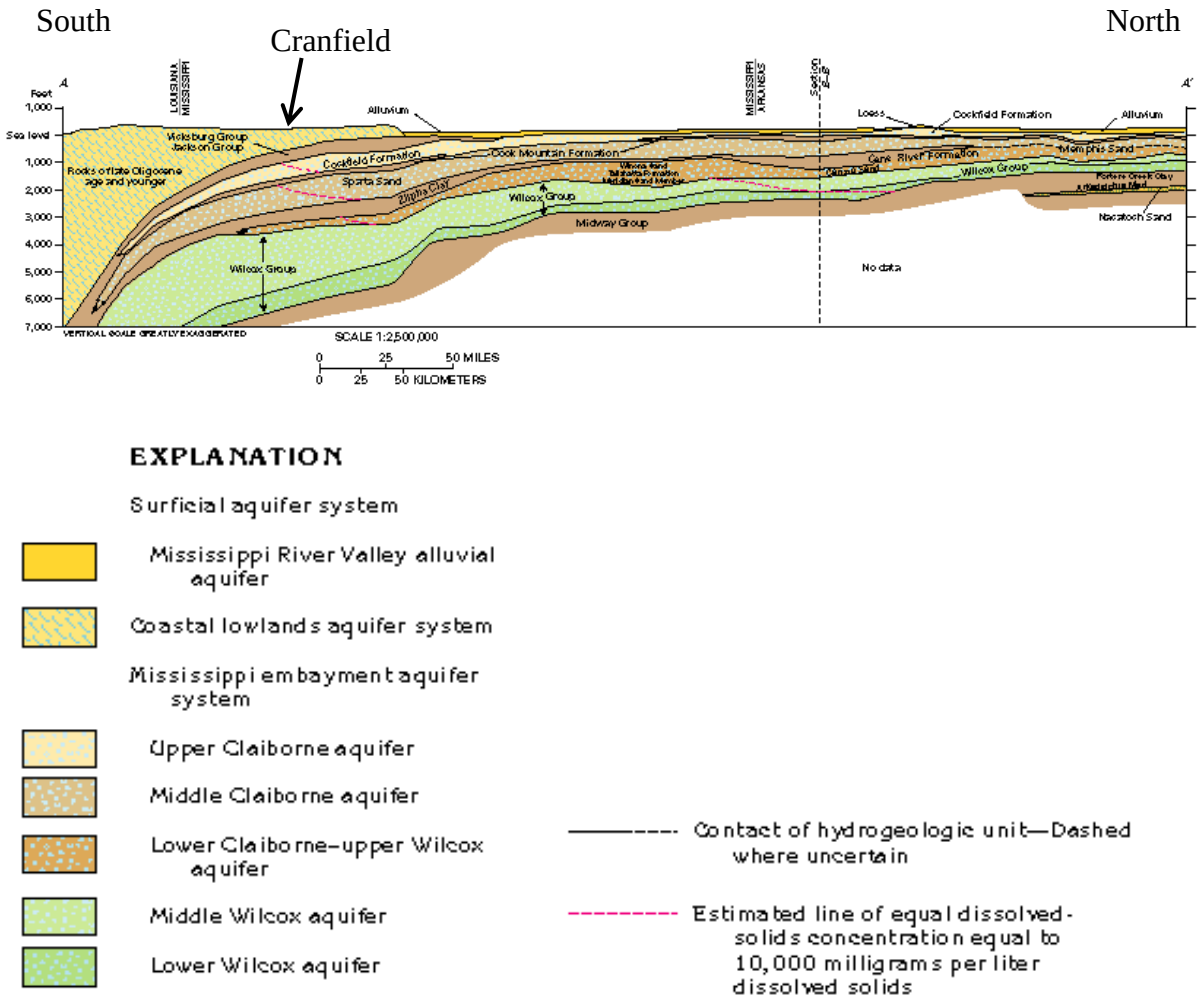

Figure 13. North-South Cross-Section 20 km East of the site Showing the Mississippi Embayment Aquifer System to Base of the Tertiary and the Coastal Lowland Aquifer System.
(Source: Renken, 1998)

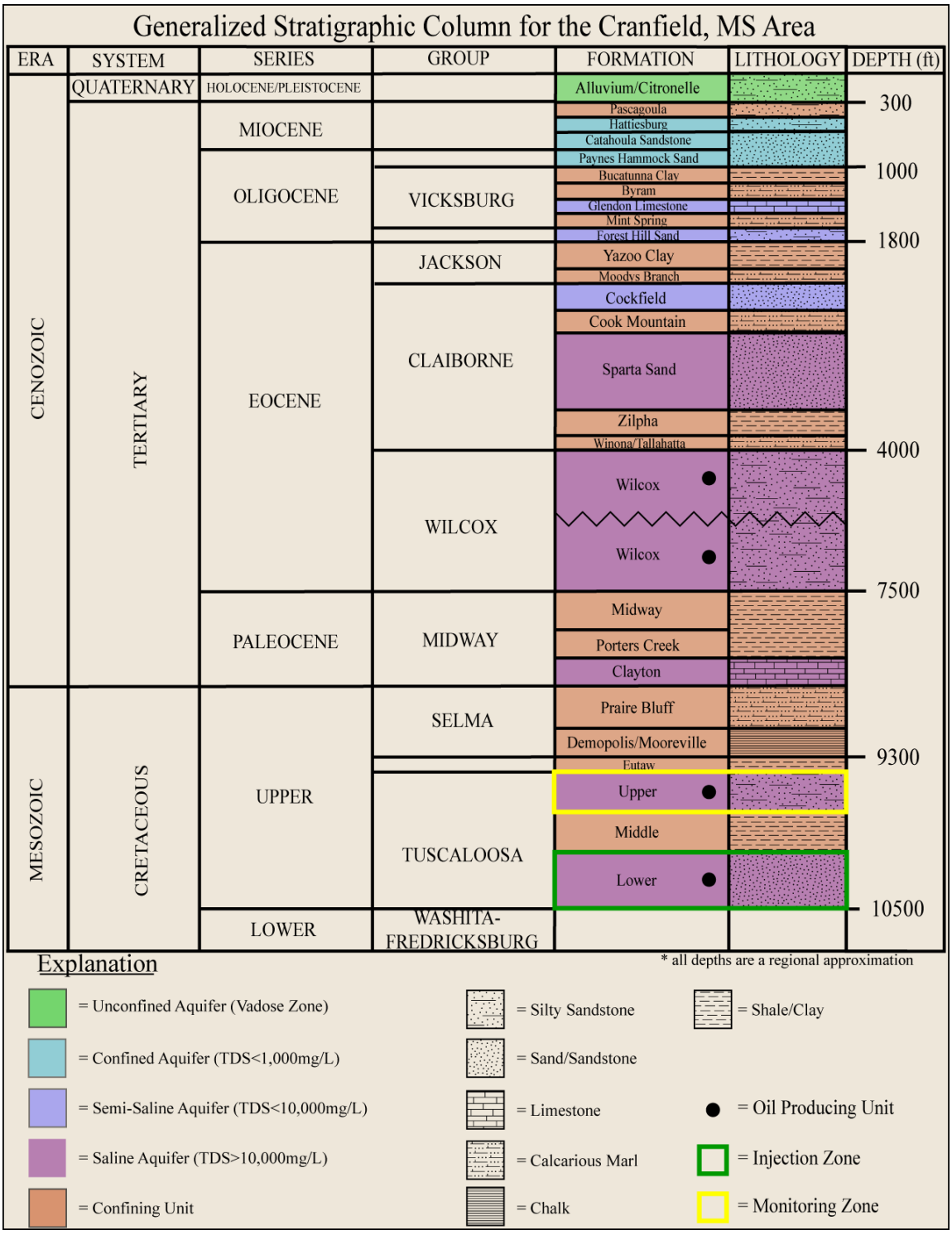

Note: the vertical depth scale is pseudo-logarithmic, expanded in the shallow subsurface.

Figure 14. Stratigraphy at the site illustrating the basic lithology and TDS for each formation from the CO_2 injection interval to the surface.
(Source: various including Childress (1976))

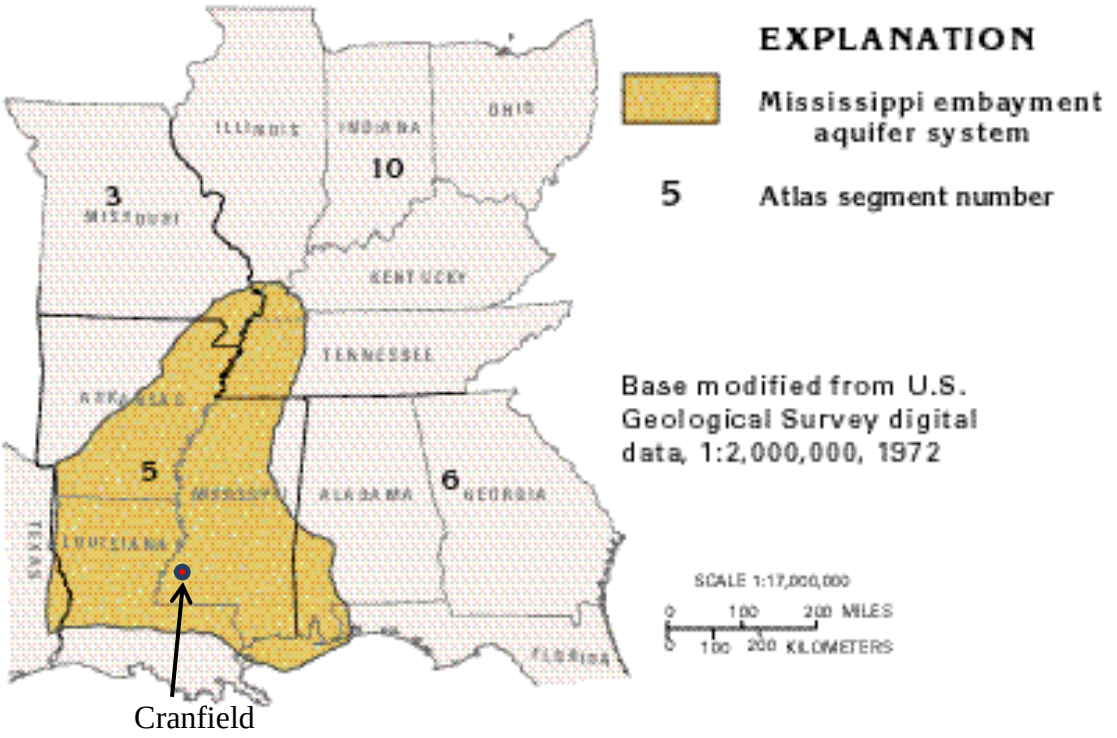

Figure 15. Footprint of Mississippi Embayment Aquifer System
(Source: Renken, 1998)

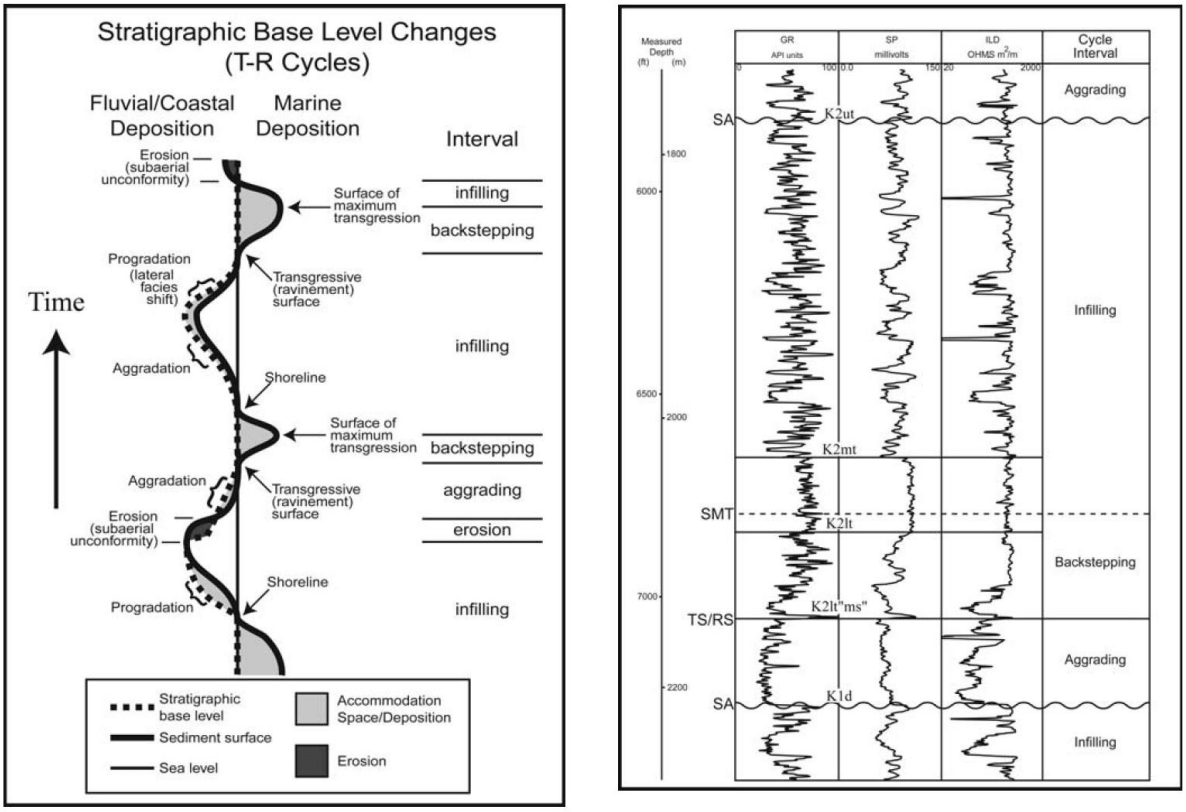

(a) (b)

Figure 16. Transgressive-Regressive Depositional Cycles for the Tuscaloosa Formation (not necessarily entirely valid at the site location)

(a) Diagram illustrating the factors affecting stratal architecture emphasizing the effect stratigraphic base level changes have on T-R cycle development in the non-marine and marine realm. Sea level is held constant to determine the behavior of strata relative to the sediment surface, sea level, and stratigraphic base level.
(b) Well log patterns from the Harrison #1 well, North Clark Field, Wayne County, Mississippi, showing the well log signature characteristics for the T-R K5 cycle and associated transgressive-regressive intervals. GR=gamma ray, SP=spontaneous potential, ILD=deep induction (resistivity). Kld=Lower Cretaceous Dantzler Formation; K2lt“ms”=Upper Cretaceous Tuscaloosa Group, “Massive sand”; K2lt=Lower Tuscaloosa Formation; K2mt=Marine Tuscaloosa, “Marine shale”; K2ut=Upper Tuscaloosa Formation. SA=subaerial unconformity, TS/RS=transgressive surface/ravinement surface, SMT=surface of maximum transgression.

(Source: Mancini and Puckett, 2005)

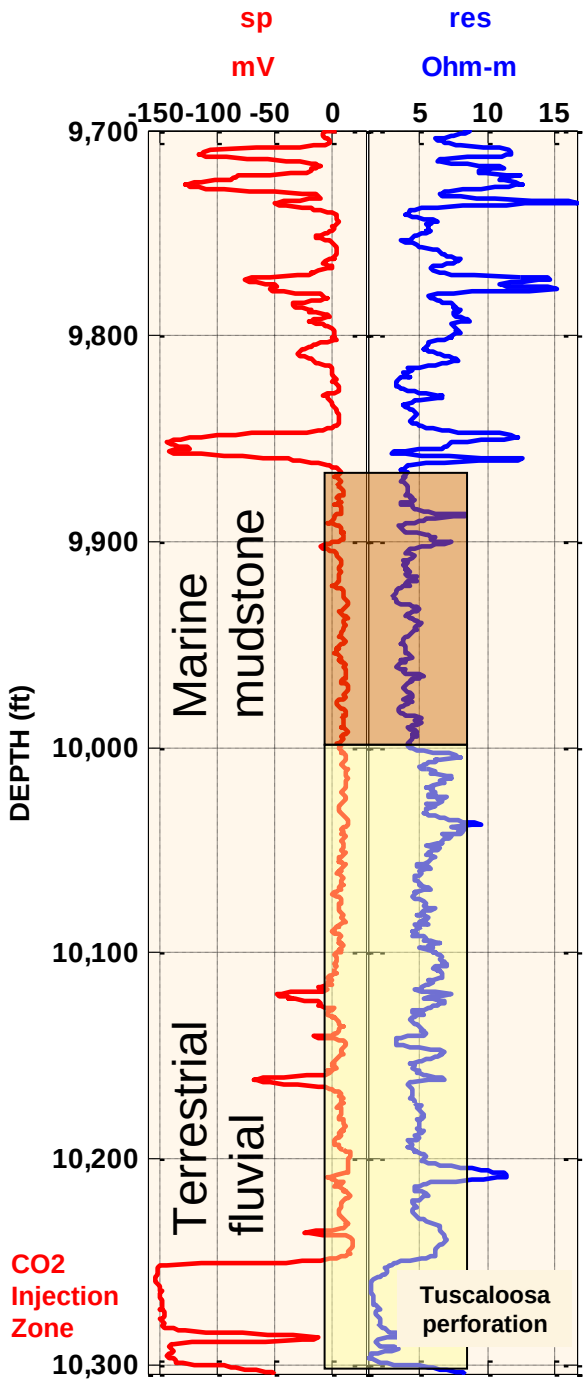

Figure 17. Type log in the study area showing the basal massive sands of the injection interval overlaid by more fluvial deposits including the local seal of the reservoir and a thick marine mudstone. A likely marine sand overlays the marine mudstone and is monitored at the site for pressure changes.

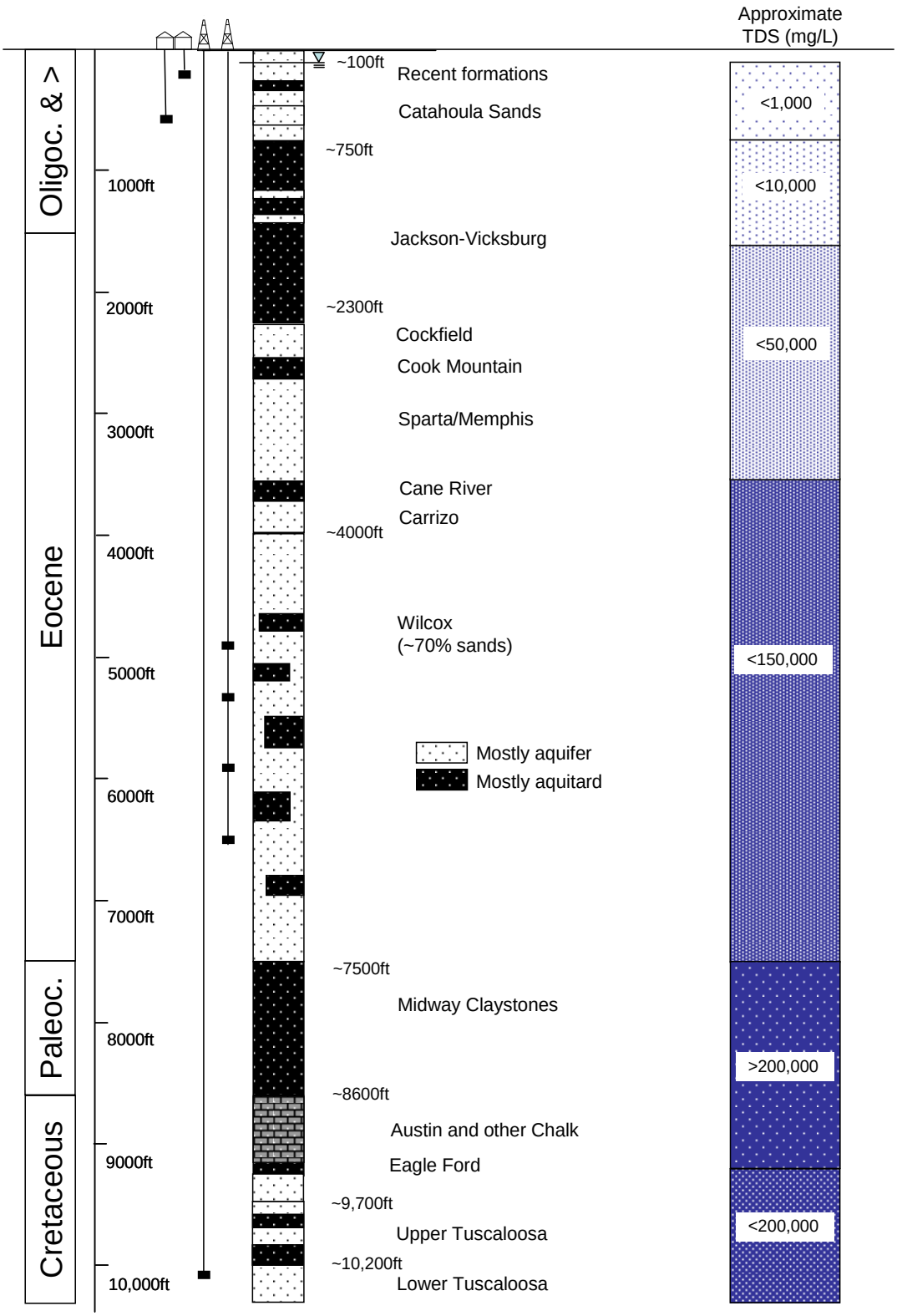

Figure 18. Simplified hydrostratigraphic column with water quality
(Source: Yang et al., 2009)

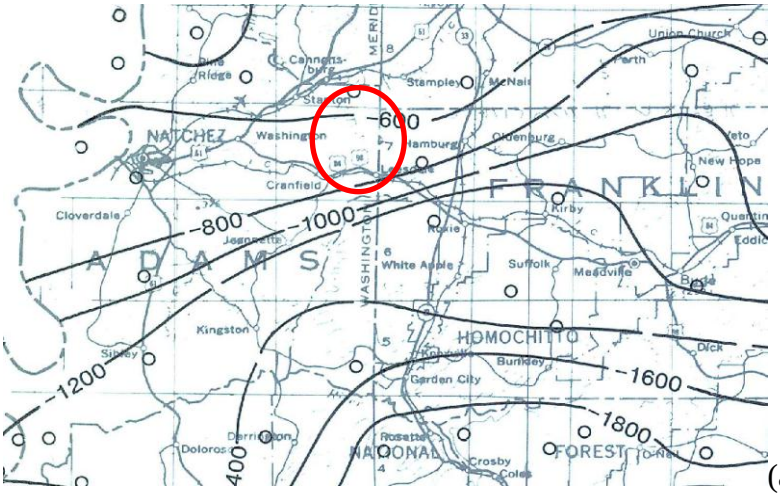

(a)

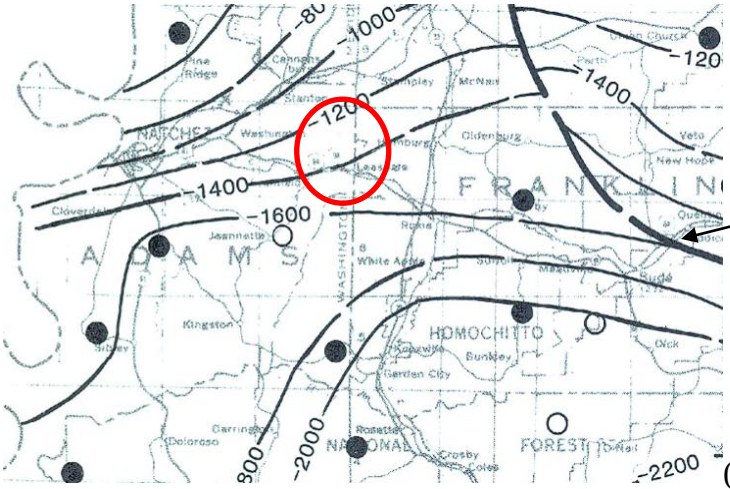

(b)

Miocene-Oligocene transition

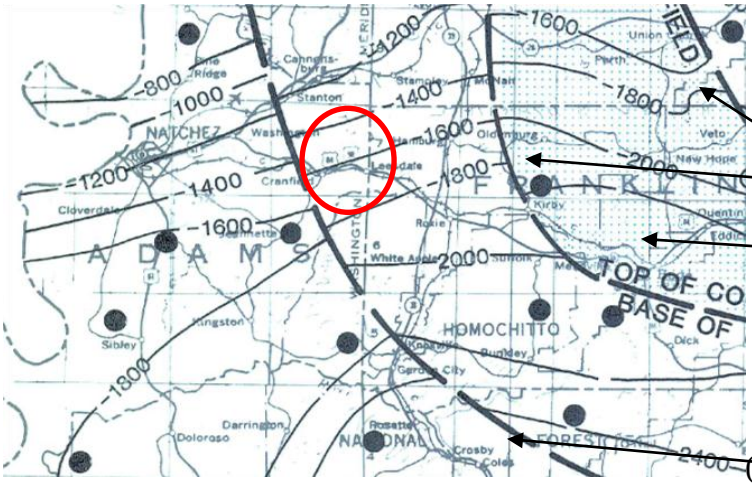

(c)

Oligocene-Cockfield transition

Stippled area: no 3,000 to 10,000 mg/L volume; direct transition from <3,000 mg/L to >10,000 mg/L

Miocene-Oligocene transition

Note: Oilfield location is denoted by red marker; dots represent data points (well logs)

Figure 19. Depth to the base of: (a) fresh water (<1,000 mg/L); (b) slightly brackish water (<3,000 mg/L); and brackish water (<10,000 mg/L)
(Source: Gandl, 1982, plates 1 to 3)

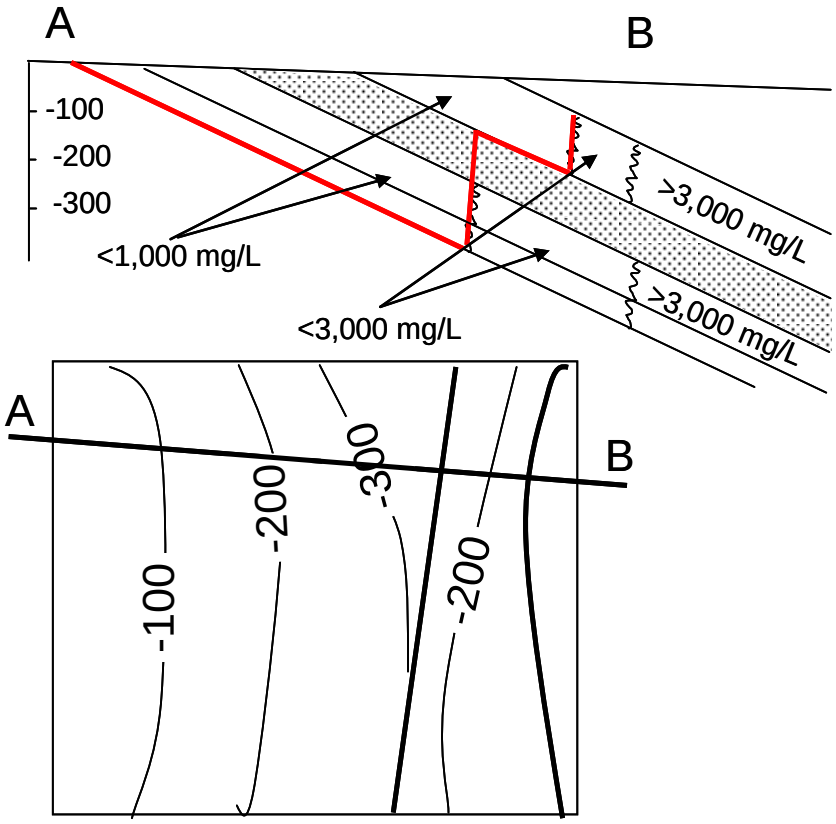

Figure 20. Cartoon demonstrating construction method of Figure 19.

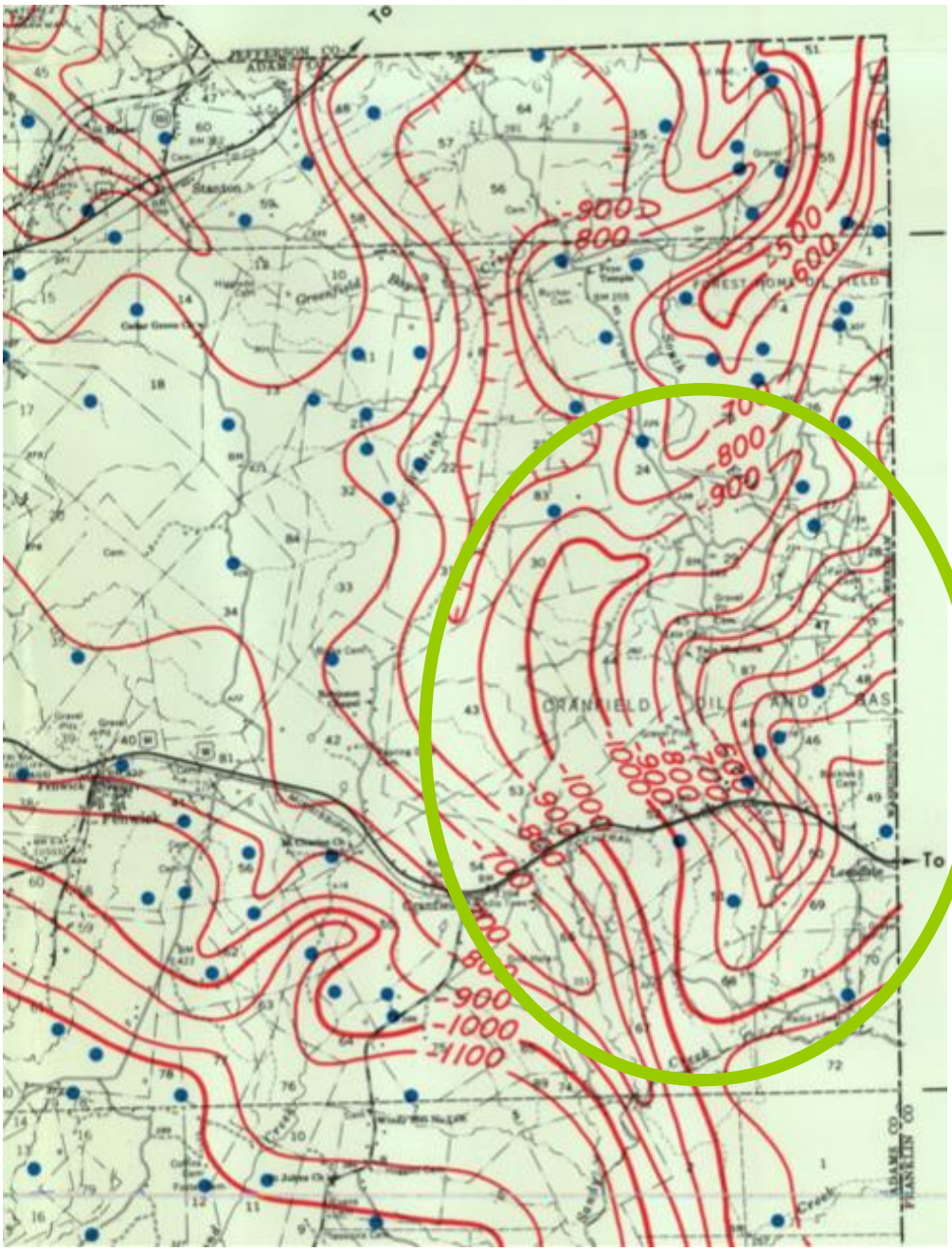

Figure 21. Base of the fresh water in Adams County
(Source: Marble (1976a))

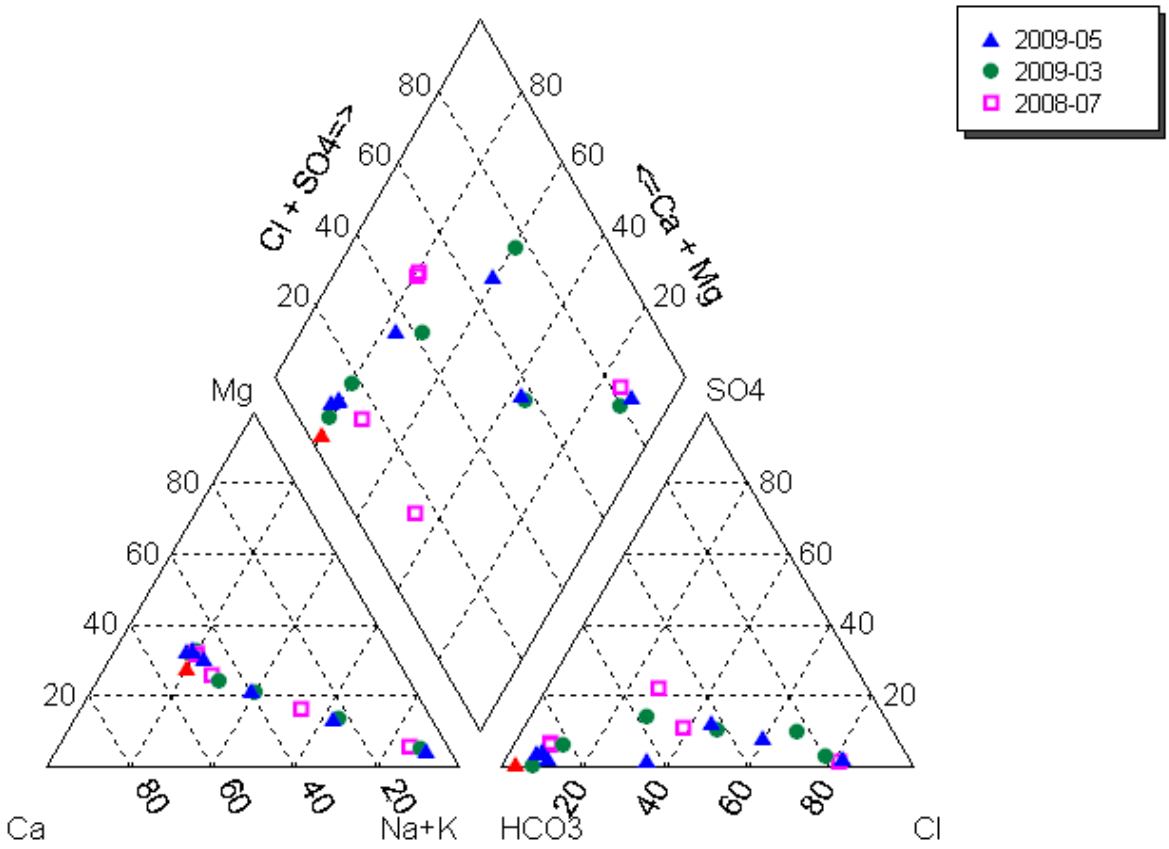

Figure 22. Piper plot of groundwater chemistry of the shallow aquifer at the site
(source: Yang, 2009, unpublished data)

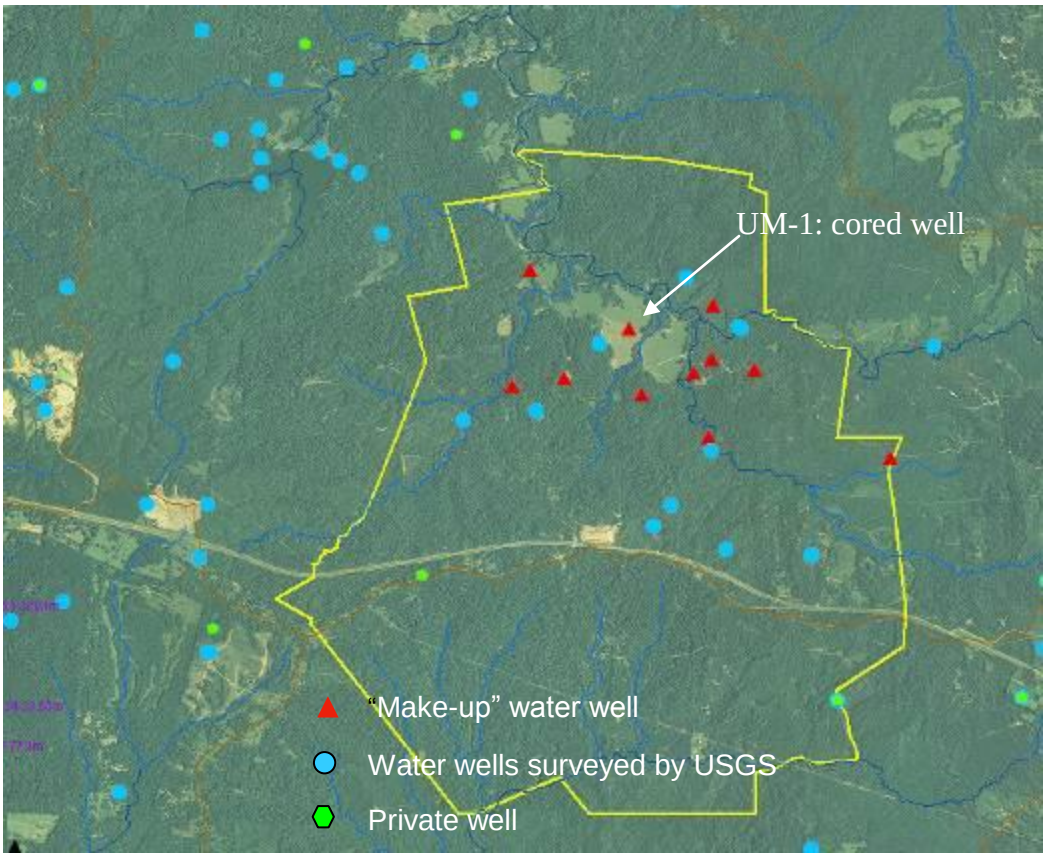

Figure 23. Location of known water wells.
(Source: Yang et al., 2009)

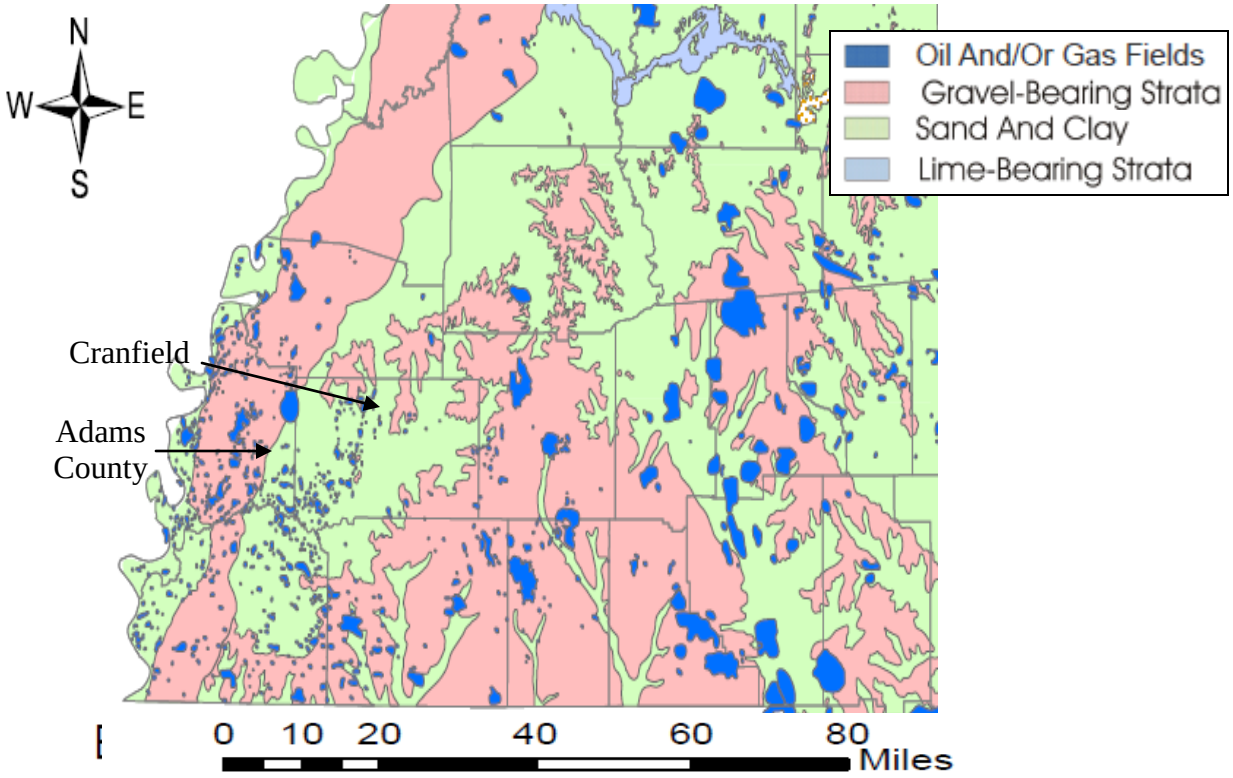

Figure 24. Map of mineral resources in the vicinity of the site
(Source: MDEQ (2009), MDEQ web site)

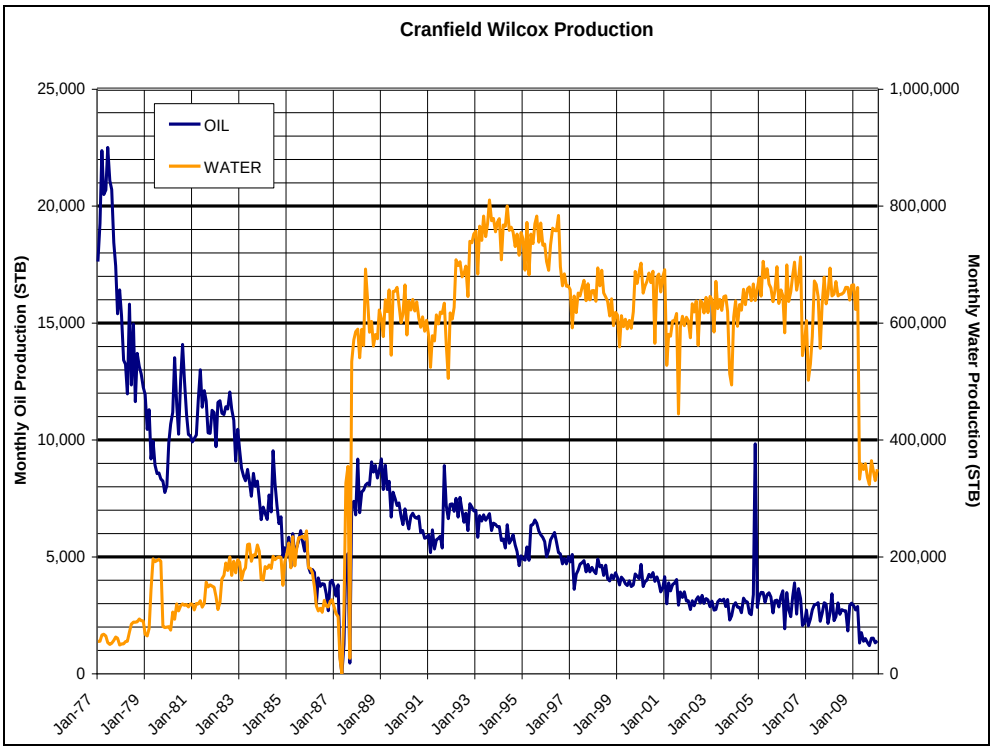

Figure 25. Monthly production data from the Wilcox formation at the site since 1977.
(Source: IHS)

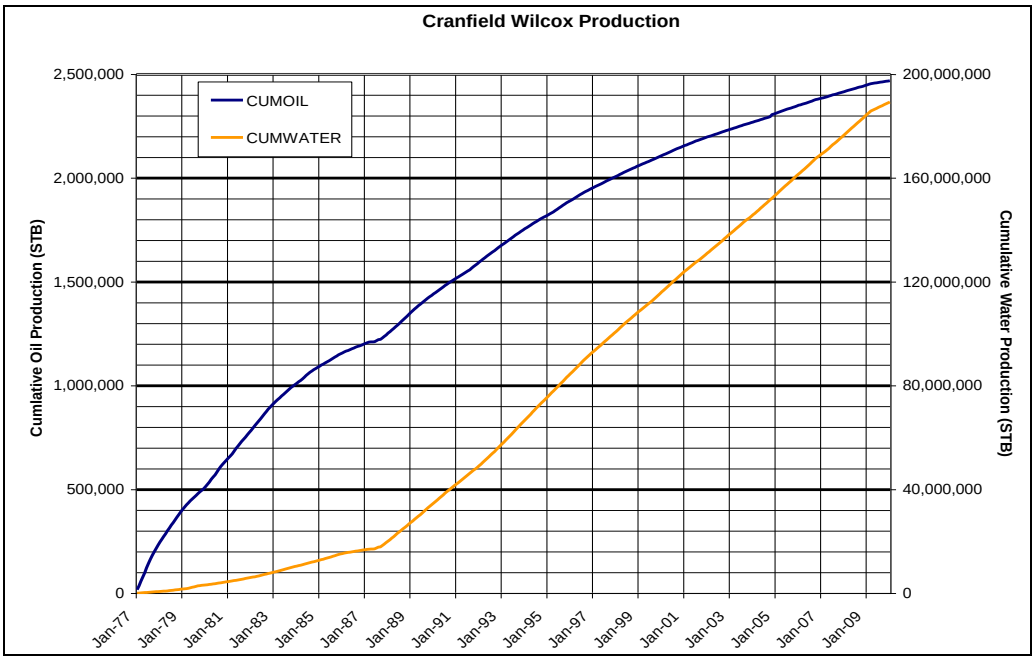

Figure 26. Cumulative production from the Wilcox formation since 1977 (oil and water) (Source: IHS)

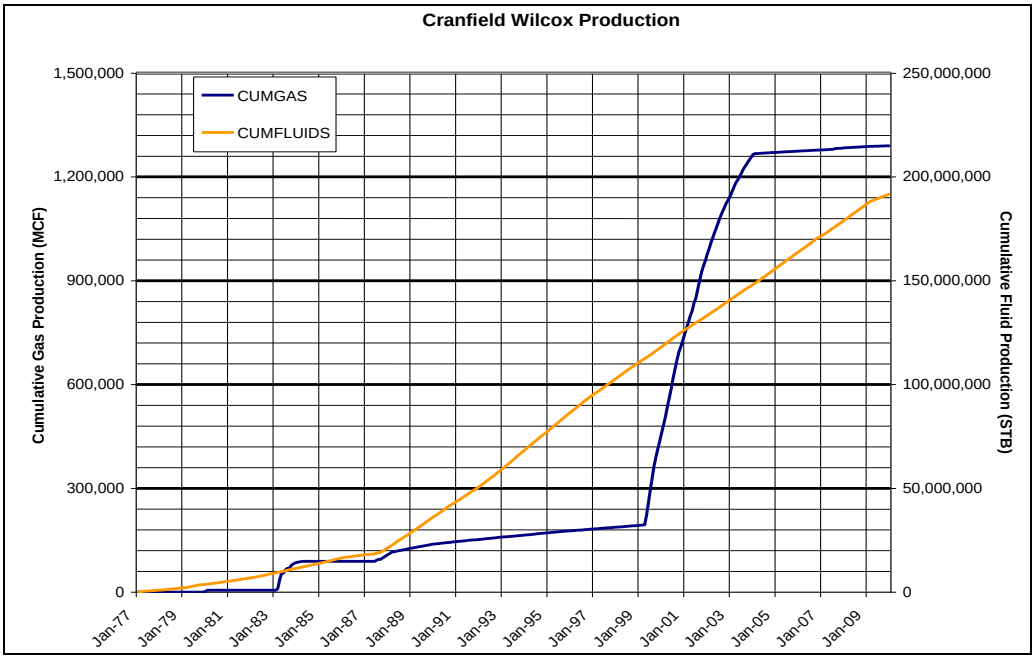

Note: oil and water are combined (total volume at surface conditions)

Figure 27. Cumulative production from the Wilcox formation since 1977 (gas and liquids) (Source: IHS)

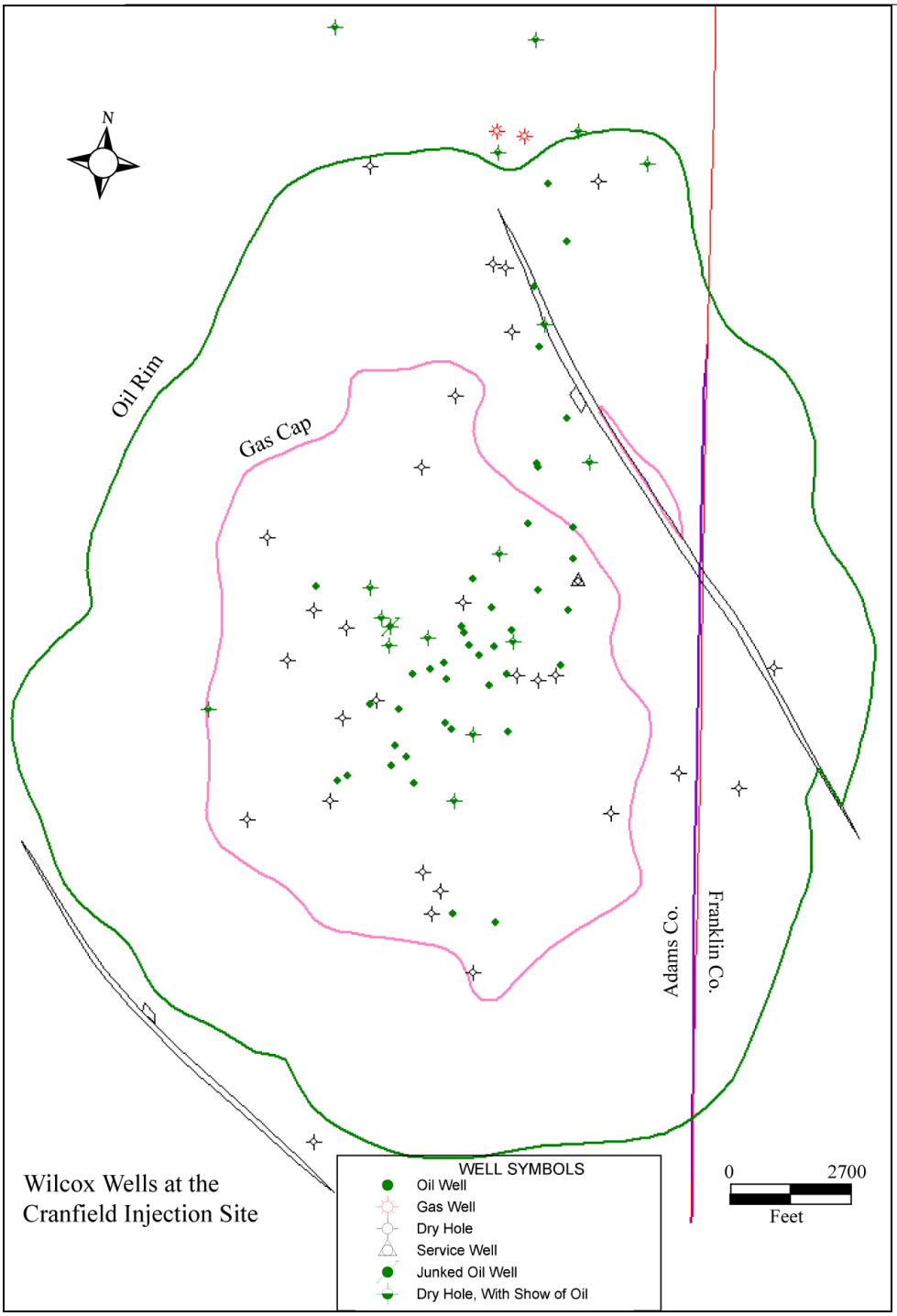

Note: oil rim and gas cap refer to production from the Tuscaloosa Fm., not the Wilcox Fm.

Figure 28. Location map showing wells drilled to the Wilcox Fm. at the injection site (Source: IHS)

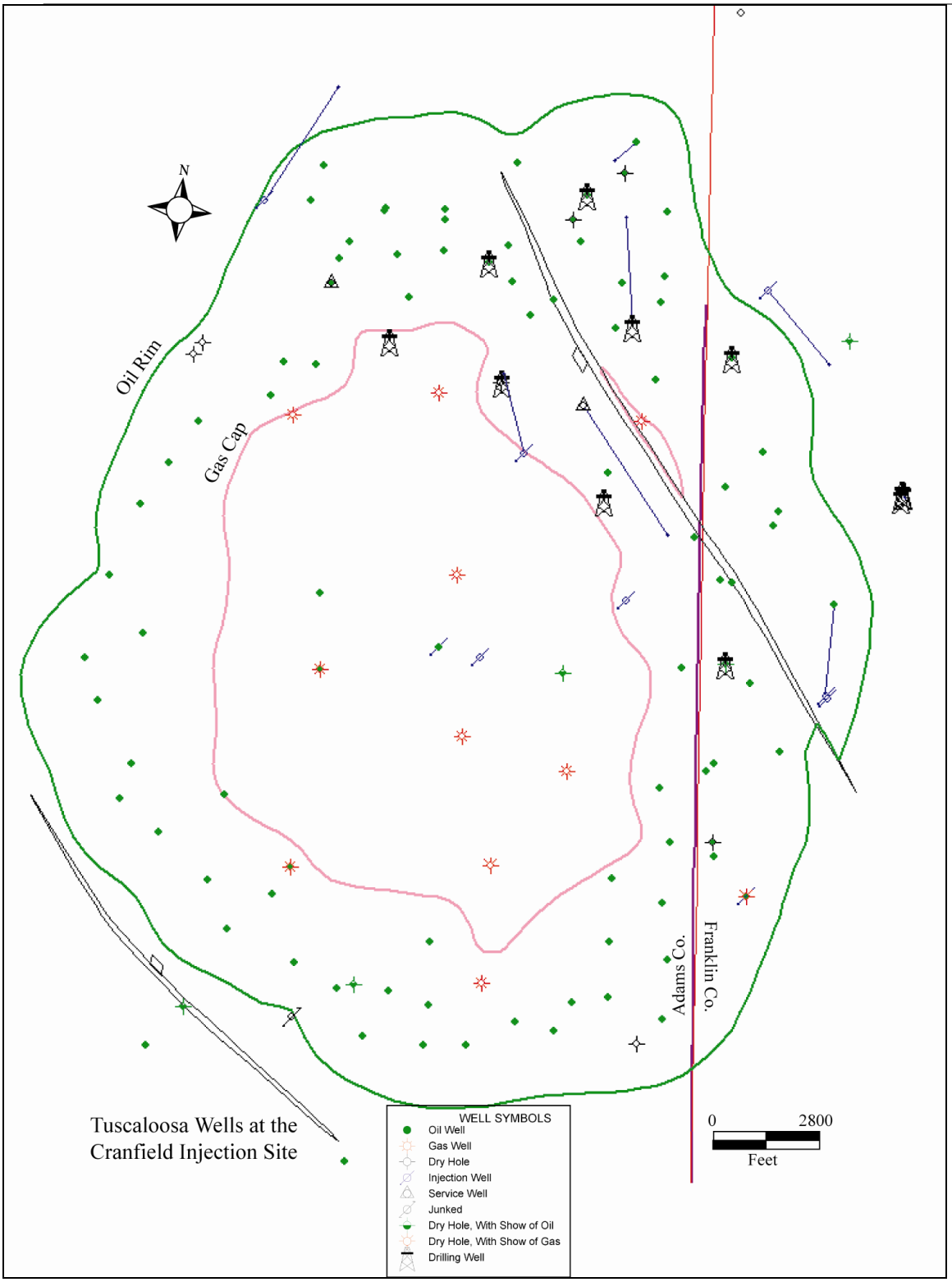

Note: because of the lag in acquiring data, map is current as of end of 2009.

Figure 29. Location map showing historical and recent wells drilled to the Tuscaloosa Fm. at the site.
(Source: IHS)

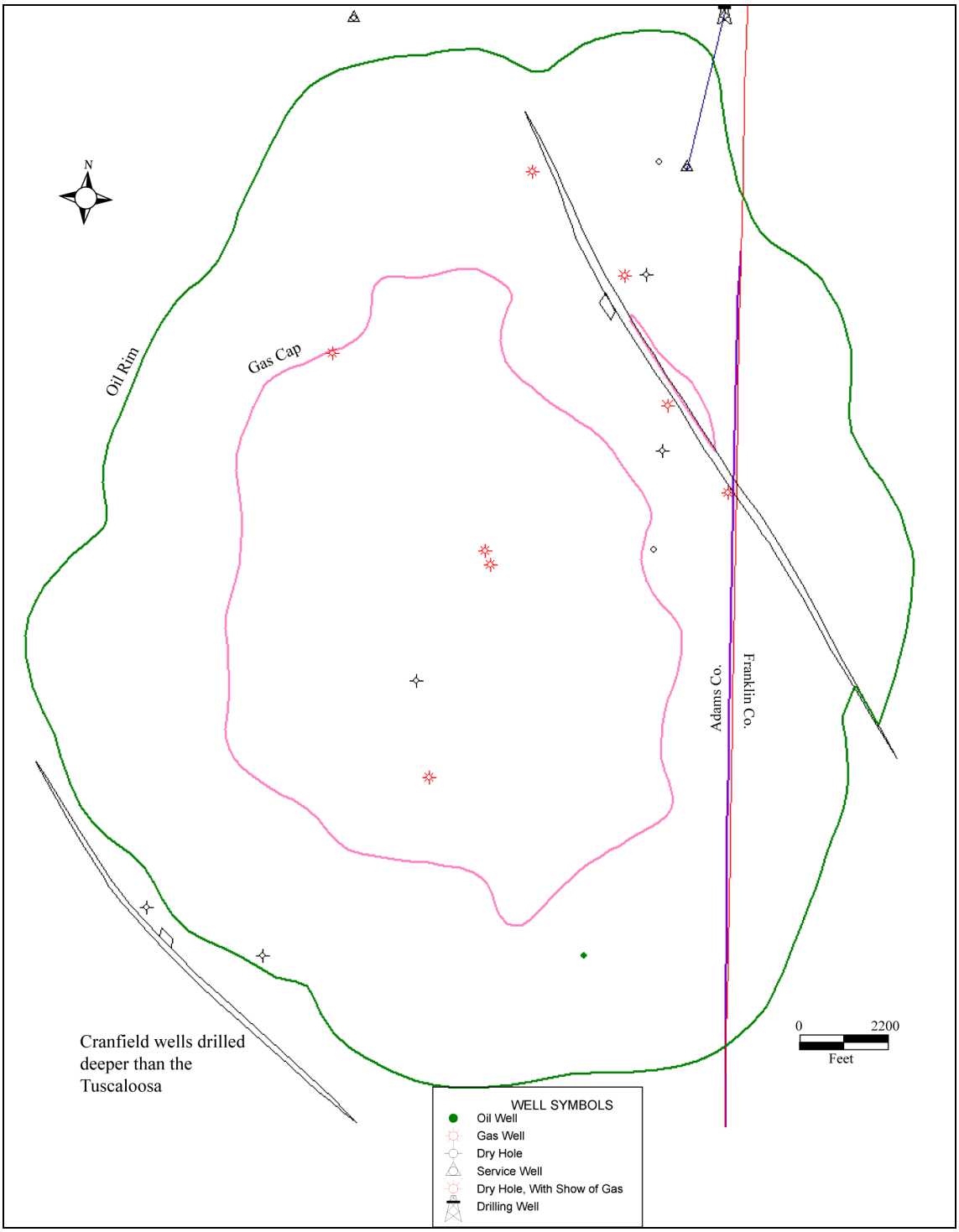

Note: oil rim and gas cap refer to production from the Tuscaloosa Fm. Most of these wells are drilled to lower Cretaceous strata, specifically the Paluxy Fm.

Figure 30. Location map showing wells drilled deeper than the Tuscaloosa Fm. (>11,000 ft) at the site
(Source: IHS)

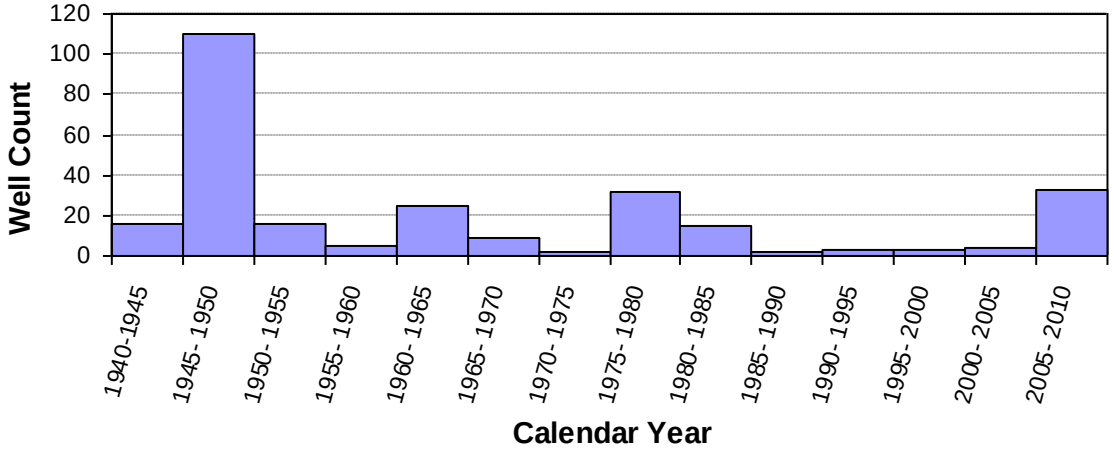

(a)

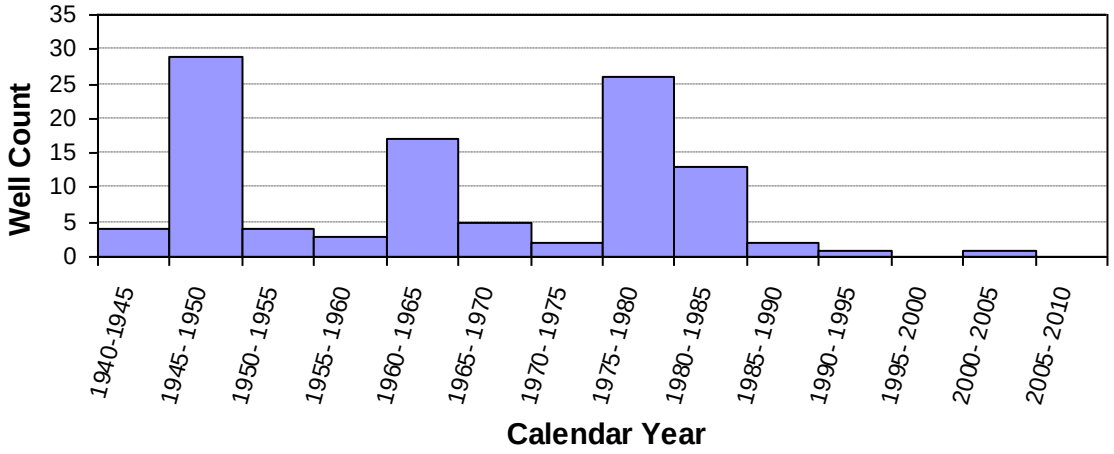

(b)

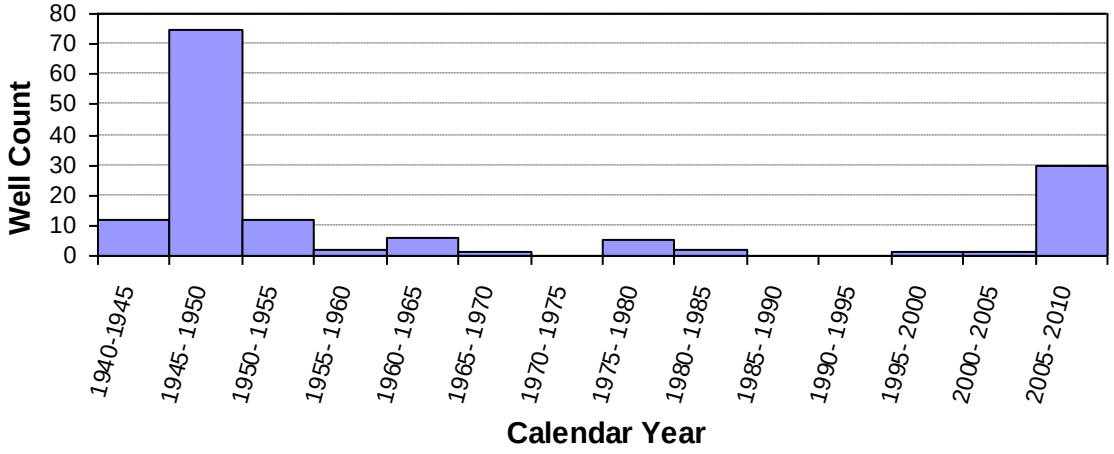

(c)

Figure 31. Annual well count for (a) all wells; (b) Wilcox wells; and (c) Tuscaloosa wells

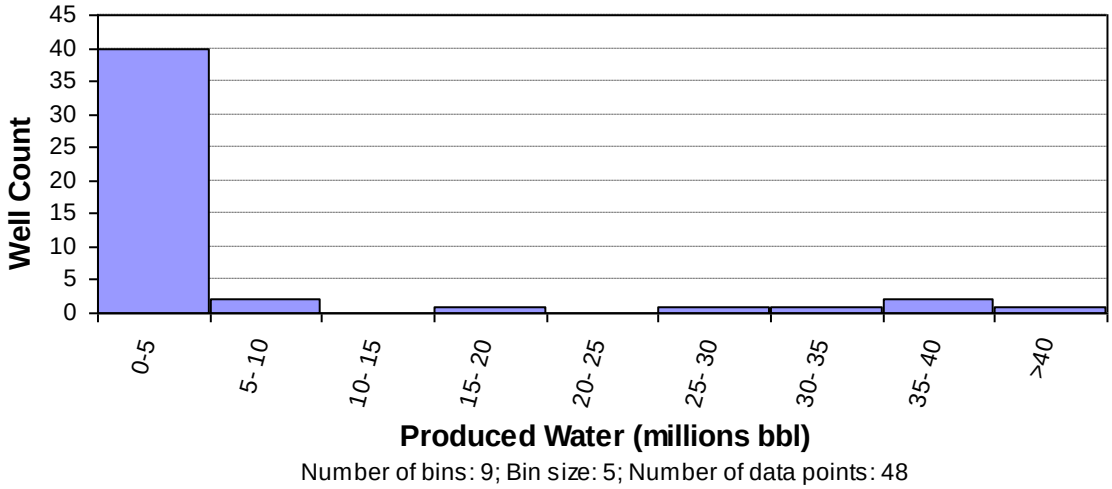

(a)

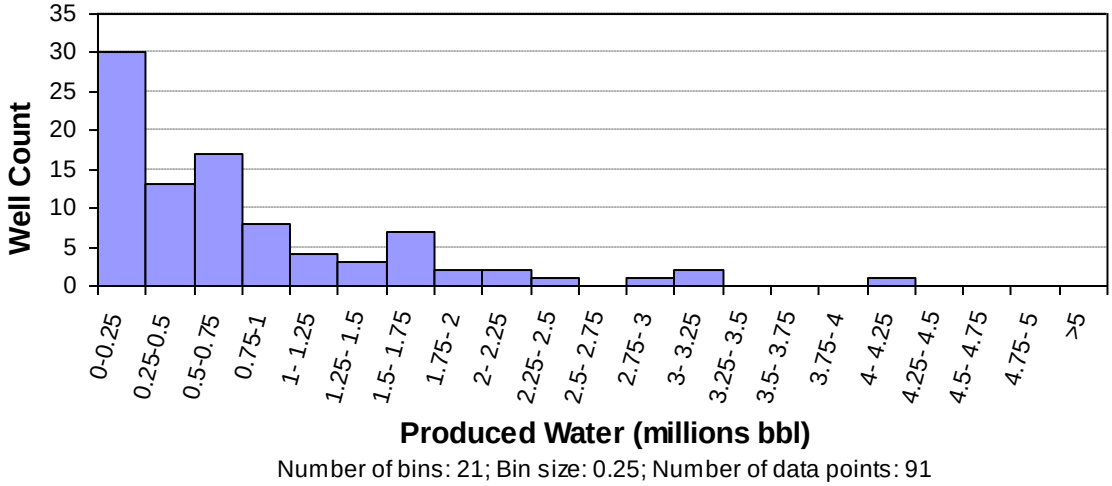

(b)

Figure 32. Produced water volume from the Tuscaloosa interval per well: (a) uncorrected and (b) corrected

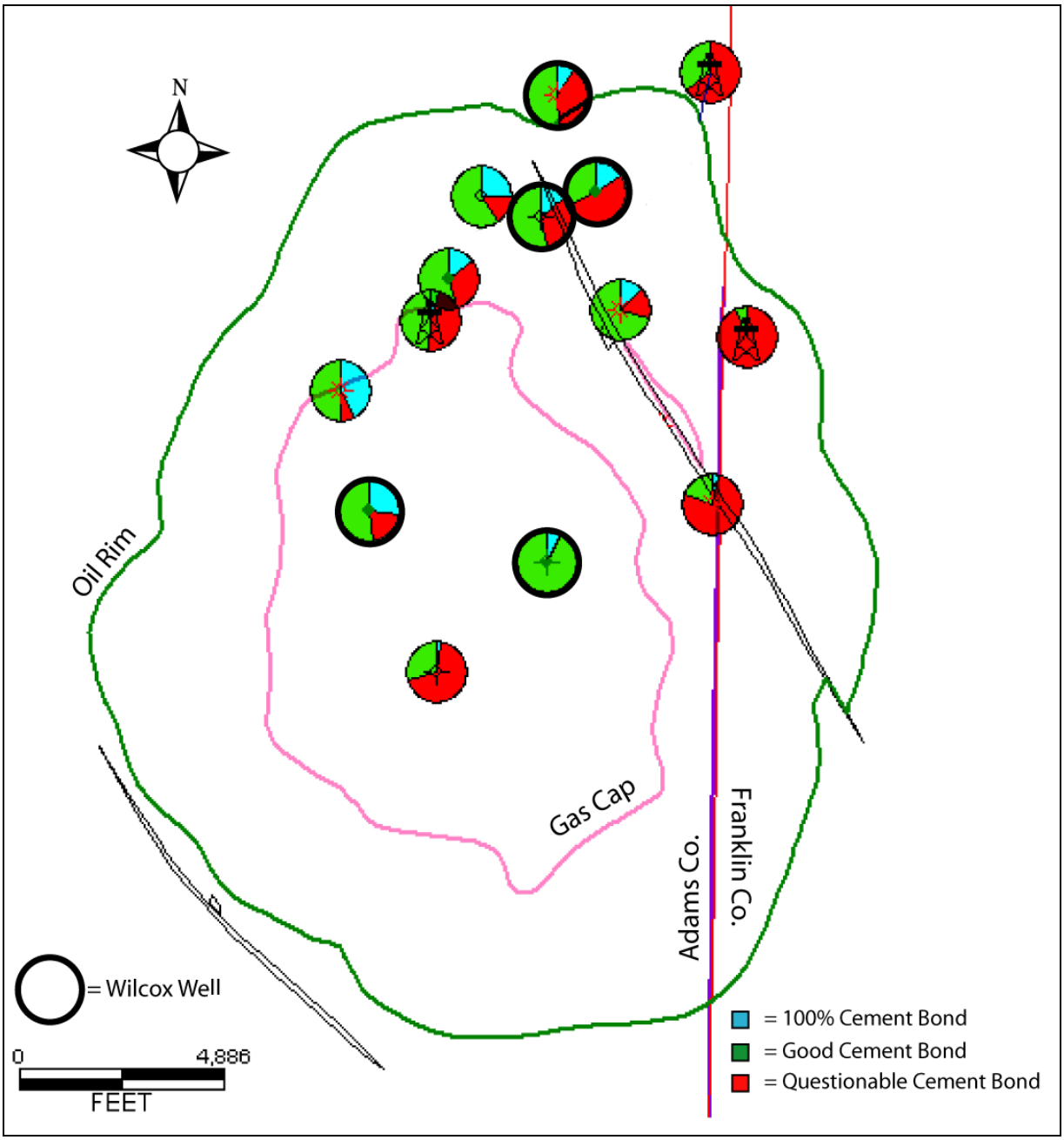

Note: The portion of each circle represents the percentage of cement that fits that defined classification. The map also shows the location and orientation of two faults associated with the oilfield.

Figure 33. Site map illustrating the location and quality of each CBL log
(Source: IHS and MOGB)

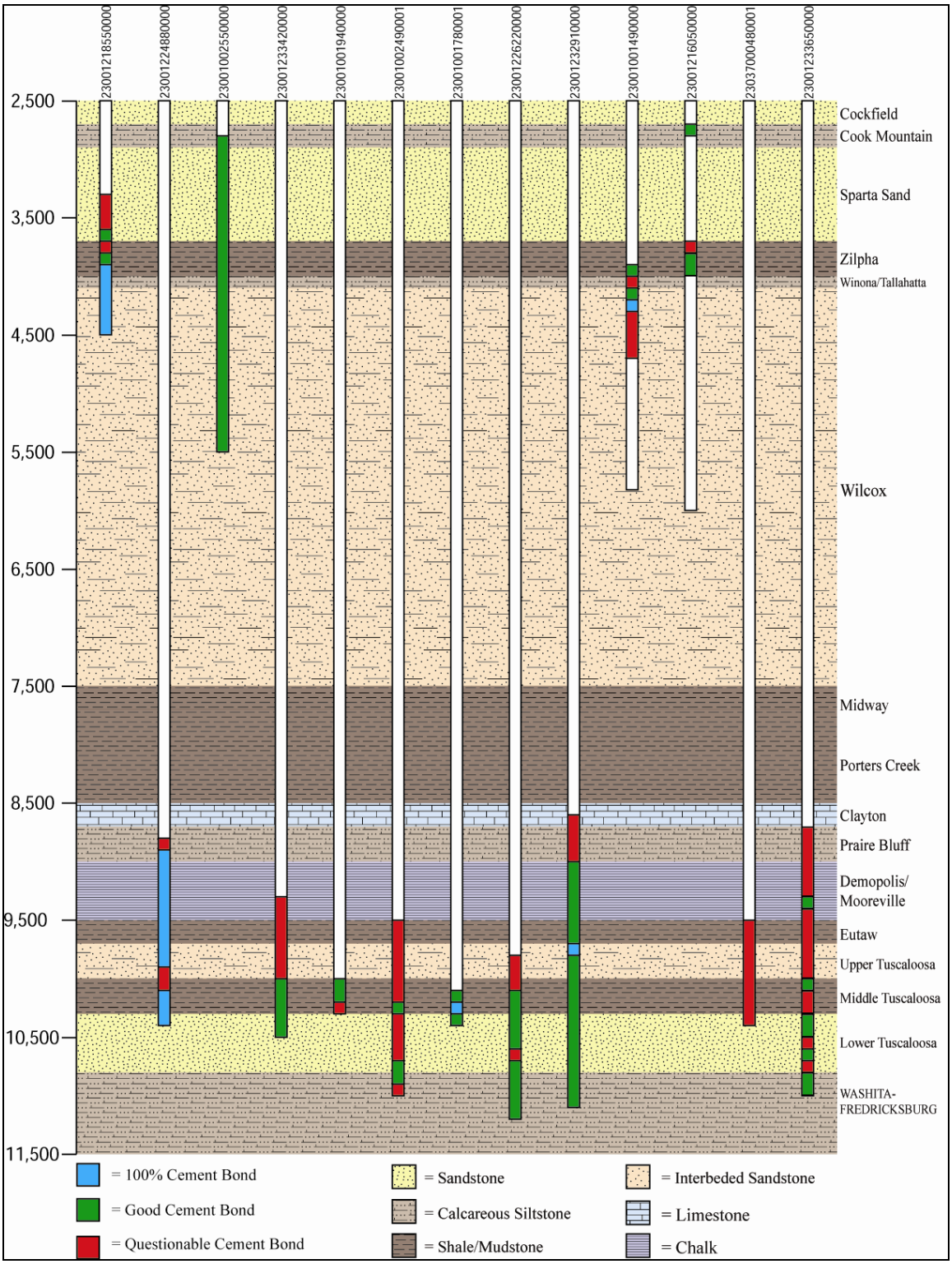

Note: Each well is labeled with their respective API number, but their spacing in this cross-section is not to scale. White sections represent lack of logs or unusable logs.

Figure 34. Cross-section illustrating cemented intervals of each well with a CBL log.

4 Reservoir Simulation

In order to assess the likelihood and consequences of CO_2 and brine leakage related to the SECARB Phase III project at the site, we have developed a numerical model of the injection process. The model domain includes only the portion of the northeastern part of the Tuscaloosa reservoir that is northeast of the fault (Figure 35) where CO_2 injection is currently in progress. The dip of the formation ranges from 1 to 3°. A fault divides the reservoir into two unequal parts.

The reservoir sandstones are petrophysically complex. Textures range from conglomerate to sandstone to mudstones, and lithological units have channel geometries incised into one another. Lateral and vertical continuity of rock types is low. Sandstones are cemented by variable amounts of authigenic chlorite, quartz and calcite. Chlorite cement is interpreted as preserving porosity, but is does not uniformly preserve permeability. The chlorite cementation adds complexity to the porosity and permeability fields that in some locations overwhelms the expected properties associated with the primary fluvial depositional system (Kordi, unpublished report; Lu, unpublished data).

Localized secondary porosity occurs due to quartz grain and carbonate cement dissolution. The average total thicknesses of the productive sand in the gas cap and in the oil zone are 63 ft (19 m) and 31 ft (9.4 m), respectively, although they vary across the field. Numerous discontinuous mudstone layers vertically compartmentalize the dominant sandstone lithology. All injection occurs in the "D" and "E" sandstones of the lower Tuscaloosa Formation.

Three-dimensional reservoir simulations of CO_2 injection and migration were carried out using CMG-GEM, a commercial multiphase compositional flow simulator. It predicts the volumetric behavior and the phase equilibrium composition of pure components or mixtures as well as their properties such as densities and viscosities. A common usage of the simulator for injection of CO_2 into brine aquifers is to handle the aqueous phase as a water-rich oil phase (and not include the water phase) to take advantage of the compositional features that are available only between the oil and gas phases. However, for the simulations carried out for this study water is treated as an individual aqueous phase and not as a component because both oil and gas phases are also present, so that the three phases coexist in the reservoir. As a consequence, partitioning of water into the other phases and of the other phase components into the aqueous phase cannot be modeled. It follows that CO_2 dissolution into the oil phase is modeled but not dissolution into the aqueous phase. Other limitations include the fact that we ignore heat transfer into and from the reservoir and that our model is an isothermal system (at 257°F (125°C)). It follows that the impact of temperature contrast and potential thermally-induced fractures are not modeled. This issue has not received wide-spread attention yet but Luo and Bryant (2010) suggested that the deeper the injection formation, the less relevant this process is. Chemical reaction with minerals of the reservoir rock matrix are not accounted for, either, since the timescale of our model is in the order of decade, whereas that for mineral trapping can be on the order of thousands of years.

We model a period of five years at which time the system has reached a quasi-steady state in terms of pressure because of the continuous CO_2 injection balancing the oil production.

Previous work shows that the oil composition has not varied since that in the historical production period (1945–1965) reported in 1960's (MOGB, 1966). Consequently, we used the

known oil composition. We chose the Peng-Robinson model for EOS. The PVT data of C2+ oil components was that internally available within CMG whereas PVT data for CO_2 and CH_4 were independently tuned for reservoir temperature of 125°C (257°F) and reservoir pressure of 32 Mpa (4,700 psi). Formation water is very saline with a TDS >150,000 mg/L and a specific gravity of ~1.1.

4.1 Storage Reservoir

4.1.1 Static Model and Flow Parameters

The static model was created based on both seismic data and well logs using the Petrel software (Schlumberger). Maximum and minimum elevations are 9,743 ft (2,970 m) and 10,433 ft (3,180 m), respectively. As the down dip section of the model is not covered by either seismic data or wells, we assume a constant dip equal to the average of that in the domain where data are available. The average dip is 2° in an approximately radial fashion away from the apex of the anticline structure. Cell size is 200 ft× 200 ft× 8 ft. The dimensions of the flow model are 20,000 ft × 20,000 ft × 80 ft, and it consists of a total of 100,000 (= 100×100×10) cells (Figure 36). It was obtained by upscaling a 50 ft× 50 ft× 1 ft Petrel grid. We used a much finer resolution in the vertical direction because of the relative abundance of data. Data from forty-five wells (logs and cores) were used as control points (Table 4). They include a mix of older and recent wells and well logs of different quality, but are located within the domain or close to it.

In order to consider the lack of permeability data in inter well areas in the horizontal direction and the difficulty to uniquely correlating rock units at an inter well scale given the fluvial stratigraphic architecture, we generated five realizations of the permeability and porosity fields using the sequential Gaussian simulation (SGS) tool within Petrel. The well data were always honored and the geostatistical parameters used are listed in Table 5. The porosity and permeability sampling were done assuming a set mean and standard deviation computed from selected wells across the field that were believed to provide good quality data and not from mean and standard deviation of the 45-well data set

The vertical range of the spherical variogram was computed from a selected set of wells but with a bigger weight from the three wells of the DAS area where the porosity and permeability are constrained by measurements on core plugs. The horizontal correlation ranges were estimated from interpreted stratal slices of seismic data (Hongliu Zheng, unpublished document) and our interpretation of depositional units based on core interpretation and outcrop analogs. The nugget was set at 0.14 to minimize the smoothing effect of upscaling and still keep some of the stratigraphic fabric. See Figure 37 and Figure 38 for example heterogeneous permeability fields.

Porosity was upscaled using simple arithmetic averaging of porosity values from the fine grid. Permeability upscaling was based on directional methods using harmonic-arithmetic average to generate k_x, k_y, and k_z. Note that the upscaled field is anisotropic even if the original field was not. The stochastically generated fields do include the domain west of the field but the information is not used in the final model.

We used only one rock type and a single set of relative permeability curves (Figure 39 and Table 6). They assume a Brooks-Corey formalism. The model is always in the drainage mode, never in

the imbibition mode as injection never stops. From MOGB (1966), water residual saturation is estimated at 0.4. Oil and gas relative permeability at residual water saturation were set at 0.65 and 0.8, respectively. A value of 0.2 is used for the oil and gas residual saturations. Water relative permeability was set at 0.5 at residual oil and gas saturation.

4.1.2 Boundary and Initial Conditions

The top and bottom boundary of the model are assumed no-flow and the injection formation is vertically bounded by low-permeability layers. The fault on the western side of the model domain is sealing and the boundary is also modeled as a no-flow boundary. The boundary on the eastern side of the domain is an open boundary with constant pressure set at hydrostatic to model an infinite-acting system. The shut-in period pressure behavior shows that there is a strong water drive and good communication with the saline aquifer as observed in the inter production period for the field. The boundary was put far from the wells and reservoir to limit its impacts on the results. Both side boundaries are also no-flow mostly for convenience. Previous work has showed that when there is a relatively balanced mix of injectors and producers, those boundaries do not matter as much, particularly since one side of the domain is open.

Initial conditions are assumed hydrostatic with no CO_2 in the system. Initial pressure at 9,976 ft (3,040 m) subsea is 4,701 psi (32 Mpa). After a short transient of a few years, the model is at numerical equilibrium and injection can start. Oil is set at residual saturation (~20%) in the reservoir domain.

4.1.3 Injection Schedule

Injection wells followed a simplified version of the field injection rates for the historical period (<2 years, exact length depends on when the well was put on line), while future injection rates are extrapolated from some measure of the previous months' activity (Figure 40). Production starts at individual production wells when the CO_2-rich oil can self-lift to the surface. Well CFU 31F-1 in the DAS area has the highest injection rate. The rate is not intended to stay continuously high but may undergo periodic boosts to test injectivity as was done during the spring/summer 2010 period. Over the whole HiVIT area (east of the fault), the total flow rate is approximately 1 million metric tonnes per year (Figure 41).

4.2 Modeling Results

We assumed results of the different realizations were acceptable when total fluid production approximately matched past Denbury production (not shown). In this results section, we focus attention on P&A wells because this is where potential leakage could occur (leakage could also occur at producers, however during production the pressure is lowered at these wells). There are seven known P&A wells in the domain (Figure 42). Maximum pressure results are listed on Table 8 and collected in Table 9. They represent pressures generated in hypothetical permeability fields but excess pressure values are mostly consistent across the different realizations and mostly below 1,000 psi (6.8 Mpa) (Figure 43). Wells Cranfield Unit 4 and H. H. Crosby et al. 1 are just below and above 1,500 psi (10 Mpa), respectively. Well Cranfield Unit 4 has been very recently reentered and upgraded by the operator and is thus considered actively managed, in good condition, and unlikely to lead to significant leakage. Pressure at H. H. Crosby et al. 1 has not reached its maximum yet at the end of the simulation because the injected CO_2 plume from nearby injectors (CFU 28-1 and 28F-1) still propagates towards it. However, well H. H. Crosby et al. 1 is located close to the (closed) northern boundary, artificially increasing its pressure

compared to the other P&A wells. Well Cranfield Unit 7 is anomalous in the sense that it has large pressure swings, including the highest excess pressure at 2,500 psi. This was the result of one realization in which the nearby injector was forced to accept a proscribed rate into a low permeability cell. Time for the excess pressure to peak is also variable and maximum excess pressures are not sustained for very long. Production wells are allowed to produce as soon as the oil-CO_2 mixture is self-lifting and able to reach the nearby processing facility without additional pumping, decreasing or at least stabilizing the bottom-hole pressure in the process. Appendix C shows the five pressure histories for each of the 7 P&A wells. A reasonable excess pressure range can then be estimated to lie between 400 and 1,500 psi.

CO_2 breakthrough is defined by the time at which its mole fraction in the gas phase is above background (1.84% naturally in the oil). In the model, as soon as CO_2 contacts oil in a cell, there is only one phase (which happens to be labeled gas) because of the assumed full miscibility between CO_2 and oil. The mole fraction of CO_2 then rises more or less quickly (Figure 44,Table 10 and Table 11). In the course of the 5 years considered in this study, some well/realization couples are still seeing the oil bank go by with a CO_2 mole fraction well below 1 (realization #1 of Cranfield Unit 7). Others have already produced all the oil within their domain of capture and the CO_2/oil miscible gas phase is ~100% CO_2 (realization #1 of Vernon Johnson 1). Others still are not contacted by CO_2 (as displayed in Figure 45 and in realizations #1 and #2 for well H H CROSBY ETAL 1). Appendix D shows the five gas saturation and oil and gas mole fraction histories for each of the 7 P&A wells. Breakthrough time varies from less that a month to beyond the time of interest (>5 years).

Table 4. Wells used to generate the static model

Name	UWI	Well Type	Surface X	Surface Y	KB	TD (TVDSS)	TD (MD)
ARMSTRONG_2	23001001510000	Oil	241468.9	394325.4	248	10061	10309
ARMSTRONG_4	23001001530000	Oil	240039.9	395194.8	264	10100	10364
29-9 (CRAN_2)	23001001590000	Oil	240462.9	391455.5	258	10053	10311
CRANFIELD_UN_4	23001001620000	Oil	243159.9	390169.1	299	10052	10351
29-3 (CRAN_UN_10)	23001001670000	Oil	240150.4	394168.1	245	10040	10285
24-3 (CRANFIELD_UN_13)	23001001720000	Oil	235555	393559.5	290	10062	10352
29-5 (CRAN_UN_14)	23001001730000	Oil	236590.6	394169.9	271	10060	10331
29-1 (CRAN_UN_17)	23001001760000	Oil	237516.7	395126.8	236	10078	10314
29-2 (CRAN_UN_21)	23001001780000	Inj. gas	238871.5	394723.5	241	10091	10332
CRAN_UN_23 (see 27-5 #2)	23001001800001	Oil	242551.3	395372.1	266	10123	10389
VERNON_JOHNSON_1	23001001890000	Oil	242393.4	392612.2	254	10060	10314
28-2 (VERNON_JOHNSON_2)	23001001900000	Oil	243423.1	392448	279	10060	10339
VERNON_JOHNSON_4	23001001910000	Oil	242562.3	391472.3	276	10060	10336
29-11 (EGL3) conv prod	23001001940000	Inj. gas	237588.9	391954.1	302	10056	10358
ELLA_G_LEES_4	23001001950000	Oil	237597.4	393059.9	271	10059	10330
29-10 (EGL5)	23001001960000	Inj. gas	236099.9	392340.3	278	10037	10315
29-6 (EGL6)	23001001980000	Oil	238632.7	392830	276	10047	10323
BEG (EGL7)	23001001990000	Well impact	239675.8	393200.4	248	10057	10305
29-4 (EGL_8)	23001002000000	Inj. gas	241261.7	393275.6	245	10060	10305
ELLA_G_LEES_10	23001002020000	Oil	236626.9	393227.5	273	10060	10333
ELLA_G_LEES_11	23001002030000	Oil	238595.7	393685.2	247	10060	10307
29-7 (EGL_17)	23001002090000	Inj. gas	240057.3	392586.3	253	10061	10314
ELLA_G_LEES_19	23001002110000	Oil	237471.6	394123.1	244	10063	10307
ELLA_G_LEES_20	23001002120000	Oil	241159.2	392083.2	250	10060	10310
R_G_CALCOTE_1	23001015540000	Oil	243253.6	394341	249	10056	10305
CRANFIELD_UN_31	23001032440000	Gas	238458.2	389975.7	280	10081	10361
27-3 (Armstrong 1)	23001033940000	Oil	242495.2	394128.4	246	10061	10307
29-13 (BLAN-ED_2)	23001225630000	Oil	239951.1	390098.9	354	10096	10450
29-12	23001333420000	Inj. gas	237464	391060	357	10165	10522
24-2		Inj. gas s	236264.72	395566	239.9	10304	10930
48-1		Inj. gas	241812.1	389834.8	285	10427	10712
26-1		Inj. gas	242561.74	393685.21	252	10290	11667
28-1		Inj. gas	242557.93	393670.74	252	10229	10671
27-4 (VERNON_JOHNSON_1)	23001232910000	Inj. gas	242189.8	390813.1	285	11375	11660
ELLA_G_LEES_17	23037003390000	Inj. gas	244881.5	386318.3	289	10096	10385

Name	UWI	Well Type	Surface X	Surface Y	KB	TD (TVDSS)	TD (MD)
31F-1 [P3 INJ]		Inj. gas	248372	387675	333.7	10312	10647
31F-2 [OBS #1]		Obser,	248572	387675	333.5	10180	10514
28F-1		Inj. gas	246264	392109	0	10500	10500
48-2 GMT OBS (Blan Ed #3)		Well impact	242785.35	388510.17	271.8	11728	12000
27-5 #2		Oil	242723.7	394879.4	266	10234	10551
28-2 #2		Oil	243388.1	391813.5	284	10234	10518
48-3 (#2) GMT INJ		Inj. gas	242089.39	387563.61	313.8	10286	10600
31F-3 (OBS #2)		Obser,	248670.4	387671.6	333.2	10458	10792
28F-3		Inj. gas	246881	390456.2	310.7	10299	10610

Table 5. Geostatistical parameter used to generate flow parameter fields

Parameter	
Mean porosity and standard deviation	19.88 and 7.26
Mean logk and standard deviation (k in md)	0.65 and 1.47
Logk variogram model	spherical
Logk variogram nugget	1.4
Vertical range of logk variogram	14 ft
Lateral NS range of logk variogram	1,000 ft
Lateral EW range of logk variogram	200 ft
Nugget	0.14

Table 6. Flow parameters for the reservoir rock in the model

Parameter	**Value**
Brooks-Corey lambda (pore size distrib. index)	2.0
Water/Oil Rel. Perm. Curve	
Water residual saturation	0.4
Oil rel. perm. end point at residual water	0.65
Oil residual saturation	0.2
Water rel. perm. end point at residual oil	0.5
Liquid/Gas Rel. Perm. Curve	
Minimum residual fluid (water)	See "Water residual saturation"
Gas rel. perm. end point at min. residual fluid	0.8
Fluid rel. perm. end point	See "Oil rel. perm. end point at res. water"

Table 7. Location of P&A wells (East of fault)

	MS Field Coordinate		**Model Cell Coordinate**	
Well name	**x.**	**y**	**i**	**j**
Origin of Model	*238000.0*	*402000.0*		
Cranfield Unit 7	245910.4	386859.9	40	76
Cranfield Unit 4	243159.9	390169.1	26	60
Vernon Johnson 1	242393.4	392612.2	22	47
Vernon Johnson 1	242189.8	390813.1	21	56
Armstrong 4	240039.9	395194.8	11	35
Armstrong 2	241468.9	394325.4	18	39
R G CALCOTE 1	243253.6	394341.0	27	39
H H CROSBY ETAL 1	244399.3	397220.1	32	24

Table 8. Pressure (psi) at P&A wells

Well name	Cranfield Unit 7	Cranfield Unit 4	Vernon Johnson 1	Armstrong 4	Armstrong 2	R G CALCOTE 1	H H CROSBY ETAL 1
(i, j)	40, 76	26, 60	22, 47	11, 35	18,39	27, 39	32,24
Realization 1							
Initial p	4648	4659	4674	4713	4680	4695	4704
Max p	6091	5553	5358	5102	4987	5071	5811
Δp	1443	894	684	389	307	376	1107
Layer	10	10	10	10	10	10	10
Date	9/1/2013	12/1/2010	3/24/2010	2/1/2011	11/28/2008	1/1/2011	12/1/2013
Realization 2							
Initial p	4648	4660	4676	4675	4682	4696	4705
Max p	5672	6408	5914	4742	5236	5480	5922
Δp	1024	1748	1238	67	554	784	1217
Layer	10	10	10	10	10	10	10
Date	6/1/2013	2/1/2011	11/1/2010	12/1/2013	12/1/2010	9/1/2011	12/1/2013
Realization 3							
Initial p	4648	4656	4673	4710	4679	4694	4701
Max p	5140	6359	5531	5232	5165	5585	6201
Δp	492	1703	858	522	486	891	1500
Layer	2	10	10	10	10	10	10
Date	9/1/2012	5/1/2011	4/1/2011	2/1/2013	7/1/2011	9/1/2011	10/1/2011
Realization 4							
Initial p	4648	4658	4671	4704	4678	4694	4702
Max p	5609	6447	5995	5580	5715	5869	6133
Δp	961	1789	1324	876	1037	1175	1431
Layer	10	10	10	10	10	10	1/10/1900
Date	4/1/2011	3/1/2011	2/1/2011	5/1/2012	5/1/2011	1/1/2012	4/1/2012
Realization 5							
Initial p	4626	4663	4677	4707	4685	4699	4707
Max p	7284	6625	5594	5269	5312	5126	6186
Δp	2658	1962	917	562	627	427	1479
Layer	4	10	10	10	10	10	10
Date	12/1/2012	5/1/2011	5/1/2011	1/1/2012	11/1/2011	4/1/2012	12/1/2013

Table 9. Excess pressure (psi) at P&A wells

Well name	Cranfield Unit 7	Cranfield Unit 4**	Vernon Johnson 1	Armstrong 4	Armstrong 2	R G CALCOTE 1	H H CROSBY ETAL 1
Realiz. 1	1443	894	684	389	307	376	1107
Realiz. 2	1024	1748	1238	67	554	784	1217
Realiz. 3	492	1703	858	522	486	891	1500
Realiz. 4	961	1789	1324	876	1037	1175	1431
Realiz. 5	2658*	1962	917	562	627	427	1479

*: prescribed rate was forced into a low permeability area

**: this well (CFU 4) has been reentered and put under production by the operator since model was constructed

Table 10. CO_2 maximum mole fraction, maximum mole fraction time, and CO_2 breakthrough time at P&A well locations.

Well name	Cranfield Unit 7	Cranfield Unit 4	Vernon Johnson 1	Armstrong 4	Armstrong 2	R G CALCOTE 1	H H CROSBY ETAL 1
(i, j)	40, 76	26, 60	22, 47	11, 35	18,39	27, 39	32,24
Realization 1							
Max Mol. F.	0.3358	0.9730	0.9993	0.5017	0.9950	0.9819	0.0184
Layer (max)	6	8	10	3	9	6	N/A
Date (max)	12/1/2013	12/1/2013	12/1/2013	12/1/2013	12/1/2013	7/1/2013	N/A
Layer (brthr)	3	1	10	1	5	6	N/A
Date (brthr)	6/1/2012	8/1/2010	9/30/2009	11/1/2010	12/1/2008	2/9/2010	N/A
Realization 2							
Max Mol. F.	0.7526	0.9526	0.9979	0.4910	0.9753	0.9811	0.0184
Layer (max)	2	9	10	6	4	3	N/A
Date (max)	12/1/2013	12/1/2013	12/1/2013	12/1/2013	12/1/2013	7/1/2013	N/A
Layer (brthr)	2	1	9	8	8	7	N/A
Date (brthr)	9/1/2011	2/9/2010	1/8/2010	4/1/2011	2/1/2009	6/9/2009	N/A
Realization 3							
Max Mol. F.	0.8766	0.9968	0.9899	0.9424	0.9736	0.9487	0.0186
Layer (max)	1	9	8	8	7	9	8
Date (max)	12/1/2013	12/1/2013	12/1/2013	12/1/2013	12/1/2013	6/1/2011	12/1/2013
Layer (brthr)	6	9	5	8	7	9	8
Date (brthr)	2/1/2011	3/24/2010	12/3/2009	8/1/2010	1/1/2009	6/25/2009	10/1/2011
Realization 4							
Max Mol. F.	0.9068	0.9804	0.9872	0.0321	0.9874	0.9800	0.0606
Layer (max)	4	8	10	4	6	7	1
Date (max)	12/1/2013	12/1/2013	12/1/2013	12/1/2013	12/1/2013	12/1/2013	12/1/2013
Layer (brthr)	4	7	8	5	8	7	1
Date (brthr)	8/1/2010	6/1/2010	12/15/2009	12/1/2010	1/1/2009	3/10/2009	2/1/2011
Realization 5							
Max Mol. F.	0.0185	0.9751	0.9885	0.8904	0.9954	0.9451	0.0184
Layer (max)	7	8	7	3	6	10	N/A
Date (max)	12/1/2013	12/1/2013	12/1/2013	12/1/2013	8/1/2010	12/1/2013	N/A
Layer (brthr)	7	8	4	3	8	3	N/A
Date (brthr)	9/1/2010	7/1/2010	10/12/2009	5/4/2010	11/28/2008	10/27/2009	N/A

Table 11. CO_2 breakthrough times at P&A well locations

Well name	Cranfield Unit 7	Cranfield Unit 4	Vernon Johnson 1	Armstrong 4	Armstrong 2	R G CALCOTE 1	H H CROSBY ETAL 1
Realiz. 1	6/1/2012	8/1/2010	9/30/2009	11/1/2010	12/1/2008	2/9/2010	N/A
Realiz. 2	9/1/2011	2/9/2010	1/8/2010	4/1/2011	2/1/2009	6/9/2009	N/A
Realiz. 3	2/1/2011	3/24/2010	12/3/2009	8/1/2010	1/1/2009	6/25/2009	10/1/2011
Realiz. 4	8/1/2010	6/1/2010	12/15/2009	12/1/2010	1/1/2009	3/10/2009	2/1/2011
Realiz. 5	9/1/2010	7/1/2010	10/12/2009	5/4/2010	11/28/2008	10/27/2009	N/A

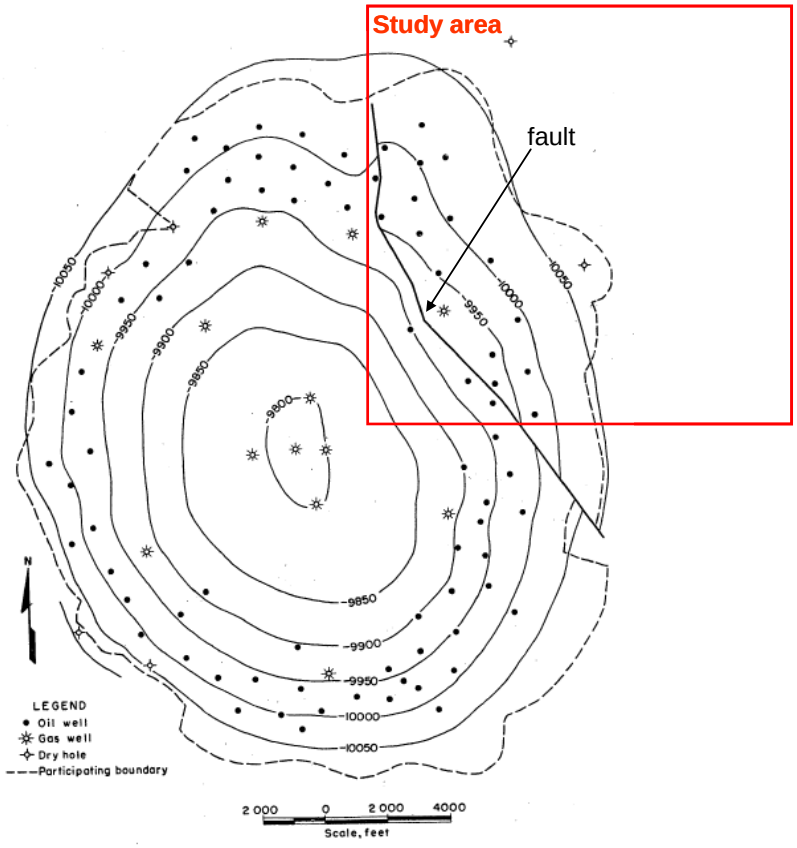

Figure 35. The model domain covers the portion of the northeast section of the field that is northeast of a non-transmissive fault (HiVIT domain)
Source: MOGB (1966)

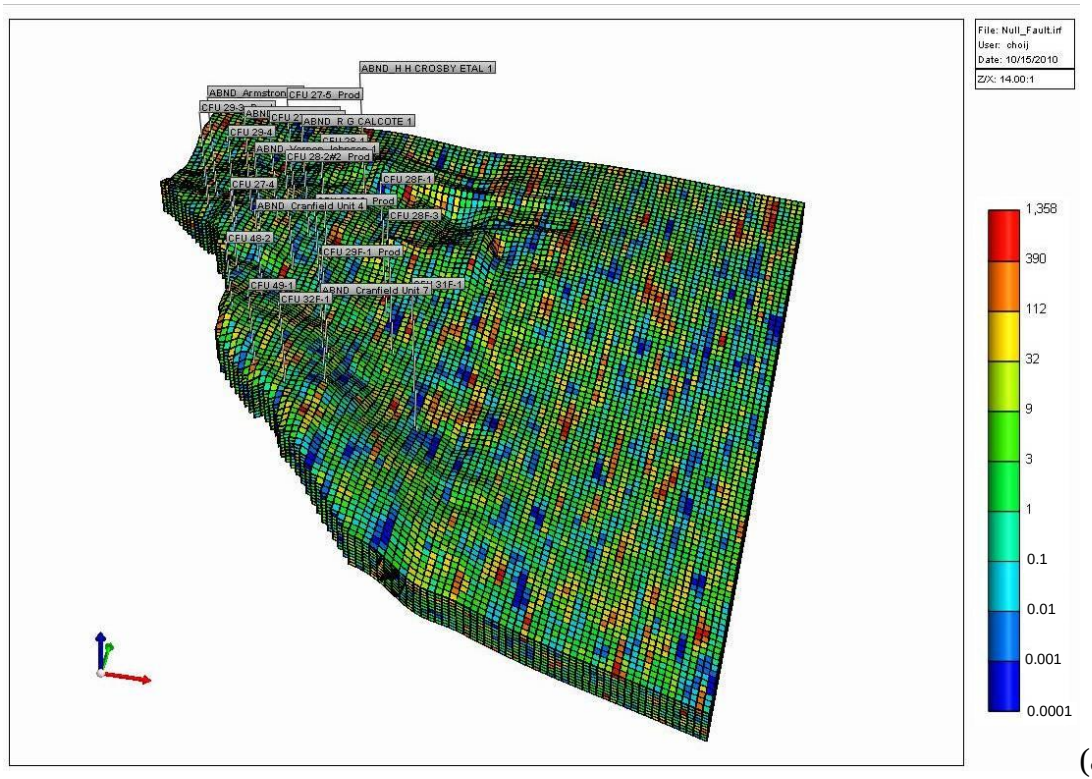

(a)

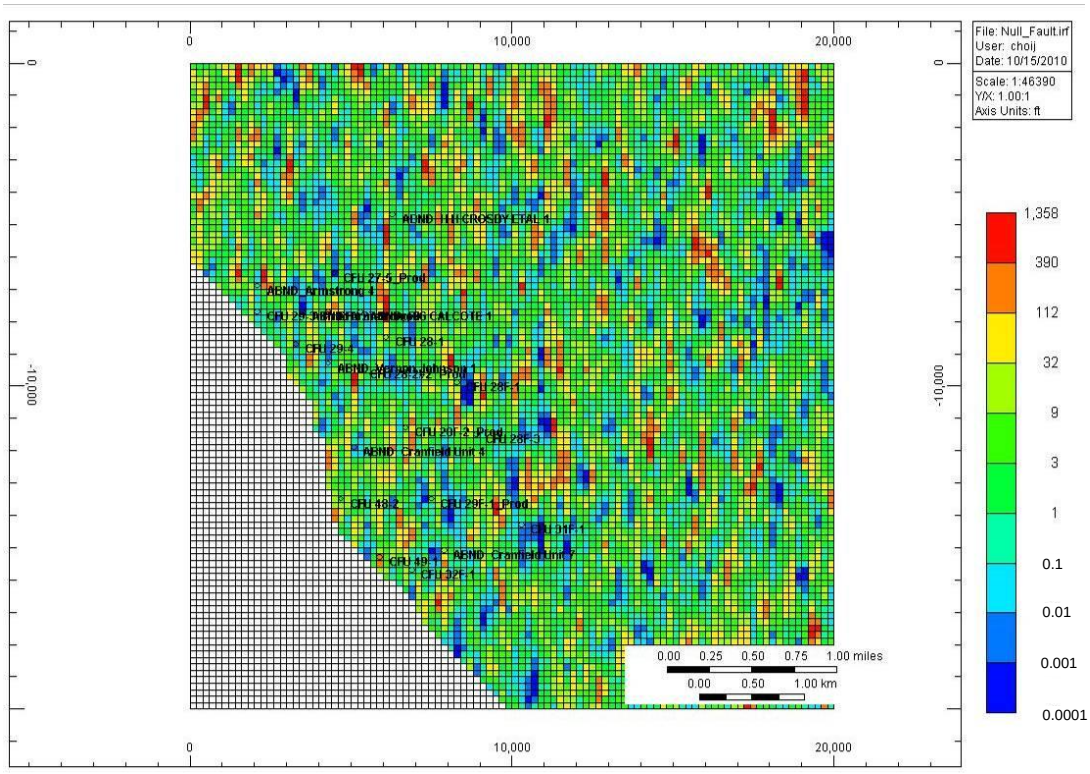

(b)

Note: red arrow in (a) indicates East direction.

Figure 36. Kx permeability distribution (layer 1, realization 1): (a) 3D view and (b) plan view.

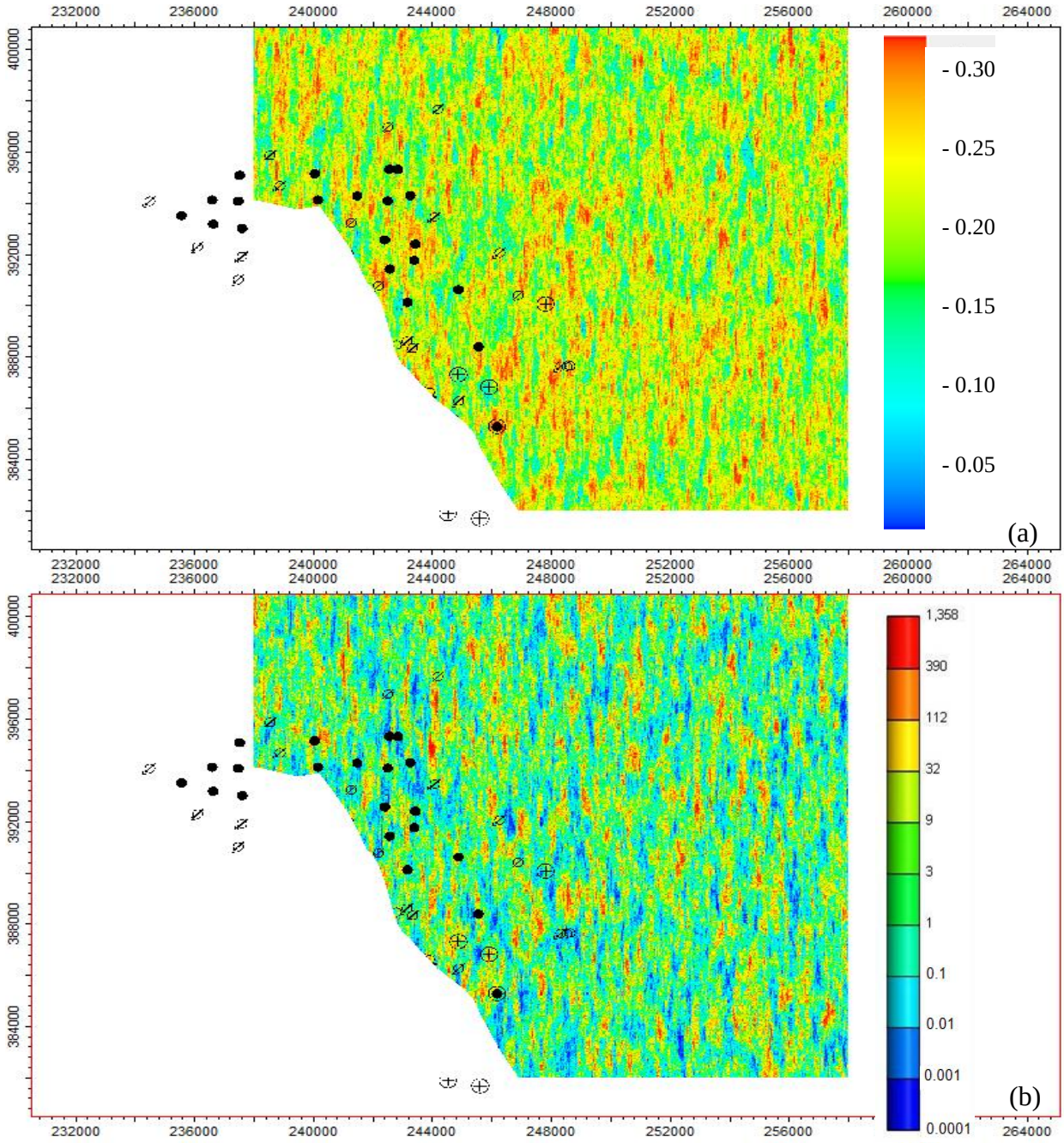

Figure 37. Porosity (a) and permeability (md) (b) with nugget of 0.14 on 50 x 50 x 8 ft (realization 1)

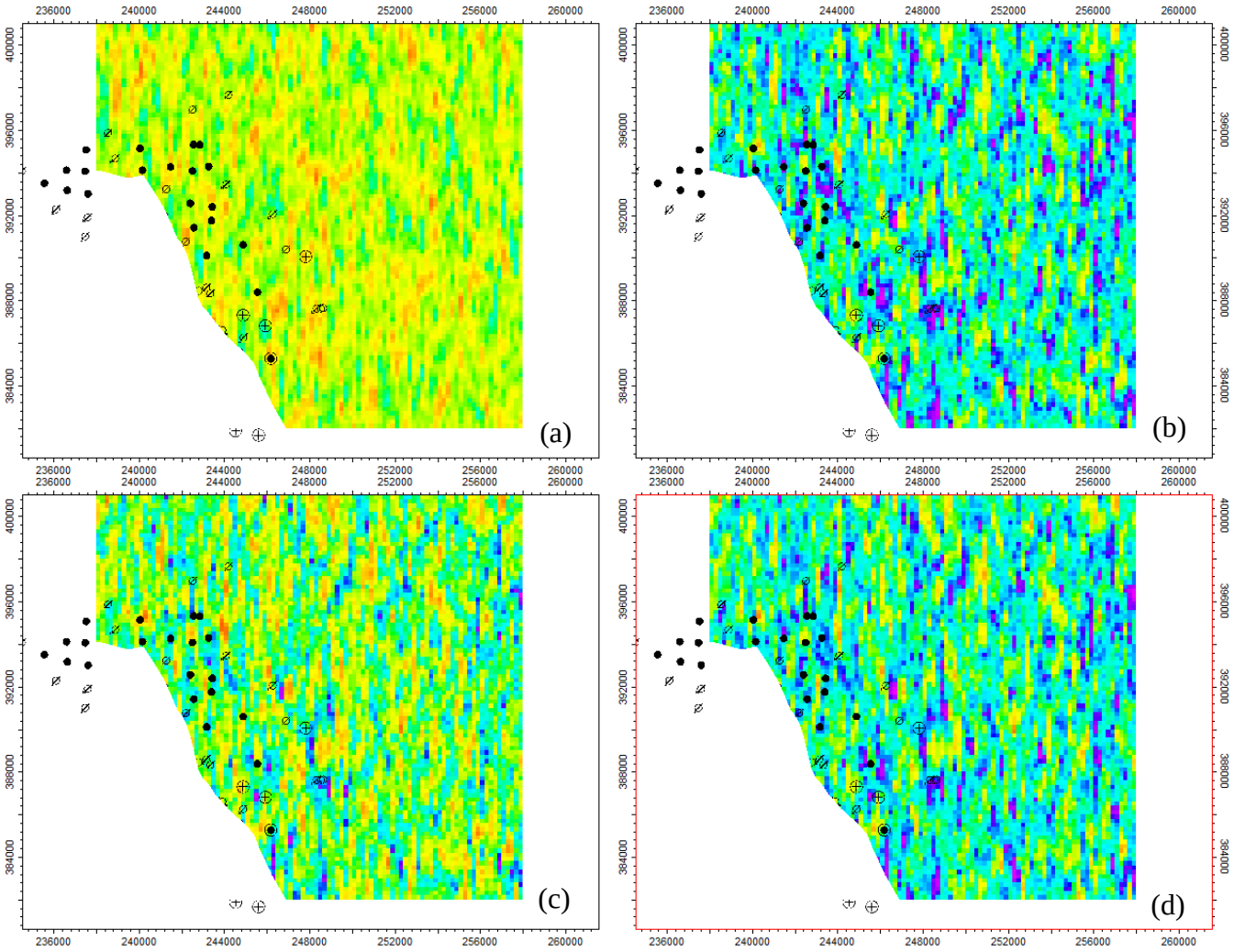

Note: same key as in Figure 37

Figure 38. Porosity (a), Kx (b), Ky (c) and Kz (d) with nugget of 0.14, upscaled 200x200x8 gt field (realization 1)

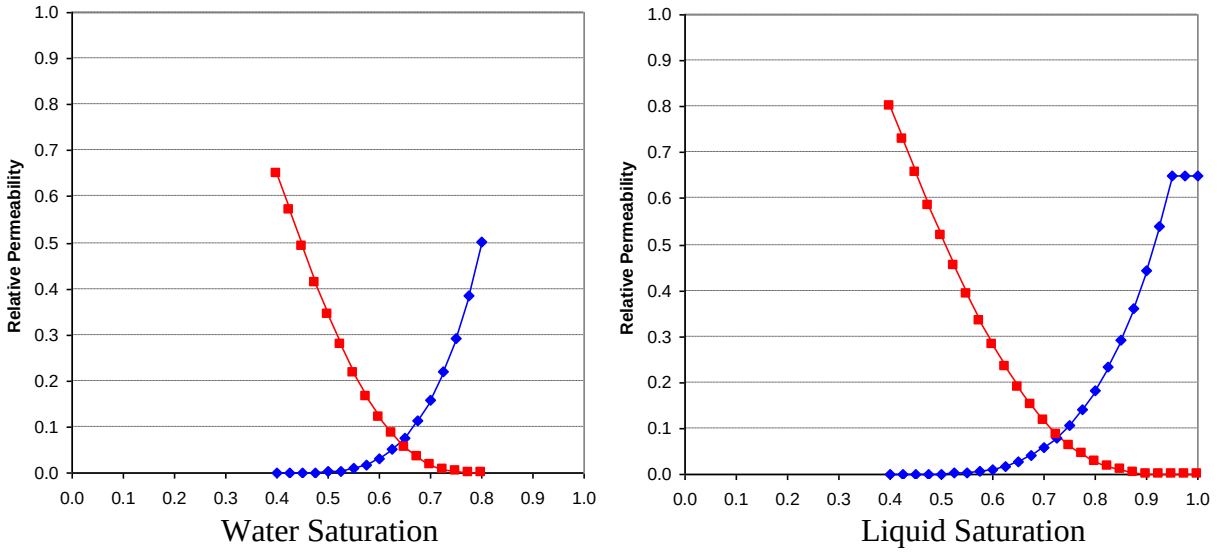

Figure 39. Relative permeability curves (oil/water and liquid/gas)

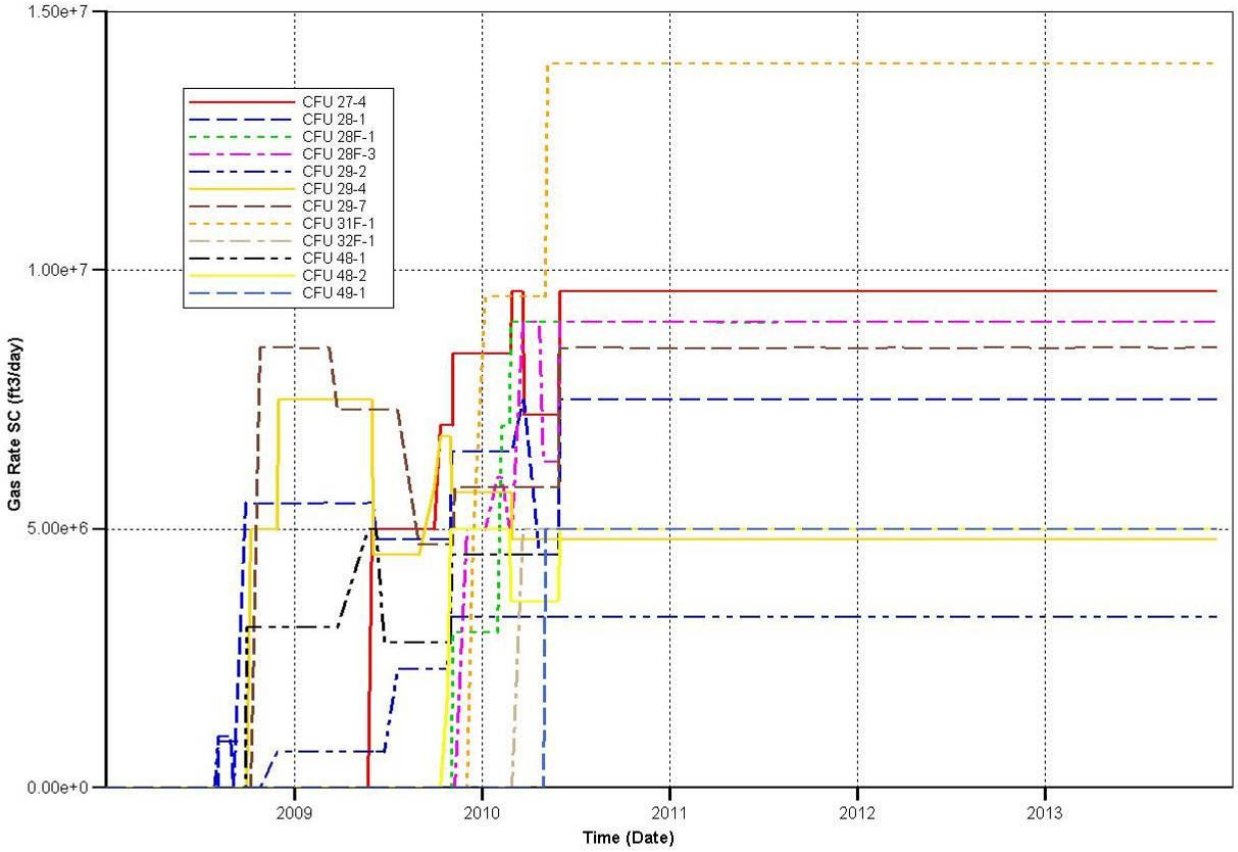

Note: this plot also includes wells CFU 29-2, 29-7 and 48-1, located in the western side of the fault; well CFU 31-1 is located in the brine leg in the DAS area

Figure 40. Injection Schedule (historical and future)

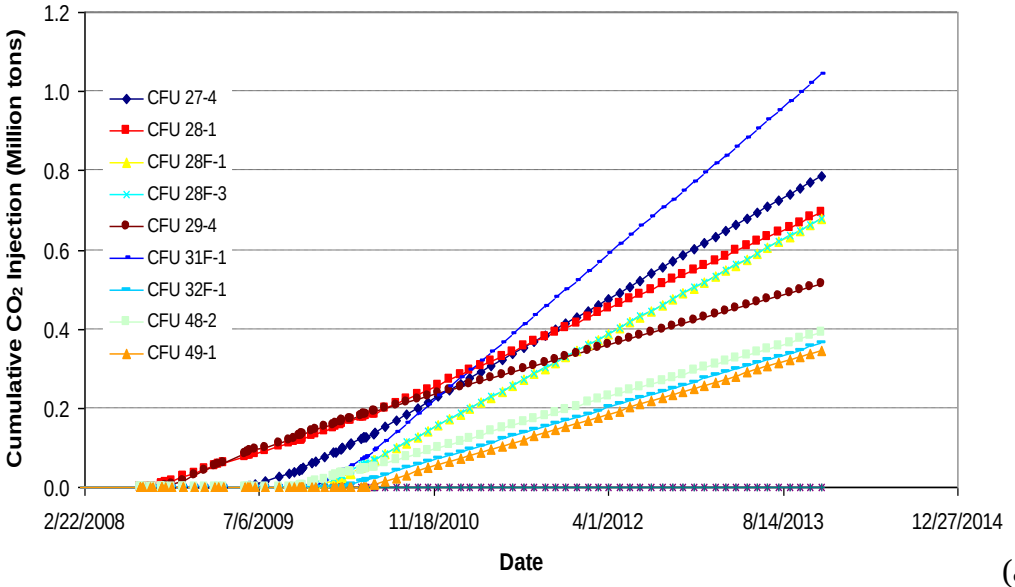

(a)

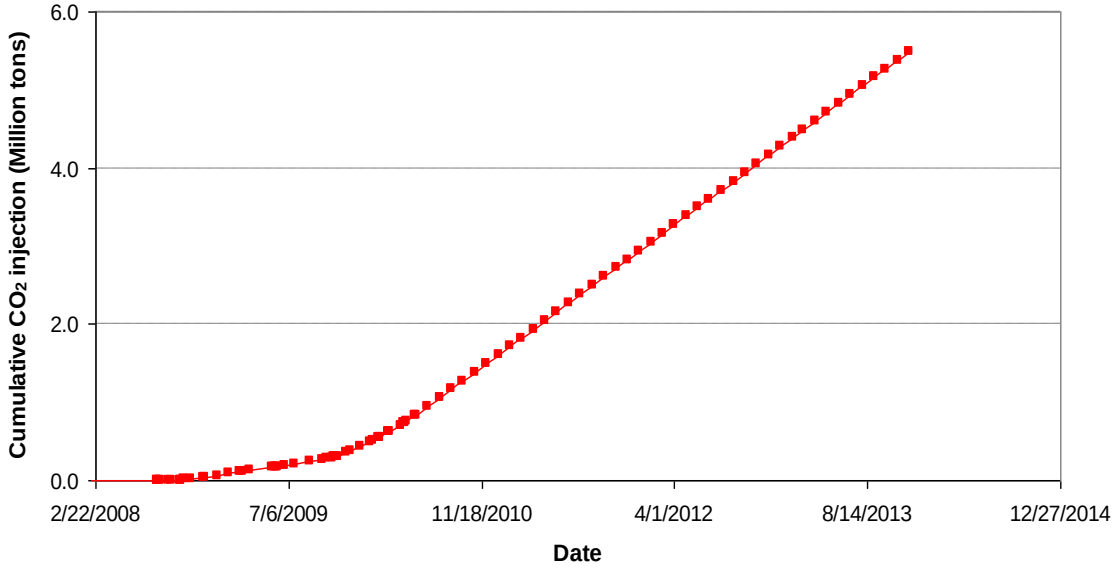

(b)

Figure 41. Cumulative injection in HiVIT wells.

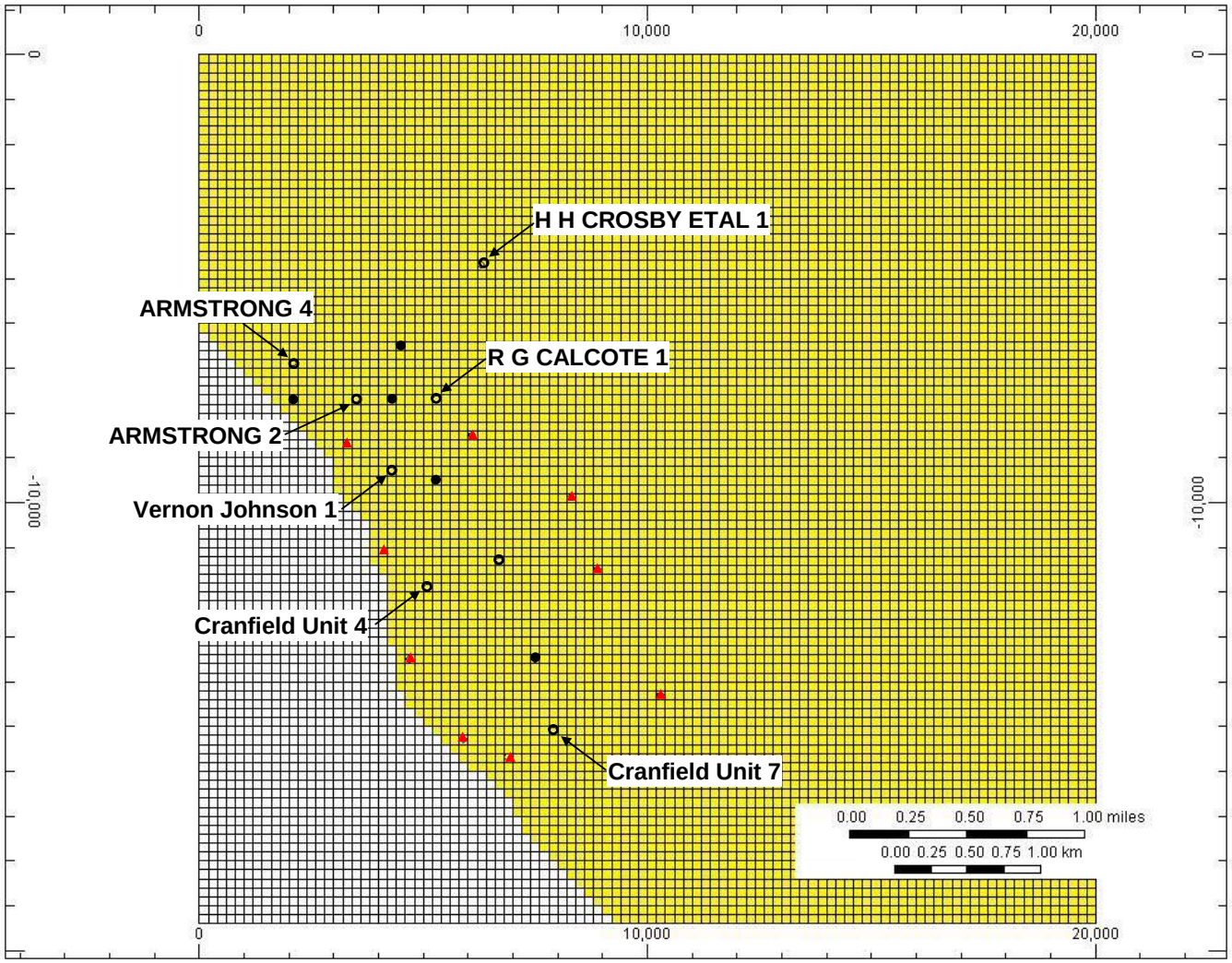

Note: only P&A wells are named, others are either injectors or producers.

Figure 42. Well location in the HiVIT domain.

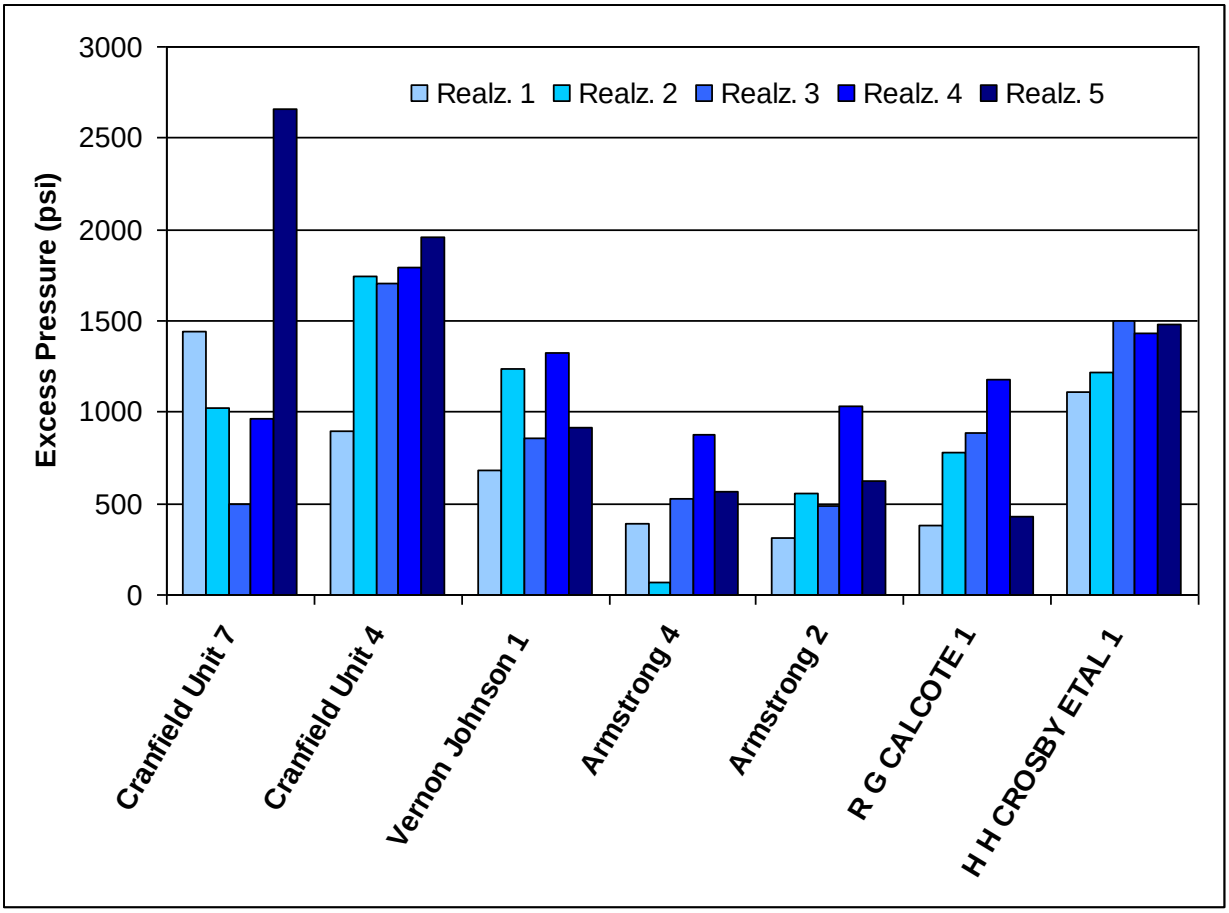

Figure 43. Comparison of excess pressure at the seven P&A wells for the five realizations

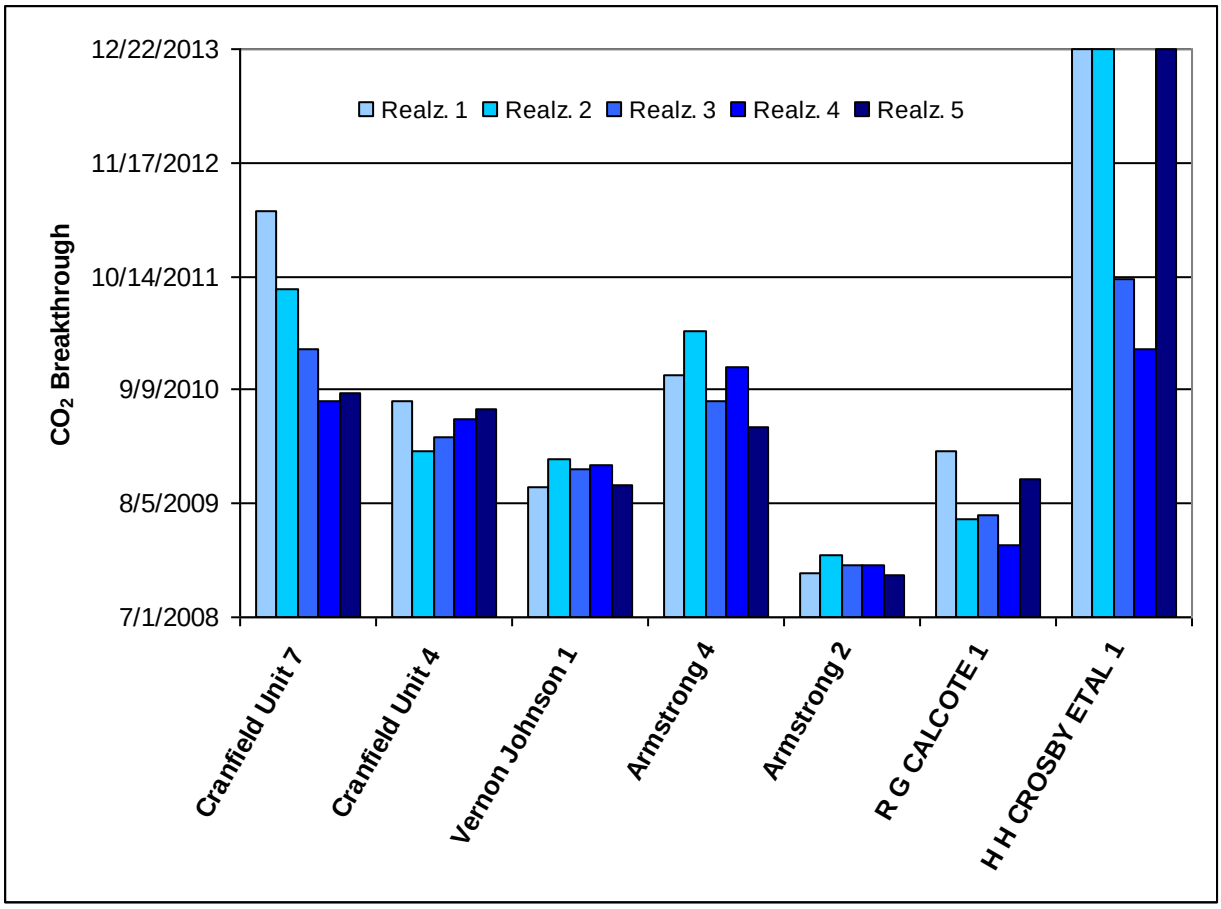

Note: The shorter the column, the sooner the breakthrough.

Figure 44. Comparison of CO_2 breakthrough times at the seven P&A wells for the five realizations

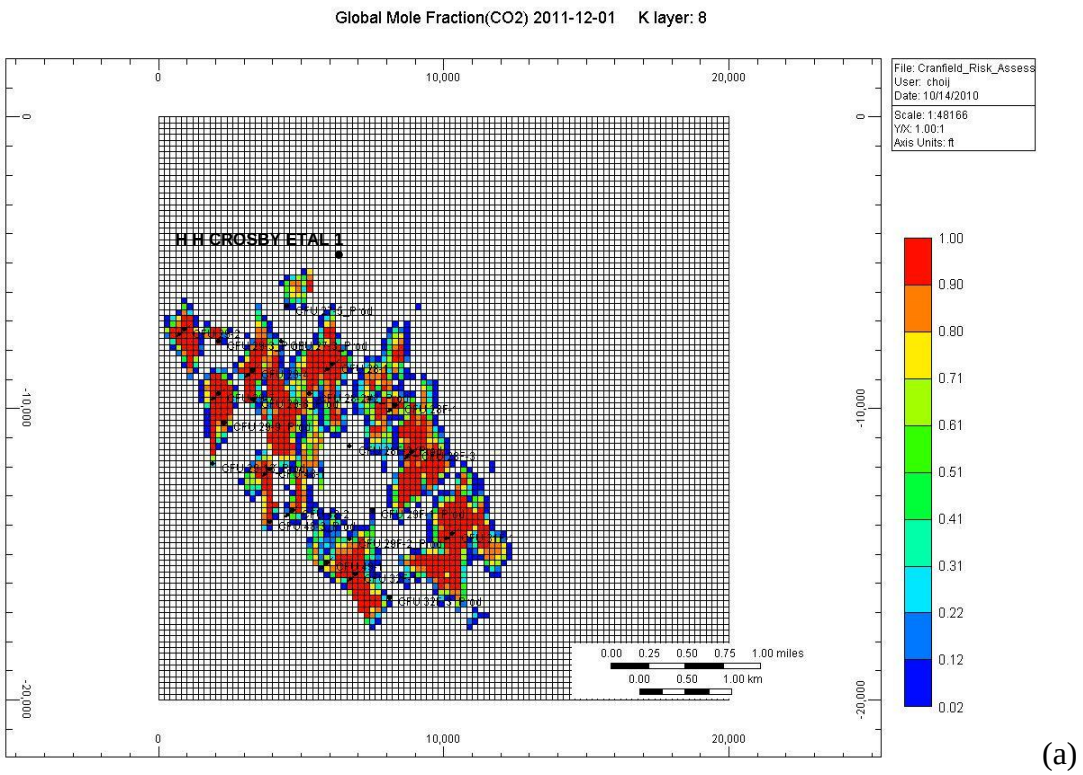

(a)

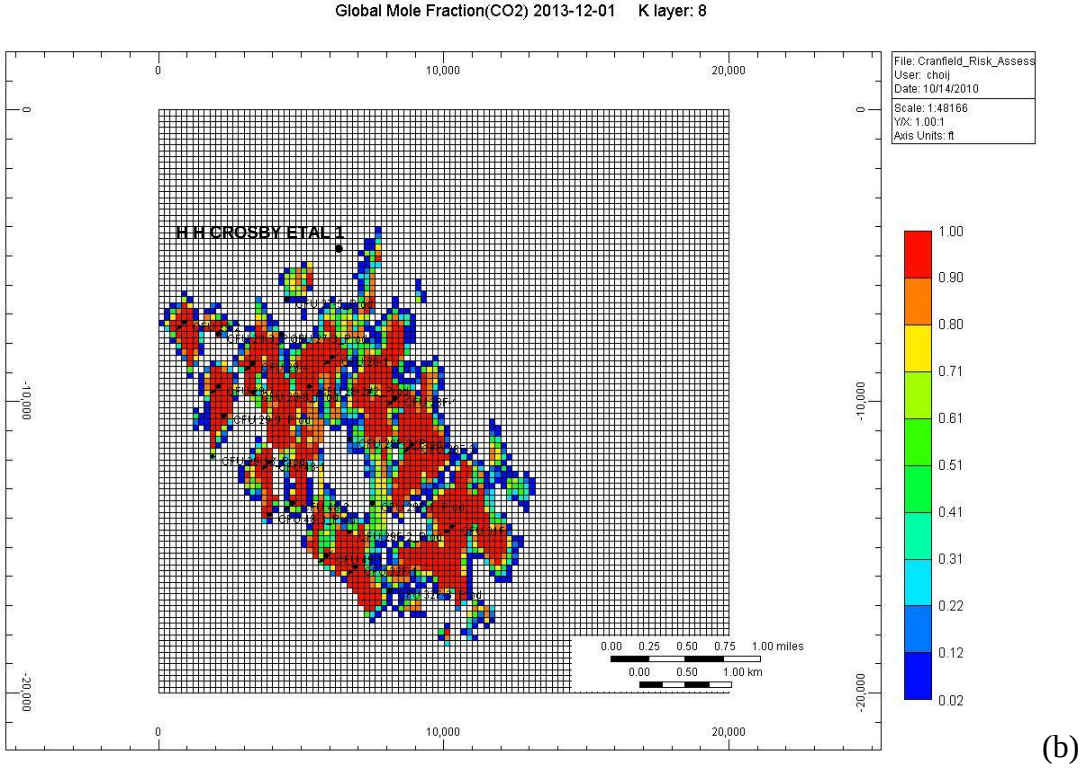

(b)

Note: Realization #1

Figure 45. Footprint of CO_2 plume in Layer 8: (a) on 12/1/2011 and (b) on 12/1/2013

5 CF Leakage Risk Assessment

5.1 Introduction

The Certification Framework (CF) definitions and concepts are presented in Appendix A. As shown there, the CF uses input on site conditions to define model properties needed to simulate CO_2 injection and migration from the injection zone (source), through the conduits (faults and wells), and potentially into compartments containing vulnerable entities. The site characterization information presented above on depths, thicknesses, and properties of the various lithologic layers combined with regional geologic experience in the area allow the development of a defensible definition of the system. Site characterization data combined with an injection plan constitutes the information needed as external input to the CF.

5.2 Storage Region

Central to the application of the CF for leakage risk assessment is the specification of the storage region, defined as the volume beyond which CO_2 migration is considered leakage. We define the storage region for the purposes of this test of the CF at the SECARB Phase III project as the subsurface volume comprised by the Tuscaloosa Fm. reservoir on the upthrown side of the fault. The lower boundary of the storage region consists of the uppermost confining unit of the Washita-Fredericksburg group, in direct contact with the Tuscaloosa. The upper boundary of the storage region is formed by the base of the regional marine mudstones overlying the Tuscaloosa. The regional seal of middle Tuscaloosa, which is an extensive marine mudstone, adds to the defense-in-depth. The non-marine mudstones at the top of the oil reservoir are not considered the storage region upper boundary because, although able to contain the hydrocarbons for millions of years, it is not as extensive as the middle Tuscaloosa. It follows that the confining system is composed of, from bottom to top: (1) non-marine local mudstones; (2) intermediate mostly low permeability rocks; (3) regional marine mudstones of the middle Tuscaloosa; (3) upper Tuscaloosa rocks: and (4) marine mudstones of the Navarro, Taylor, and equivalent Fms. The updip limit is the fault. The downdip limit (to the northeast and east) of the storage region is arbitrarily placed 10 mi (16 km) from the original oil-water contact in all other directions.

5.3 Terminology for Degree of Likelihood, Impact, and Risk

In the evaluation and communication of risk, descriptions and measures of likelihood, impact severity, and level of risk are needed whether or not these components have actually been quantified. The CF project has defined some terminology to describe approximate likelihoods as shown in Table 12. In the discussion below, likelihood terminology can be referenced to this table to understand the implied range of probability for the occurrence of the various events and scenarios.

In this demonstration of the CF approach, we rely on qualitative descriptions to convey impact severity and risk. These terms are presented in Table 13 and Table 14. We use the words negligible, low, moderate, and high to describe the severity of impacts. Negligible means that it would be difficult to even detect or measure an impact. Low severity in this report implies that the impacts are small but measurable but are expected to only have a minor effect on the value of any compartment (see Section 5.7 for definitions of compartments).. A moderate impact is one that could noticeably degrade the perceived value of one or more compartments.. A high impact

means that one or more compartments will suffer severe or even complete loss of the perceived value. This latter category includes the so-called high-consequence low likelihood events that are of great concern and are very challenging to mitigate and manage.

In terms of risk terminology, we use the term de minimis to indicate a risk that is so low that for all practical purposes (e.g., as a target of mitigation), it can be ignored. A low risk implies a risk that should be acknowledged but does not warrant large expense or focus for mitigation. A moderate risk is one that should be mitigated to reduce the risk. A high risk clearly requires focused mitigation. The lowering of risks through mitigation, monitoring, and enhanced understanding is at the heart of risk management.

5.4 Likelihood of CO_2 and Brine Encountering Leakage Pathways

Because the storage region is capped by multiple thick mudstones and the non-transmissive fault dies out in the thick Midway mudstones, there is no natural pathway for brine or CO_2 to leak upward. Indeed the reservoir has held natural gas and oil in the structure over geologic time. Despite some elevation in pressure, the pressure gradient stays well below lithostatic at a modeled maximum of <0.73 psi/ft (Table 8). Therefore the only leakage pathways that need to be considered are the wells in the area. The only wells that penetrate the Tuscaloosa are the deep wells related to oil and gas exploration and production, including the CO_2 injection well(s).

Simulation results described in Section 4 show that CO_2 and displaced brine at elevated pressures will encounter multiple P&A wells during the Phase III project. This result confirms the production strategy which is to pressurize the reservoir and re-enter P&A wells ahead of time and changing them into producing wells when the oil becomes self-lifting. This means that for the CF approach the likelihood of potential leakage pathways (in this case P&A wells) being intersected by CO_2 and brine at elevated pressure is high. Therefore, the calculation of leakage risk in the CF reduces to a calculation of leakage impact severity along any conduits that exist through flaws in the cement placed in the rock-casing annulus. In the CF, impacts are evaluated on the basis of proxy leakage fluxes, as presented below.

5.5 Upward CO_2 Leakage

The wells that must be considered as possible leakage conduits are the P&A wells as discussed in Section 3.3.5. Below, we evaluate the potential leakage flux from such wells to quantify this single recognized leakage scenario. Here, only the impact of chronic flow of CO_2 through wells is considered. Such flows by definition do not significantly disrupt the wellbore conditions. This may be distinguished from a complete loss of wellbore integrity in a "blowout" where the cement plugging and casing can be substantially damaged resulting in a high-rate uncontrolled release of CO_2. Because the impact severity of a blowout is expected to be moderate to high depending on the duration of the blowout, the main variable in terms of overall risk regarding blowouts is the probability of occurrence. This aspect will be treated in Section 5.8.

5.5.1 Model for Leakage up P&A Wells

An investigation of potential flow in P&A wells was conducted for the site. The analysis is for a steady-state flow condition, based on one-dimensional (vertical), single-phase flow in the well coupled with horizontal (radial) single-phase flow from the well into the formation. A

description of the mathematical model is given in Appendix B. The base-case calculations use the hydrostratigraphy given in Table 15:

The Wilcox is designated as "i" and "i+1" in Table 15 because it is divided into a total of 23 layers. The layers have alternating high and low permeability representing sand and mudstone. Each permeable layer has a thickness of 61 m and each impermeable layer has a thickness of 30 m. The total depth of the entire section is 3,095 m. Other base-case parameters are given in Table 16: The viscosity and density of the fluid flowing in the well corresponds to CO_2. The bottom pressure rise is fixed at the interface of the lower Tuscaloosa and middle Tuscaloosa. The pressure rise of 2,000 psi (14 Mpa) is close to the highest pressure expected (Sec. 4, Figure 43). The results for the base case and sensitivity cases are shown in Figure 46.

The base case shows a small flux in the well within the middle Tuscaloosa that is quickly dissipated within the upper Tuscaloosa. The residual flux moving up the well is equivalent to about 0.6 tonnes of CO_2 per year per well. Two sensitivity cases were evaluated. Sensitivity Case 1 increases wellbore permeability from 1.4×10^{-14} m^2 to 6.2×10^{-14} m^2 (see next section). This change causes the flow in the well to increase significantly within the middle Tuscaloosa. Although the flow is dissipated within the permeable upper Tuscaloosa, the increased wellbore permeability results in a residual flux moving up the well annulus that is about 4.5 times larger than the base case (2.8 tonnes CO_2 per year per well). Sensitivity Case 2 uses the increased wellbore permeability plus a reduction in the upper Tuscaloosa permeability from 1.64×10^{-14} to 1.64×10^{-16} m^2. The result for this sensitivity case is that excess pressure is able to move farther into the upper Tuscaloosa before it is dissipated within this unit. Residual CO_2 flux up the well is unchanged. The analysis shows that the residual flux penetrating above the Wilcox is a sensitive function of the wellbore permeability. This analysis is expected to be conservative because current oil production activities in the Wilcox have reduced the static formation pressure, leading to conditions that would tend to more readily dissipate flow through the well than represented in this analysis.

5.5.1.1 Effective Permeability of P&A Wells

The sensitivity analysis indicates that the effective permeability of P&A wellbores is a critical parameter for estimating CO_2 leakage. To investigate this further, we considered cement bond log (CBL) data from the site. A small subset of wells has CBL measurements. These measurements are shown in Figure 34. The well permeability analysis is based on interpretation of the nine CBLs available for P&A wells that penetrate the Tuscaloosa (see Section 5.5.1.3). Part of this interpretation is that cement falling in the "100%" or "good" categories results in a tight seal. This means that all but one of the nine P&A wells with CBL measurements have tight cement seals. Therefore, about 89% of the P&A wells are expected to have negligible CO_2 leakage. The remaining 11% may have higher permeabilities that could lead to higher CO_2 leakage rates. This fraction of P&A wells with more permeable cement seals is similar to the leakage-occurrence rate of 14% found by Watson and Bachu (2009) for cased P&A wells in Alberta, Canada.

A P&A well permeability distribution was developed from the CBL data and measurements of permeability through cement/simulated casing samples to provide more realistic estimates of CO_2 leakage through wells (Appendix B). This distribution only applies to the higher-

permeability subset (~ 11%) of P&A wells. However, data from all nine wells were included in the permeability distribution by using the CBLs to quantify the distribution of lengths of cemented sections for P&A wells, as explained in Appendix B. The resulting well permeability distribution is shown in Figure 47. The mean and standard deviation for the log-permeability data points are -13.9 and 0.32, respectively. These correspond to a mean permeability of 1.4×10^{-14} m^2 and a two-standard-deviation range of 3.2×10^{-15} m^2 to 6.2×10^{-14} m^2. The figure also shows the fitted log-normal distribution with the same mean and standard deviation.

5.5.1.2 Modeled CO_2 Leakage Rate up Wells

The CO_2 mass flow rates at the ground surface were computed over the range of wellbore permeabilities from 7×10^{-16} m^2 to 6×10^{-13} m^2 and weighted by the log-normal probability distribution. This was computed from a set of 35 cases with varying wellbore permeabilities ranging from four standard deviations below the mean to five standard deviations above the mean based on the fitted log-normal distribution in Figure 47.

The mean CO_2 mass flow rate for these wells is 0.9 tonnes/yr per well, with standard deviation of 0.8 tonnes/yr. The distribution of CO_2 mass flow rates is given in Figure 48. As shown in this figure, the releases range from less than 0.1 tonnes per year to more than 10 tonnes/yr. For wells with "100%" or "good" cement bonds, the maximum permeability of 1.3×10^{-19} m^2 was used. Based on the CBLs available at the site, 8/9 of the P&A wells have some amount of "100%" or "good" cement bonds and, therefore, are assigned the lower permeability of 1.3×10^{-19} m^2. The CO_2 mass flow rate for wells with 100% cement bonds is negligible (5.8×10^{-6} tonnes/yr).

5.5.1.3 Additional Mitigating Elements

Some recent field observations tend to reduce P&A well integrity concerns created by the CBL logs that show questionable cement. During the Phase II project, the SECARB team contracted Denbury Onshore LLC., the field operator, and Sandia Technologies LLC, the experiment field service provider, to reenter and recomplete a typical P&A 1954 production well, ELLA G Lees#7 which provides information about well performance. Multiple mechanical integrity tests and Schlumberger Ultrasonic Imager Tool (USIT) cement and casing integrity logs were run during workover of this well.

The permitted cement and drilling mud plugs inside the casing were located where the P&A records reported, and they had pressure integrity. The 7" casing had some damage because of corrosion in the 3306' and 3457' depth interval which required repair before the well could be returned to service. However, it provided no migration pathways because cement inside the well at greater depth was shown to be intact by repeated pressure testing.

The USIT run to total depth showed poor cement quality, therefore to support the test plan the casing was perforated and a cement squeeze was placed in the zone showing the greatest void on the USIT. The zone that appeared most open proved to have inadequate communication to circulate cement. Furthermore, during the cement squeeze, no pressure was communicated to a pressure gage hung below the bridge plug and in communication with the injection zone through the historic perforations. It follows that the Ella G Lees # 7 was therefore shown to have no communication through what cement bond logs indicated was poor quality cement.

Further studies conducted under SECARB Phases II and III target assessment of the possibility that fluids could migrate along wellbores through poor or non-existent cements, the possible rates and pathways of such fluid migration, and the indicators that may show minor fluid migration. In other words, questionable cement does not necessarily translate into a fluid pathway along the wellbore. Actually, some practitioners think that the likelihood of false positives based on CBLs (stating that there is a flow pathway where there is none) is greater than that of false negatives (stating there is no pathway where there is one).

In addition, several studies by Warner et al., (1997) and Watson and Bachu (2009) provide factors applicable to this study that may limit the ability of a wellbore to maintain open space in the rock-casing annulus even in the absence of cement. Mitigating effects such as the presence of sloughing (caving in) or squeezing (expanding) mudstones in the Gulf Coast can be expected and is well documented (Warner et al., 1997). For example, corroborating drillers' experience in the Gulf Coast, a controlled test performed at a depth of about 900 m (2,953 ft) and presented by Clark et al., (2003) effectively observed well closure through these mechanisms.

All those elements combined tend to suggest that the modeling analysis presented above is conservative and that CO_2 leakage fluxes up P&A wells, if any occurs at all, are likely to be lower than the model shows. If the specific values of leakage flux estimated here are ever a concern, we recommend more detailed modeling (e.g., including accurate CO_2 properties) be carried out to refine the estimates.

5.5.2 Leakage through Active Producers

The operator has retrofitted 10 P&A wells as producers (all injectors are new wells). It is possible that some of these wells share the same flaws as untouched P&A wells. The leakage driving force due to pressure is smaller because of the oil production but there could be exposure to CO_2 after it comes out of solution with the oil upon decompression.

A report on production wells on the outer continental shelf (Bourgoyne and Scott, 1999) indicates that many have experienced sustained casing pressure. The sources of sustained casing pressure are tubing and casing leaks and flow paths through the cemented annulus. This suggests that sustained casing pressure may be used as a surrogate measure for leakage along production wells. Based on Figure 3.2 of Bourgoyne and Scott (1999) approximately 11% of the wells have sustained casing pressure. This percentage is the same as used for the percentage of P&A wells that may experience a higher level of CO_2 leakage (see Section 5.5.1.1). Therefore, the estimate of overall potential CO_2 leakage through wells is based on 10 P&A wells retrofitted as producers and seven unaltered P&A wells, for a total of 17 wells. Because there is no additional information concerning the potential permeability distribution of leaking P&A wells retrofitted for production, the permeability distribution for these wells is assumed to be the same as for the unaltered P&A wells.

5.6 Brine Leakage

Brine leakage can be difficult to identify because of the extensive oil and gas history in Adams and Franklin counties going back to the first half of the 20th century when surface disposal of produced brines was the norm. Contamination (for example, Kalkhoff, 1986; Childress, 1976)

next to a P&A well could have been caused by past practices rather than because of a defective cement job. Several studies on the impact of P&A wells on groundwater resources have been released in the past decades including one on the lower Tuscaloosa trend of Southwestern Mississippi and Eastern Louisiana (Warner and McConnell, 1990, 1993). In the context of brine injection, they concluded that injection into the Tuscaloosa Fm. is not likely to impact USDWs.

5.6.1 Analysis of Upward Brine Leakage

Although CO_2 leakage could bring up some brine with it in a potential leakage event, this section concerns brine leakage alone. Brine leakage is analyzed using the same methodology as discussed for CO_2 leakage in Section 5.4.1. The significant difference between CO_2 and brine is the density. CO_2 is forced up a wellbore by injection pressure and buoyancy effects because of its low density relative to formation brine. Because salinity generally increases with depth and temperature equilibrates rapidly with the formation, there is no buoyancy to move brine up a well. In fact, any buoyancy effect of the mobilized brine relative to the formation brine may be expected to reduce the movement of brine up a well. The analysis shows that no brine flow is expected to occur in wells above the upper Tuscaloosa, even for the highest wellbore permeability investigated for CO_2.

5.6.2 Along-Dip Leakage of CO_2 and Brine

The western part of the storage region is bounded by the non-transmissive fault which is expected to provide an effective barrier to leakage in this direction. There is no barrier to migration of brine or CO_2 locally downdip to the northeast and east. However, given that there are no vulnerable resources in this direction (Figure 24) that could be impacted by injection into the reservoir, the consequences of down-dip leakage of either CO_2 or brine are negligible.

5.7 Impact to Compartments

From bottom to top, the compartments in the CF containing vulnerable entities are the Hydrocarbon and Mineral Resources (HMR), Underground Sources of Drinking Water (USDW), Near-Surface Environment (NSE), Health and Safety (HS), and Emission Credits and Atmosphere (ECA). Because the oilfield is under CO_2-EOR, and no other significant mineral resources are recognized in the area, we conclude that there are no potential negative impacts of CO_2 on the hydrocarbon resource at the site.

As discussed in Section 3, there are significant USDWs in the area that could be impacted if CO_2 or brine leaked up a P&A well and out of the storage region beyond the Wilcox Formation. There are 17 wells that may be impacted by the Phase III CO_2 injection. Given the results in Section 5.5, it is expected that one-ninth, or about two of these wells, may be expected to present a higher-permeability pathway. This leads to a total CO_2 leakage rate estimate of about 1.8 tonnes per year. The remaining 15 wells are expected to have sufficiently tight cement closures to limit releases from those wells to the negligible level of 9×10^{-5} tonnes/yr. Strom et al., (1995) reports on groundwater pumping rates from 24 wells in the Natchez area. The smallest rate of water withdrawal is 0.024 million gallons per day, which is nearly an order of magnitude smaller than the next lowest pumping rate for any of the other 23 wells. If the entire 900 kg per year of CO_2 leaking up a single well was captured in this low-rate water supply well, the mass ratio of leaked CO_2 to water in the withdrawal would be about 3e-5. This may be compared with the natural bicarbonate levels in groundwaters used for water supply as reported by Boswell and Bodnar (1985). The average bicarbonate level is 287 mg/L (as $CaCO_3$) or an equivalent CO_2 to

water mass ratio of about 1e-4. The corresponding standard deviation is 48 mg/L or an equivalent CO_2 to water mass ratio of about 2e-5. Therefore, the leaked CO_2 release is not expected to significantly perturb natural CO_2 levels in groundwater withdrawn from the USDW because the perturbation is similar to the natural variations in equivalent CO_2 content and a factor of 3 less than the average equivalent CO_2 content.

The impact of 1.8 tonnes per year of CO_2 leakage on the NSE may be better understood by comparison with soil gas CO_2 mass flow rates. Biological activity in soil produces CO_2 and there is a natural flux of CO_2 from the soil gas into the atmosphere. Klusman (2005) measured CO_2 soil gas fluxes at Teapot Dome oil field, Wyoming. The measurements were conducted in the winter and as such represent minimum values. Based on measurements at 40 locations, the CO_2 flux from soil gas gives an average value of about 250 mg/m^2/day (0.091 kg/m^2/year), a standard deviation of about 240 mg/m^2/day (0.088 kg/m^2/year) without noticeable damage to natural flora. CO_2 flux values during summer are expected to be higher by an order of magnitude or more (Klusman, 2005). This suggests that damage to flora will not occur if the leakage flux is less than about 2500 mg/m^2/day (0.91 kg/m^2/year). Assuming similar natural soil gas CO_2 fluxes at the site, the flux from one leaking well, 0.9 tonnes/year, must disperse over an area of about 1,000 m^2 or more to remain below 2,500 mg/m^2/day (0.91 kg/m^2/year). Therefore, for two leaking wells, there is a risk of damage to flora for a maximum area of about 2,000 m^2. Similar measurements and study are currently being conducted at the site.

Regarding the HS compartment, in the absence of homes or enclosed buildings on top of P&A wells, such low fluxes will not lead to hazardous concentrations in open-air conditions. A suitable comparison for the HS compartment is the rate of ecosystem utilization of CO_2. The net ecosystem exchange (amount of CO_2 taken up and emitted by plants and soil) is typically around 4.4×10^{-7} kg/m^2/s or 14 kg/m^2/yr. Therefore, the well leakage rate is similar to the rate of CO_2 usage by an 11 m by 11 m plot of land with natural vegetation. The small area of equivalent ecosystem exchange indicates that the impacts of CO_2 leakage through wells to the HS are negligible.

A suitable comparison of CO_2 flux rates for the ECA is the ratio of CO_2 leakage to CO_2 injection. One goal of the Phase III study is to inject 1 million tonnes of CO_2 per year. Thus, the well leakage rate is seen to be about 0.0002% of the injection rate.

5.8 Overall CO_2 and Brine Leakage Risk

As discussed above, with 100% probability of overpressured CO_2 and brine encountering potential leakage pathways provided by P&A wells, the leakage risk assessment is based directly on the assessment of impacts. In consideration of the leakage probability and impact severities given above, we conclude that the overall risk of leakage to the USDW, ECA, or the HS compartments is low (see Table 14). Based on the analyses of impact severity in Section 5.7 for the HMR, USDW, and HS, the potential leakage fluxes of CO_2 through wells are expected to have negligible impacts.

In the case that the P&A wells were improperly plugged at the ground surface only and leaking CO_2 somehow discharged into the shallow vadose zone, it is possible that CO_2 concentrations could build up to high levels in the soil locally around the well affecting the NSE. The reason for

this is that there is less potential for dissipation of CO_2 in the soil than above ground (Oldenburg and Unger, 2003). High concentrations in the root zone could cause plant stress which would be visible in wilting leaves and/or dying trees or plants. The risk to the NSE compartment is considered low because this would be a very local impact and the presence of stressed vegetation would in fact alert the operator to the potential problem which could then be mitigated by various well workover processes.

A specific impact analysis for blowouts is not provided because of the uncertainty regarding how blowouts may interact with the different compartments. The Sheep Mountain blowout (Lynch et al., 1985) may be considered representative of a highly-improbable "worst case". Sheep Mountain is a natural CO_2 reservoir in Colorado that was developed for use in Permian Basin enhanced oil recovery operations. The blowout required 17 days to control and lost approximately 125,000 tonnes of CO_2 (to the atmosphere). Even though the impact severity may range from moderate to high and could vary between compartments, the risk is greatly reduced by the probability of occurrence. Jordan and Benson (2008) report that the blowout rate in oil fields using steam injection is one per 98,000 P&A wells per year; similar rates for blowouts are expected for CO_2 sequestration operations. Thus the impact severity is offset by a low occurrence rate. Furthermore, during the operational period for oil recovery and carbon sequestration activities, any blowout would be immediately recognized and mitigation measures would be implemented. In the case of steam blowouts, the wells were brought under control for 95% of the cases in less than 3.5 days (Jordan and Benson, 2008), resulting in an even lower probability for long-duration blowouts and associated higher impact severity.

Table 12. Likelihood terminology

Occurrence expectation terminology	If there were 100 projects like this one,
Improbable	…less than once in the 100 projects
Unlikely	…in 1 to 5 of the 100 projects
Somewhat likely	…in 6 to 10 of the 100 projects
Likely	…in 11 to 50 of the 100 projects
Very likely	… more than 50 times within the 100 projects

Source: modified from Hnottavange-Telleen, Schlumberger Carbon Services

Table 13. Impact terminology

Severity of impact	Qualitative Description
Negligible	So small that it is difficult to detect or measure
Low	Small but measurable effect; minor impact on compartment values
Moderate	Noticeably degrades value of one or more compartments
High	One or more compartments will suffer severe or complete loss of value

Table 14. Risk terminology

Risk level	Qualitative description
De minimis	Can be ignored for all practical purposes
Low	Should be acknowledged, and mitigated if feasible
Moderate	Should be mitigated to reduce risk
High	Requires focused mitigation

Table 15. Well leakage base case hydrostratigraphy

Layer	Permeability (m^2)	Thickness (m)
Recent and Catahoula Sands	3.55292E-11	229
Jackson-Vicksburg	0	472
Cockfield	4.11547E-14	61
Cook Mountain	0	53
Sparta/Memphis	5.06292E-14	244
Cane River	0	61
Wilcox i	4.94449E-14	61
Wilcox i+1	0	30
Midway Claystones	0	335
Austin Chalk	2.37E-14	213
Eagle Ford	1.64E-14	122
Eutaw	0	53
Upper Tuscaloosa	1.64E-14	99
Middle Tuscaloosa	0	91

Source: Carlson (2010)

Table 16. Well leakage base case parameters (for definitions of parameters, see Appendix B)

Parameter	Value
k_w	1.40E-14 m^2
r_w	0.11 m
μ	5.71E-05 kg/m-s
ρ	693.844 kg/m^3
p_b	13889520 Pa (2,000 psi)
d	1,102 m
Δz	1 m

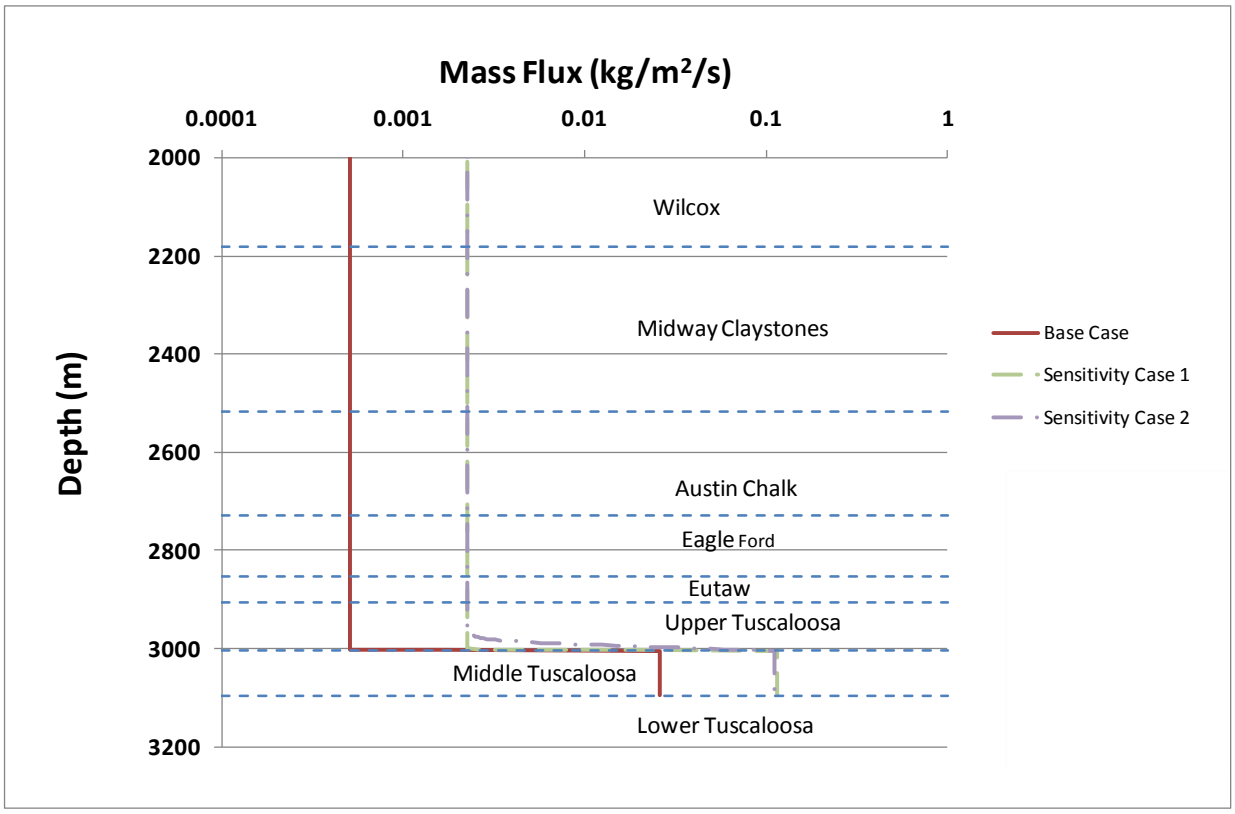

Figure 46. Results for Flow in P&A Wells at the site

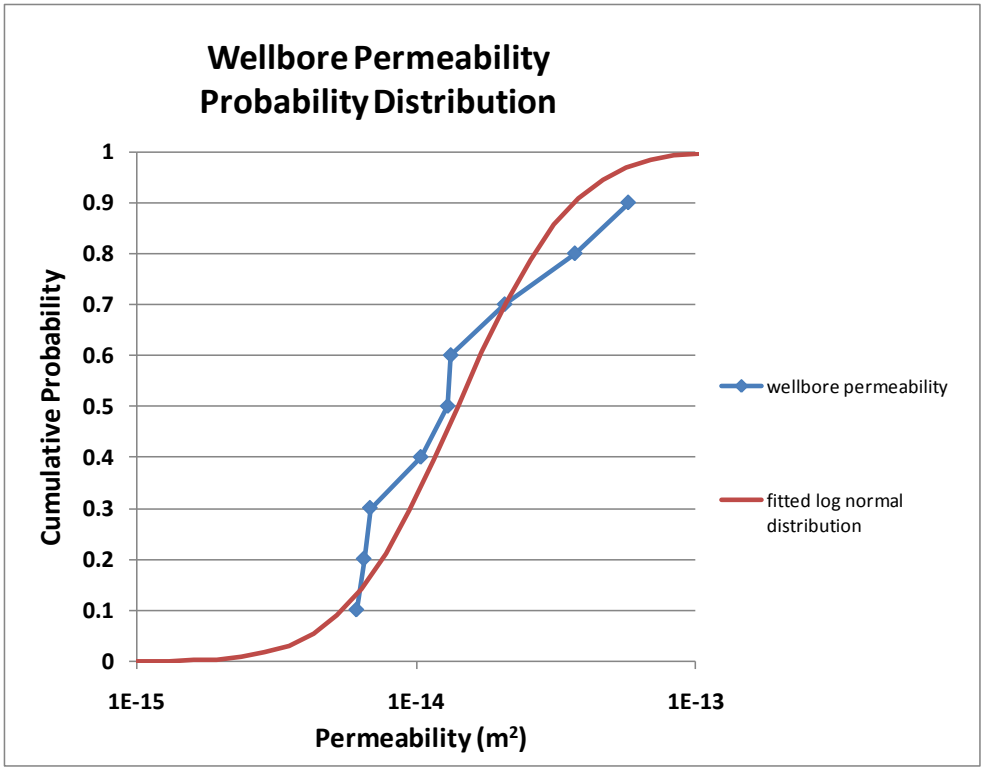

Figure 47. Wellbore Permeability Distribution for Wells without 100% Cement Bonds

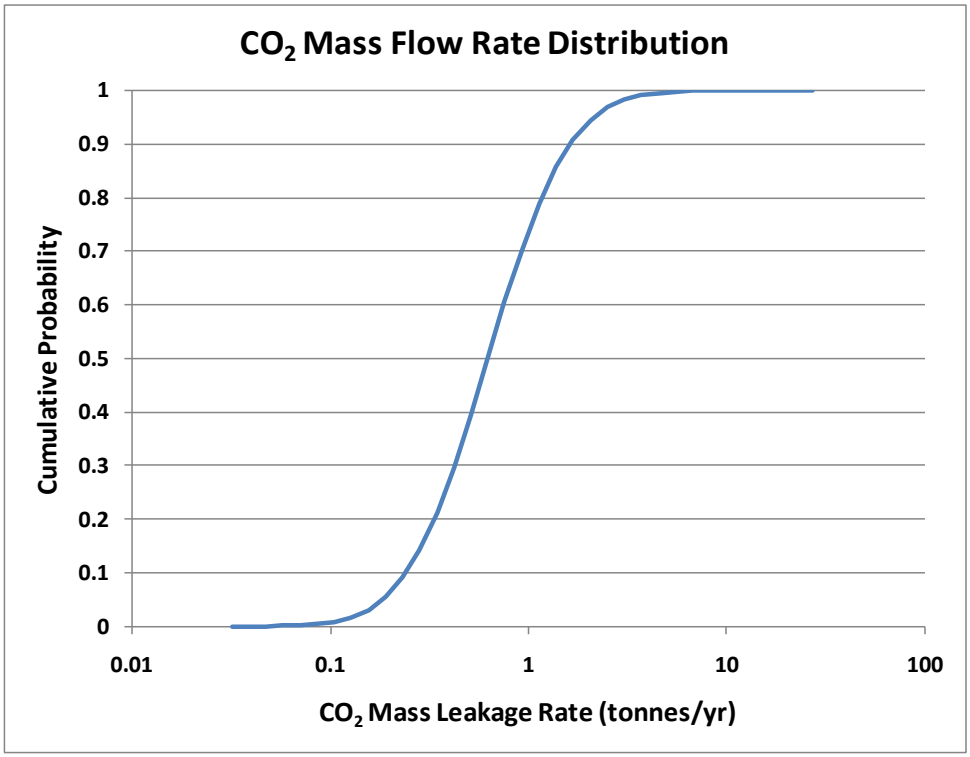

Figure 48. CO_2 Mass Leakage Rate Distribution for Wells without 100% Cement Bond

6 References

Bachu, S. and D.B. Bennion, 2009. Experimental Assessment of Brine and/or CO_2 Leakage through Well Cements at Reservoir Conditions, International Journal of Greenhouse Gas Control 3, 494–501.

Boswell, E.H. and G.A. Bednar, 1985. Ground-water resources of the Natchez area, Mississippi: U.S. Geological Survey Water-Resources Investigations Report WRI84-4341, 53p.

Bourgoyne, A.T. and S.L. Scott, 1999. A Review of Sustained Casing Pressure Occuring on the OCS, Louisiana State University, March 24-25, 1999.

Carlson, D., 2010, Influence of lithology on scaling factors for permeability of Louisiana geologic units: Gulf Coast Association of Geological Societies Transactions, v. 60, p. 87-101.

Chasteen, H.R., 1983. DOI: 10.1306/A1ADDABD-0DFE-11D7-8641000102C1865D, GCAGS Transactions.

Childress, S.C., 1976. Geology and Man in Adams County, Mississippi: *in* Environmental Geology Series, v. 4, S.C. Childress, M. Bograd, and J.C. Marble editors: Jackson, MS, State of Mississippi, 188 p.

Clark, J.E., D.K. Bonura, P.W. Papadeas and R.R. McGowen, 2003. Gulf Coast borehole closure test well near Orange, Texas: Proceedings of the 2nd International Symposium on Underground Injection Science and Technology, Lawrence Berkeley National Laboratory, Berkeley, California,October 22–23, LBNL-53837, unpaginated.

Cushing, E.M., E.H. Boswell and R.L. Hosman, 1964. General geology of the Mississippi embayment. U.S. Geol. Surv. Prof. Paper 448-B, 28 pp.

Gandl, L.A., 1982. Characterization of aquifers designated as potential drinking-water sources in Mississippi, U.S. Geological Survey Open-File Report OFR 81-550

Hines, L.E., 1950. The Cranfield Unit, cycling-pressure maintenance, part 1 – basis of the unitization agreement, World Oil, February.

Hovorka, S.D., J.-W. Choi, T.A. Meckel, R.H. Trevino, H. Zeng, M. Kordi, F.P. Wang, and J.-P. Nicot, 2009. Comparing Carbon Sequestration in an Oil Reservoir to Sequestration in a Brine Formation—Field Study, Energy Procedia 1 (2009) 2051–2056.

Huber, B.T., R.M. Leckie, R.D. Norris, T.J. Bralower and E. CoBabe, 1999. Foraminiferal Assemblage and Stable Isotopic Change Across the Cenomanian–Turonian Boundary in the Subtropical North Atlantic, Journal of Foraminiferal Research, v. 29, no. 4, p. 392–417.

IEA, 2005. A Review of Natural CO_2 Occurrences and Releases and their Relevance to CO_2 Storage, IEA Greenhouse Gas R&D Programme, Report 2005/8.

Jordan, P.D. and S.M. Benson, 2008. Well Blowout Rates and Consequences in California Oil and Gas District 4 from 1991 to 2005: Implications for Geological Storage of Carbon Dioxide, Lawrence Berkeley National Laboratory, http://escholarship.org/uc/item/2t05f9kc , 21 pp.

Kalkhoff, S.J., 1986. Brine Contamination of Freshwater Aquifers and Streams in Petroleum Producing Areas in Mississippi, Jackson, MS, U.S. Geological Survey Water Resources Investigations RepOrt WRI85-4117, 106p.

Klusman, R.W. 2005. Baseline Studies of Surface Gas Exchange and Soil-Gas Composition in Preparation for CO_2 Sequestration Research: Teapot Dome, Wyoming, AAPG Bulletin, v. 89, no. 8, pp. 981-1003.

Lynch, R.D., E.J. McBride, T.K. Perkins and M.E. Wiley, 1985. Dynamic Kill of an Uncontrolled CO_2 Well, Journal of Petroleum Technology, Society of Petroleum Engineers, July 1985, pp. 1267-1275.

Lu, J., K. Milliken, R. M. Reed, and S. Hovorka, 2011, Diagenesis and sealing capacity of the middle Tuscaloosa mudstone at the Cranfield carbon dioxide injection site, Mississippi, Environmental Geosciences, v. 18, no. , p.1-19

Luo, Z. and S. Bryant, 2010. Influence of Thermo-Elastic Stress on Fracture Initiation During CO_2 Injection and Storage, Proceedings of GHGT-10

Mancini, E.A., R.M. Mink, J.W. Payton and B.L. Bearden, 1987. Environments of Deposition and Petroleum Geology of Tuscaloosa Group (Upper Cretaceous), South Carlton and Pollard Fields, Southwestern Alabama, AAPG Bulletin, Volume 71, Issue 10. (October), Pages 1128 – 1142.

Mancini. E. A., 2005. Basin Analysis and Petroleum System Characterization and Modeling, Interior Salt Basins, Central and Eastern Gulf of Mexico, Annual Progress Report for Year 2, Department of Energy Award Number DE-FC26-03NT15395, 195p.

Mancini, E.A. and T.M. Puckett, 2005. Jurassic and Cretaceous Transgressive-Regressive (T-R) Cycles, Northern Gulf of Mexico, USA, Sedimentology, Vol. 2, No. 1, pp. 31-48.

Marble, J.C., 1976a. Configuration of the base of fresh water, Adams County, Mississippi: Mississippi Geological Survey.

Marble, J.C., 1976b. Water Resources: *in* Environmental Geology Series, v. 4, S. C. Childress, M. Bograd, and J. C. Marble editors: Jackson, MS, State of Mississippi, 188 p.

Mississippi Oil and Gas Board (MOGB), 1966. Cranfield Field, Cranfield unit, basal Tuscaloosa reservoir, Adams and Franklin Counties, p. 42- 58.

MDEQ, 2009. Records of public-supply wells in Mississippi: Mississippi Department of Environmental Quality, Office of Land and Water Resources, Groundwater Planning and Protection Division, May 22, 2009, 147p.

Meckel, T.A. and S.D. Hovorka, 2009. Results from continuous downhole monitoring (PDG) at a field-scale CO_2 demonstration project, Cranfield, MS, SPE 127087, Proceedings of 2009 SPE International Conference on CO_2 Capture, Storage, and Utilization, San Diego, California, USA, November 2-4, 2009.

Meckel, T.A., and S.D. Hovorka, 2010. Above-Zone Pressure Monitoring as a Surveillance Tool for Carbon Sequestration Projects, SPE paper # 139720.

Oldenburg, C. M., S.L. Bryant and J.-P. Nicot, 2009. Certification framework based on effective trapping for geologic carbon sequestration: International Journal of Greenhouse Gas Control, v. 3, p. 444–457.

Oldenburg, C.M. and A.J.A. Unger, 2003. On leakage and seepage from geologic carbon sequestration sites: unsaturated zone attenuation, *Vadose Zone Journal*, 2(3): 287-296, August 2003.

Renken, R. A., 1985. The hydrogeologic framework for the southeastern Coastal Plain aquifer system of the United States, U.S. Geological Survey Water-Resources Investigations Report WRI 84-4243

Renken, R.A., 1998. Ground Water Atlas of the United States: Segment 5, Arkansas, Louisiana, Mississippi: U.S. Geological Survey Hydrologic Atlas HA 730-F, 28p., http://pubs.usgs.gov:80/ha/ha730/index.html, last accessed October 2009.

Schlumberger, 2009. CBL Parameters from Schlumberger Interpretation Charts, Houston, TX, , Appendix A, calculated from the Interpretation Chart M-1 (in Schlumberger, 1989, Schlumberger Interpretation Charts Cased-Hole Log Principles/Applications, Houston, TX, Schlumberger).

Studlick, J.R.J., R.D. Shew, G.L. Basye and J.R. Ray, 1990. A giant carbon dioxide accumulation in the Norphlet Formation, Pisgah Anticline, Mississippi, in Sandstone Petroleum Reservoirs, eds J. H. Barwis, J. G. McPherson, and J. R. J. Studlick, p.181-203.

Stevens, S., 2005. Natural CO_2 Fields as Analogs for Geologic CO_2 Storage, in Thomas, D.C. 2005. Carbon Dioxide Capture for Storage in Deep Geologic Formations, Volume 2, Elsevier.

Strom, E.W., D.E. Burt Jr., and W.T. Oakley, 1995. Hydrogeology and Analysis of Groundwater Withdrawal from the Catahoula Aquifer System in the Natchez Area, Adams County, Mississippi, USGS Water Resources Investigation Report 95-4171. 32 pp.

Warner, D.L. and C.L. McConnell, 1990. Abandoned oil and gas industry wells-A quantitative assessment of their environmental implications: with emphasis upon the Lower Tuscaloosa sand

oil-producing trend of Mississippi and Louisiana, prepared for the American Petroleum Institute, June 1990, 45p.+Appendices

Warner, D.L. and C.L. McConnell, 1993. Assessment of environmental implications of abandoned oil and gas wells, Journal of Petroleum Technology, September 1993, p.874-880; also listed as SPE20692 (1996).

Warner, D.L., L. Koederitz and R.C. Laudon, 1997. Application of an area-of-review (AOR) concept to the east Texas field and other selected Texas oil fields: University of Missouri–Rolla, Final Report for U.S. Department of Energy Grant No. DE-FG22-94MT-94002, 402 p.

Watson. T.L. and S. Bachu, 2009. Evaluation of the Potential for Gas and CO_2 Leakage along Wellbores, SPE# 106817-PA.

Williamson, A.K. and H.F. Grubb, 2001. Ground-water flow in the Gulf Coast aquifer systems, south-central United States, U.S. Geological Survey Professional Paper, PP 1416-F, 173p. + 11 plates.

Yang, C., K. Romanak, S.D. Hovorka, J. Paine, J. Lu, R. Trevino, R. Holt and J. Lindner, 2009. Phase III Task 9.1.3b: Surface Monitoring Plan SECARB Phase III (Early) Project at Cranfield: Milestone report, October 12, 2009: prepared for SSEB.

Zhou, Z., C.J. Ballentine, M. Schoell and S. Stevens, 2007. Noble Gases in Jackson Dome Gas Deposits: Identifying and Quantifying Natural CO_2 Sequestration Processes, Proceedings of the 4th Mini Conference on Noble Gases in the Hydrosphere and in Natural Gas Reservoirs held at GFZ Potsdam, Germany, 28.02.-02.03.2007.

Websites:

Southeast Regional Carbon Sequestration Partnership:
http://www.secarbon.org/secarbprogrambackground.html

U.S. Climate Data:
http://www.usclimatedata.com/climate.php?location=USMS0255

USGS (Historic Earthquakes: New Madrid Earthquakes 1811-1812):
http://earthquake.usgs.gov/earthquakes/states/events/1811-1812.php.

USGS (Historic Earthquakes: Near Charlseton, Mississippi Co, Missouri):
http://earthquake.usgs.gov/earthquakes/states/events/1895_10_31.php.

USGS (Mississippi):
http://earthquake.usgs.gov/earthquakes/states/mississippi/history.php.

USGS (Louisiana):

http://earthquake.usgs.gov/earthquakes/states/louisiana/history.php.

USGS programs such as the Regional Aquifer-System Analysis (RASA); all reports available at: http://ms.water.usgs.gov/

The EPA web site provided information on sole source aquifers: http://cfpub.epa.gov/safewater/sourcewater/sourcewater.cfm?action=SSA

MDEQ website. MDEQ includes the State Geological Survey (Office of Geology): http://www.deq.state.ms.us/MDEQ.nsf/page/Geology_home?OpenDocument)

MDEQ website. MDEQ includes the State Geological Survey (Office of Land and Water): http://www.deq.state.ms.us/MDEQ.nsf/page/L&W_Home?OpenDocument

MDEQ has a searchable dataset "Oil and Gas Online Search": (http://library.geology.deq.state.ms.us/) but it does not seem to include wells more recent than 1996 or to allow bulk download of well information.

Mississippi Oil and Gas Board: http://www.ogb.state.ms.us/

IHS Energy, a private vendor of energy-related information and prospective: http://www.ihs.com/

Natchez, Mississippi profile: http://www.city-data.com/city/Natchez-Mississippi.html

Sole Source Aquifer Program: http://www.epa.gov/region04/water/groundwater/r4ssa.html#shills

Index of downloads (Climate/Windrose/Mississippi): http://www.wcc.nrcs.usda.gov/ftpref/downloads/climate/windrose/mississippi/

Mississippi Wildlife, Fisheries, and Parks: http://www.epa.gov/region04/water/groundwater/r4ssa.html - shillshttp://home.mdwfp.com/pdfgallery.aspx?Albumid=84&Page=2

7 Appendix A. Certification Framework Concepts and Definitions

7.1 Overview

The purpose of the CF is to provide a framework for project proponents, regulators, and the public to analyze the risks of geologic CO_2 storage in a simple and transparent way to certify startup and decommissioning of geologic CO_2 storage sites. The CF currently emphasizes leakage risk associated with subsurface processes and excludes compression, transportation, and injection-well leakage risk. The CF is designed to be simple by (1) using proxy concentrations or fluxes for quantifying impact rather than complicated exposure functions, (2) using a catalog of pre-computed CO_2 injection results, and (3) using a simple framework for calculating leakage risk. For transparency, the CF endeavors to be clear and precise in terminology in order to communicate to the full spectrum of stakeholders. Definitions are presented in the next section, followed by brief description of the framework structure.

7.2 Definitions

- *Effective Trapping* is the proposed overarching requirement for safety and effectiveness.
- *Storage Region* is the 3D volume of the subsurface intended to contain injected CO_2.
- *Leakage* is migration across the boundary of the Storage Region.
- *Compartment* is a region containing vulnerable entities (e.g., environment and resources).
- *Impact* is a consequence to a compartment, evaluated by proxy concentrations or fluxes.
- *Risk* is the product of probability and consequence (impact).
- *CO_2 Leakage Risk* is the probability that negative impacts will occur to compartments due to CO_2 migration.
- *Effective Trapping* implies that CO_2 Leakage Risk is below agreed-upon thresholds.

7.3 Compartments and Conduits

In the CF, impacts occur to compartments, while wells and faults are the potential leakage pathways. Figure A-1 shows how the CF conceptualizes the system into source, conduits (wells and faults), and compartments HMR, USDW, HSE, NSE, and ECA, where

- ECA = Emission Credits and Atmosphere
- HS = Health and Safety
- NSE = Near-Surface Environment
- USDW = Underground Source of Drinking Water
- HMR = Hydrocarbon and Mineral Resource

7.4 Risk and Flow Chart

Figure A-2 shows the concepts of likelihood of the CO_2 source intersecting conduits, and the conduits having likelihood of intersecting compartments. In the CF, the probability of CO_2 leaking from the source to a compartment is the product of the two intersection probabilities.

Figure A-3shows a flow chart of CF logic and inputs and outputs.

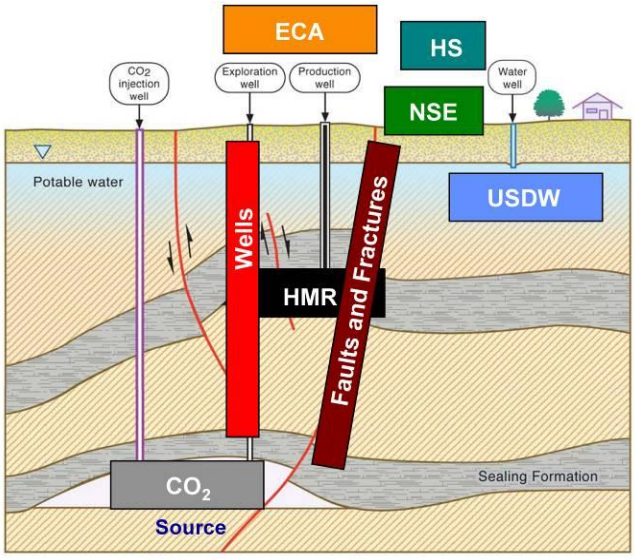

Figure A-1. Generic schematic of compartments and conduits in the CF.

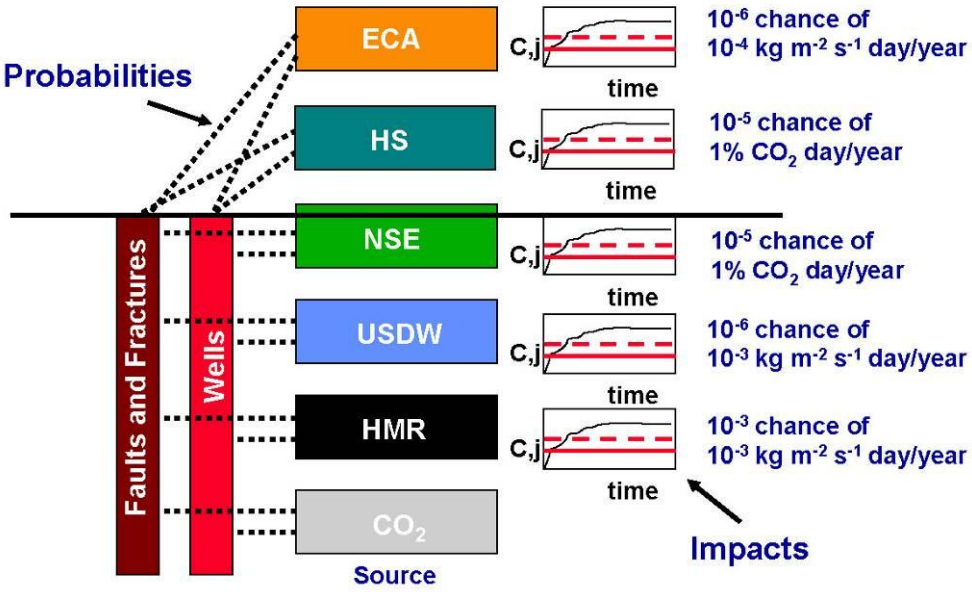

Figure A-2. CO_2 leakage risk schematic.

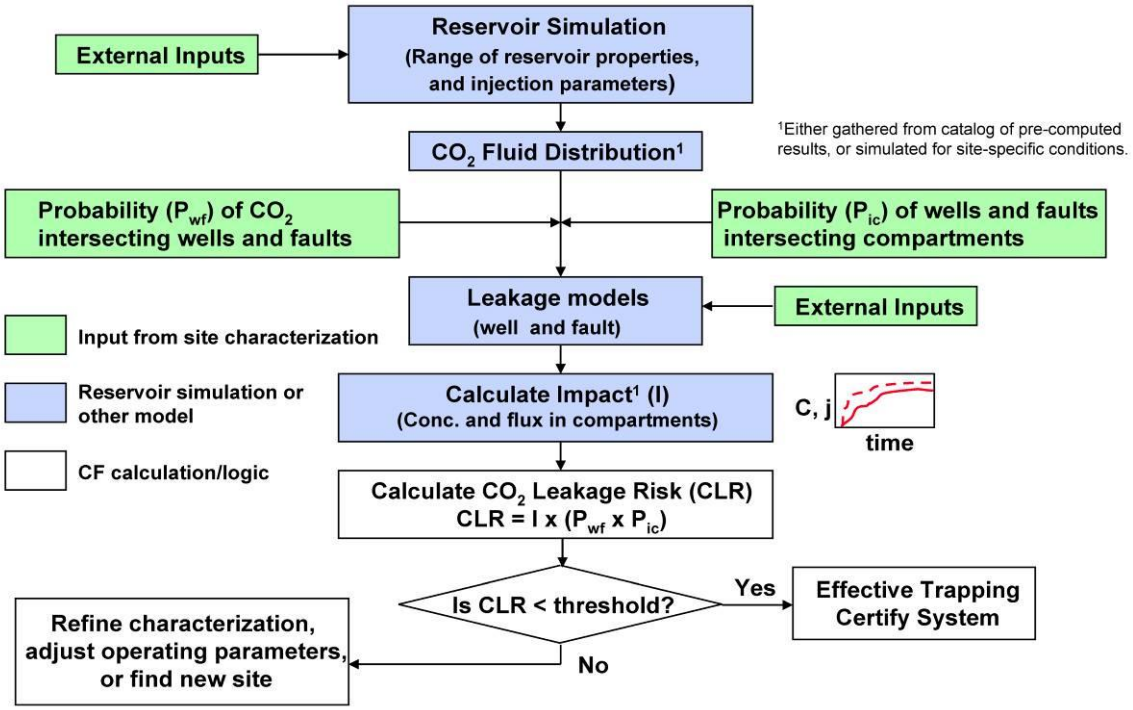

Figure A-3. Flow chart of CF process showing logic and inputs and outputs.

Table A.1. Tasks and Steps in the CF approach.

Task	Step	Name	Description
1	1	Project definition	Gather information on location, injection depth, properties of the formation, injection rate, number of wells, duration of injection, etc.
	2	Define storage region	Supplement the project definition with a practical and acceptable definition of the boundaries of the storage region.
	3	Identify vulnerabilities	E.g., wells and faults are potential leakage pathways; hydrocarbon and mineral resources, potable groundwater, near-surface environment, health and safety, and the atmosphere are potentially vulnerable entities that are grouped into "compartments" in the CF.
2	4	Characterize vulnerabilities	Determine properties of wells, faults, cap rock to the extent possible; determine properties of the compartments in which impacts may occur.
3	5	Injection and migration modeling	Simulate injection and migration of CO_2 and brine pressurization (or use catalog or other existing results) to estimate sizes of CO_2 plume and pressure perturbation.
	6	Estimate likelihood of leakage	From simulation results and spatial characterization of leakage conduits, estimate probability of leakage.
	7	Model impacts of leakage	Use specialized models in the CF to calculate fluxes or concentrations in the compartments as a function of time.
4	8	Risk calculation	Calculate CO_2 Leakage Risk (CLR) and Brine Leakage Risk (BLR) (CLR = likelihood of leakage x impact of leakage)

8 Appendix B. Flow Induced in P&A Wells by CO_2 Injection Pressure

An investigation of potential flow in P&A wells was conducted for the study site. The analysis is for a steady-state flow condition, based on one-dimensional (vertical), single-phase flow in the well coupled with horizontal (radial) single-phase flow from the well into the formation. The governing equations are:

Darcy's law for steady, single-phase flow in one-dimensional wellbore:

$$Q = -\frac{\pi r_w^2 k_w}{\mu}\left(\frac{dp}{dz} - \rho_C g\right) \tag{1}$$

where

Q = flow rate in well

r_w = radius of the well

k_w = permeability of the P&A wellbore

p = pressure at the well

μ = fluid viscosity

ρ_C = fluid density

g = gravitational acceleration

For steady-state, horizontal, radial flow from the wellbore over a wellbore depth increment dz,

$$dQ_\ell = \frac{2\pi k_f}{\mu \ln\left(\frac{d}{r_w}\right)}(p - p_e)dz \tag{2}$$

where

dQ_ℓ = differential leakage flow rate over depth increment dz

k_f = permeability of the formation

d = distance to constant pressure external boundary far from well

$p_e = \rho_f g z + p_s$ = hydrostatic pressure at external boundary

ρ_f = formation brine density

The leakage results in a change in flow rate in the well, which follows the following differential mass balance equation:

$$dQ = -dQ_\ell \tag{3}$$

Substituting from Equations (1) and (2) into Equation (3) gives,

$$\frac{\pi r_w^2 k_w}{\mu} d\left(\frac{dp}{dz}\right) = \frac{2\pi k_f}{\mu \ln\left(\frac{d}{r_w}\right)}(p - p_e)dz \tag{4}$$

and in the limit as $dz \to 0$,

$$\frac{d^2 p}{dz^2} = \frac{2k_f}{r_w^2 k_w \ln\left(\frac{d}{r_w}\right)}(p - p_e) \tag{5}$$

Introduce the following dimensionless variables,

$$\hat{p} = \frac{p - p_e}{p_b} = \frac{p(z) - \rho_f g z - p_s}{p_b} \tag{6}$$

$$\hat{z} = \frac{z}{r_w} \tag{7}$$

where p_b = pressure rise at the bottom of wellbore above hydrostatic such that $\hat{p}_b = 1$. The dimensionless surface pressure boundary condition is $\hat{p}_s = 0$.

Also, let

$$\omega^2 = \frac{2k_f}{k_w \ln\left(\frac{d}{r_w}\right)} \tag{8}$$

Simplifying Equation (5) using the dimensionless variables gives,

$$\frac{d^2\hat{p}}{d\hat{z}^2} = \omega^2 \hat{p} \tag{9}$$

Analytical solutions to Equation (9) can be developed, however, for the case of a multi-layer system, implementation of the analytical solution becomes complex. Therefore, a numerical solution scheme was developed. A finite difference expression for Equation (9) is,

$$-\hat{p}_{j-1} + \left(2 + \omega_j^2 \Delta\hat{z}^2\right)\hat{p}_j - \hat{p}_{j+1} = 0 \tag{10}$$

For $j = 2$ to $n-1$.

For $j = 1$,

$$\left(2 + \omega_j^2 \Delta\hat{z}^2\right)\hat{p}_j - \hat{p}_{j+1} = 0 \tag{11}$$

For $j = n$,

$$-\hat{p}_{j-1} + \left(2 + \omega_j^2 \Delta\hat{z}^2\right)\hat{p}_j = 1 \tag{12}$$

where n is the number of grids. The tridiagonal system represented by Equations (10) through (12) is solved using the Thomas algorithm.

The numerical method was verified using analytical results for a single-layer system and a two-layer system.

Single-Layer Test Case

The single-layer system has a depth of 140 m, a formation permeability of 10^{-16} m^2, and is described by the parameters in Table B-1:

Table B-1. Single-Layer Test Case Parameters

Parameter	Value
$\mathbf{k_w}$	1.00E-12 m^2
$\mathbf{r_w}$	0.05 m
μ	5.71E-05 kg/m-s
ρ	693.844 kg/m^3
$\mathbf{p_b}$	500 Pa
d	1102 m
$\Delta\mathbf{z}$	1 m

The analytical solution to Equation (9) for mass flux subject to the surface and bottom pressure boundary conditions is given by,

$$\dot{m} = -\frac{\rho_C k_w p_b}{\mu r_w}\left(\omega \frac{\exp\left(\omega\{\hat{z}-\hat{z}_b\}\right)+\exp\left(-\omega\{\hat{z}+\hat{z}_b\}\right)}{1-\exp\left(-2\omega\hat{z}_b\right)}+\frac{\Delta\rho g r_w}{p_b}\right) \tag{13}$$

This result is written so that flux is positive upward. The results for the analytical and numerical solution are shown in Figure B-1.

.

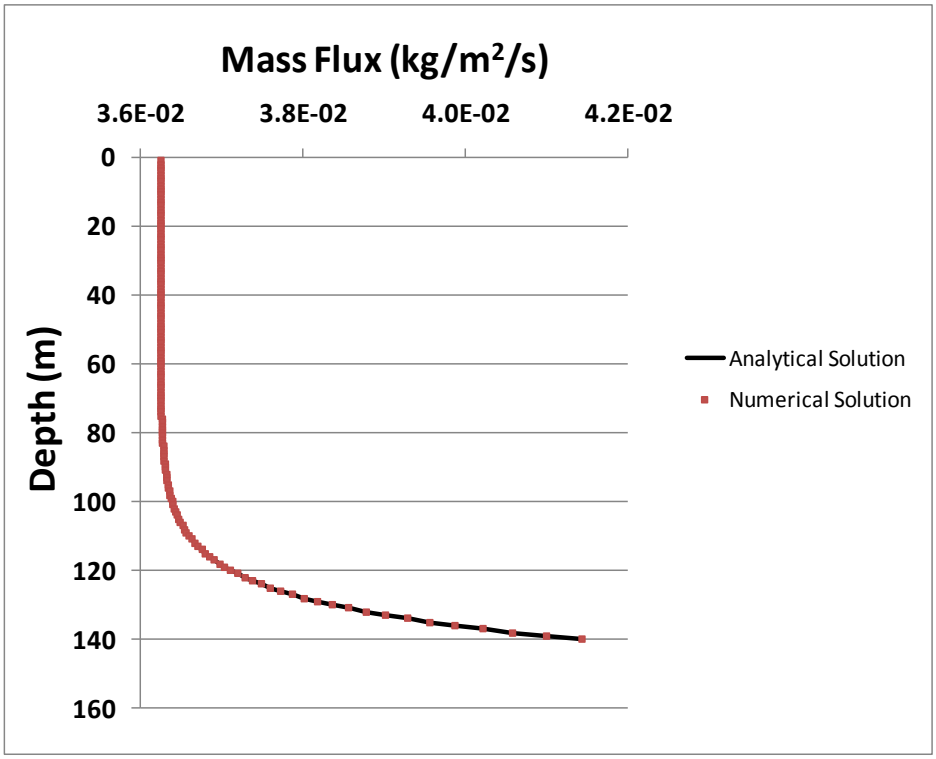

Figure B-1. Comparison of Analytical and Numerical Results for Single-Layer Test Case

Two-Layer Test Case

The two-layer test case consists of a 10-m layer at the base with a permeability of 10^{-13} m^2 and the remaining 130 m of overlying rock is impermeable, for a total depth of 140 m. For the two-layer case there are conditions requiring continuity of pressure and pressure gradient at the interface of the two layers in addition to the surface and bottom boundary pressure conditions. The two-layer system is described by the following parameters:

Table B-2. Two-Layer Test Case Parameters

Parameter	Value
$\mathbf{k_w}$	1.00E-12 m^2
$\mathbf{r_w}$	0.05 m
μ	5.71E-05 kg/m-s
ρ	693.844 kg/m^3
$\mathbf{p_b}$	500 Pa
D	1102 m
Δ**z**	1 m
$\mathbf{z_I}$	130 m

where z_I is the depth to the interface between layers 1 and 2.

The analytical solution to Equation (9) for mass flux in the upper layer is given by,

$$\dot{m} = -\frac{\rho_C k_w p_b}{\mu r_w} \times \left(\frac{2\omega_2}{\{\omega_2 \hat{z}_I - 1\}\exp(\omega_2 \hat{z}_I)\exp(-\omega_2 \hat{z}_b) + \{\omega_2 \hat{z}_I + 1\}\exp(-\omega_2 \hat{z}_I)\exp(\omega_2 \hat{z}_b)} + \frac{\Delta\rho g r_w}{p_b} \right) \tag{14}$$

where ω_2 refers to the value of ω in the second (lower) layer. This result is written so that flux is positive upward. The value of ω is zero in the upper layer, which leads to a linear pressure profile and a constant mass flux in that layer.

The analytical solution to Equation (9) for mass flux in the lower layer is given by,

$$\dot{m} = -\frac{\rho_C k_w p_b}{\mu r_w} \times \left(\frac{\omega_2\{\omega_2 \hat{z}_I + 1\}\exp(-\omega_2 \hat{z}_I)\exp(\omega_2 \hat{z}) - \omega_2(\omega_2 \hat{z}_I - 1)\exp(\omega_2 \hat{z}_I)\exp(-\omega_2 \hat{z})}{\{\omega_2 \hat{z}_I - 1\}\exp(\omega_2 \hat{z}_I)\exp(-\omega_2 \hat{z}_b) + \{\omega_2 \hat{z}_I + 1\}\exp(-\omega_2 \hat{z}_I)\exp(\omega_2 \hat{z}_b)} + \frac{\Delta\rho g r_w}{p_b} \right) \tag{15}$$

The results for the analytical and numerical solution are shown in Figure B-2. This result is written so that flux is positive upward.

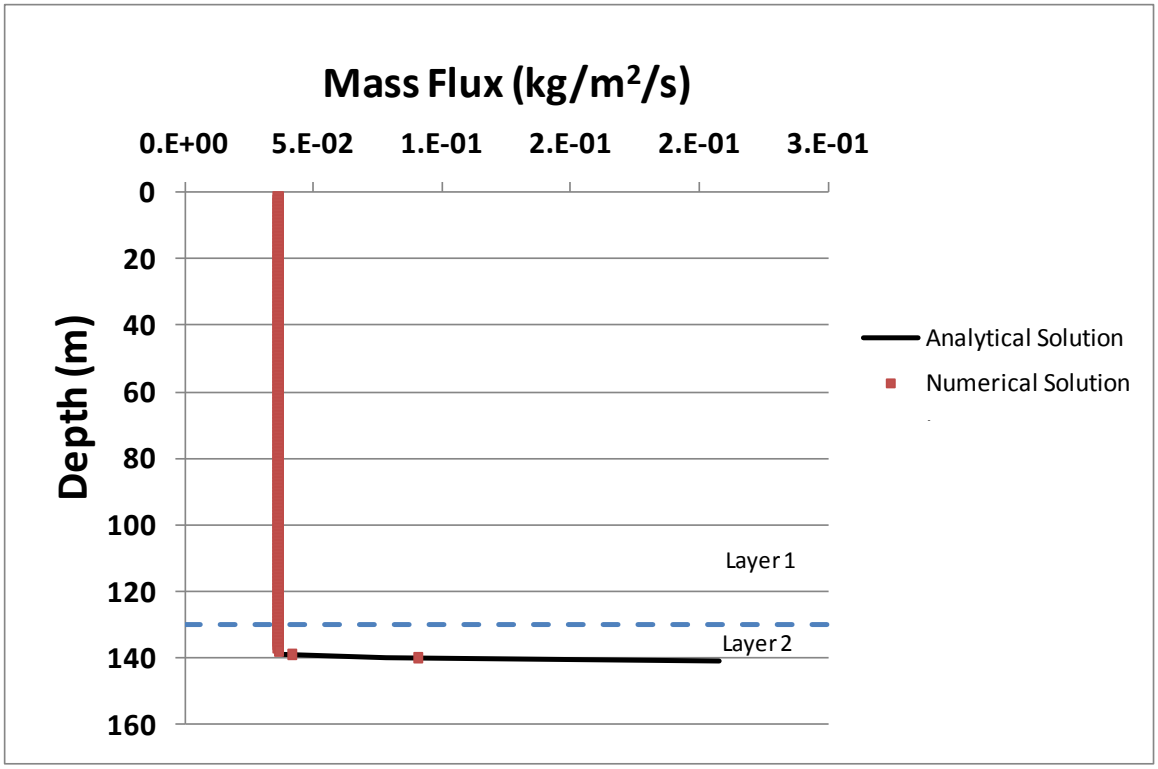

Figure B-2. Comparison of Analytical and Numerical Results for Two-Layer Test Case

Analysis of Wellbore Permeability

Data from cement bond logs (CBLs) were used to evaluate wellbore permeability. A small subset of wells at the site have (CBL) measurements. These measurements are shown in Figure 34. To quantify the cement bond logs, measured permeabilities for intact and degraded cement made by Bachu and Bennion (2009) are used. These measurements indicate that intact cement has a very low permeability, 10^{-21} m^2, whereas degraded cement has permeability on the order of 10^{-15} m^2. The degraded cement contained annular gaps and cracks in the cement. The intact cement permeability is assigned to the "100%" and "good" categories from the CBL and the degraded cement permeability is assigned to the "bad" category. No specific measurements are available for the uncemented intervals. These are assigned a value of 10^{-11} m^2 to allow for quantitative evaluation. A permeability of 10^{-11} m^2, or about 10 darcies, is similar to that of a uniform 0.1 mm fine sand. The mean well permeability is not particularly sensitive to the higher permeability of the uncemented section because the averaging is harmonic, as discussed below.

Mean permeabilities for the wells were computed using the permeability assignments given above and the lengths of the sections in the CBL shown in Figure 34. The means are harmonic because of the serial nature of the permeability variations. The mean permeability is given by the following,

$$k_m = \frac{L}{\sum_{j=1}^{4} \frac{\ell_j}{k_j}} \tag{1}$$

where j denotes the CBL category, ℓ_j is the length of wellbore within a given category, k_j is the permeability of the CBL category, and $L = \sum_{j=1}^{4} \ell_j$ is the total wellbore length from the top of the upper Tuscaloosa to the ground surface. The results of the averaging for wells that penetrate the Tuscaloosa are given in Table B-3. Note that the eight wells with any (even a small) section of 100% or good cement bonds have mean permeabilities, about 10^{-19} m^2 or lower. These permeabilities are orders of magnitude lower than well 23037000480001, which has a mean permeability of 1.3×10^{-14} m^2. Therefore, well permeability is negligible unless all of the cement falls into the "bad" category on the CBL. The fact all of the cement is identified as "bad" in only one of the nine wells is used to segregate the total population of P&A wells into a smaller group of more permeable wells (1/9 of the total) and the remainder of the P&A wells that would have very low permeabilities and, as a result, negligible CO_2 releases.

The permeability of wells with exclusively "bad" cement is a harmonic average of the permeability of the section with bad cement and the permeability of the section without cement. Because the permeabilities of these sections are fixed, the distribution of well permeabilities is a function only of the lengths of the two sections. If it is assumed that there is no correlation between the length of the cemented section and the cement categories on the CBL, the variable lengths of the cemented sections in the other eight wells can be used to develop a distribution of mean well permeability for the more permeable group of wells. Using this approach, the permeabilities of the nine wells with CBLs were computed by assigning the permeability of "bad" cement to all of the cement in the CBLs. The harmonic mean permeabilities for the nine wells were then expressed as a probability distribution based on an ordered ranking of the values. The empirical cumulative probabilities were assigned using the relationship $P_j = \frac{j}{n+1}$, where $n = 9$ is the total number of wells in the sample. The empirical distribution was fit to a theoretical log-normal distribution with the same mean and standard deviation as the data for use in the analysis. The results are shown in Figure 45.

Table B-3. Mean Wellbore Permeabilities for Wells with CBLs that Penetrate the Tuscaloosa

Well ID (Figure 1)	Mean Wellbore Permeability (m^2)
23001232910000	8.01025E-21
23001224880000	8.67778E-21
23001233420000	3.71904E-20
23001233650000	5.20663E-20
23001226220000	5.20666E-20
23001001940000	5.20666E-20
23001001780001	5.78519E-20
23001002490001	1.30166E-19
23037000480001	1.3001E-14

9 Appendix C. Pressure history at P&A well locations

1 Realization #1 (ten cells of a vertical profile displayed on each plot)

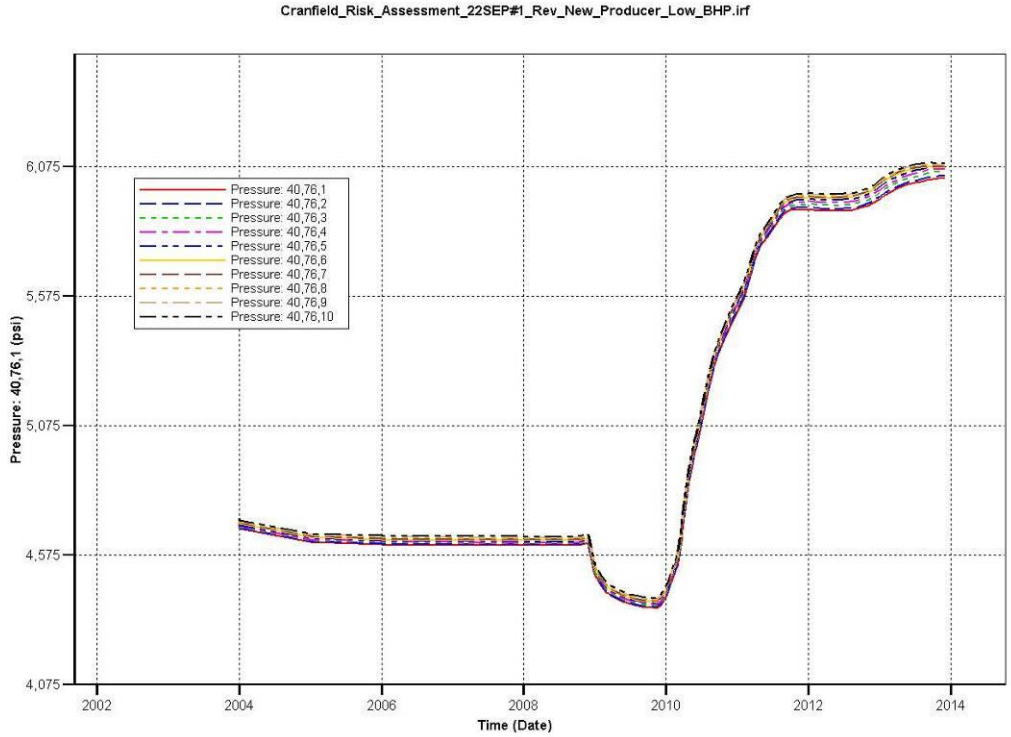

Pressure history at Cranfield Unit 7 (40, 76)

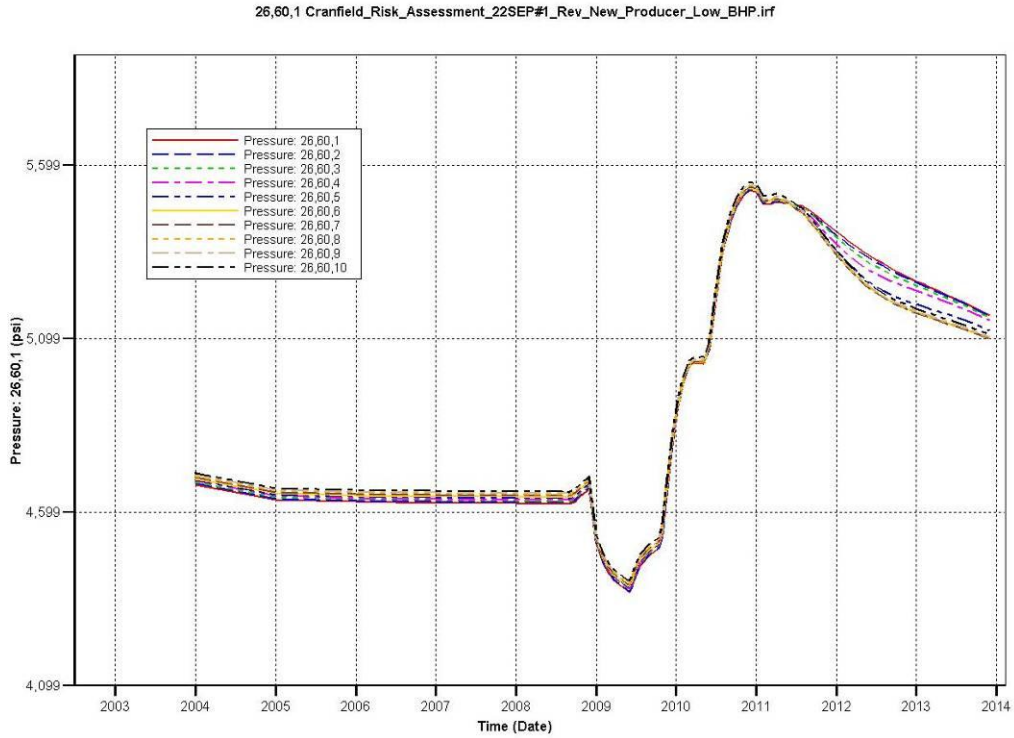

Pressure history at Cranfield Unit 4 (26, 60)

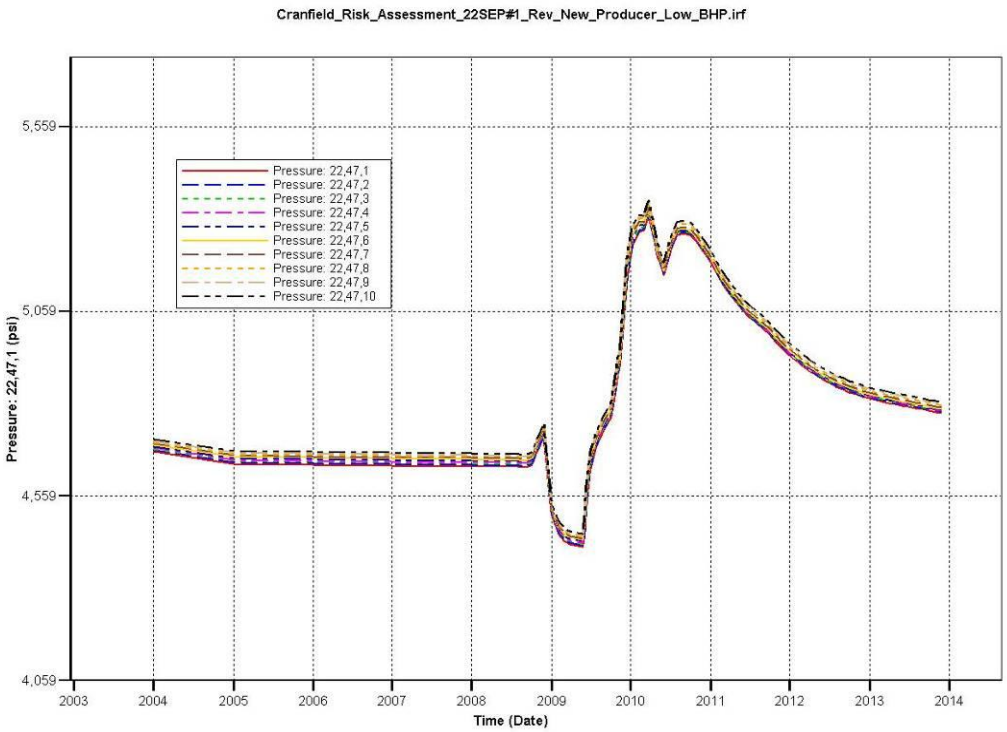

Pressure history at Vernon Johnson 1 (22, 47)

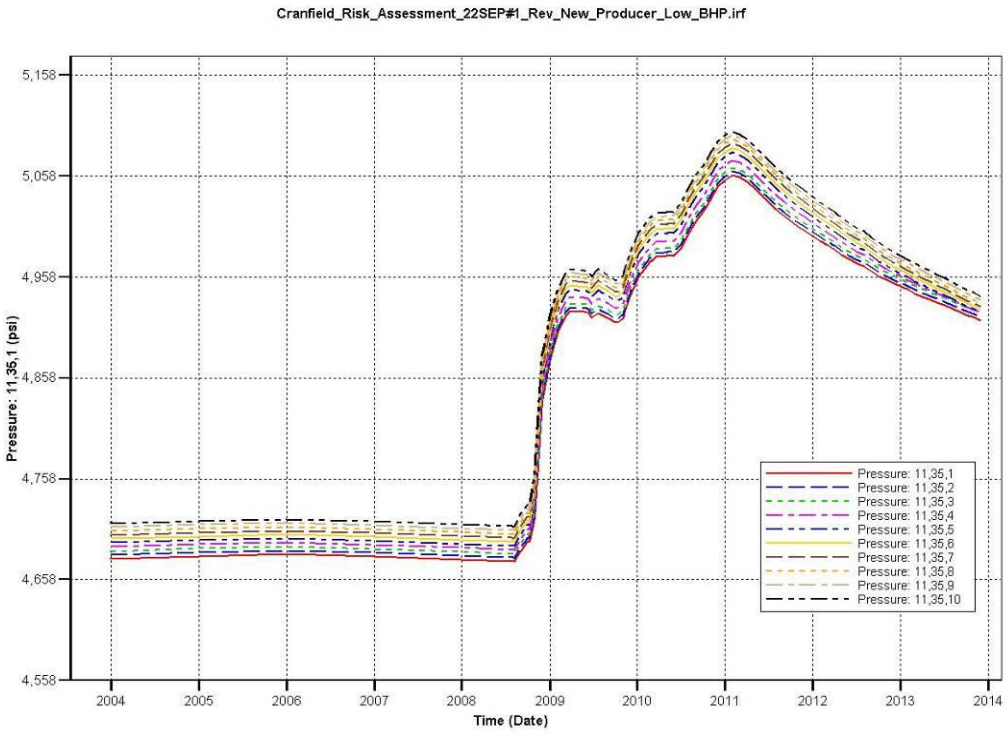

Pressure history at Armstrong 4 (11, 35)

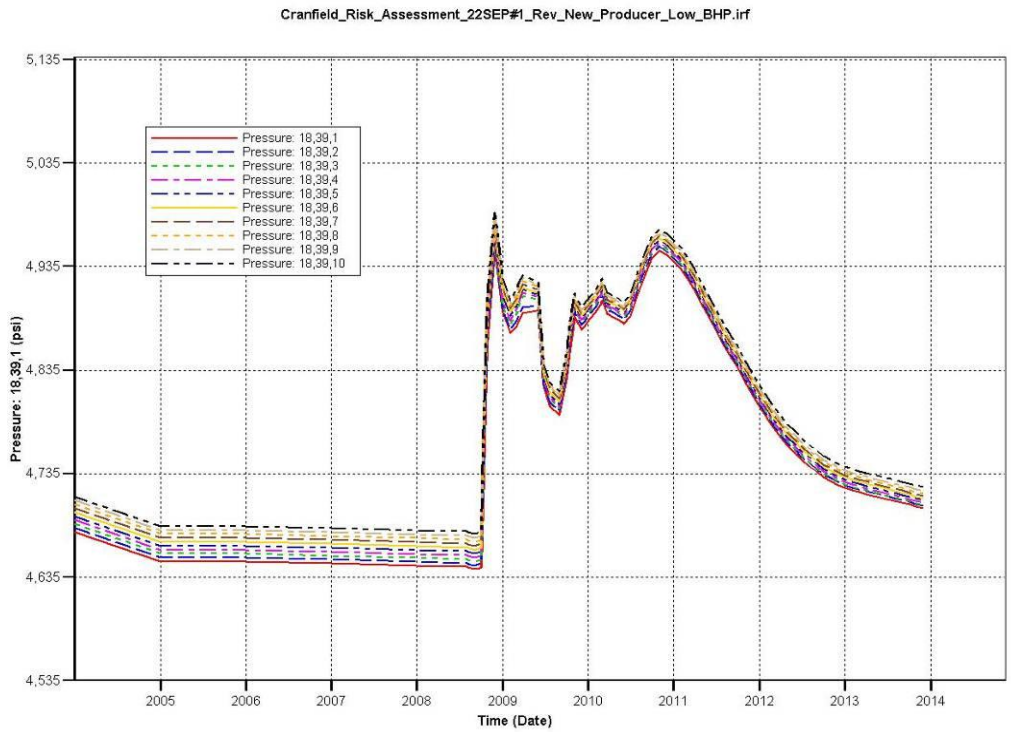

Pressure history at Armstrong 2 (18, 39)

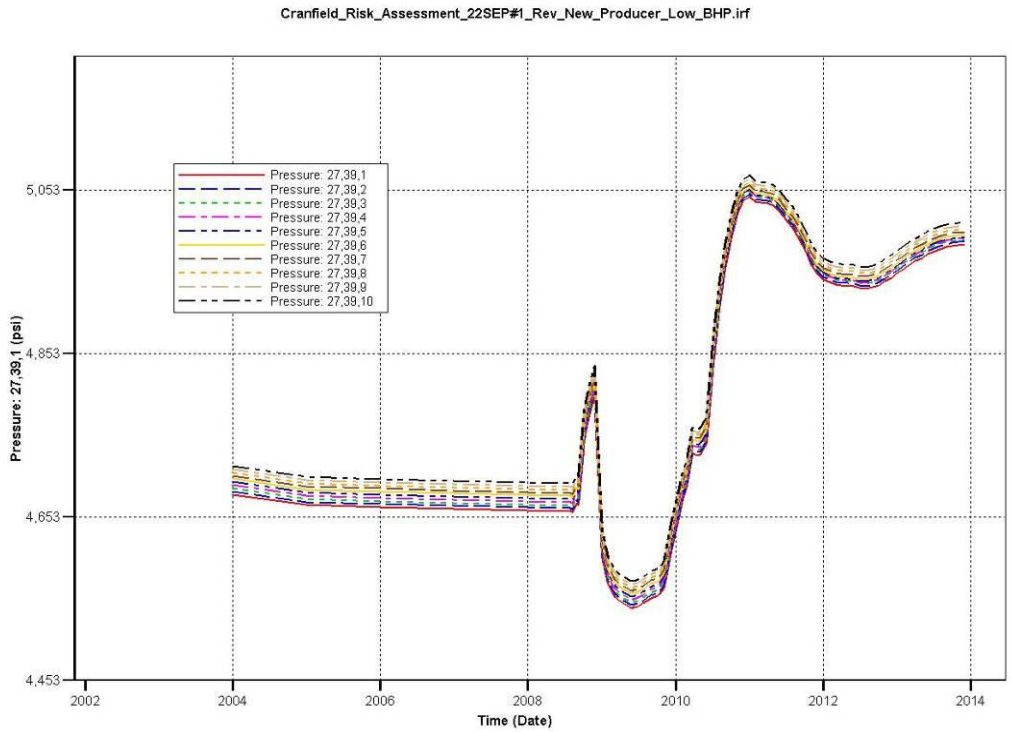

Pressure history at R G CALCOTE 1 (27, 39)

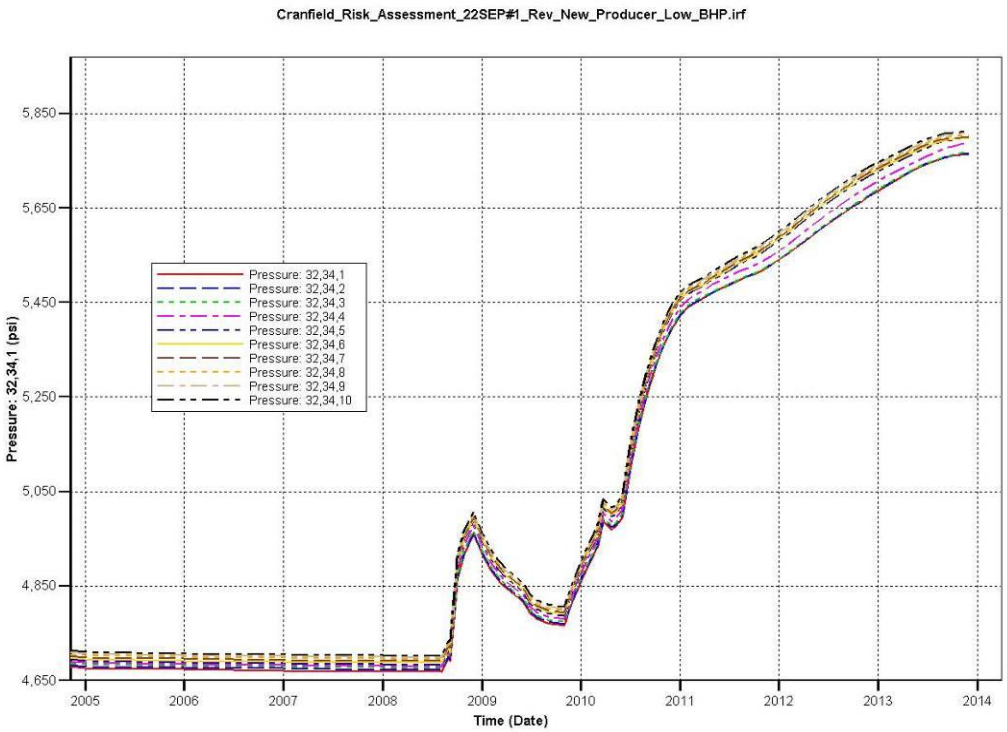

Pressure history at H H CROSBY ETAL 1 (32, 24)

2 Realization #2 (ten cells of a vertical profile displayed on each plot)

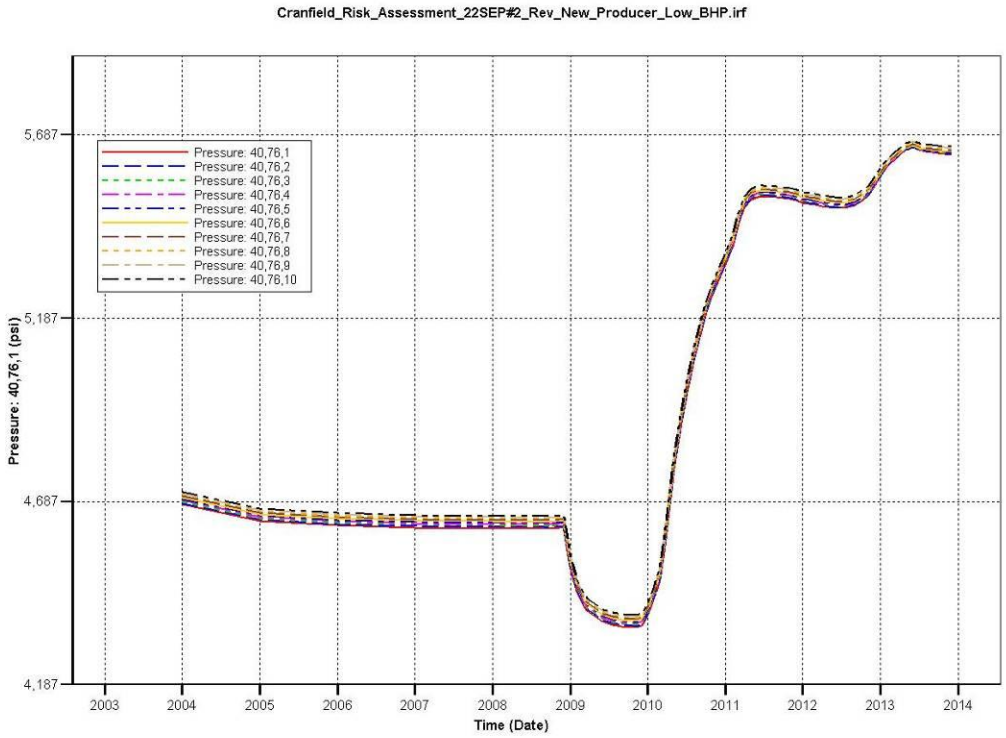

Pressure history at Cranfield Unit 7 (40, 76)

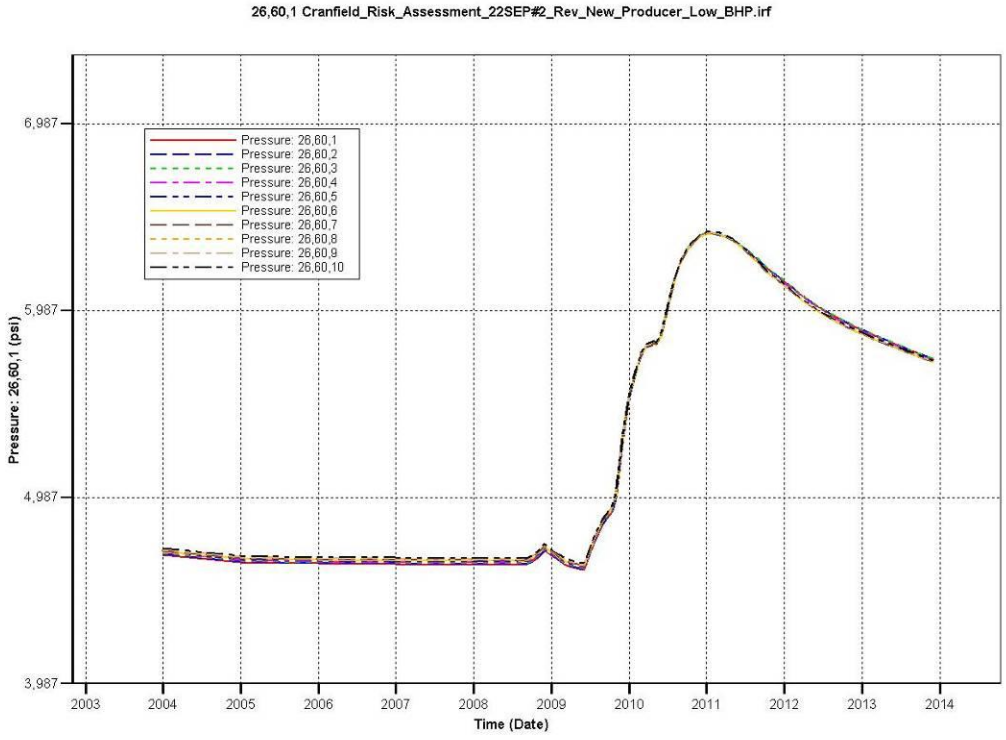

Pressure history at Cranfield Unit 4 (26, 60)

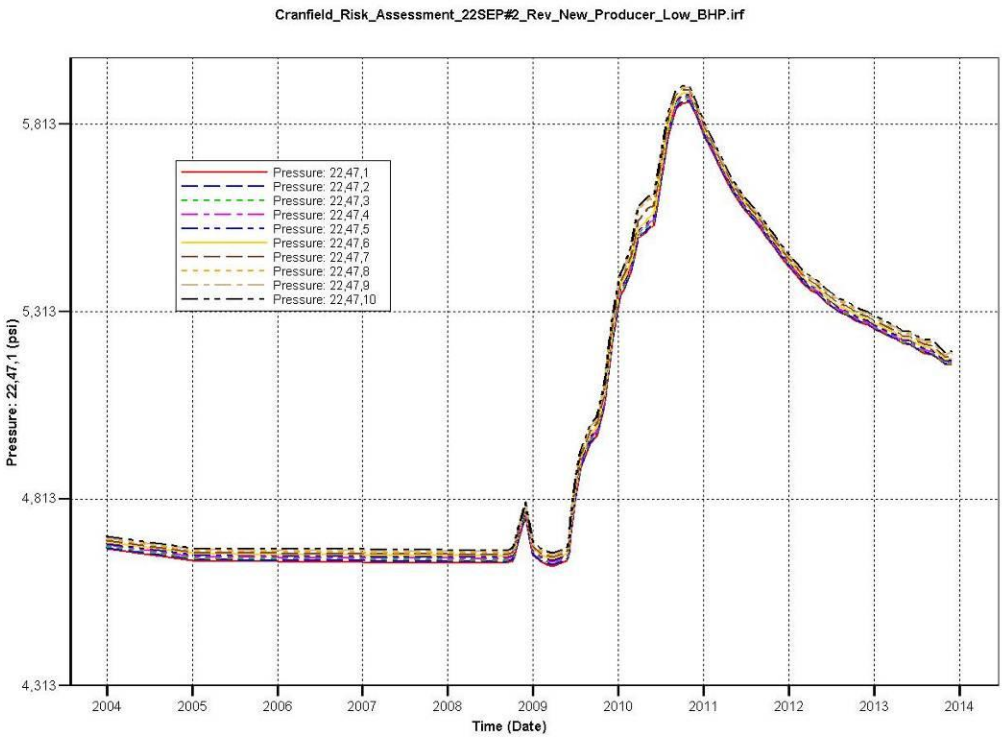

Pressure history at Vernon Johnson 1 (22, 47)

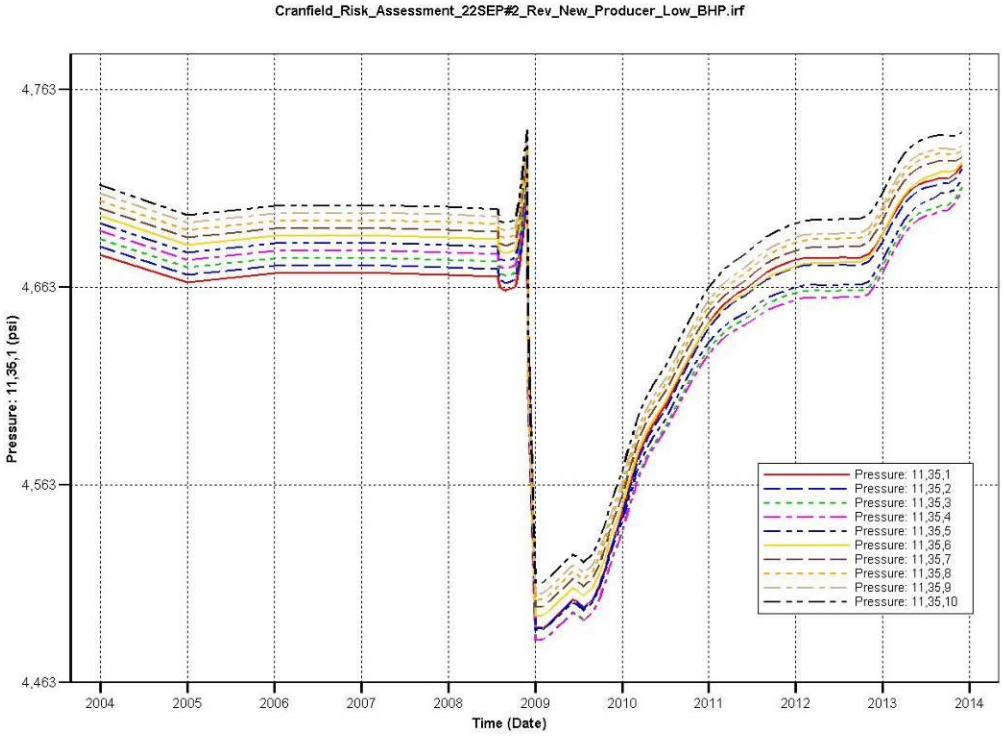

Pressure history at Armstrong 4 (11, 35)

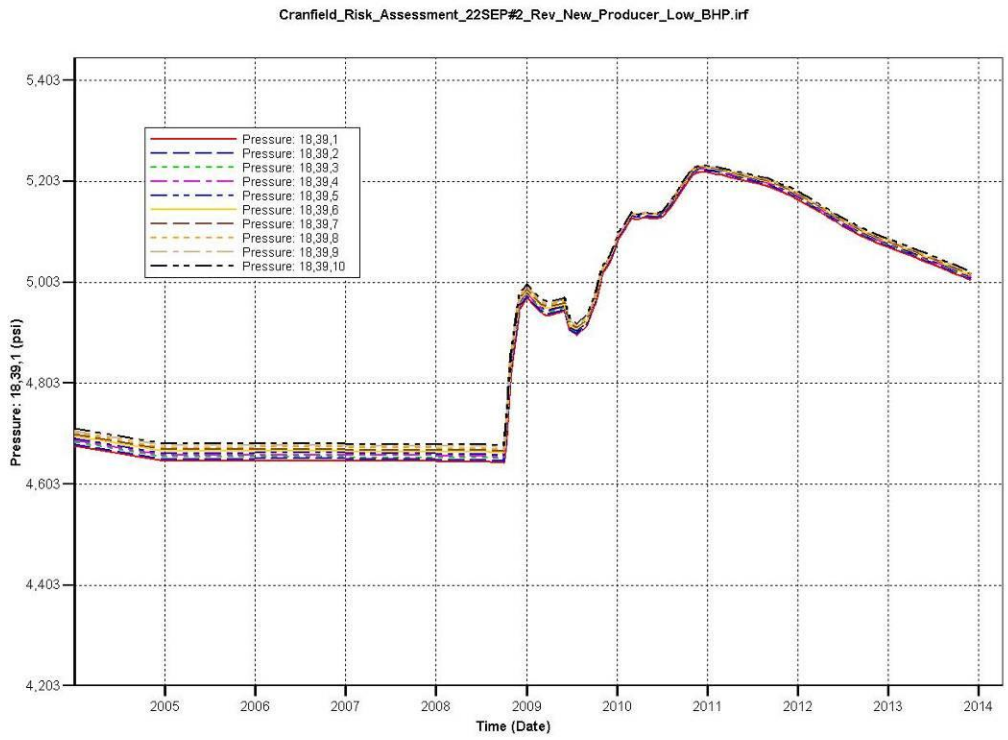

Pressure history at Armstrong 2 (18, 39)

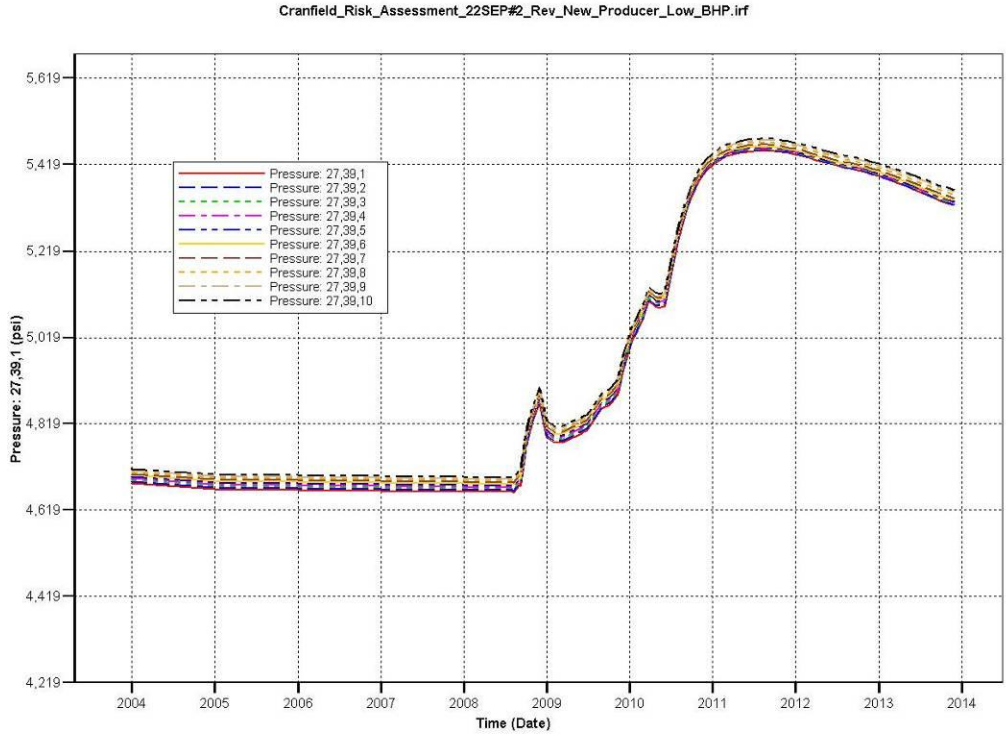

Pressure history at R G CALCOTE 1 (27, 39)

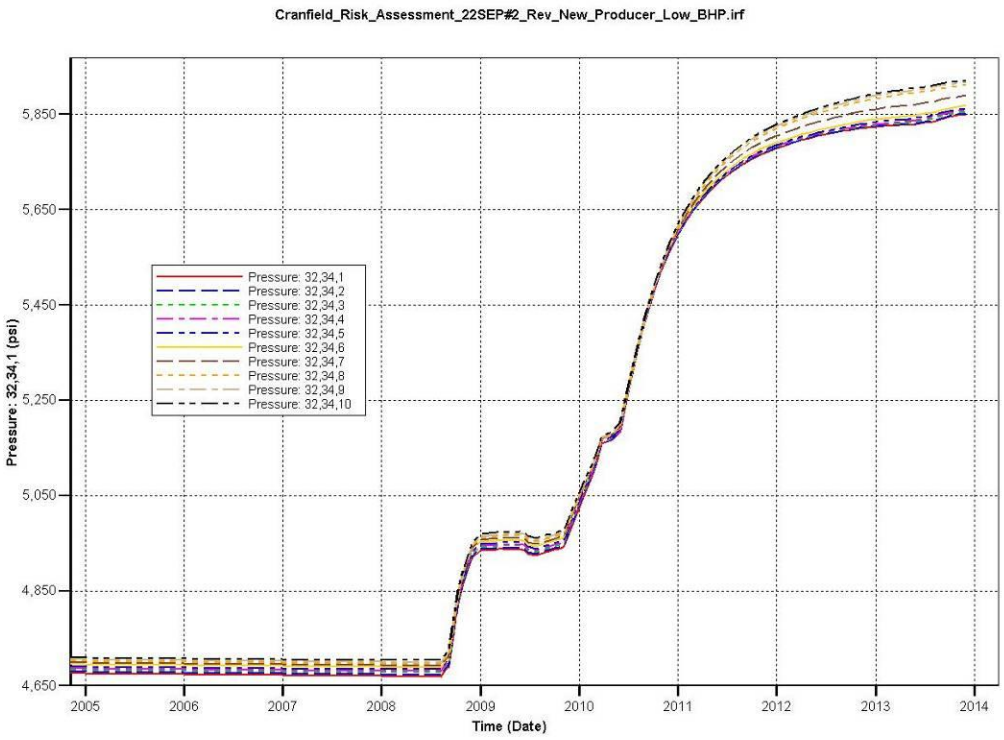

Pressure history at H H CROSBY ETAL 1 (32, 24)

3 Realization #3 (ten cells of a vertical profile displayed on each plot)

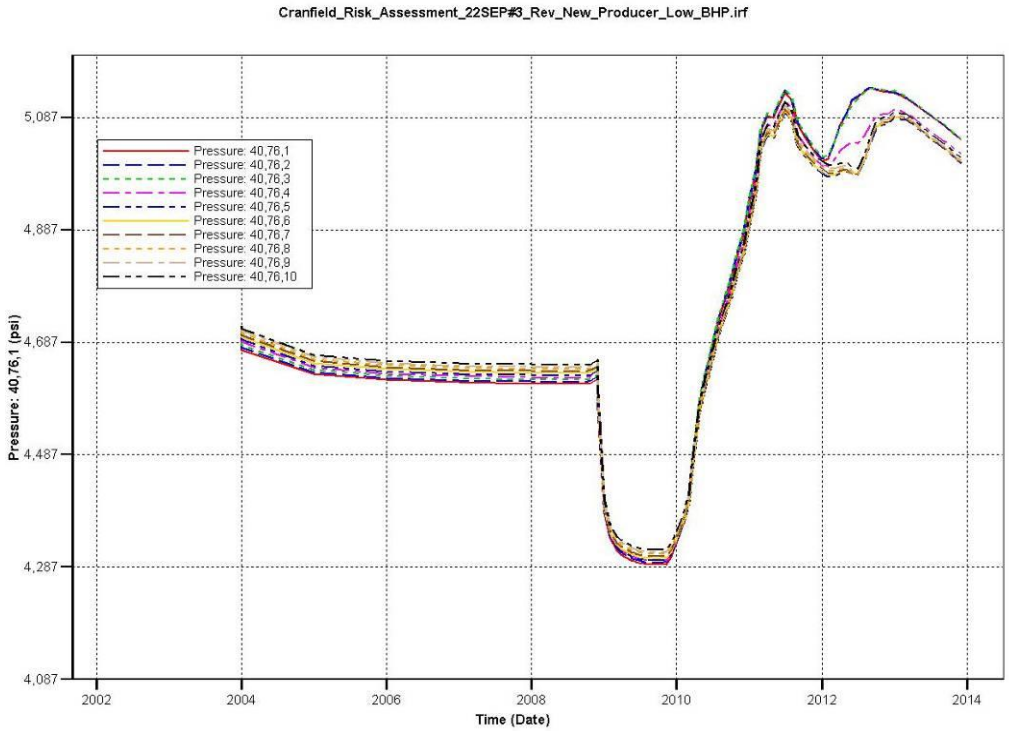

Pressure history at Cranfield Unit 7 (40, 76)

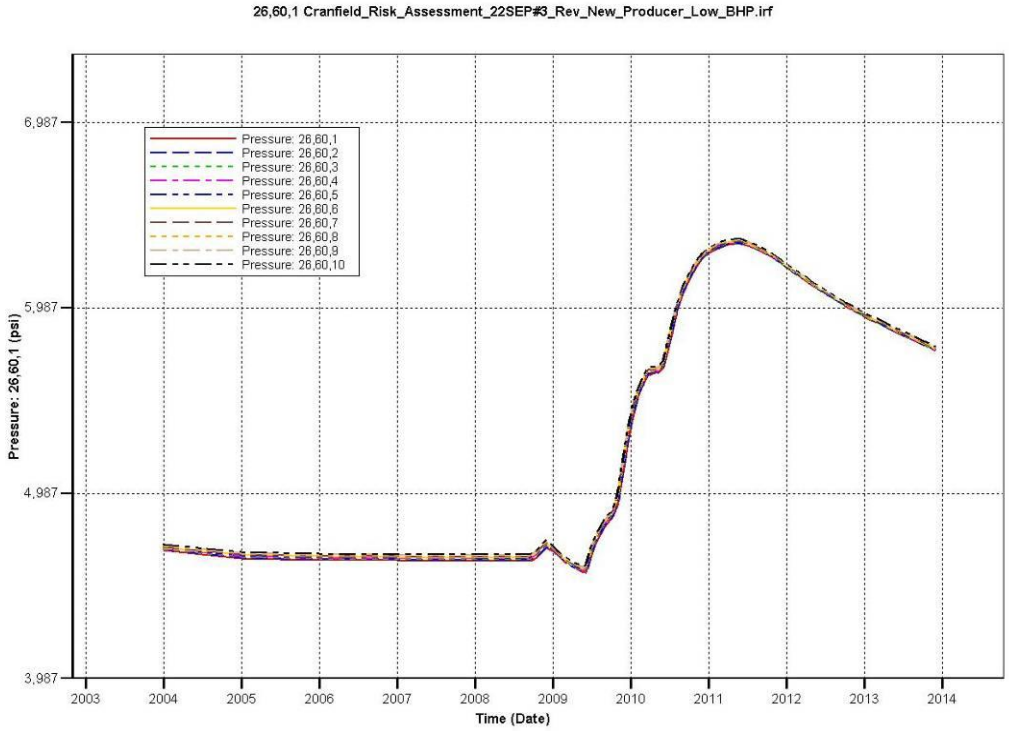

Pressure history at Cranfield Unit 4 (26, 60)

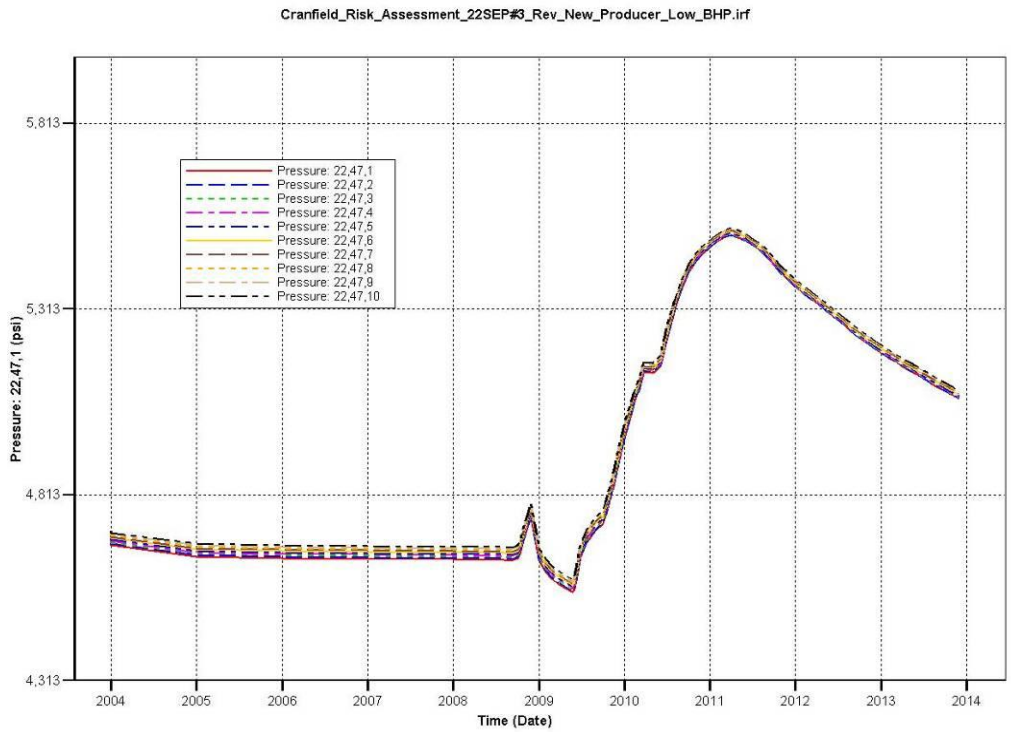

Pressure history at Vernon Johnson 1 (22, 47)

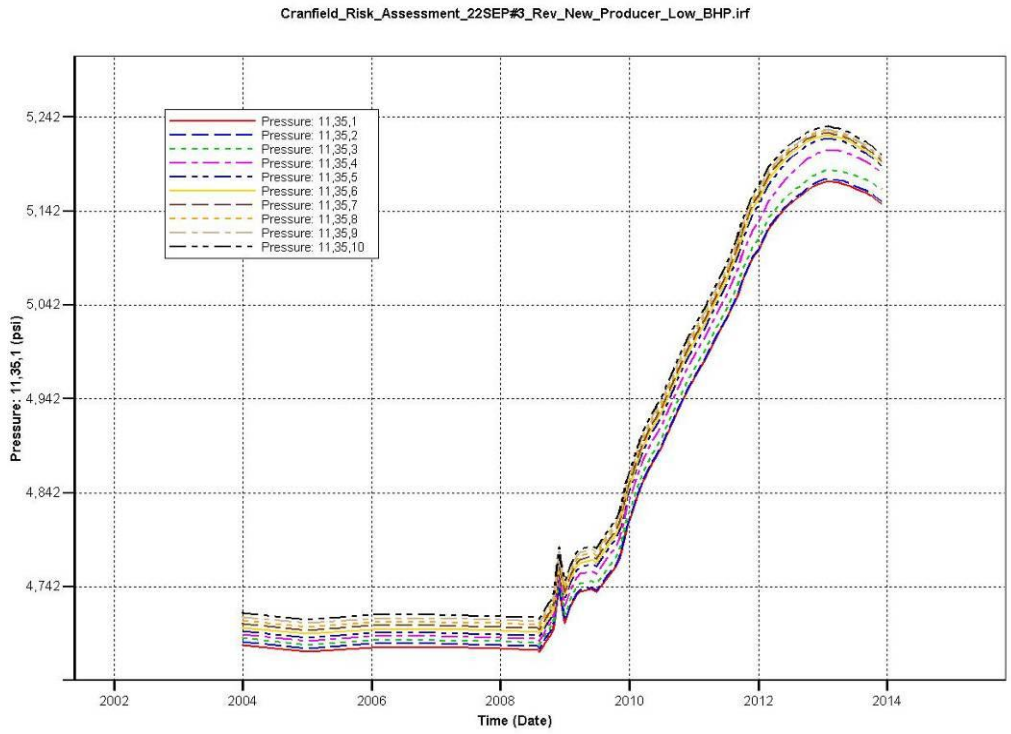

Pressure history at Armstrong 4 (11, 35)

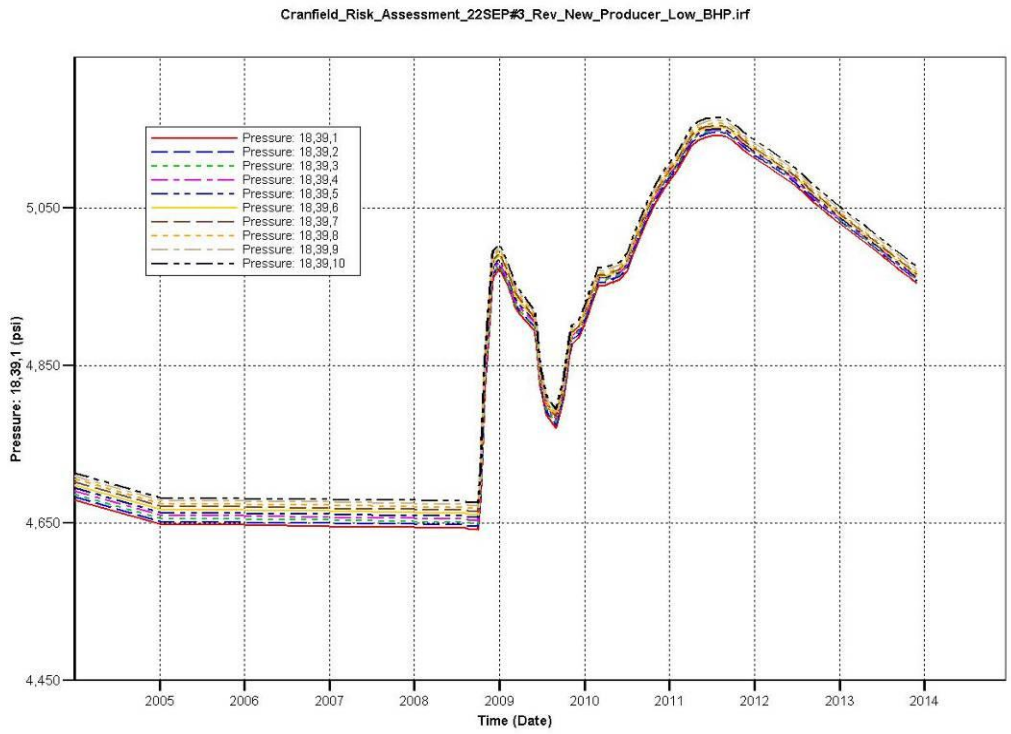

Pressure history at Armstrong 2 (18, 39)

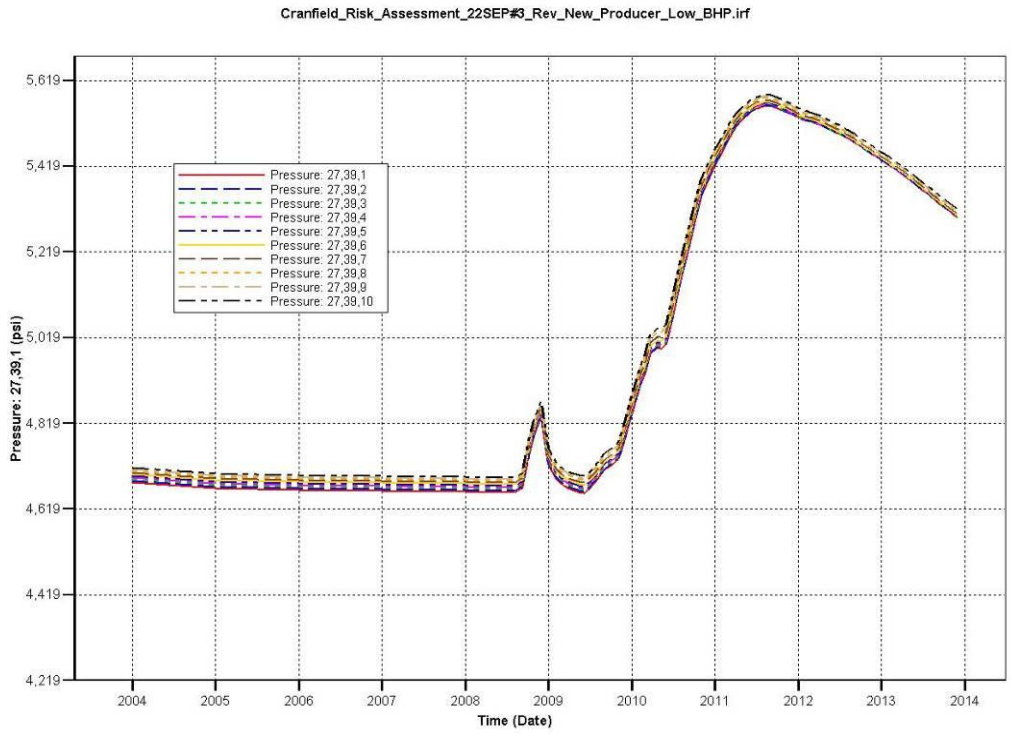

Pressure history at R G CALCOTE 1 (27, 39)

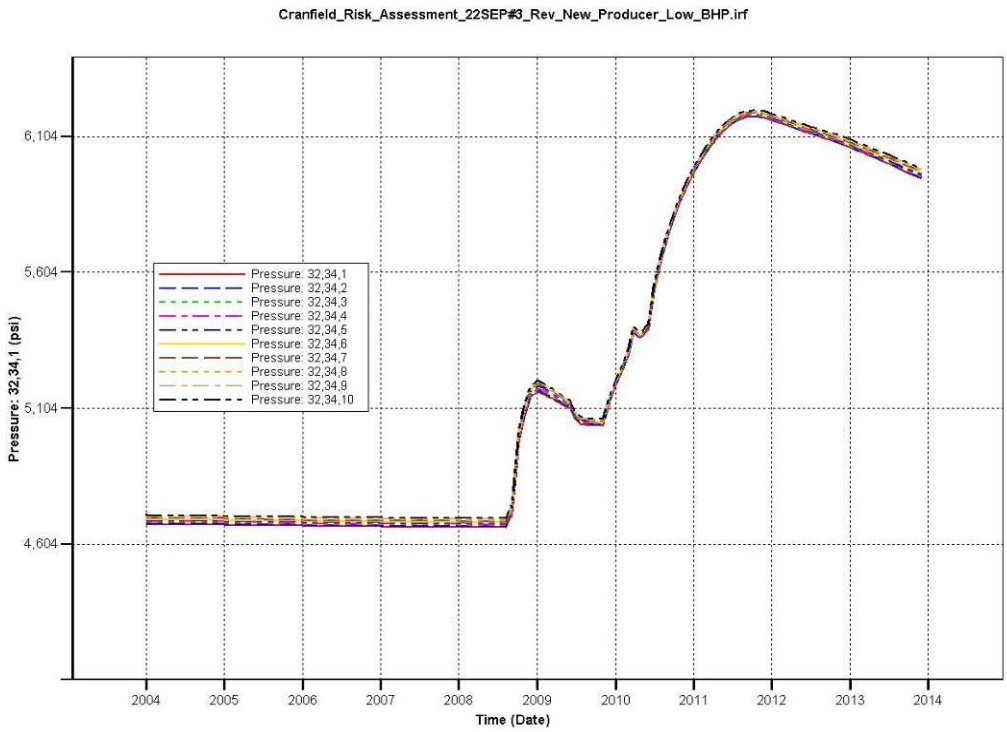

Pressure history at H H CROSBY ETAL 1 (32, 24)

4 Realization #4 (ten cells of a vertical profile displayed on each plot)

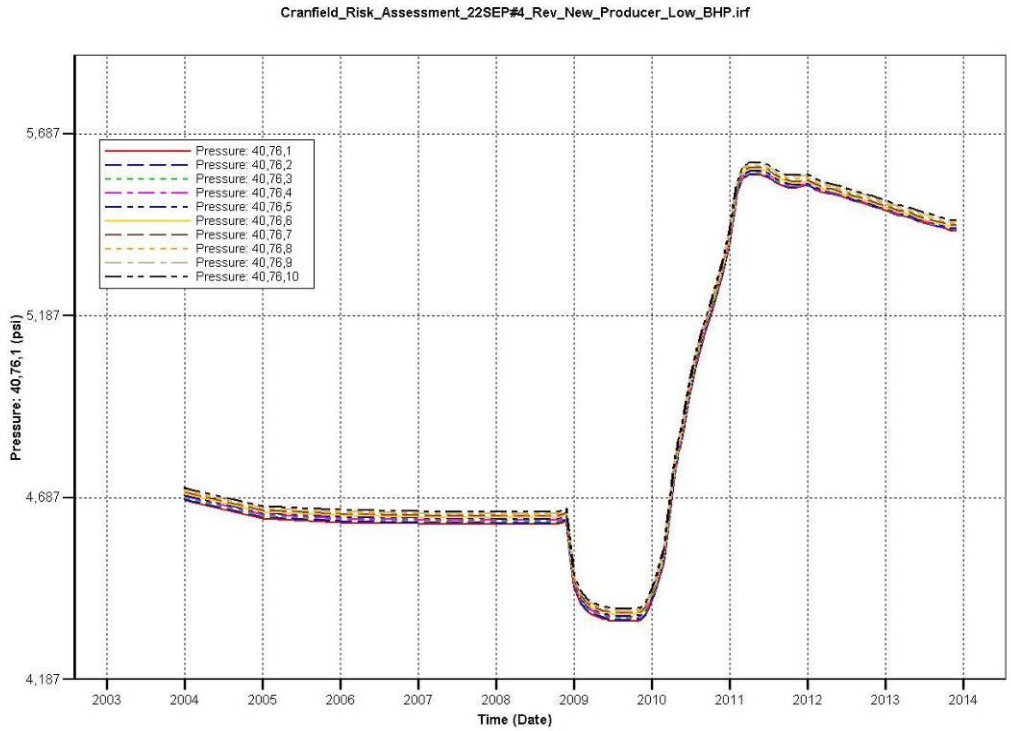

Pressure history at Cranfield Unit 7 (40, 76)

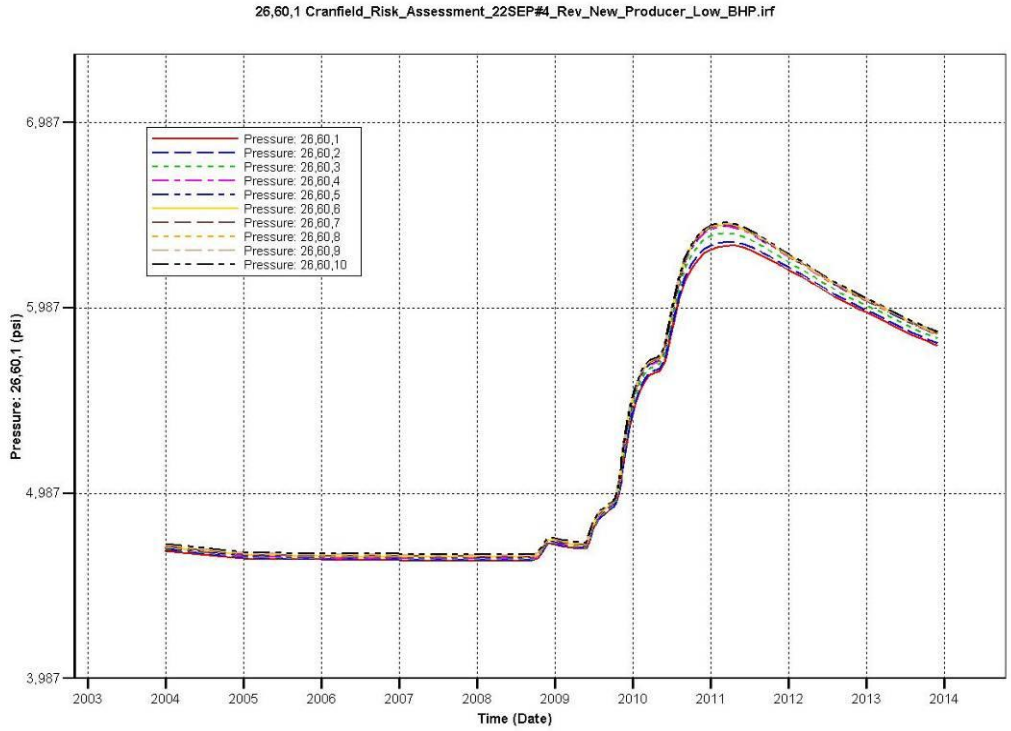

Pressure history at Cranfield Unit 4 (26, 60)

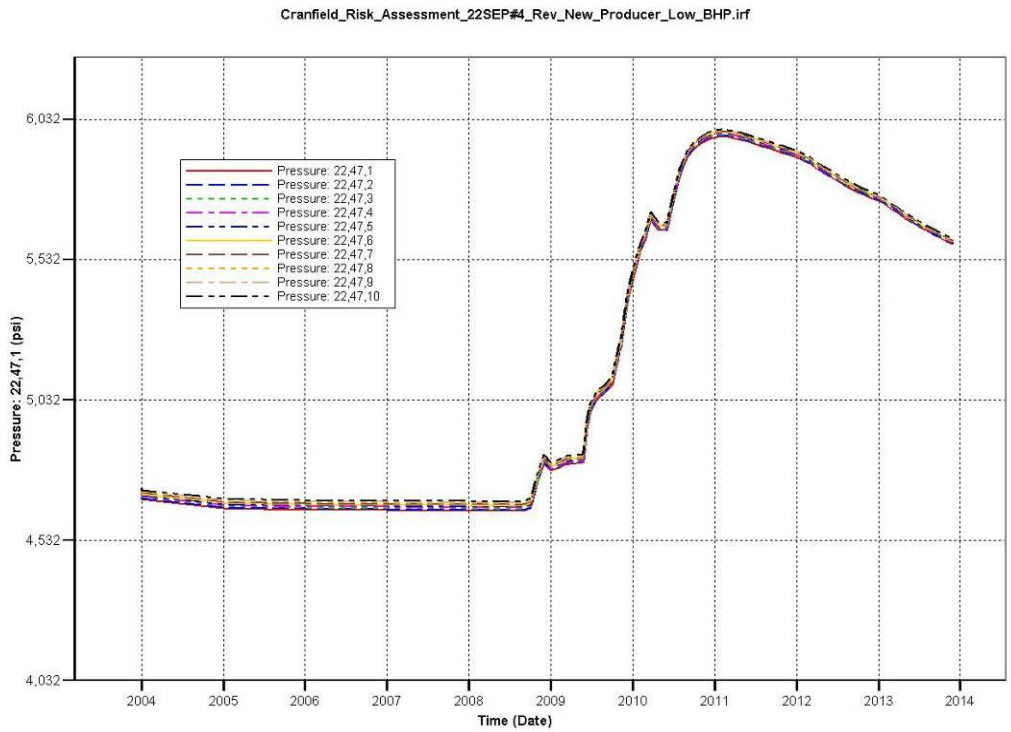

Pressure history at Vernon Johnson 1 (22, 47)

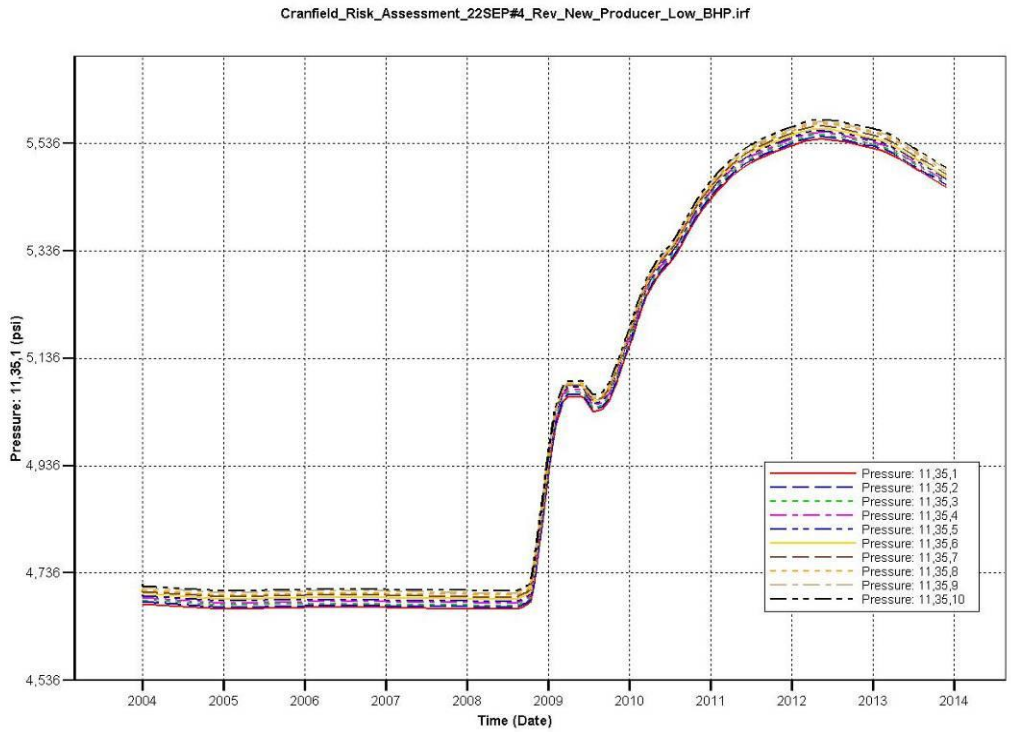

Pressure history at Armstrong 4 (11, 35)

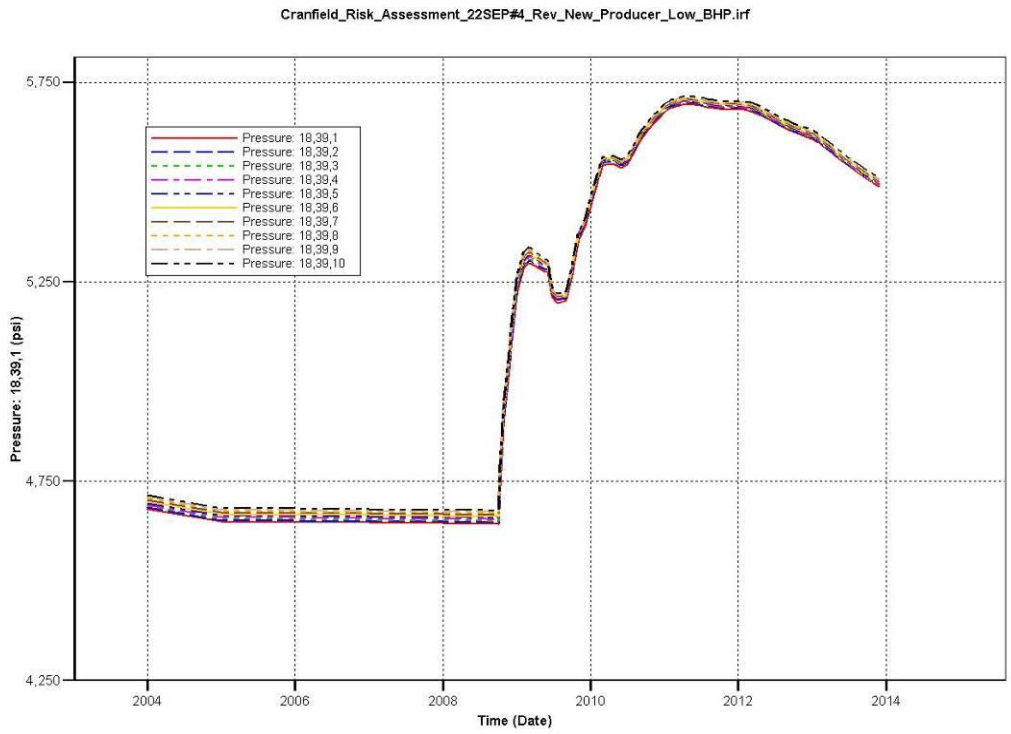

Pressure history at Armstrong 2 (18, 39)

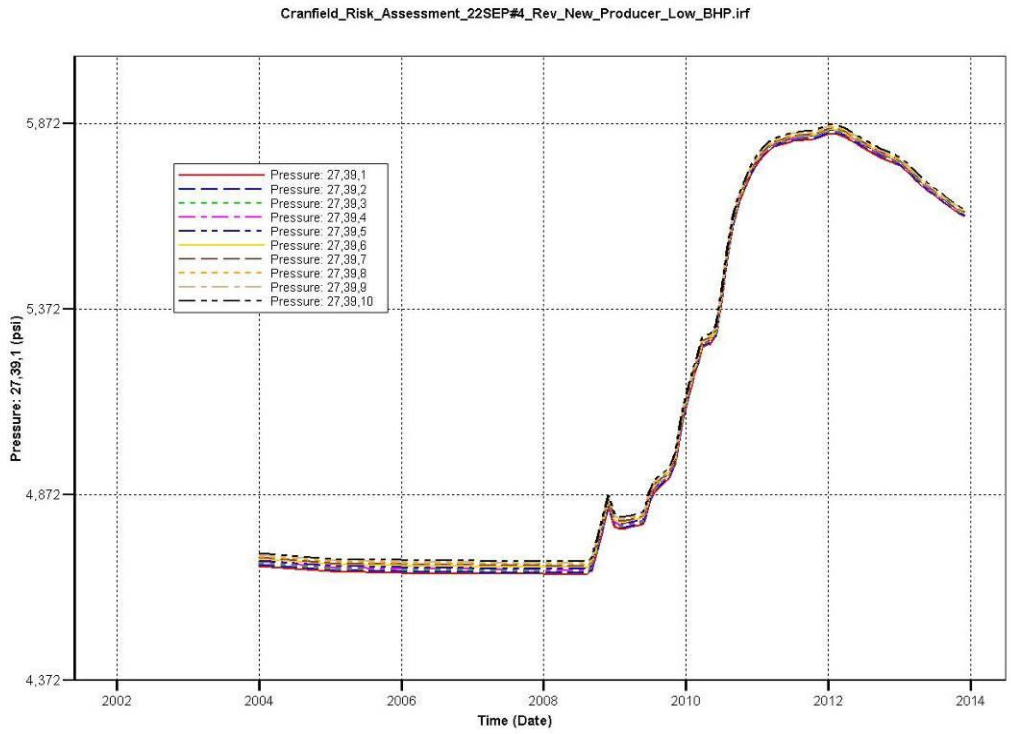

Pressure history at R G CALCOTE 1 (27, 39)

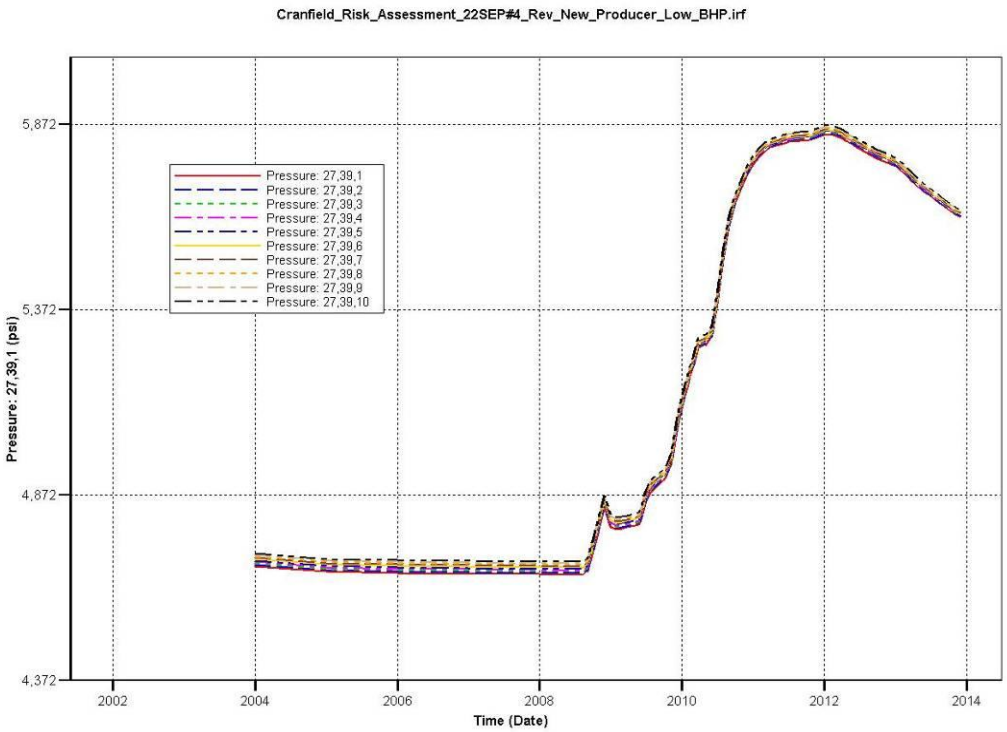

Pressure history at H H CROSBY ETAL 1 (32, 24)

5 Realization #5 (ten cells of a vertical profile displayed on each plot)

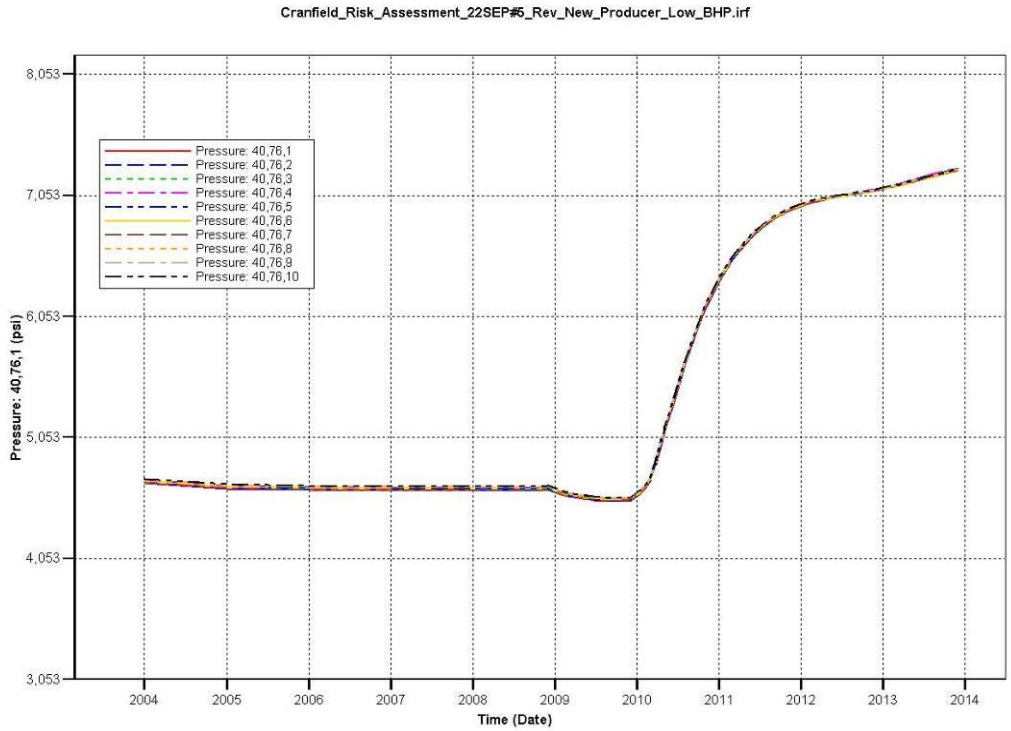

Pressure history at Cranfield Unit 7 (40, 76)

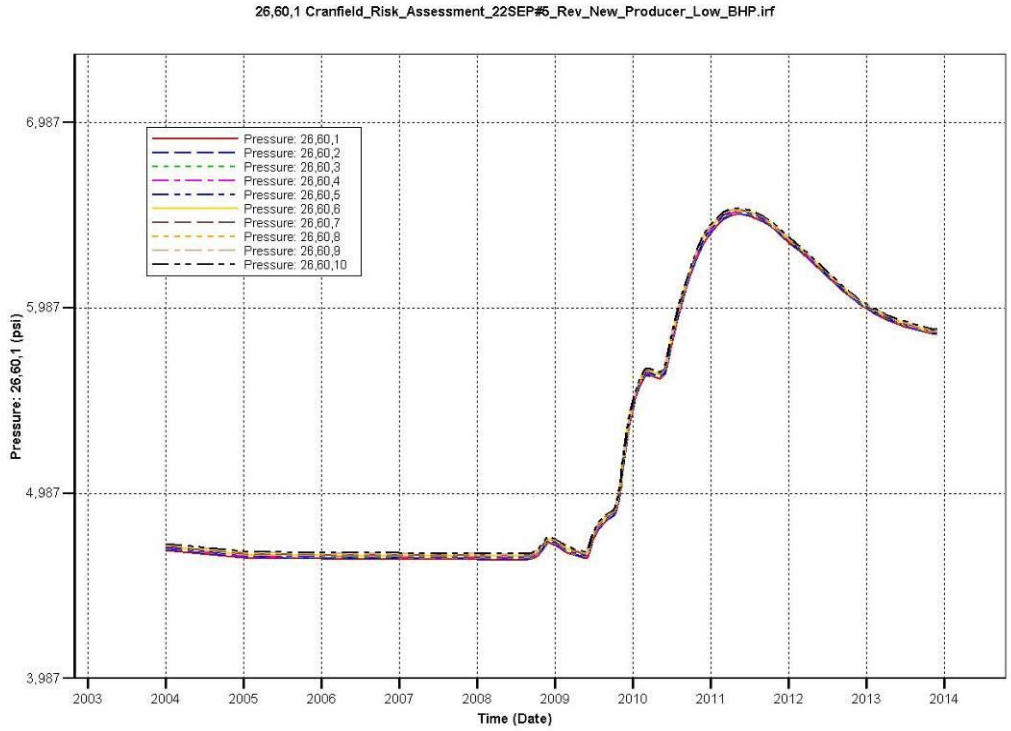

Pressure history at Cranfield Unit 4 (26, 60)

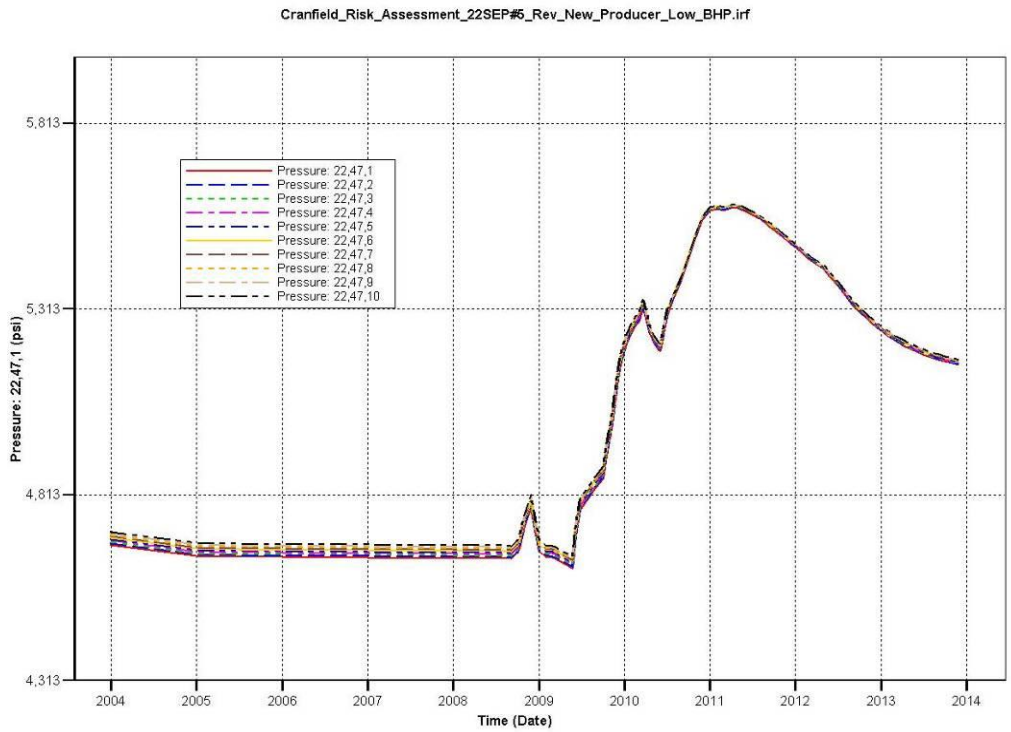

Pressure history at Vernon Johnson 1 (22, 47)

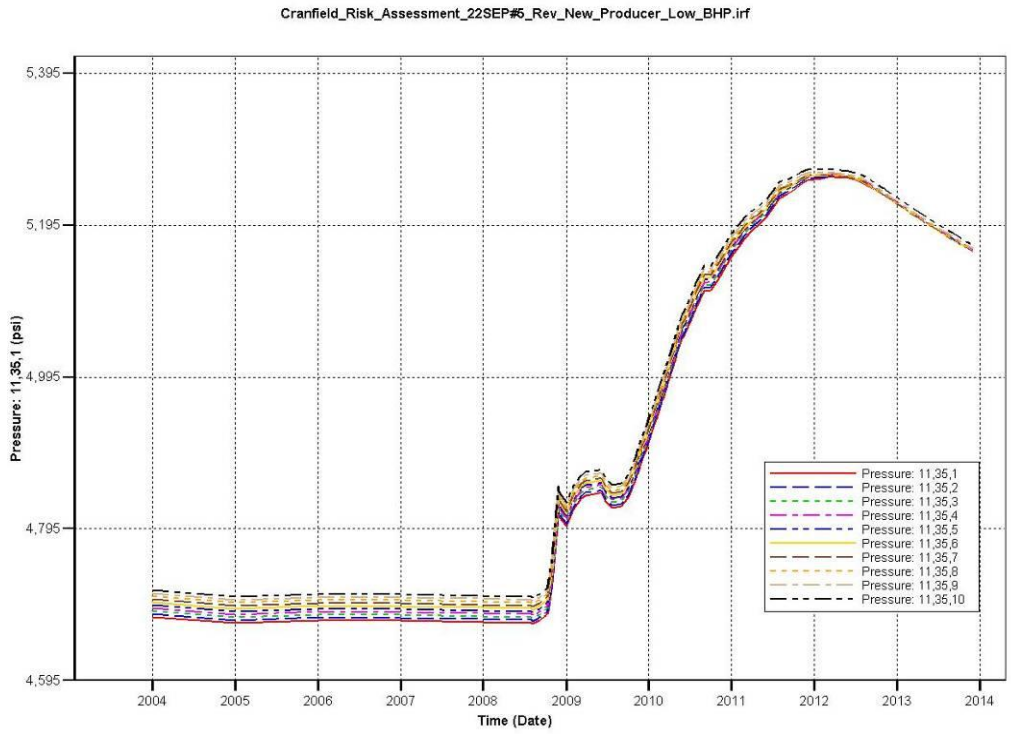

Pressure history at Armstrong 4 (11, 35)

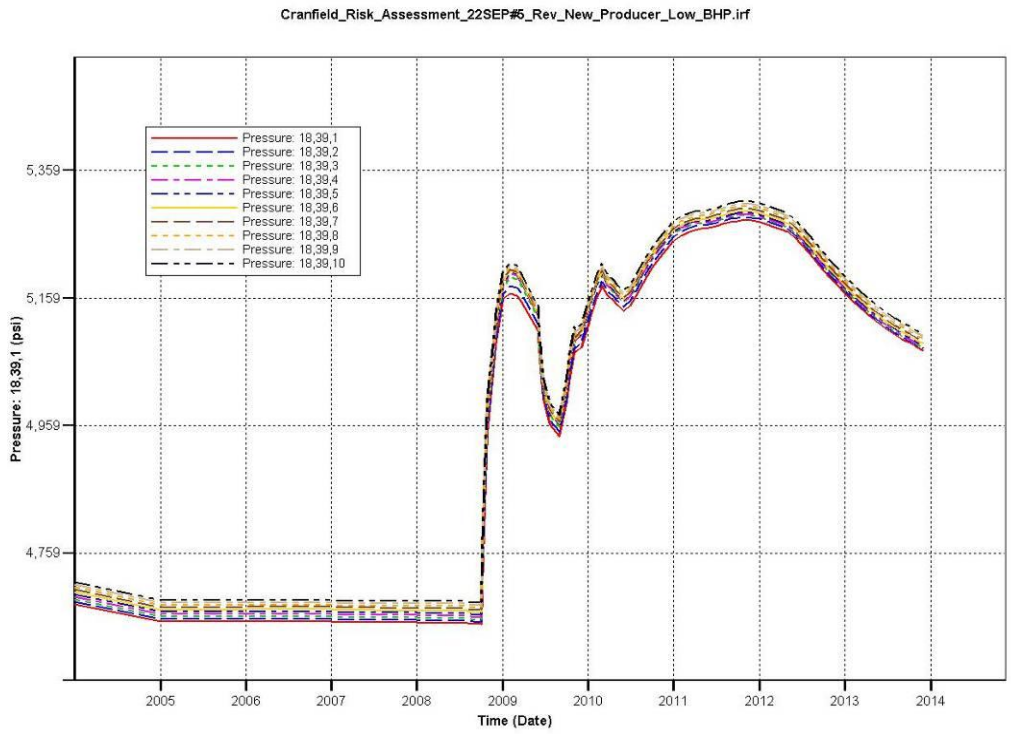

Pressure history at Armstrong 2 (18, 39)

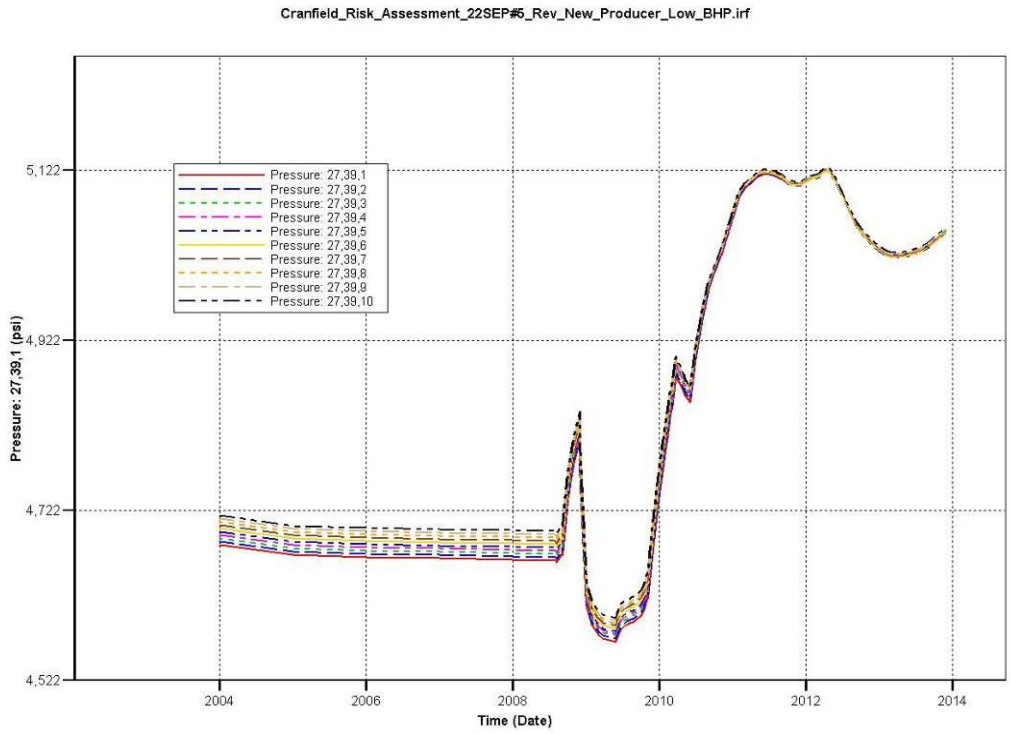

Pressure history at R G CALCOTE 1 (27, 39)

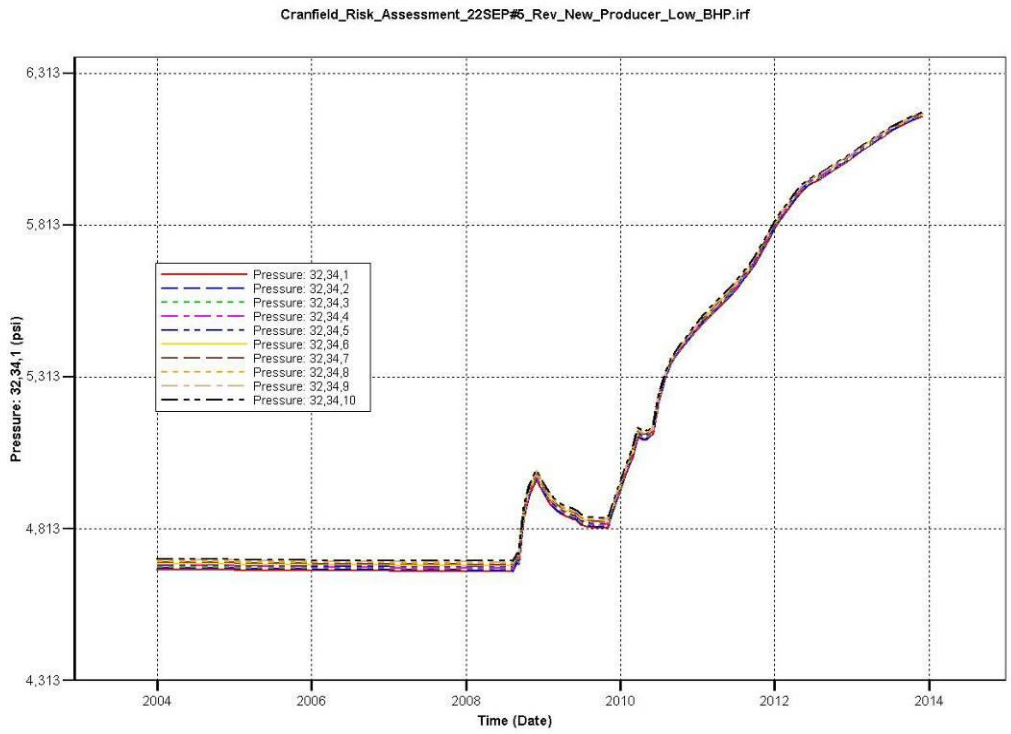

Pressure history at H H CROSBY ETAL 1 (32, 24)

10 Appendix D. Saturation history at P&A well locations

1 Realization #1 (ten cells of a vertical profile displayed on each plot)

Gas saturation Real.1
Cranfield Unit 7 (40,76)

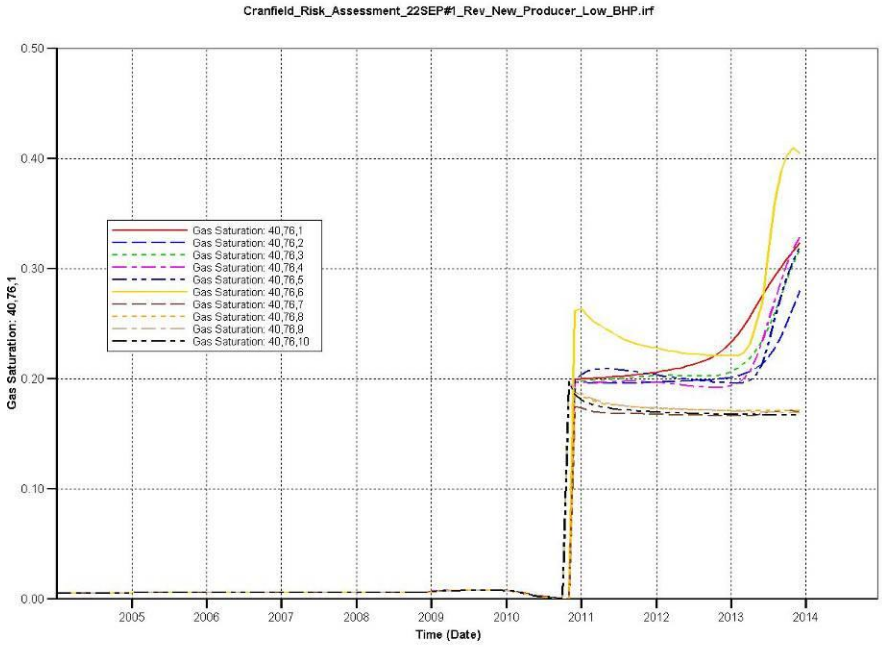

Gas saturation Real.1
Cranfield Unit 4 (26,60)

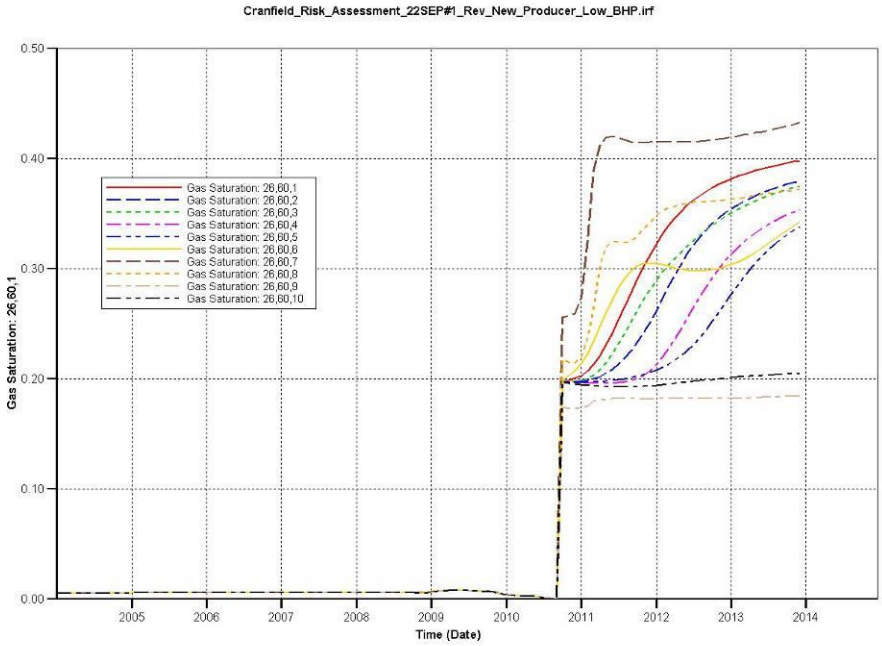

Gas saturation Real.1
Vernon Johnson 1 (22,47)

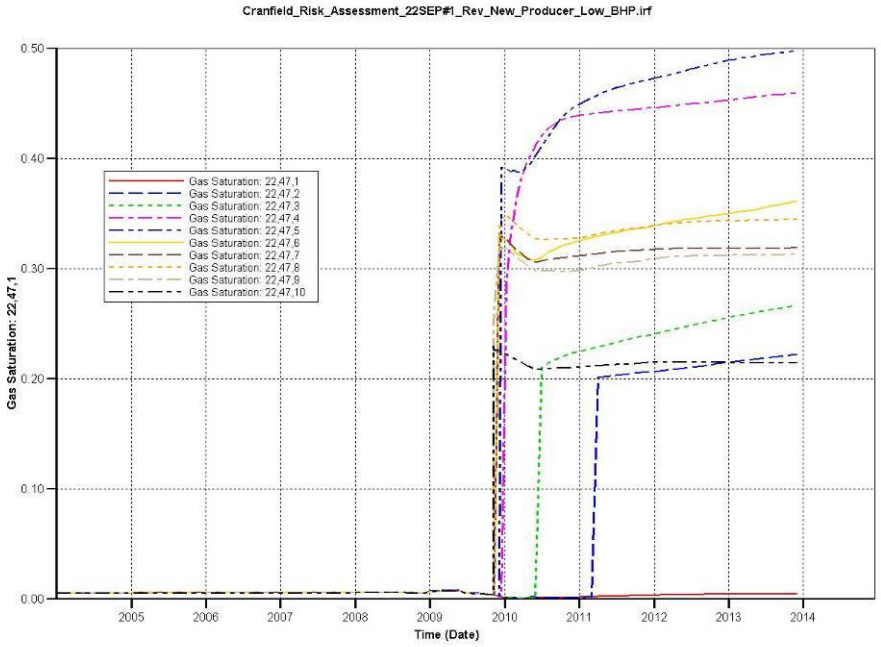

Gas saturation Real.1
Armstrong 4 (11,35)

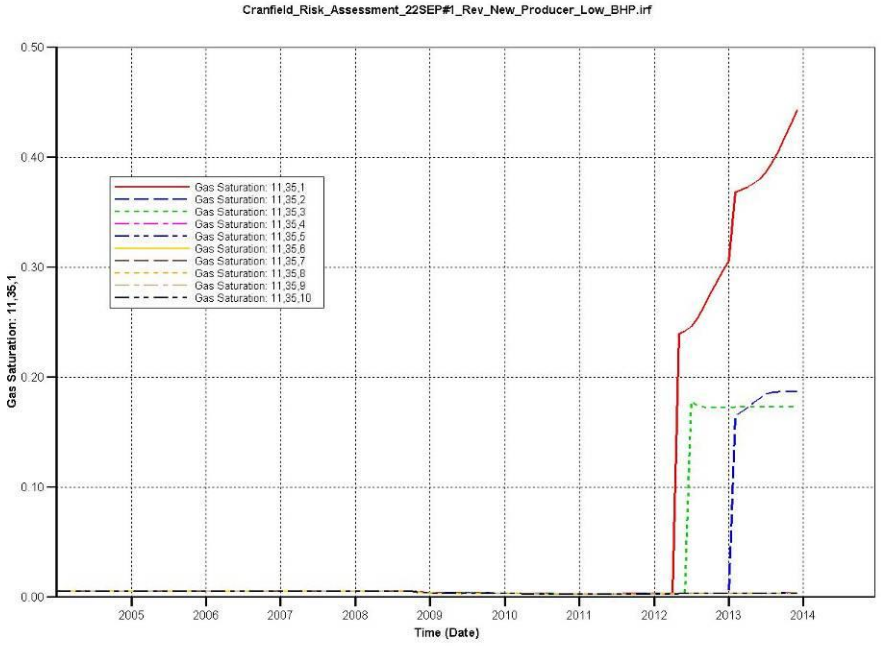

Gas saturation Real.1
Armstrong 2 (18,39)

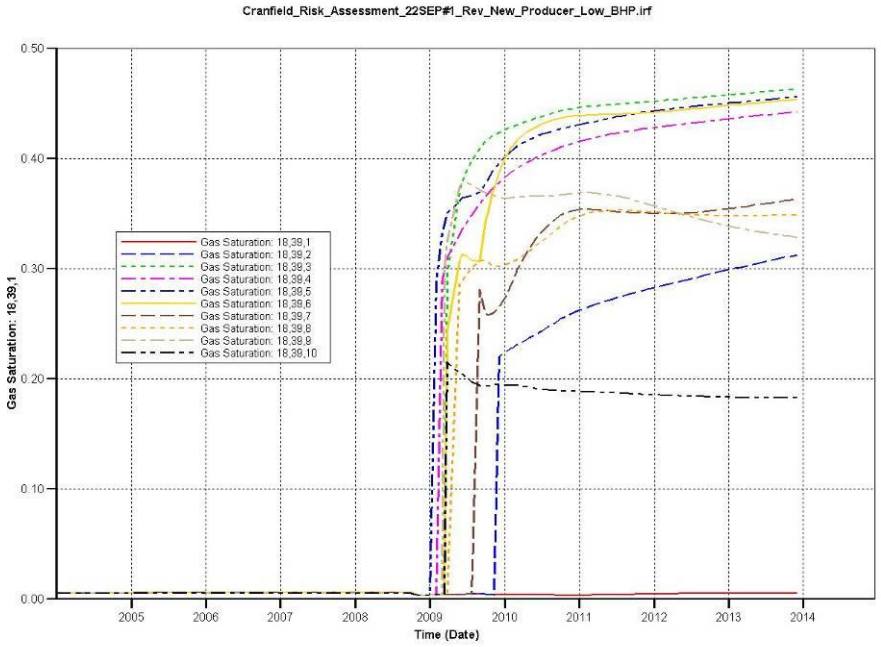

Gas saturation Real.1
R G CALCOTE 1 (27,39)

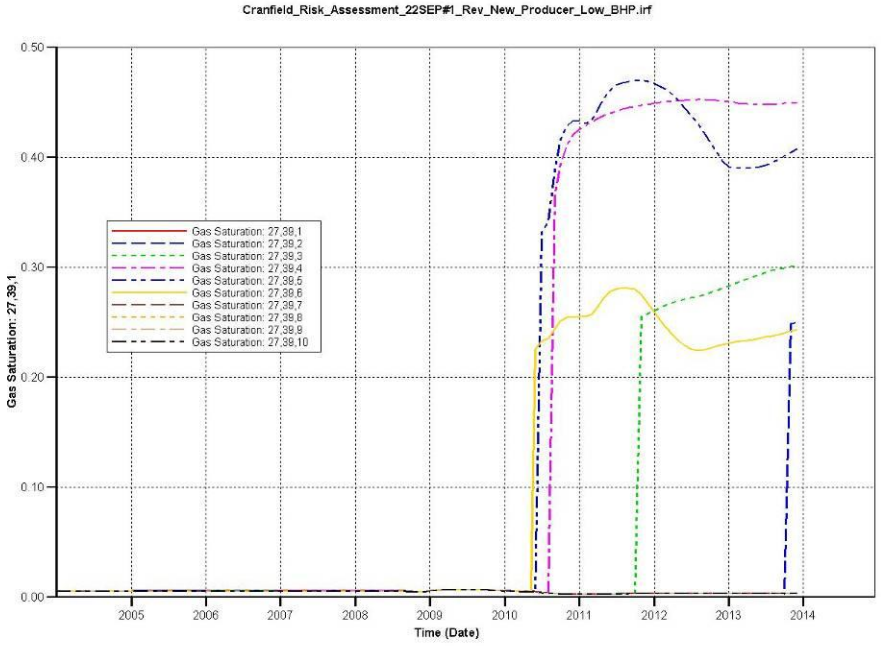

Gas saturation Real.1
H H CROSBY ETAL 1 (32,24)

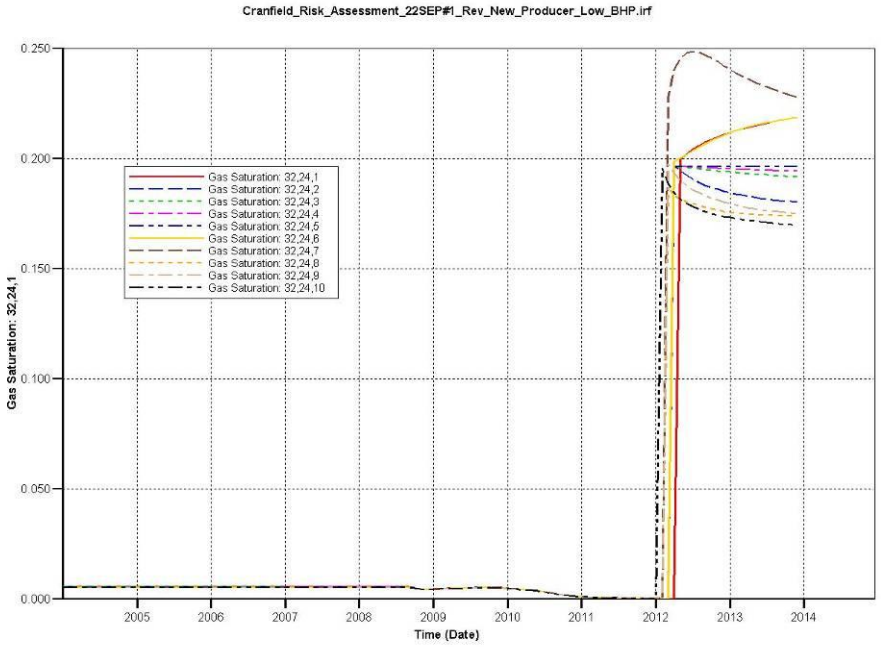

Global mole fraction of CO_2 Real.1
Cranfield Unit 7 (40,76)

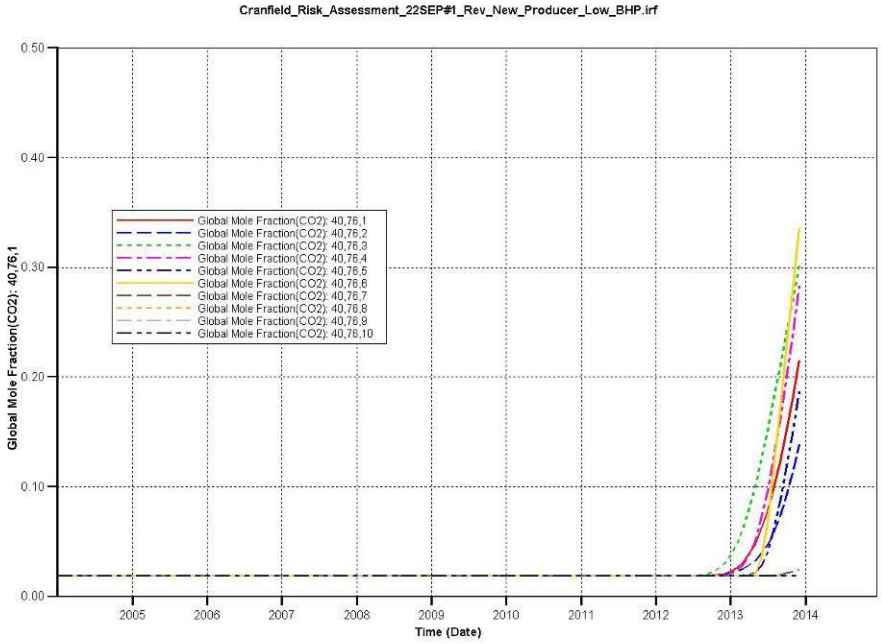

Global mole fraction of CO_2 Real.1
Cranfield Unit 4 (26,60)

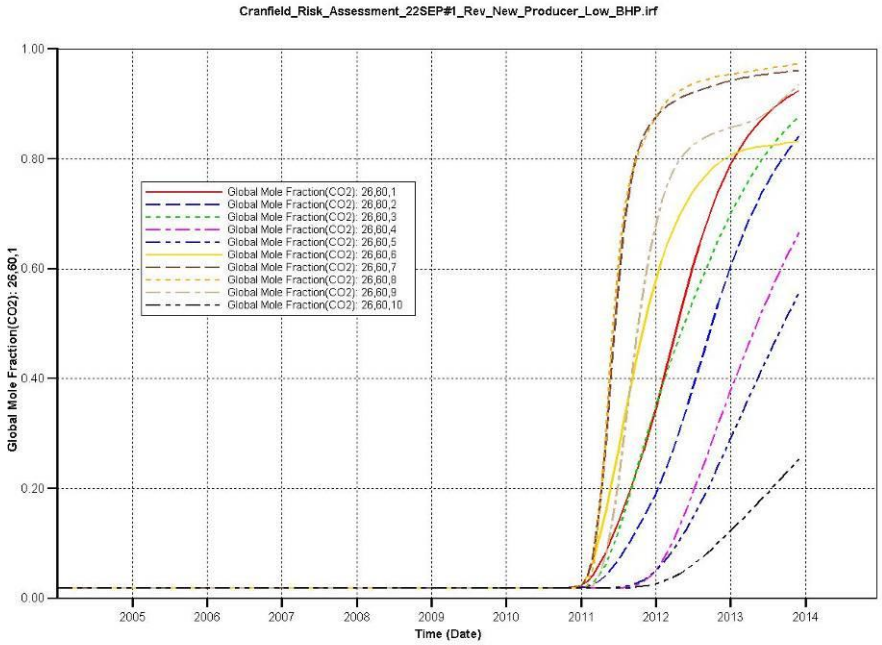

Global mole fraction of CO_2 Real.1
Vernon Johnson 1 (22,47)

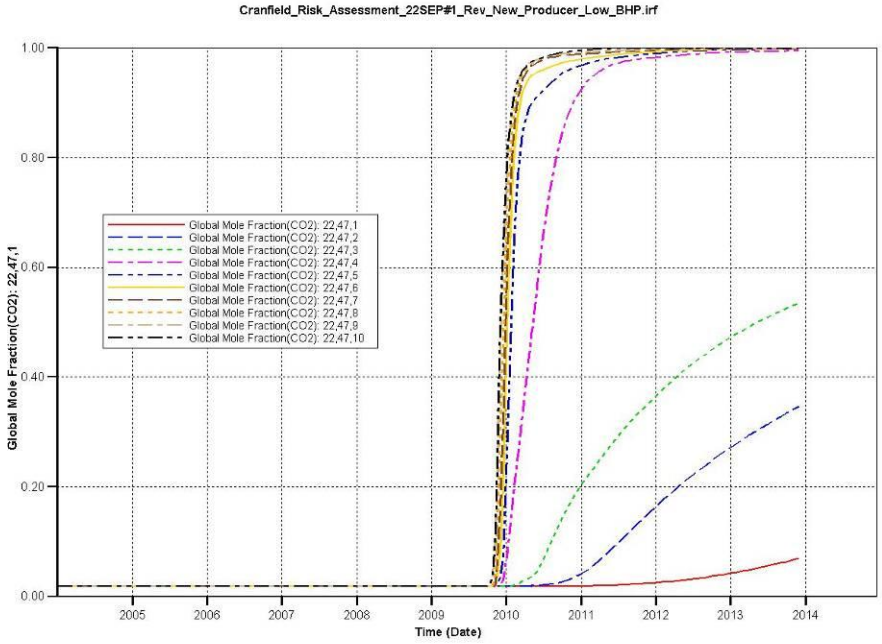

Global mole fraction of CO_2 Real.1
Armstrong 4 (11,35)

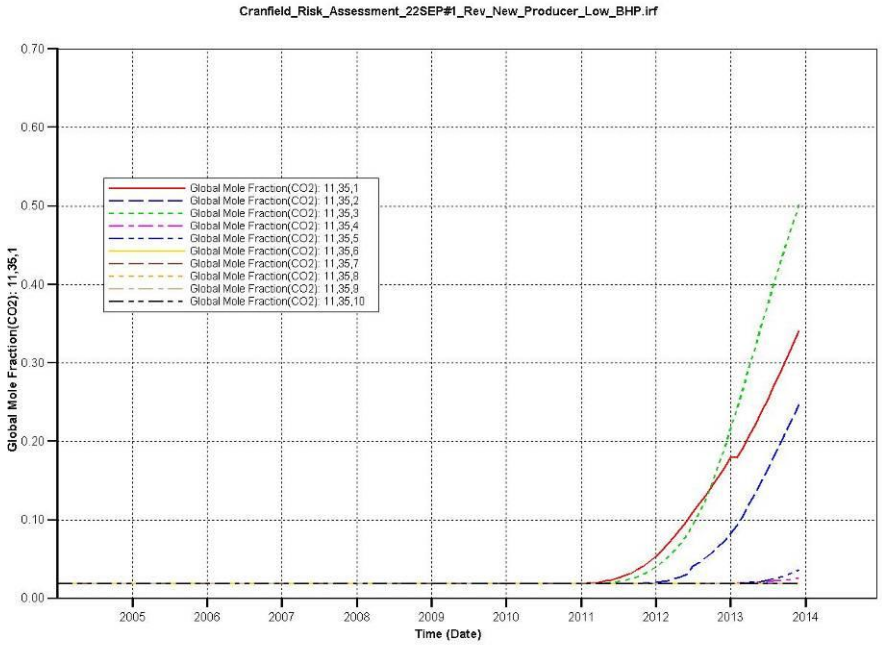

Global mole fraction of CO_2 Real.1
Armstrong 2 (18,39)

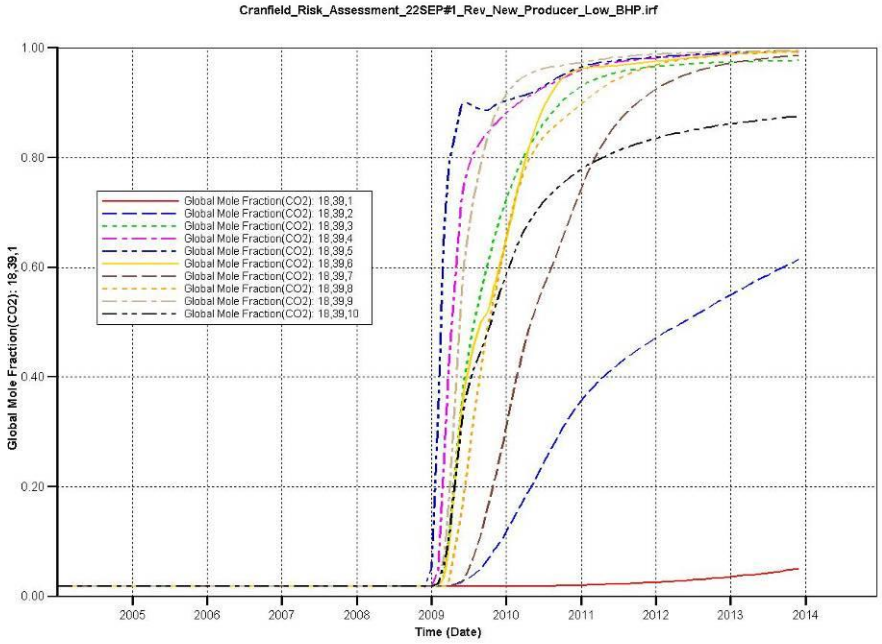

Global mole fraction of CO_2 Real.1
R G CALCOTE 1 (27,39)

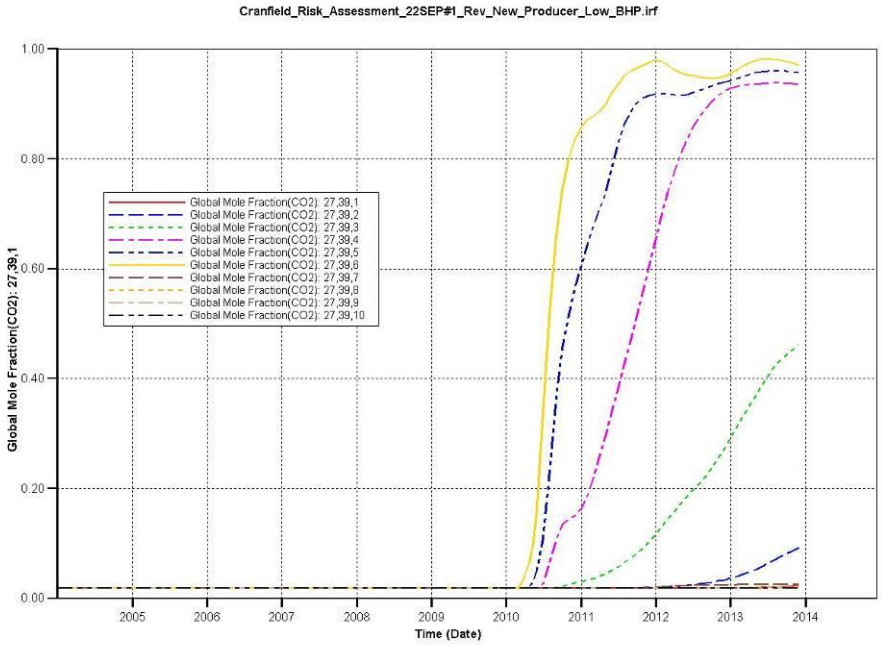

Global mole fraction of CO_2 Real.1
H H CROSBY ETAL 1 (32,24)

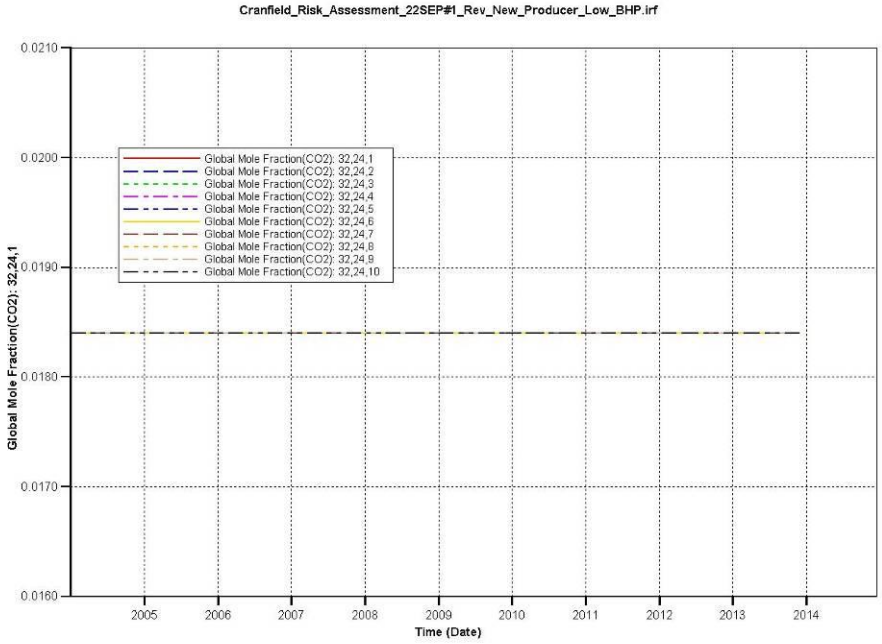

Oil mole fraction of CO_2 Real.1
Cranfield Unit 7 (40,76)

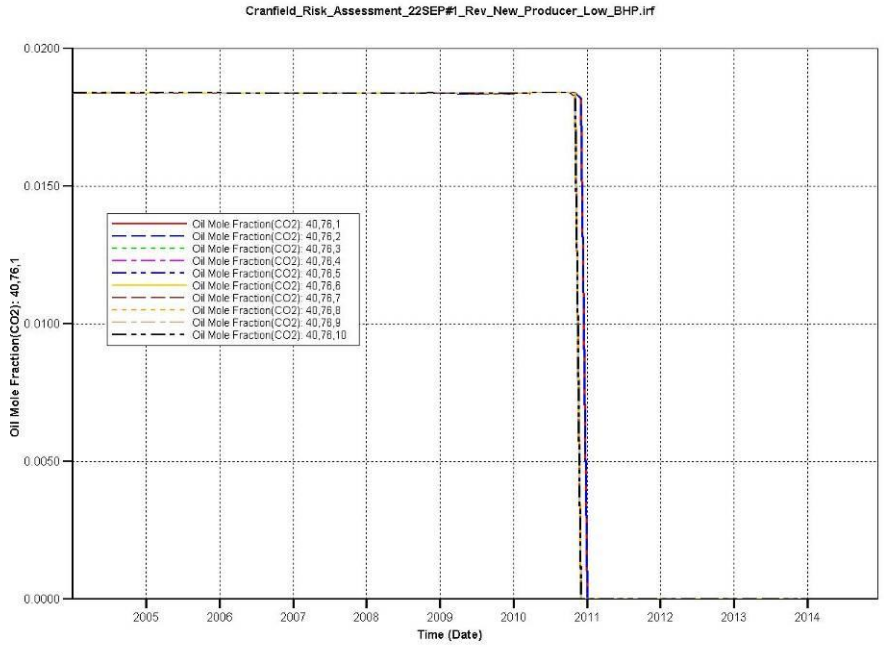

Oil mole fraction of CO_2 Real.1
Cranfield Unit 4 (26,60)

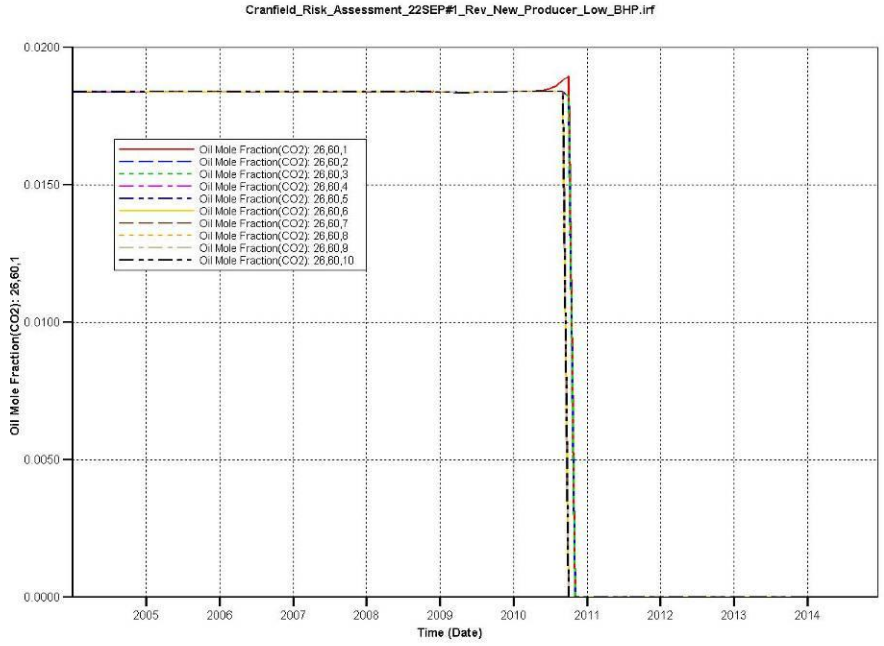

Oil mole fraction of CO_2 Real.1
Vernon Johnson 1 (22,47)

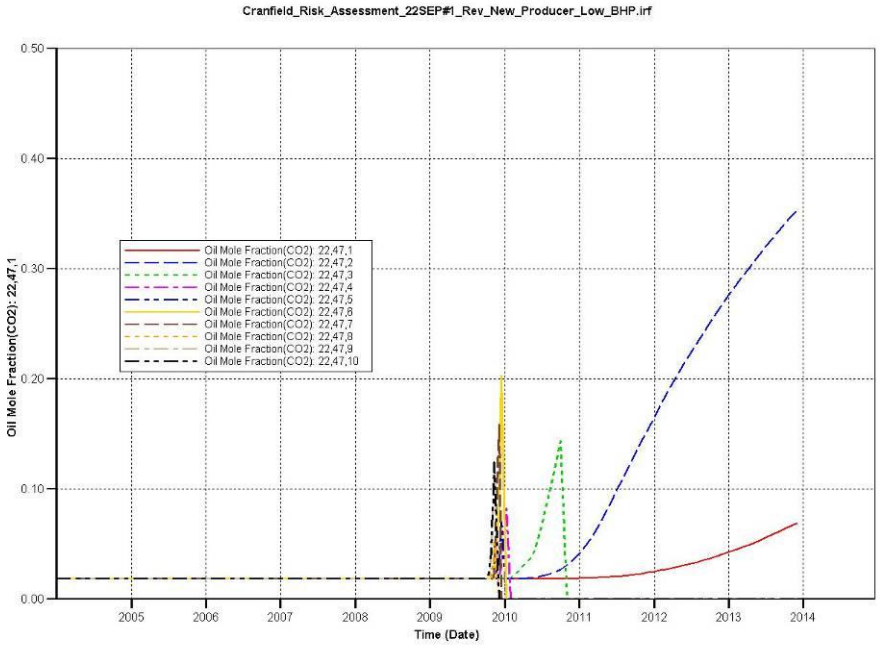

Oil mole fraction of CO_2 Real.1
Armstrong 4 (11,35)

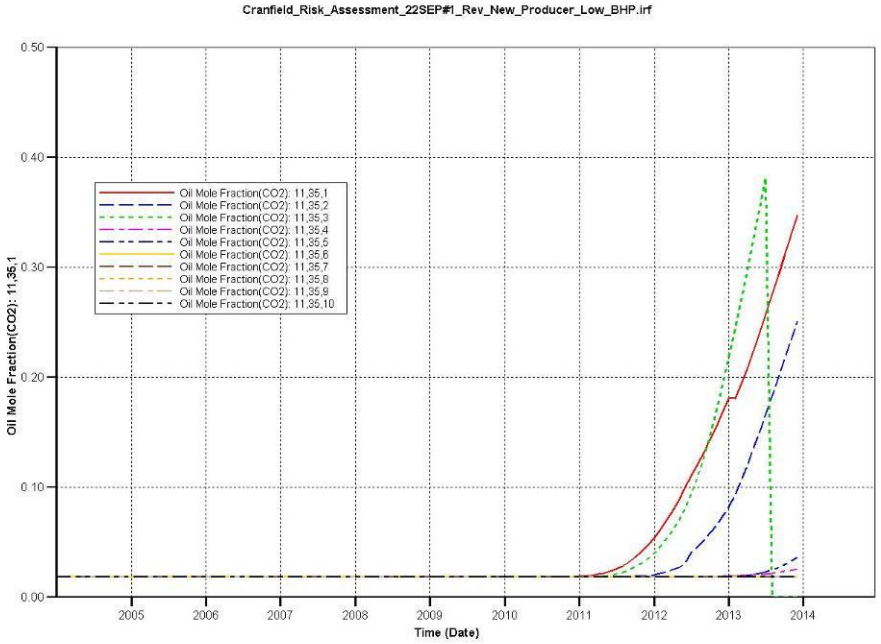

Oil mole fraction of CO_2 Real.1
Armstrong 2 (18,39)

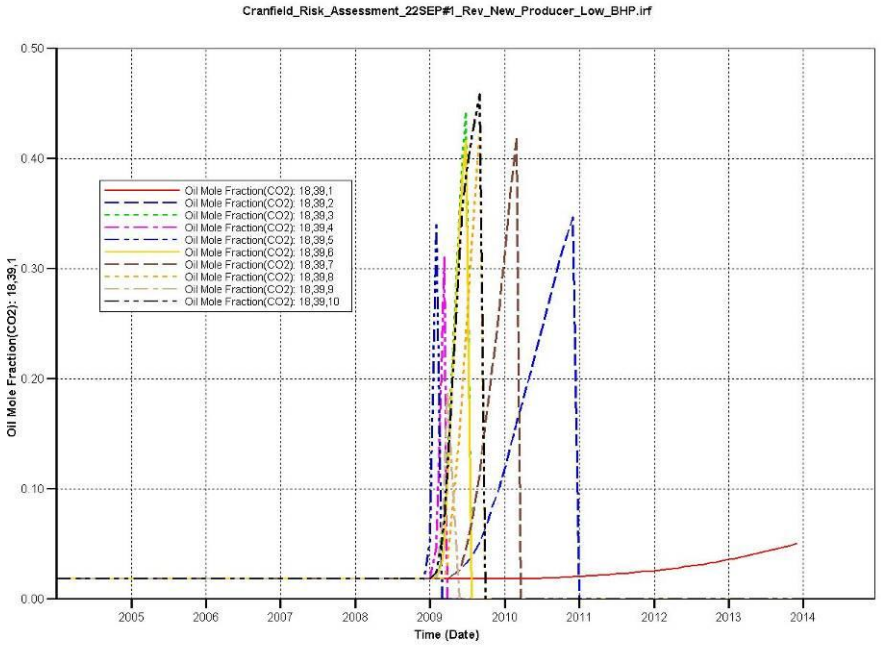

Oil mole fraction of CO_2 Real.1
R G CALCOTE 1 (27,39)

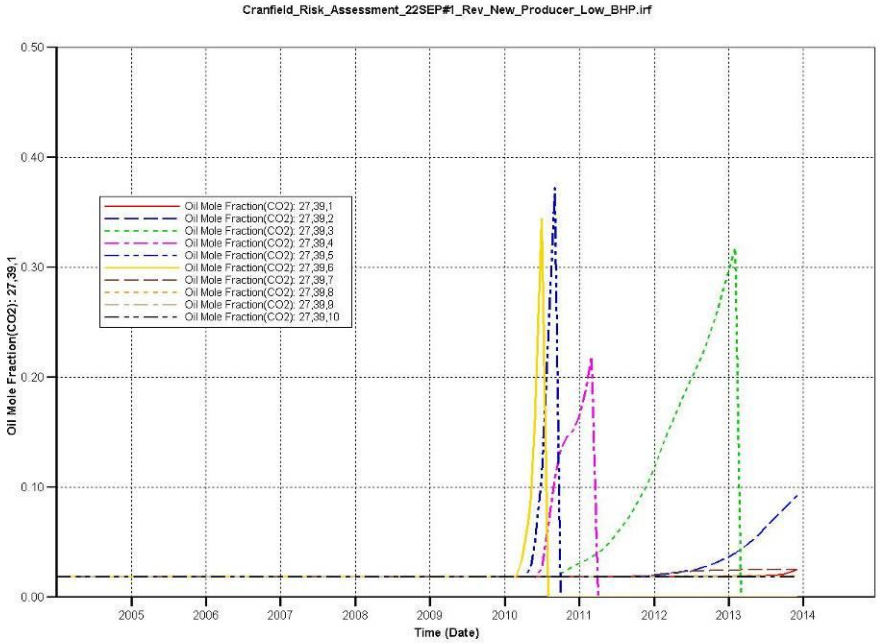

Oil mole fraction of CO_2 Real.1
H H CROSBY ETAL 1 (32,24)

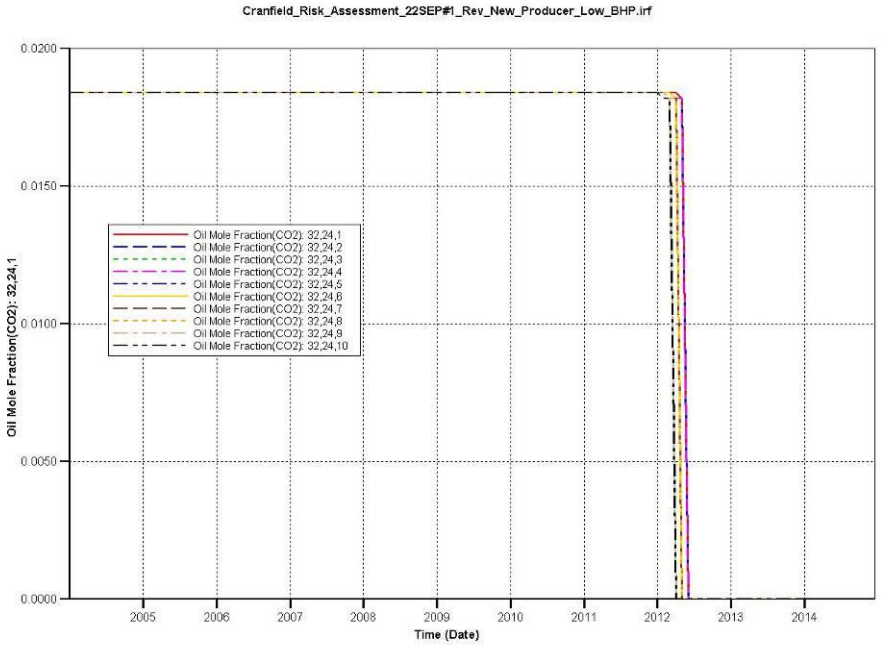

2 Realization #2 (ten cells of a vertical profile displayed on each plot)

Gas saturation Real.2
Cranfield Unit 7 (40,76)

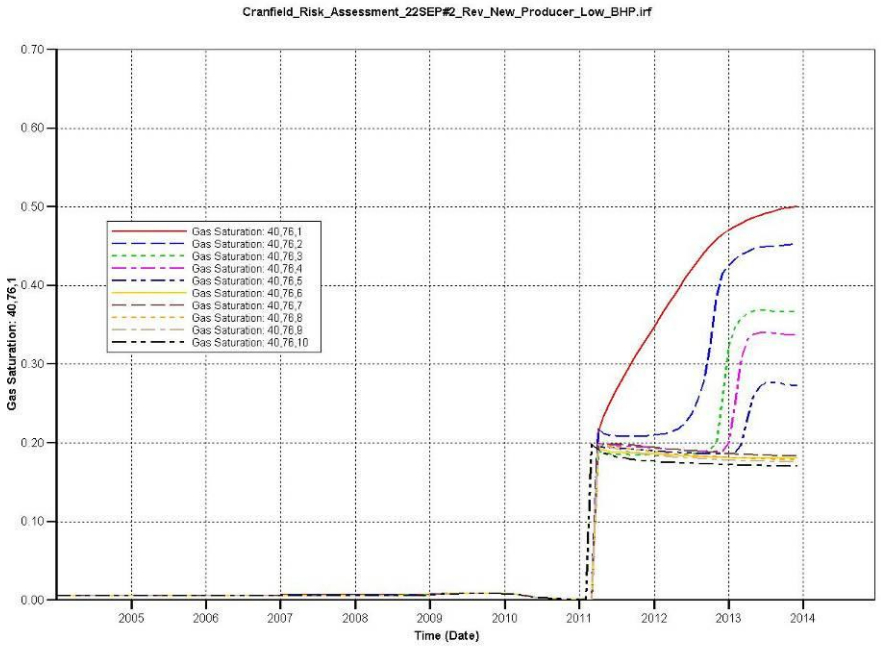

Gas saturation Real.2
Cranfield Unit 4 (26,60)

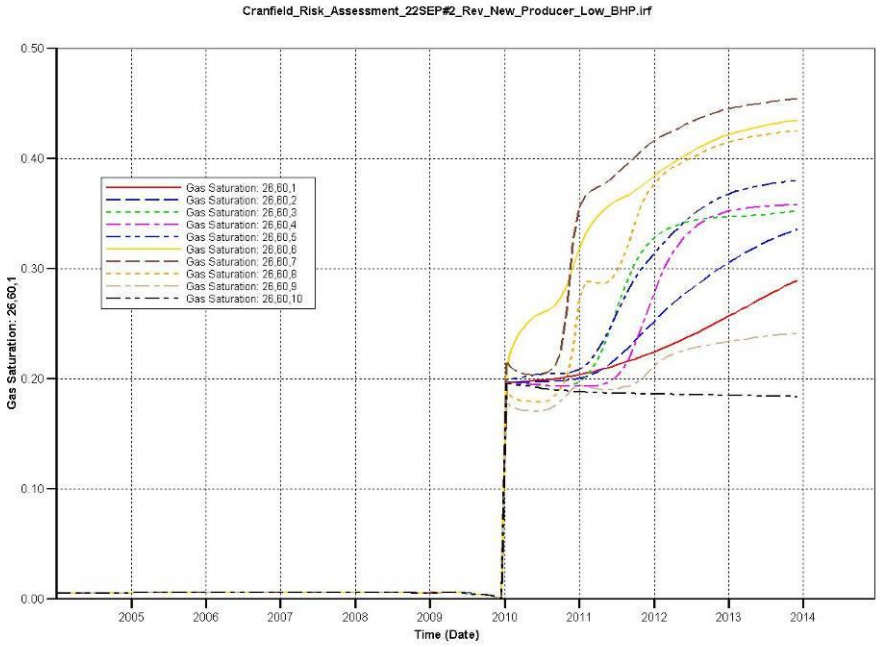

Gas saturation Real.2
Vernon Johnson 1 (22,47)

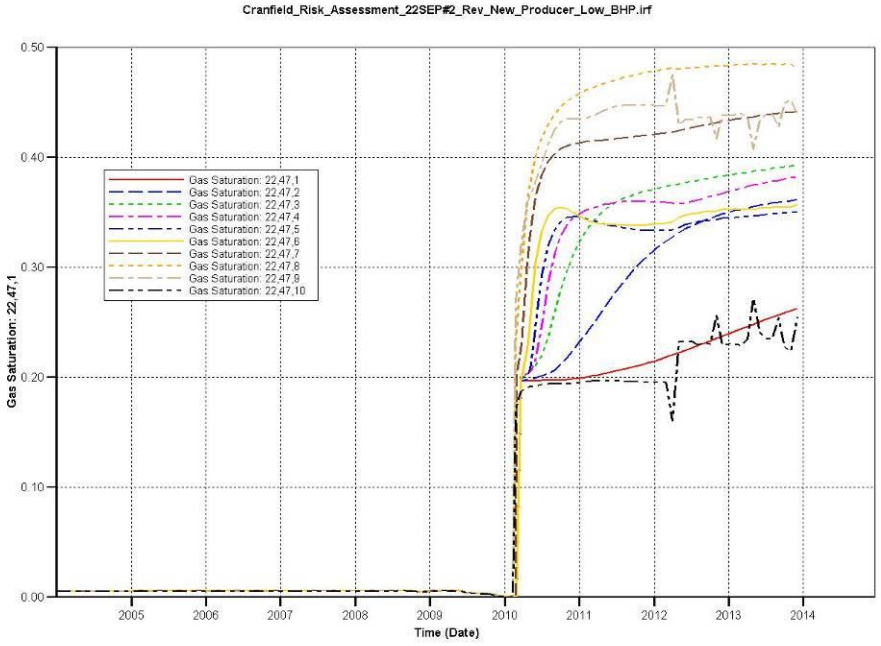

Gas saturation Real.2
Armstrong 4 (11,35)

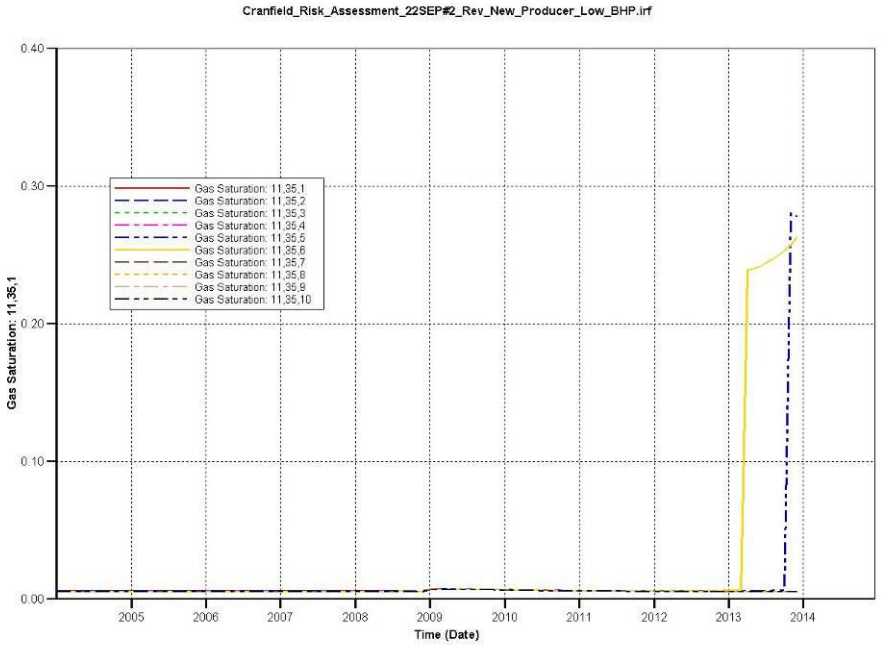

Gas saturation Real.2
Armstrong 2 (18,39)

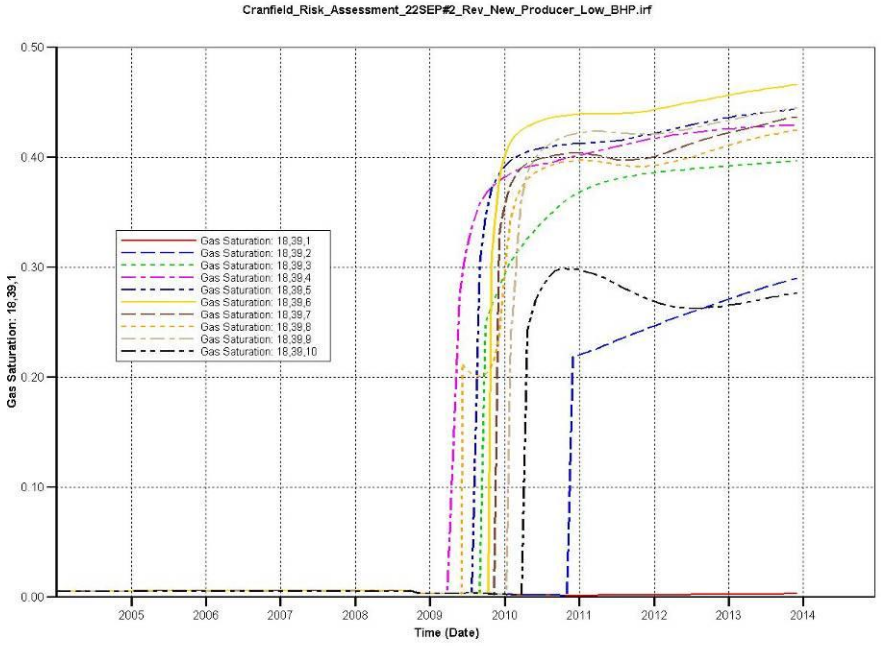

Gas saturation Real.2
R G CALCOTE 1 (27,39)

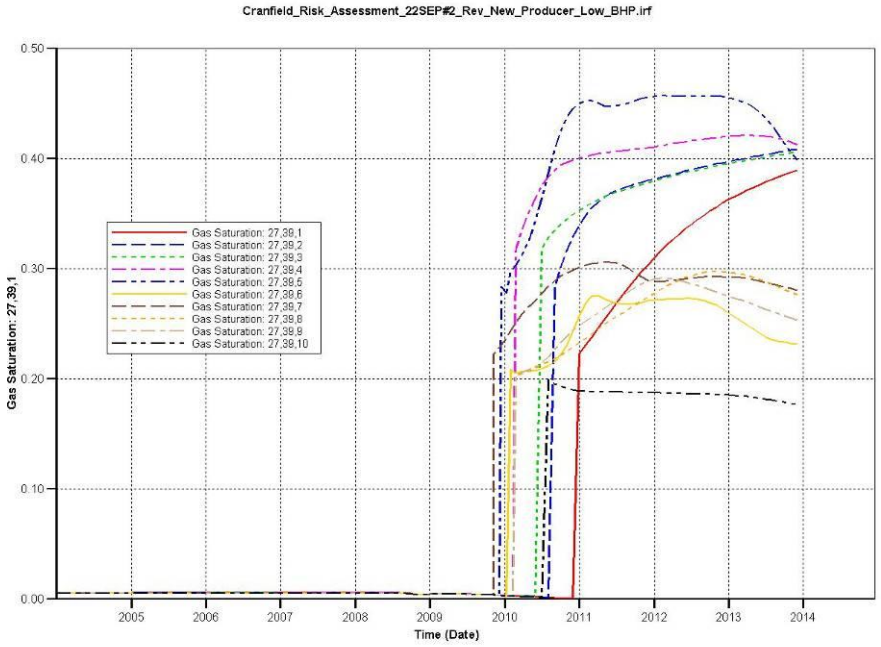

Gas saturation Real.2
H H CROSBY ETAL 1 (32,24)

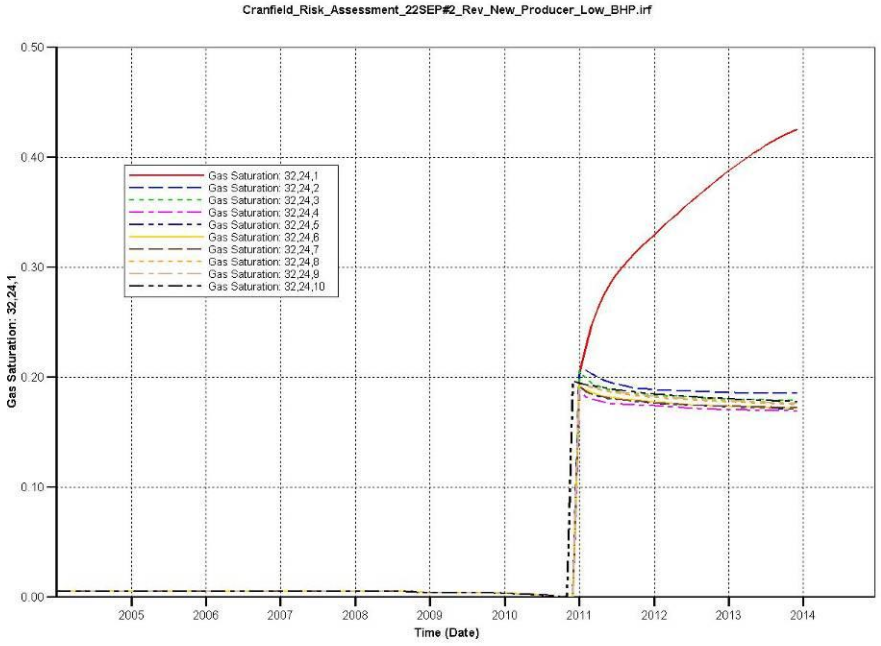

Global mole fraction of CO_2 Real.2
Cranfield Unit 7 (40,76)

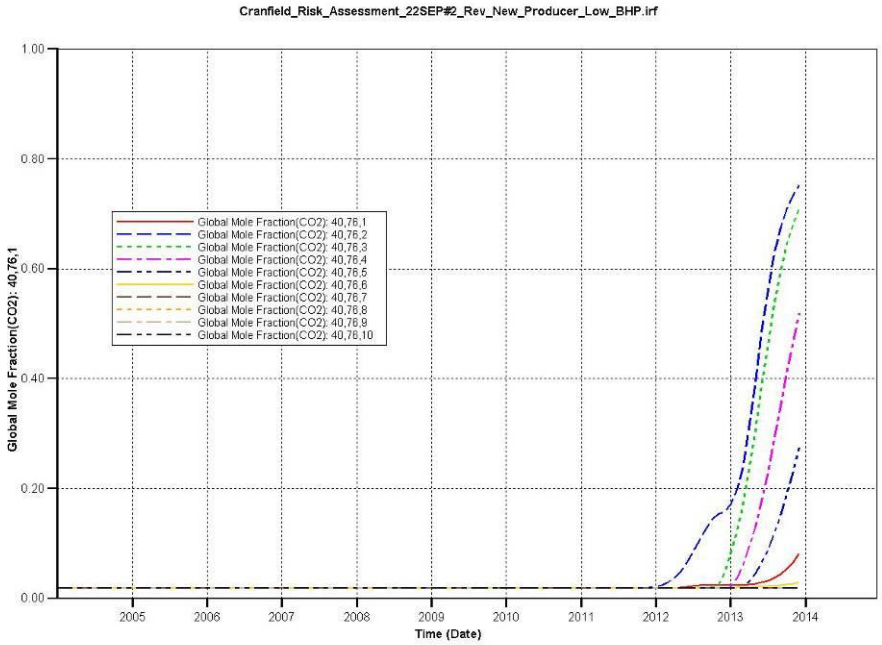

Global mole fraction of CO_2 Real.2
Cranfield Unit 4 (26,60)

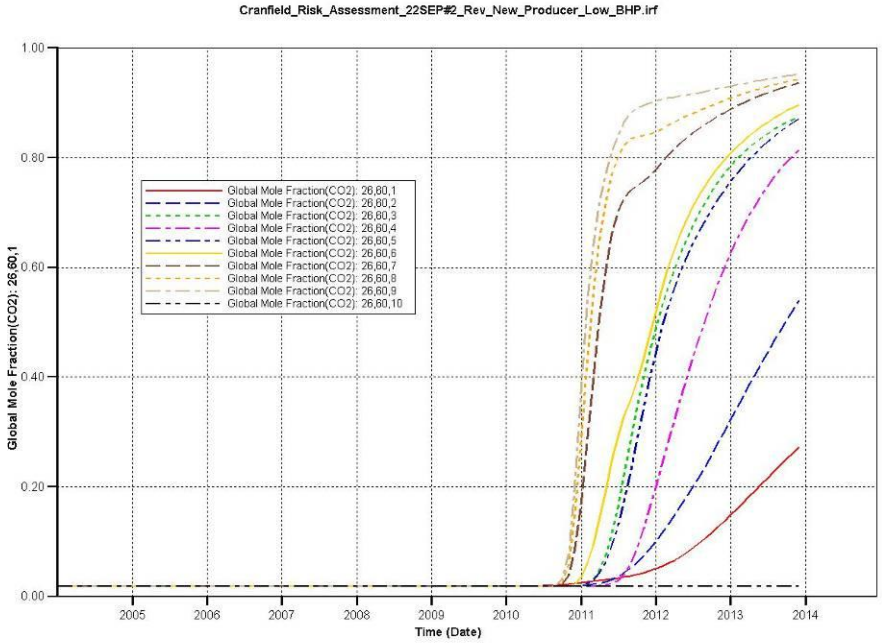

Global mole fraction of CO_2 Real.2
Vernon Johnson 1 (22,47)

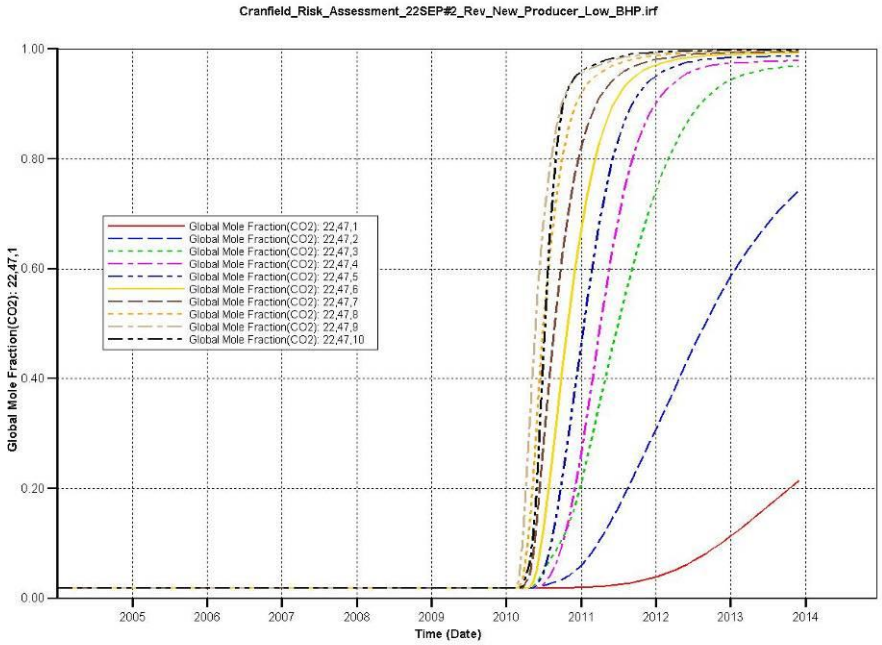

Global mole fraction of CO_2 Real.2
Armstrong 4 (11,35)

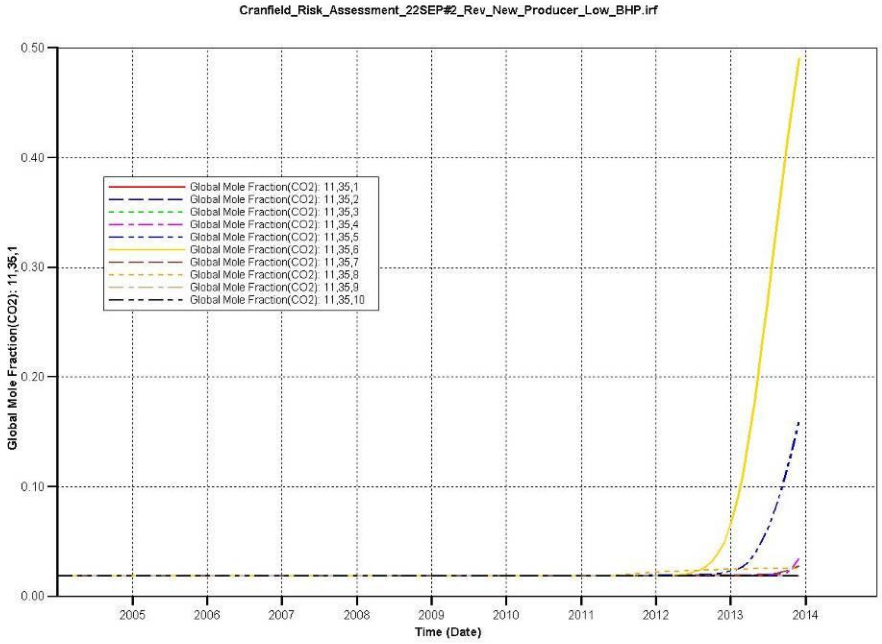

Global mole fraction of CO_2 Real.2
Armstrong 2 (18,39)

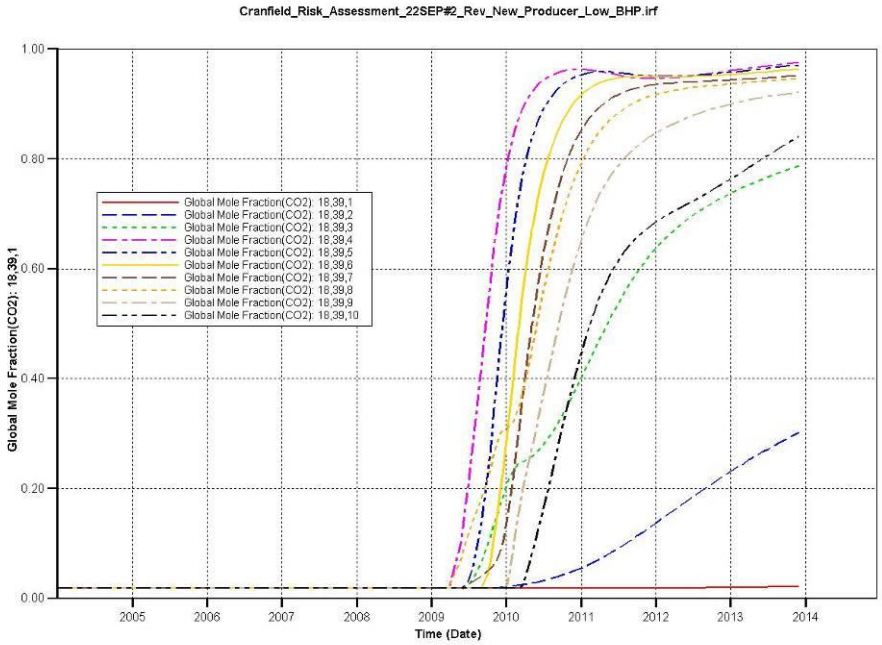

Global mole fraction of CO_2 Real.2
R G CALCOTE 1 (27,39)

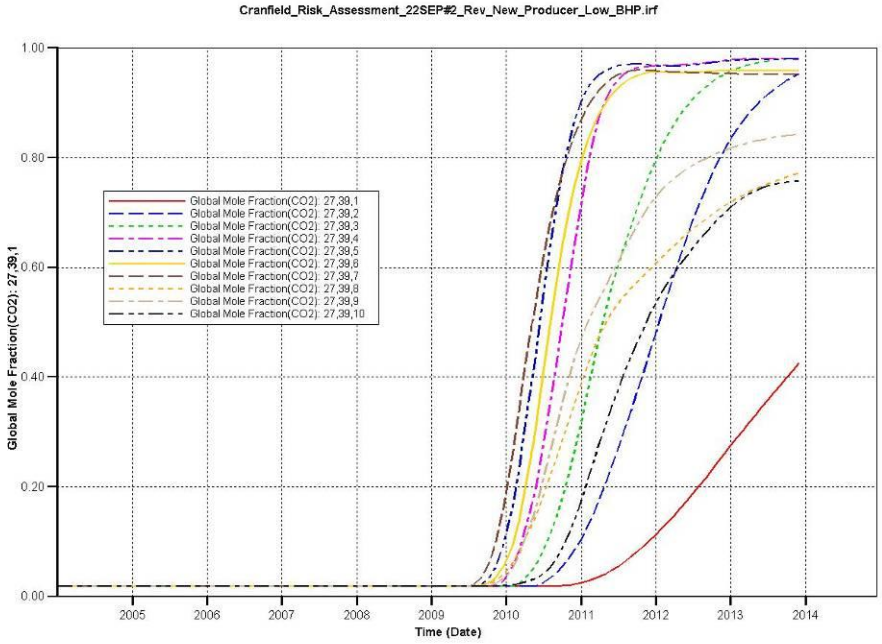

Global mole fraction of CO_2 Real.2
H H CROSBY ETAL 1 (32,24)

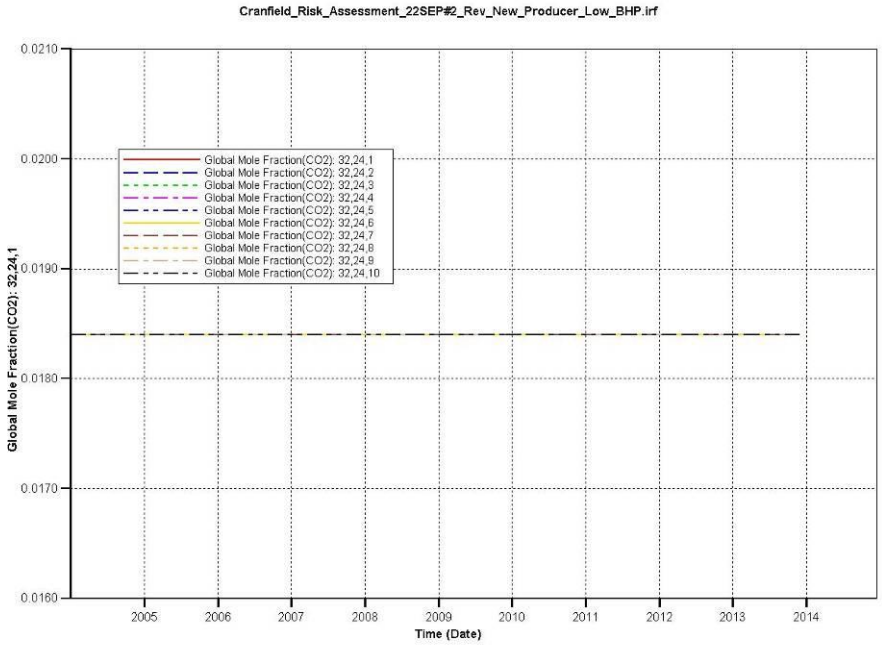

Oil mole fraction of CO_2 Real.2
Cranfield Unit 7 (40,76)

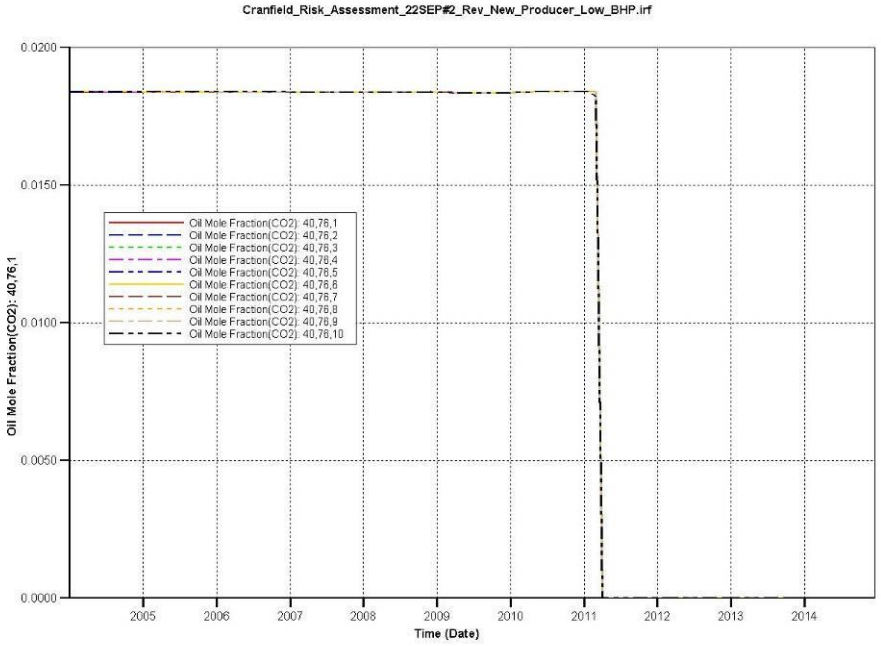

Oil mole fraction of CO_2 Real.2
Cranfield Unit 4 (26,60)

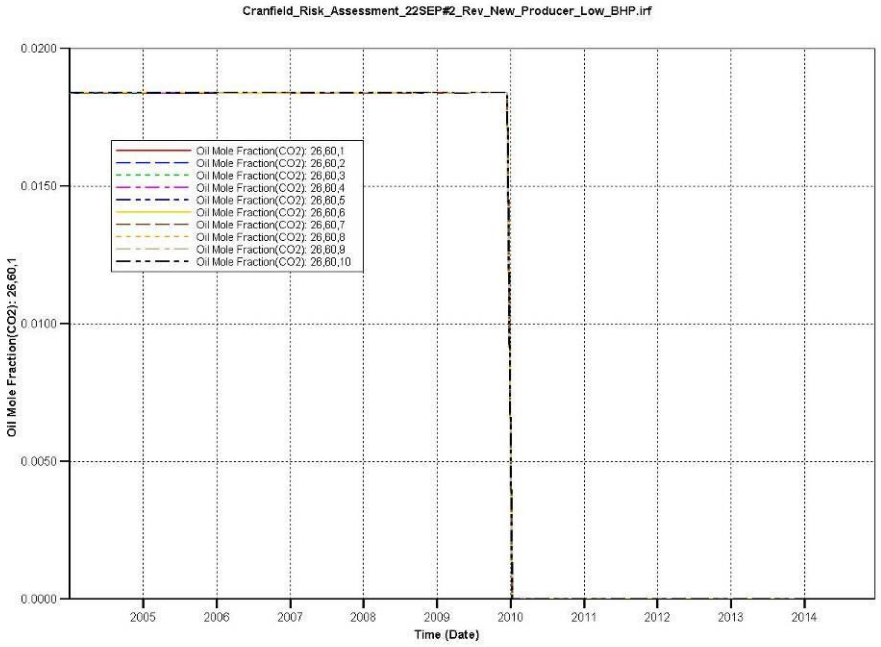

Oil mole fraction of CO_2 Real.2
Vernon Johnson 1 (22,47)

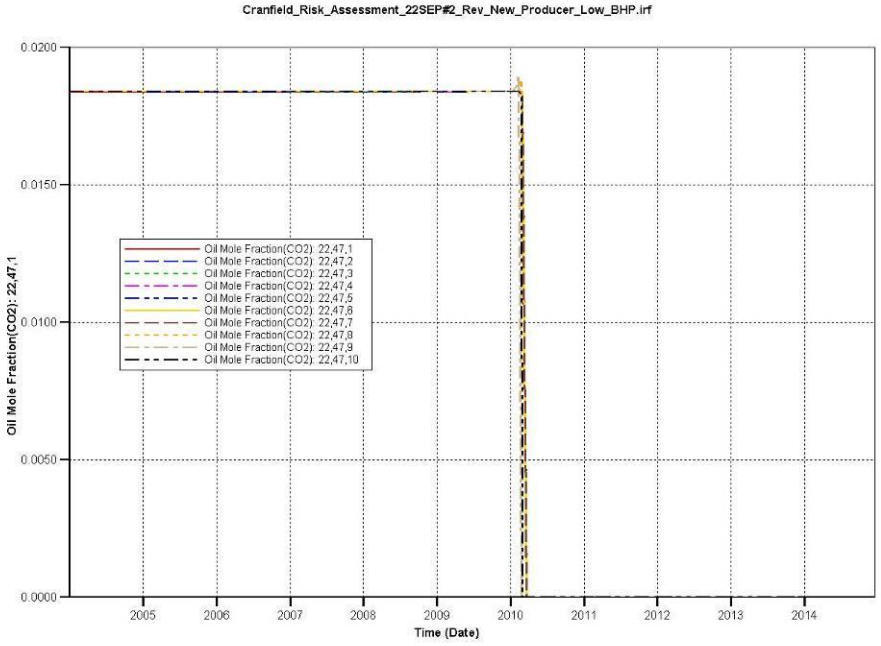

Oil mole fraction of CO_2 Real.2
Armstrong 4 (11,35)

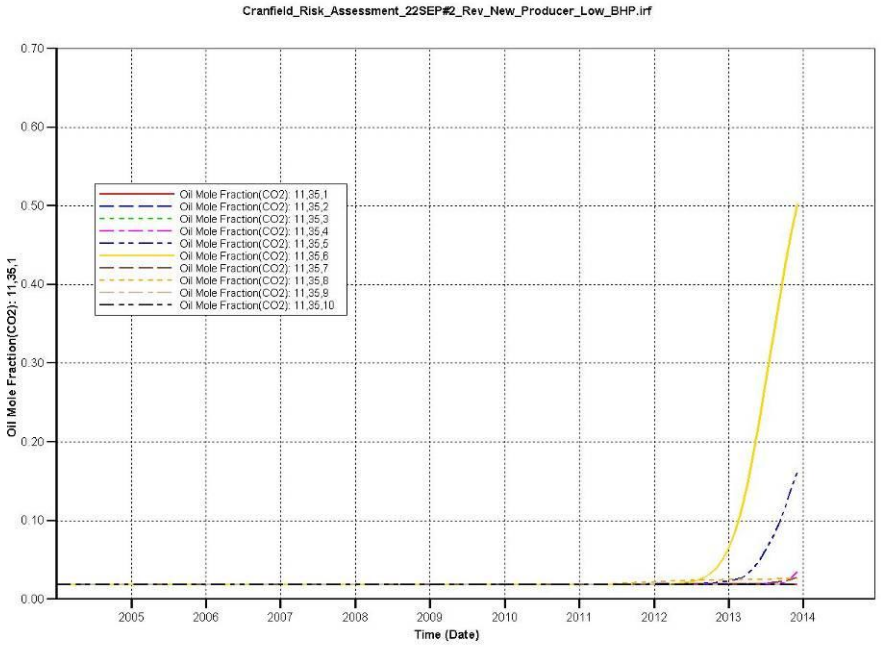

Oil mole fraction of CO_2 Real.2
Armstrong 2 (18,39)

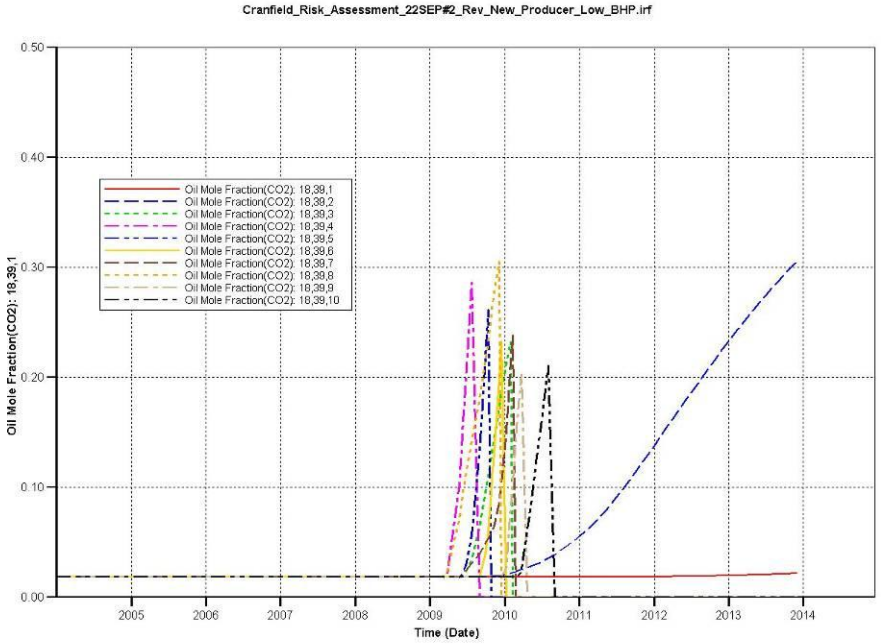

Oil mole fraction of CO_2 Real.2
R G CALCOTE 1 (27,39)

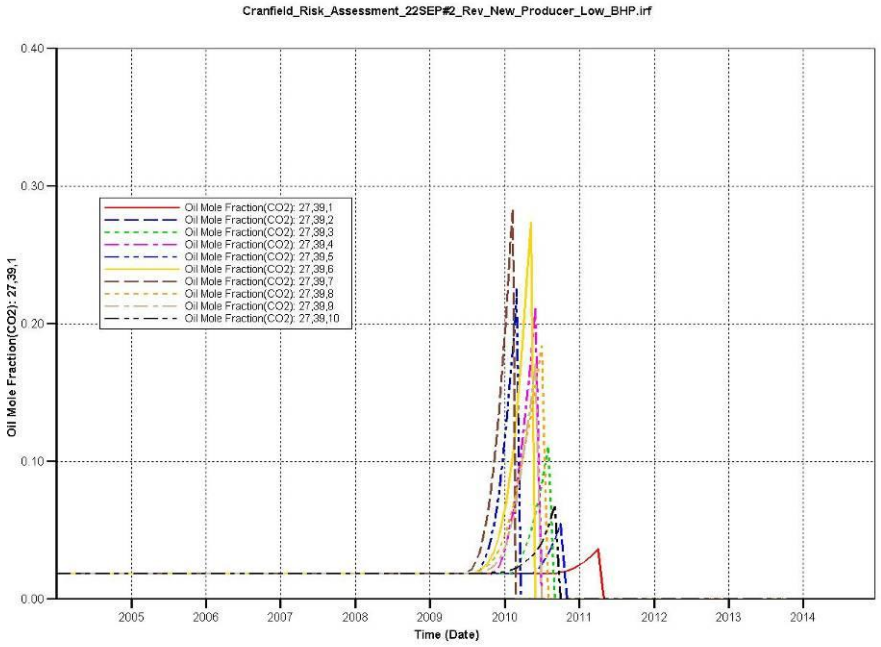

Oil mole fraction of CO_2 Real.2
H H CROSBY ETAL 1 (32,24)

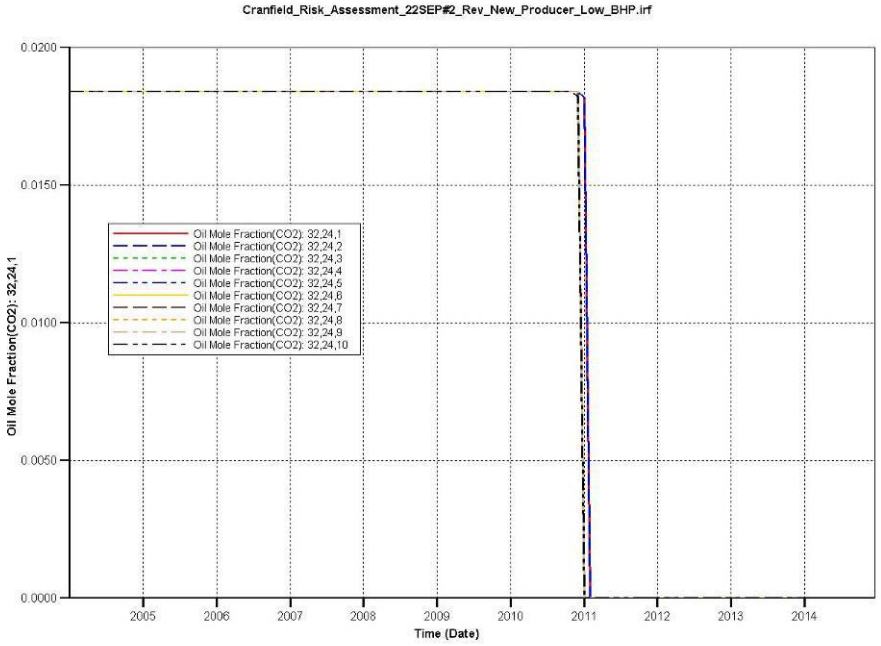

3 Realization #3 (ten cells of a vertical profile displayed on each plot)

Gas saturation Real.3
Cranfield Unit 7 (40,76)

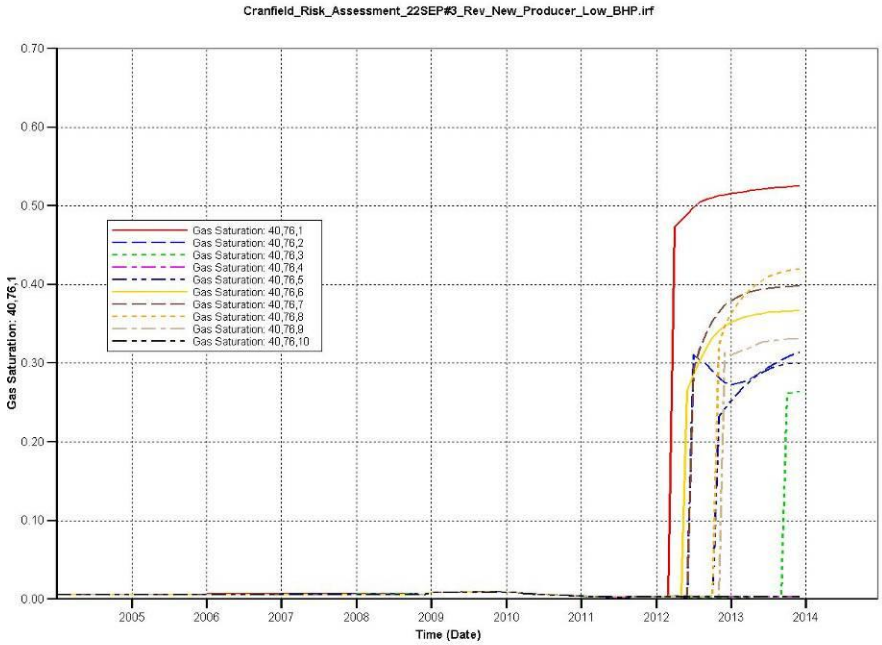

Gas saturation Real.3
Cranfield Unit 4 (26,60)

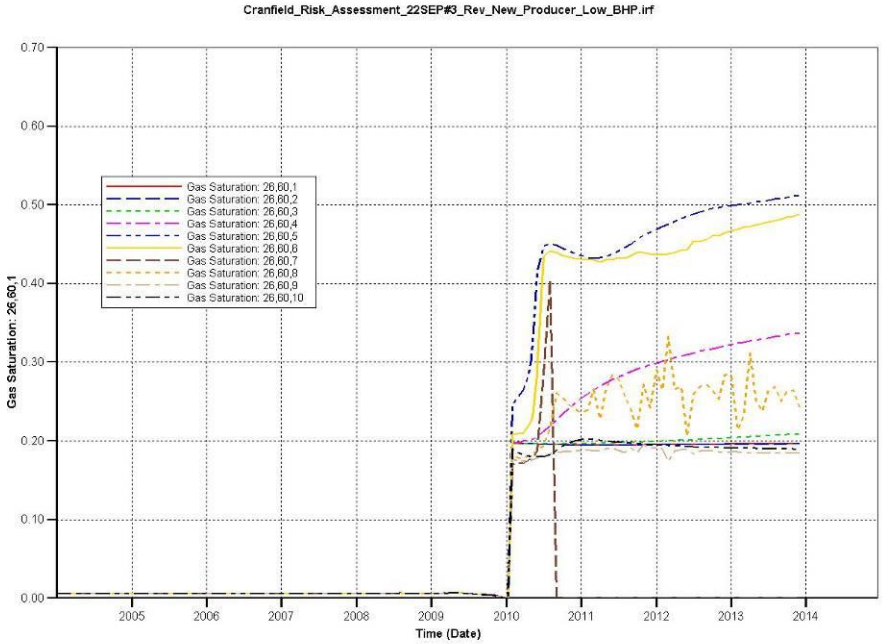

Gas saturation Real.3
Vernon Johnson 1 (22,47)

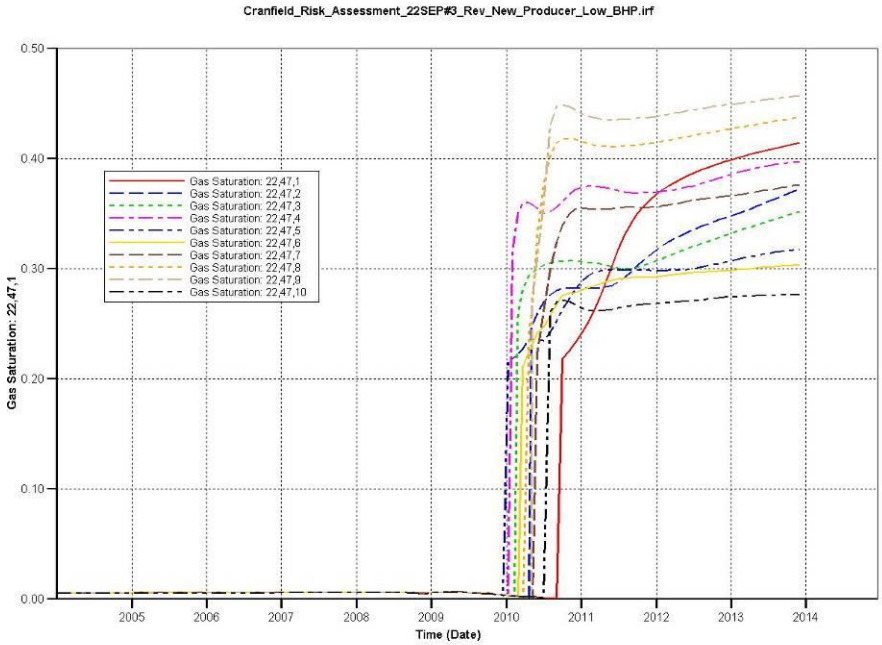

Gas saturation Real.3
Armstrong 4 (11,35)

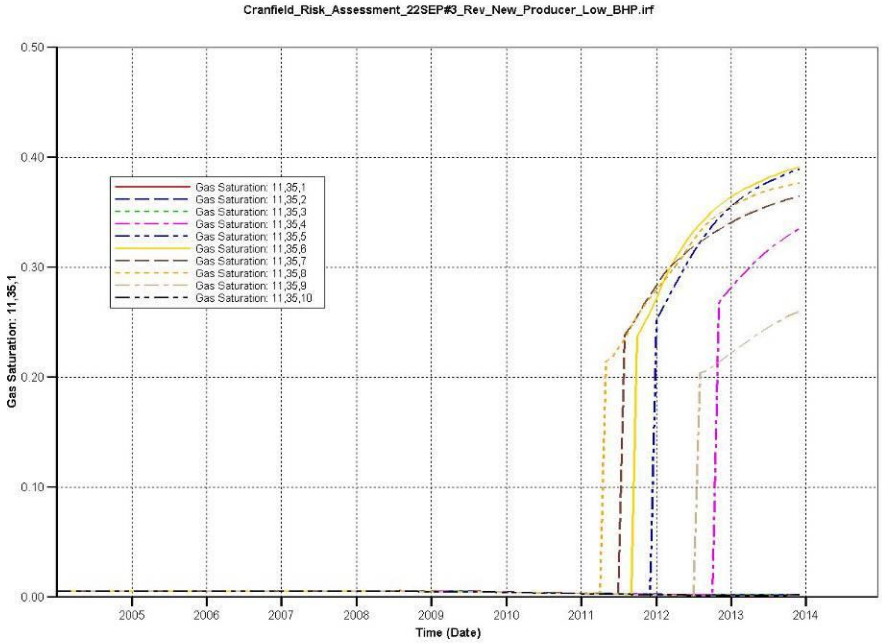

Gas saturation Real.3
Armstrong 2 (18,39)

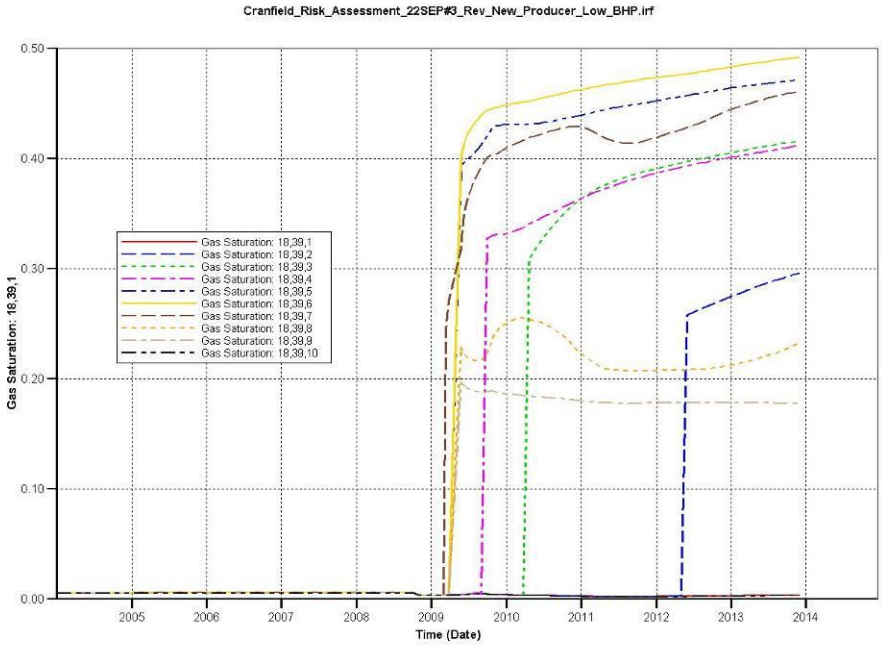

Gas saturation Real.3
R G CALCOTE 1 (27,39)

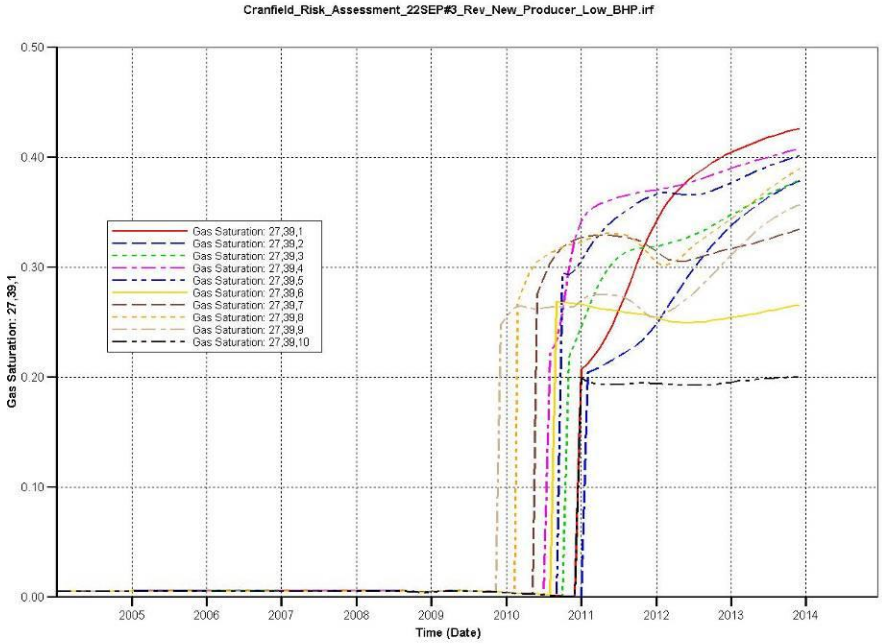

Gas saturation Real.3
H H CROSBY ETAL 1 (32,24)

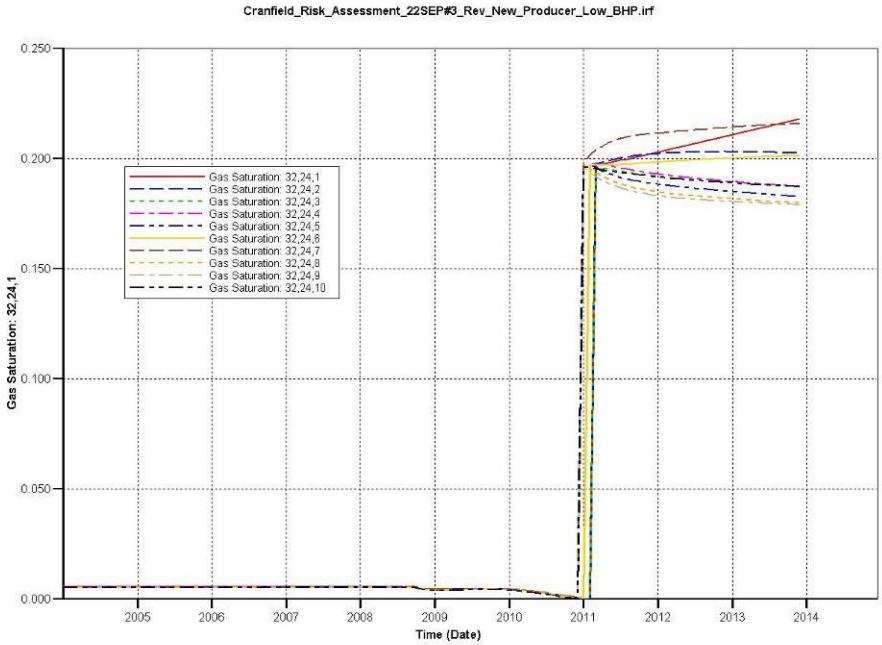

Global mole fraction of CO_2 Real.3
Cranfield Unit 7 (40,76)

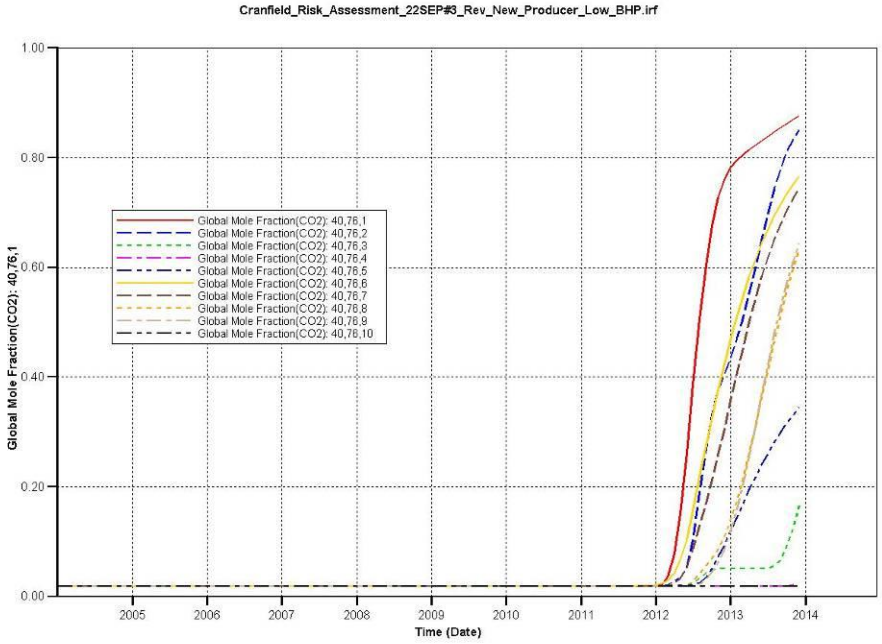

Global mole fraction of CO_2 Real.3

Cranfield Unit 4 (26,60)

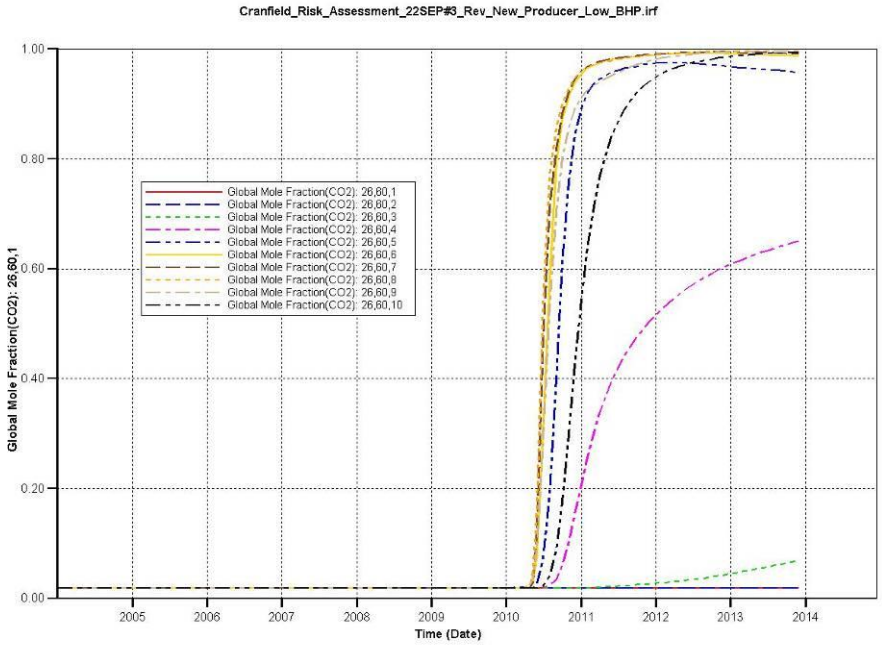

Global mole fraction of CO_2 Real.3

Vernon Johnson 1 (22,47)

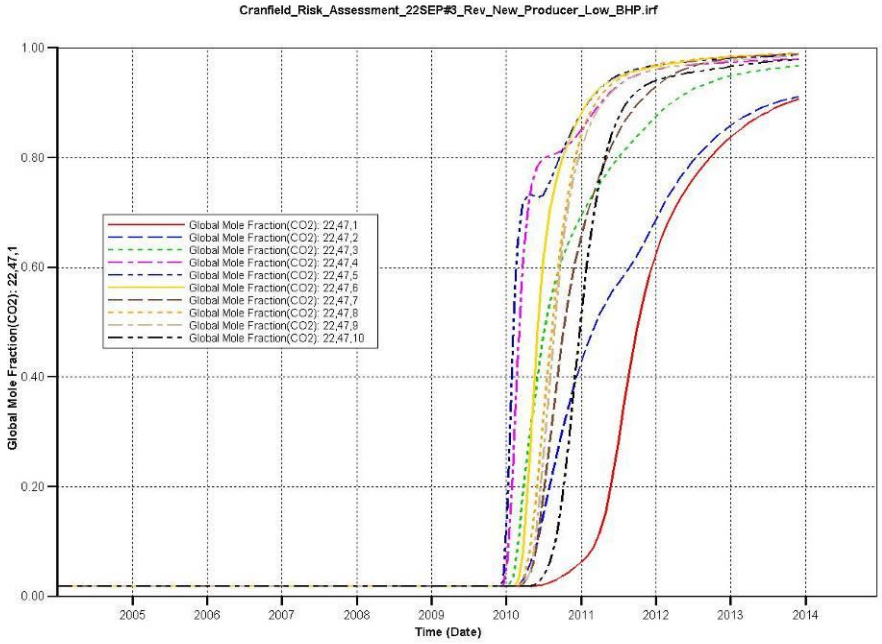

Global mole fraction of CO_2 Real.3
Armstrong 4 (11,35)

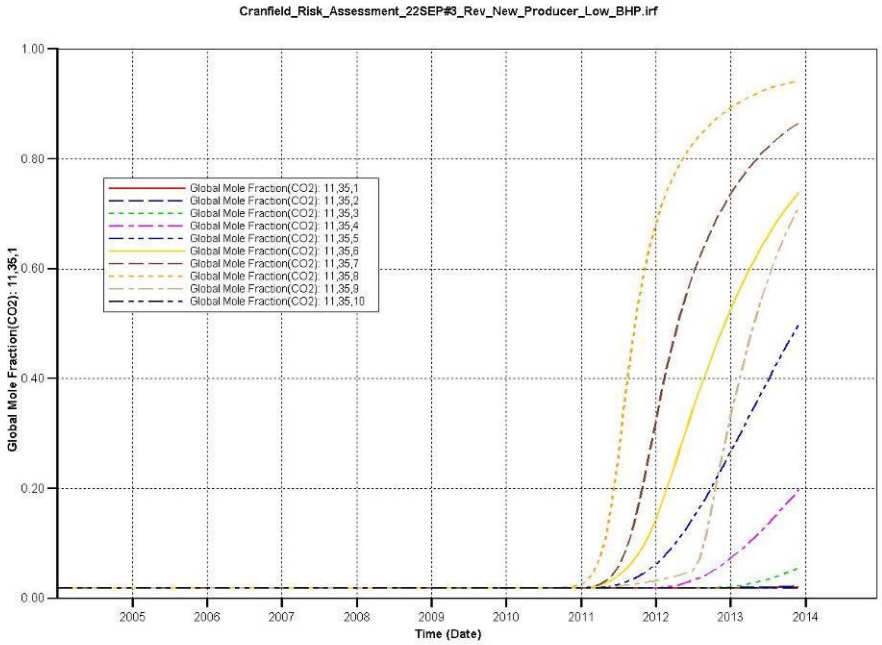

Global mole fraction of CO_2 Real.3
Armstrong 2 (18,39)

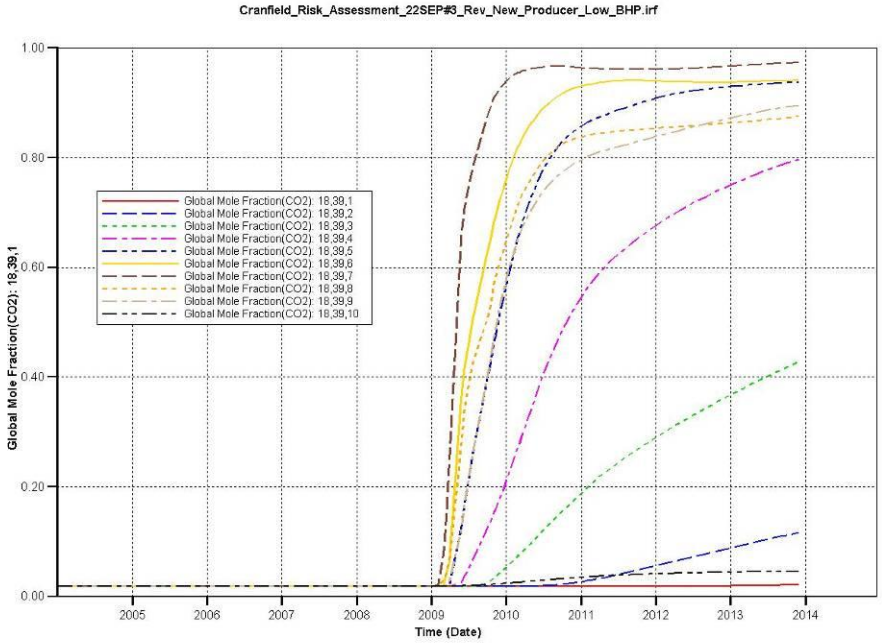

Global mole fraction of CO_2 Real.3
R G CALCOTE 1 (27,39)

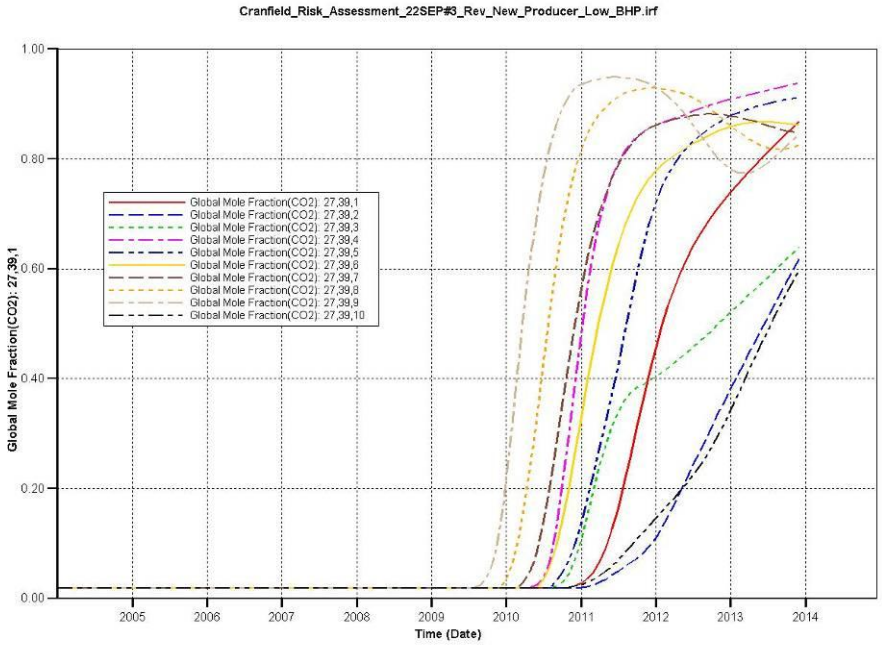

Global mole fraction of CO_2 Real.3
H H CROSBY ETAL 1 (32,24)

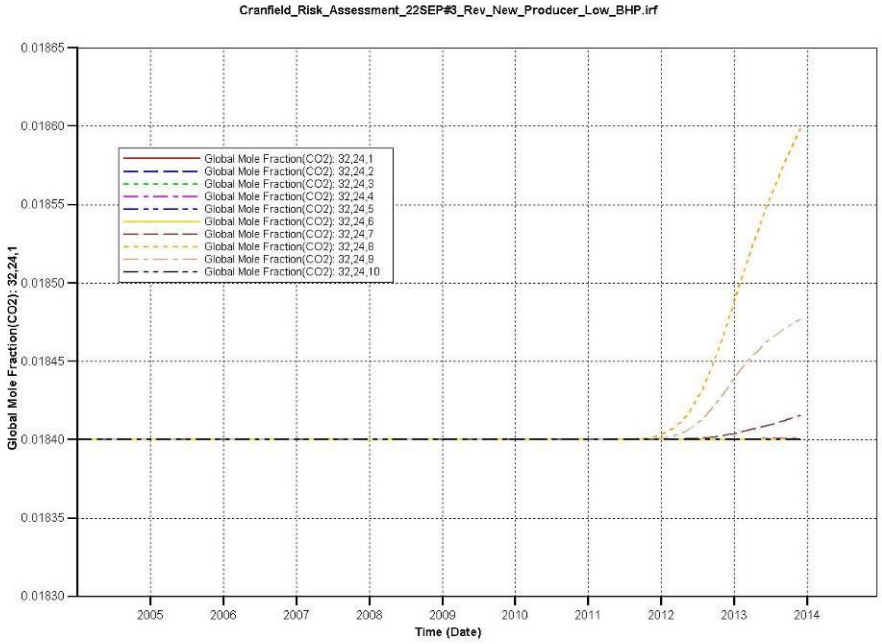

Oil mole fraction of CO_2 Real.3
Cranfield Unit 7 (40,76)

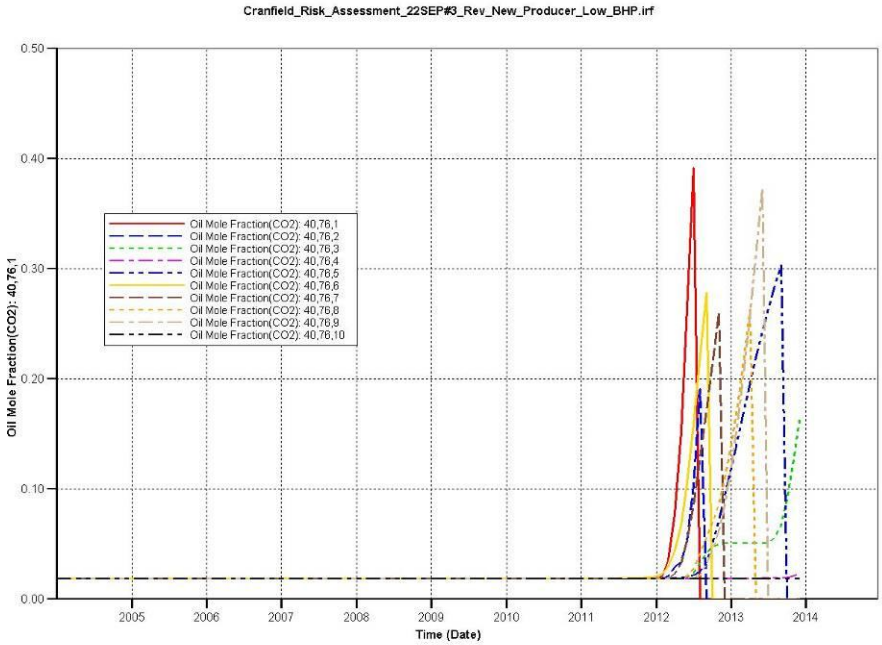

Oil mole fraction of CO_2 Real.3
Cranfield Unit 4 (26,60)

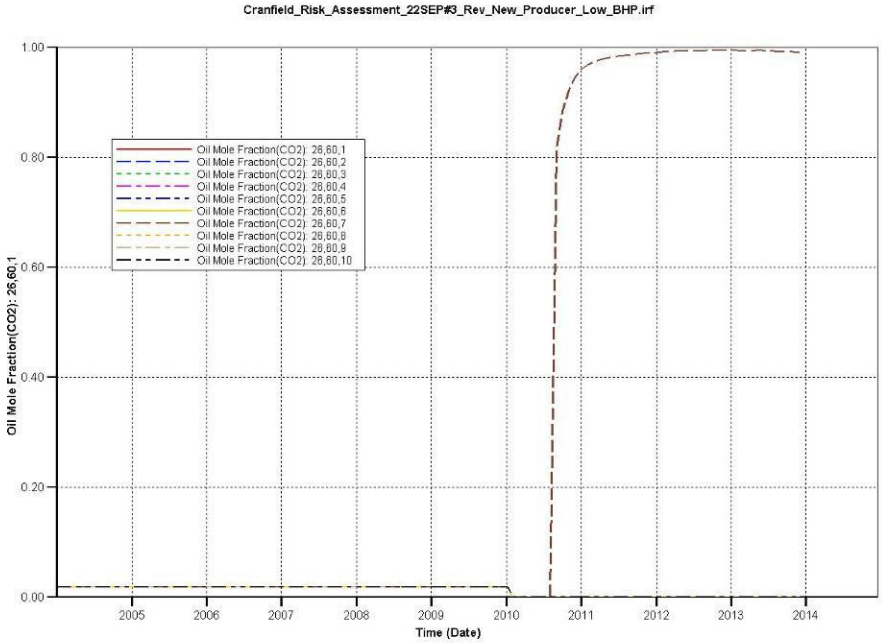

Oil mole fraction of CO_2 Real.3

Vernon Johnson 1 (22,47)

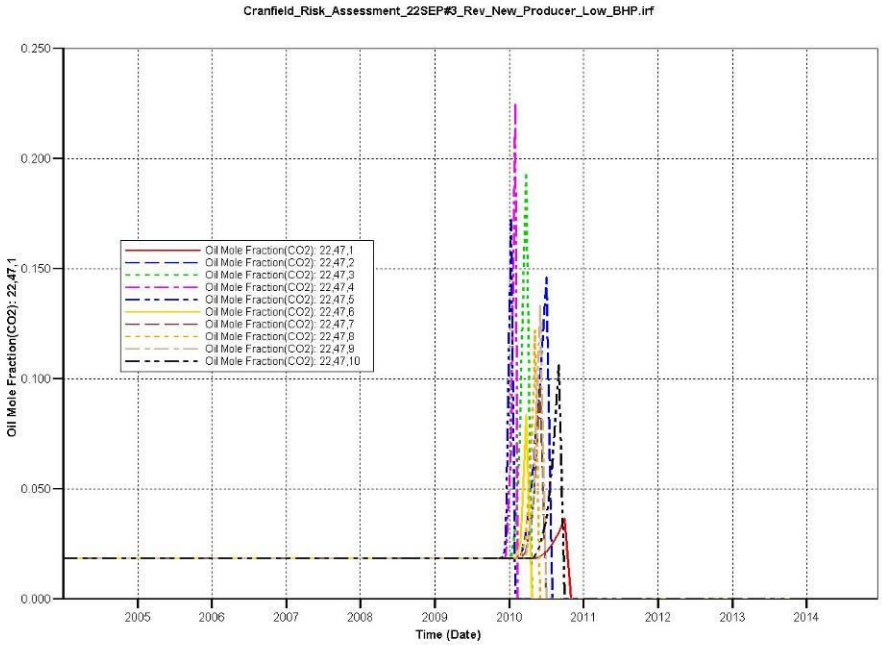

Oil mole fraction of CO_2 Real.3

Armstrong 4 (11,35)

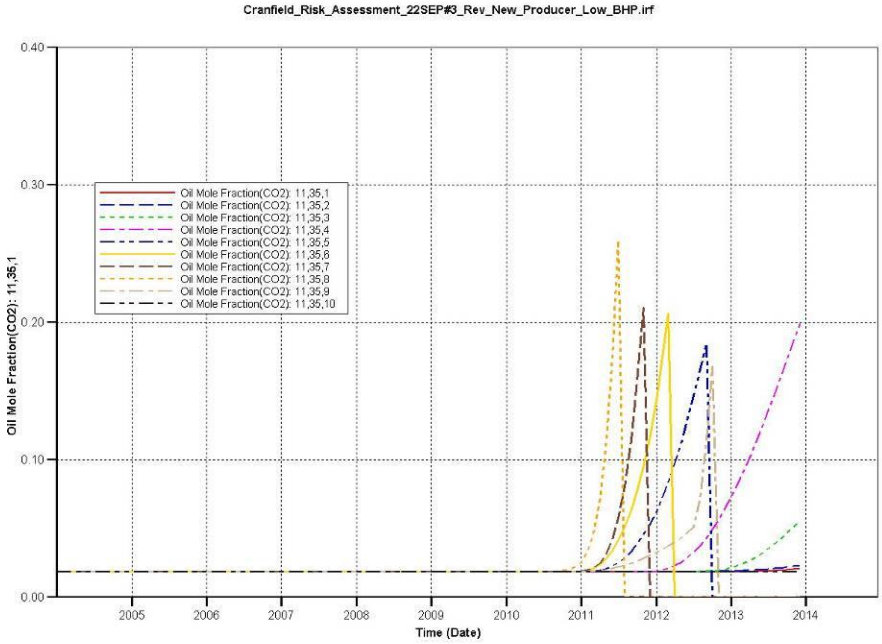

Oil mole fraction of CO_2 Real.3
Armstrong 2 (18,39)

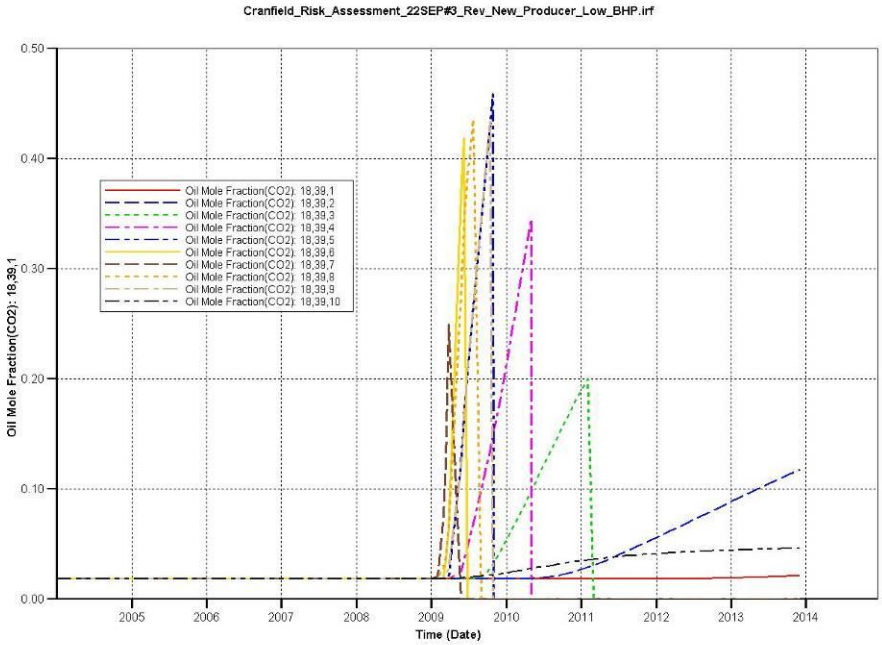

Oil mole fraction of CO_2 Real.3
R G CALCOTE 1 (27,39)

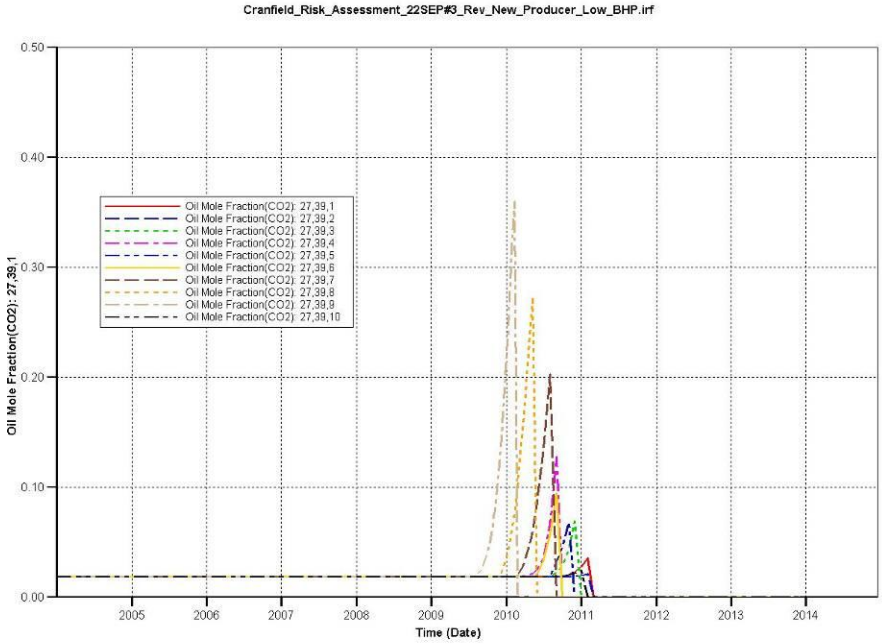

Oil mole fraction of CO_2 Real.3
H H CROSBY ETAL 1 (32,24)

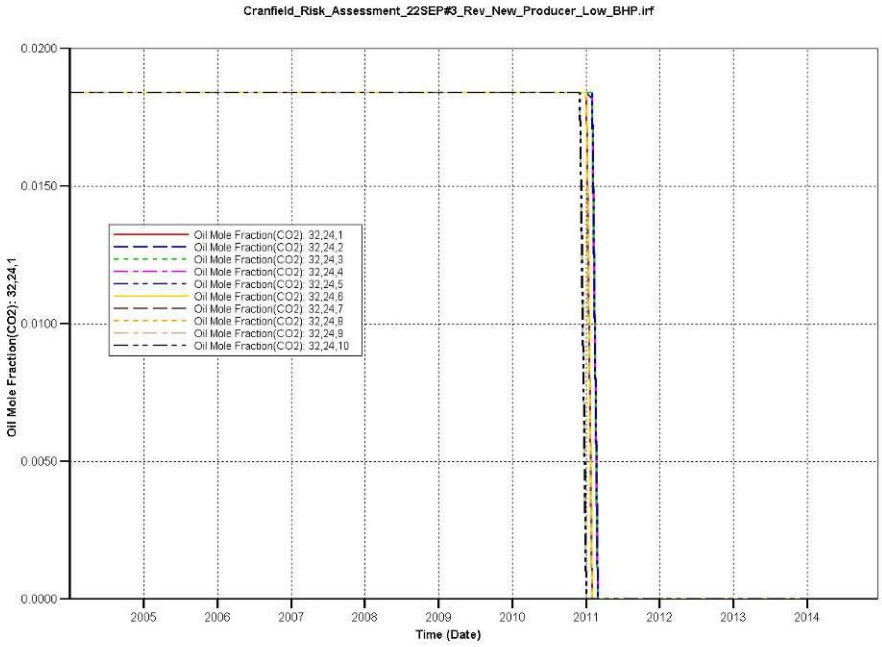

4 Realization #4 (ten cells of a vertical profile displayed on each plot)

Gas saturation Real.4
Cranfield Unit 7 (40,76)

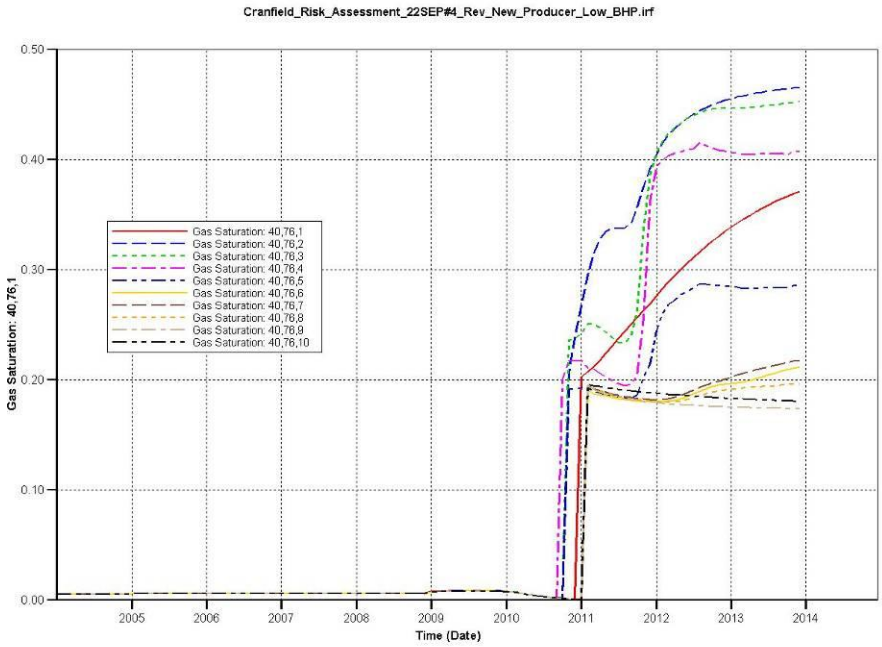

Gas saturation Real.4
Cranfield Unit 4 (26,60)

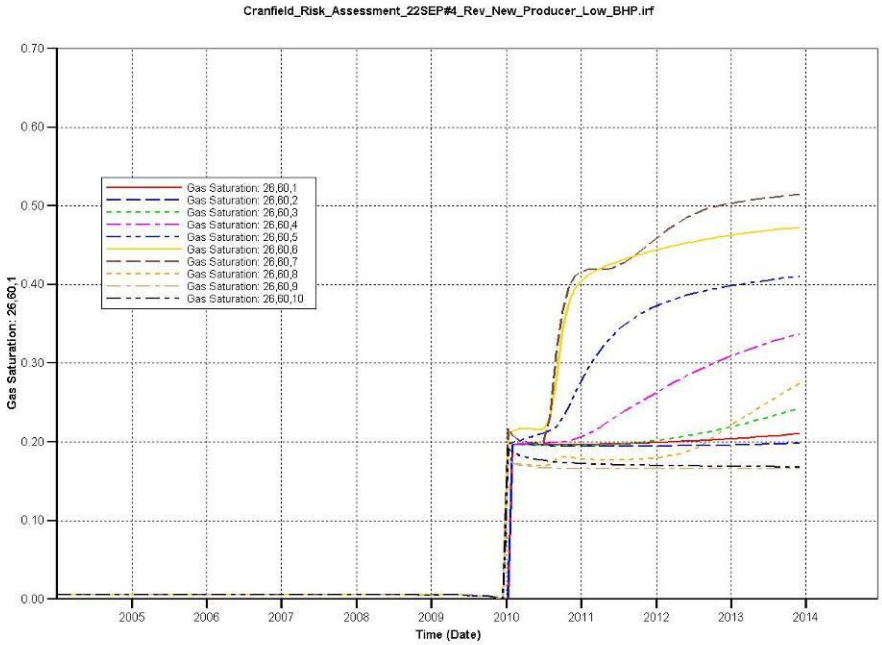

Gas saturation Real.4
Vernon Johnson 1 (22,47)

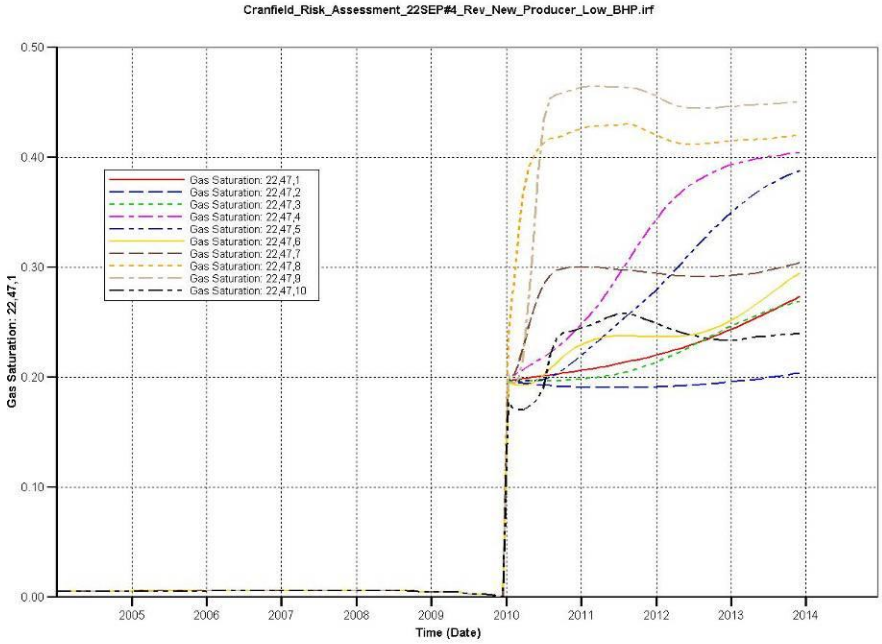

Gas saturation Real.4
Armstrong 4 (11,35)

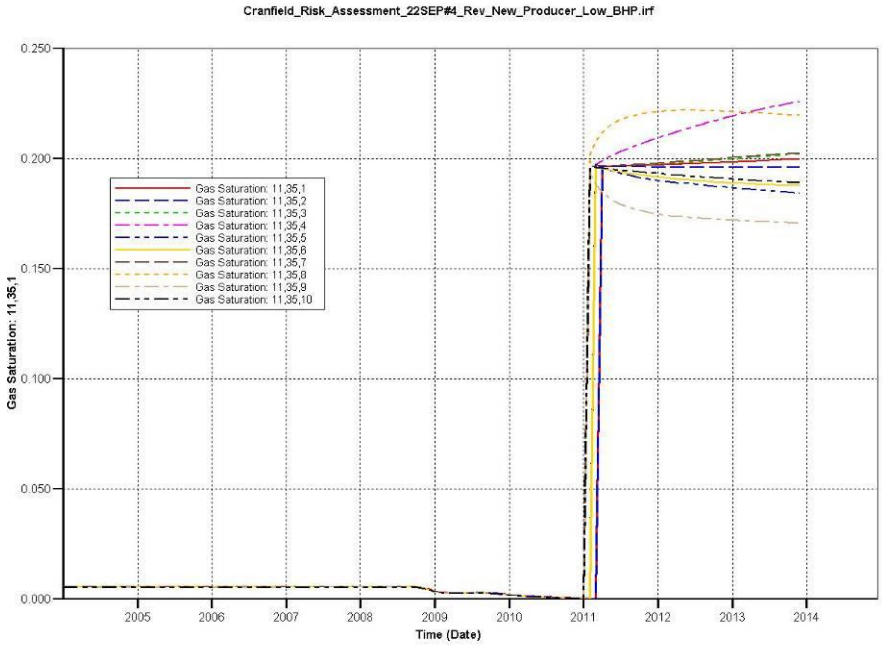

Gas saturation Real.4
Armstrong 2 (18,39)

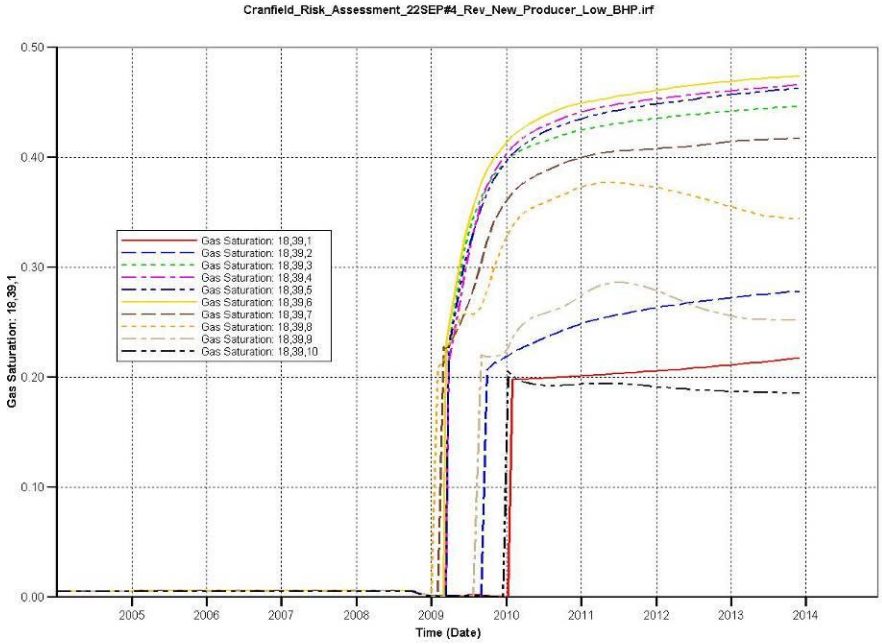

Gas saturation Real.4
R G CALCOTE 1 (27,39)

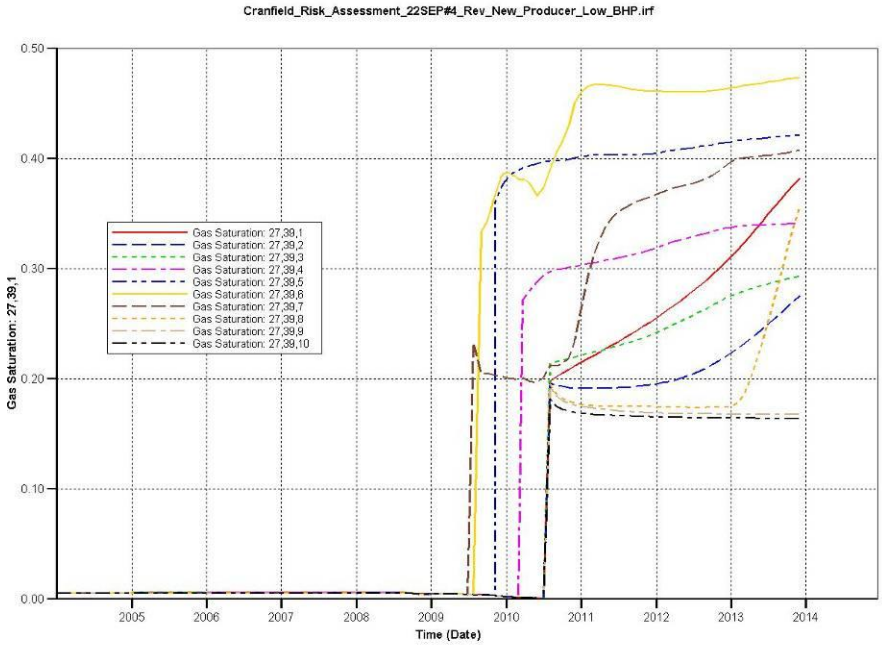

Gas saturation Real.4
H H CROSBY ETAL 1 (32,24)

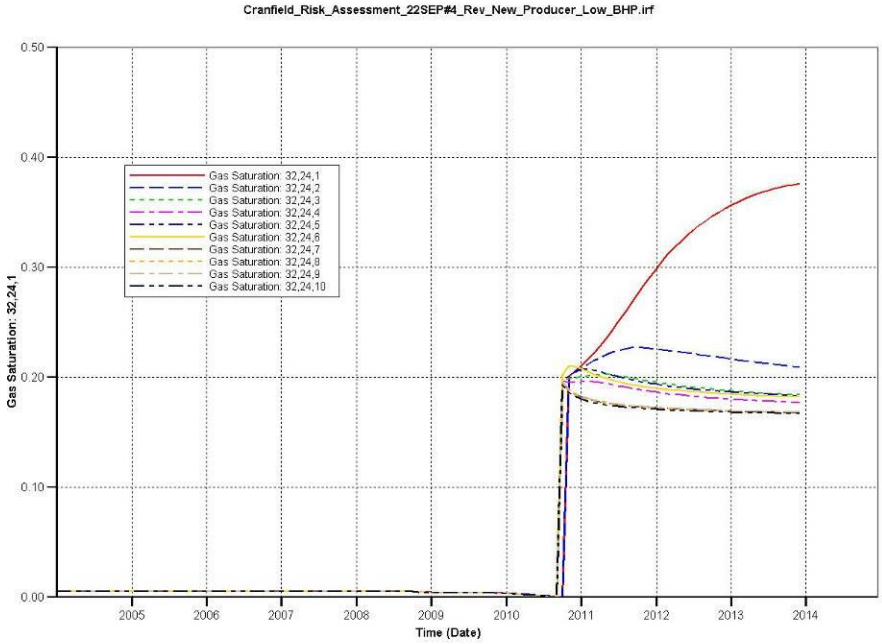

Global mole fraction of CO_2 Real.4
Cranfield Unit 7 (40,76)

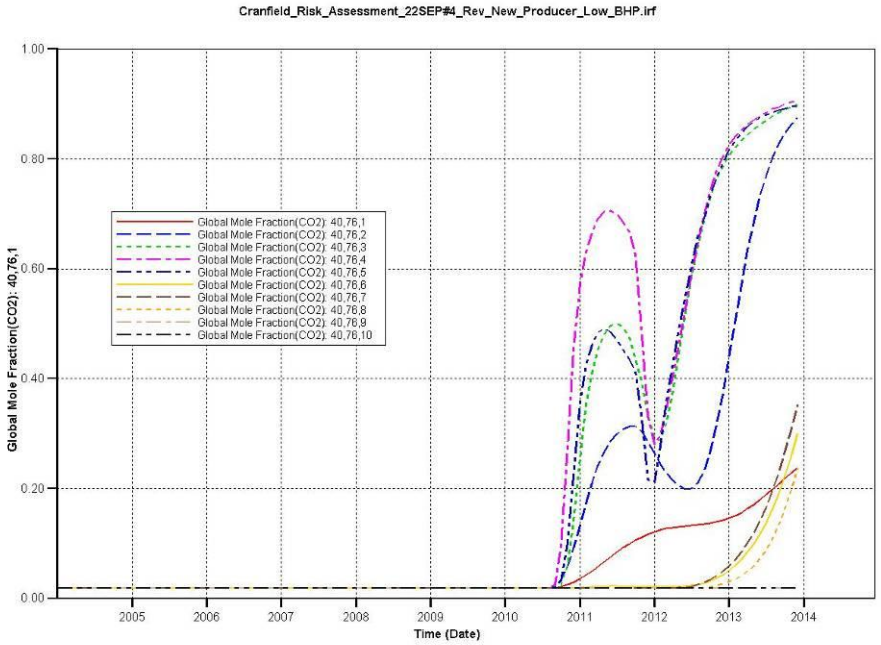

Global mole fraction of CO_2 Real.4
Cranfield Unit 4 (26,60)

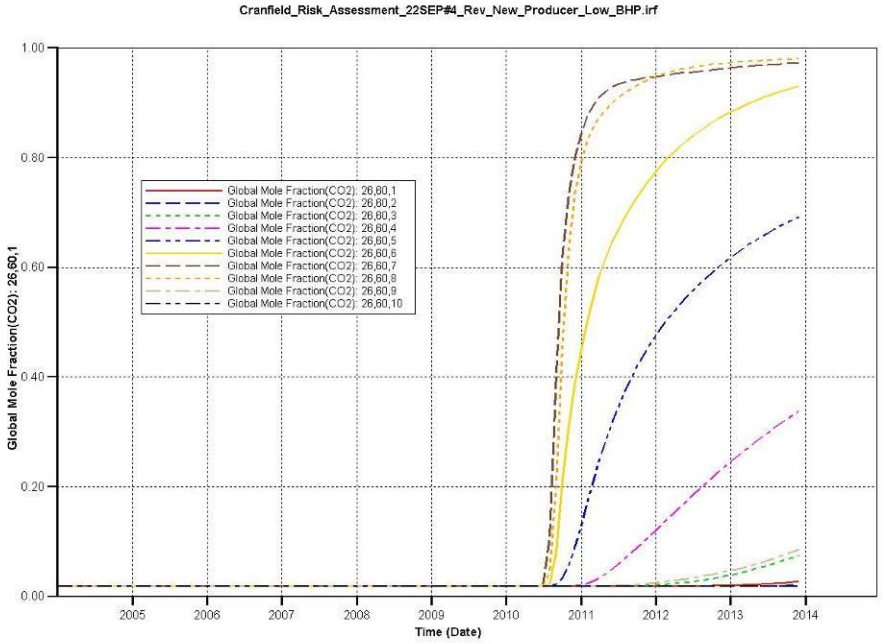

Global mole fraction of CO_2 Real.4
Vernon Johnson 1 (22,47)

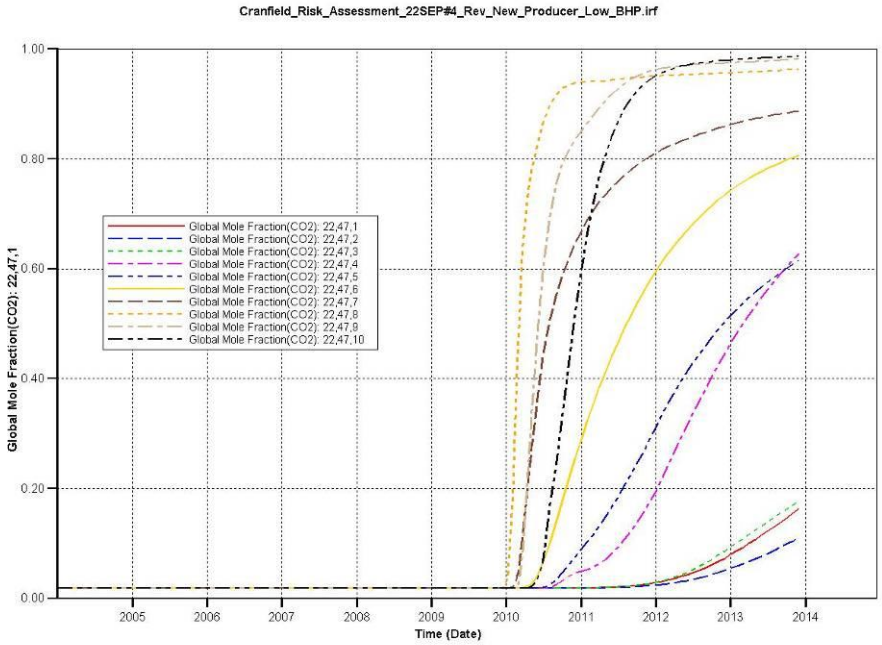

Global mole fraction of CO_2 Real.4
Armstrong 4 (11,35)

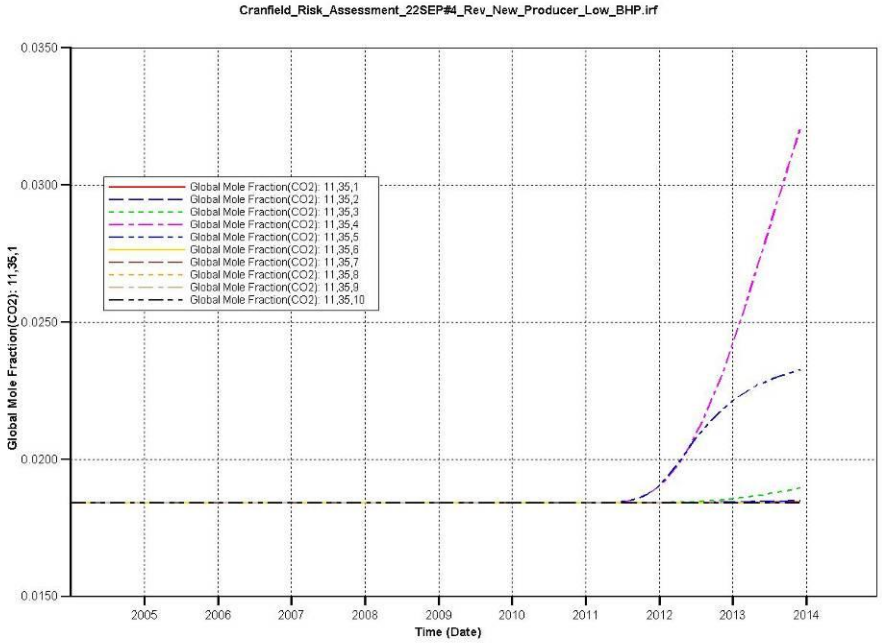

Global mole fraction of CO_2 Real.4
Armstrong 2 (18,39)

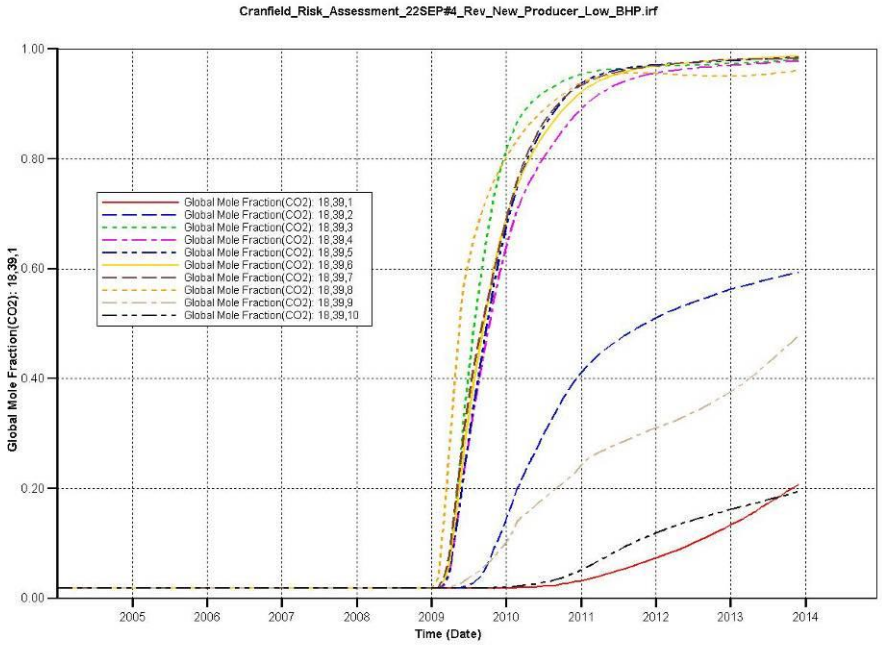

Global mole fraction of CO_2 Real.4
R G CALCOTE 1 (27,39)

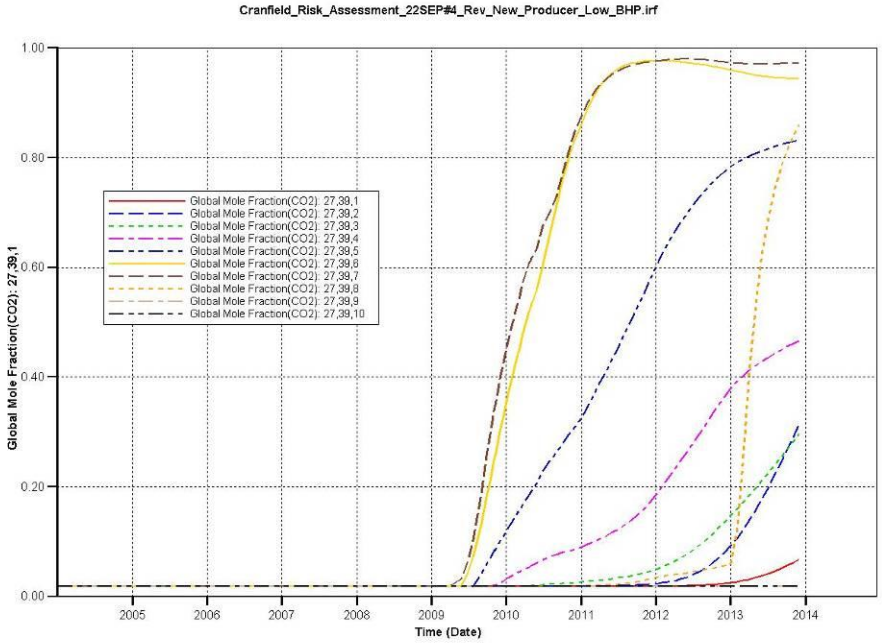

Global mole fraction of CO_2 Real.4
H H CROSBY ETAL 1 (32,24)

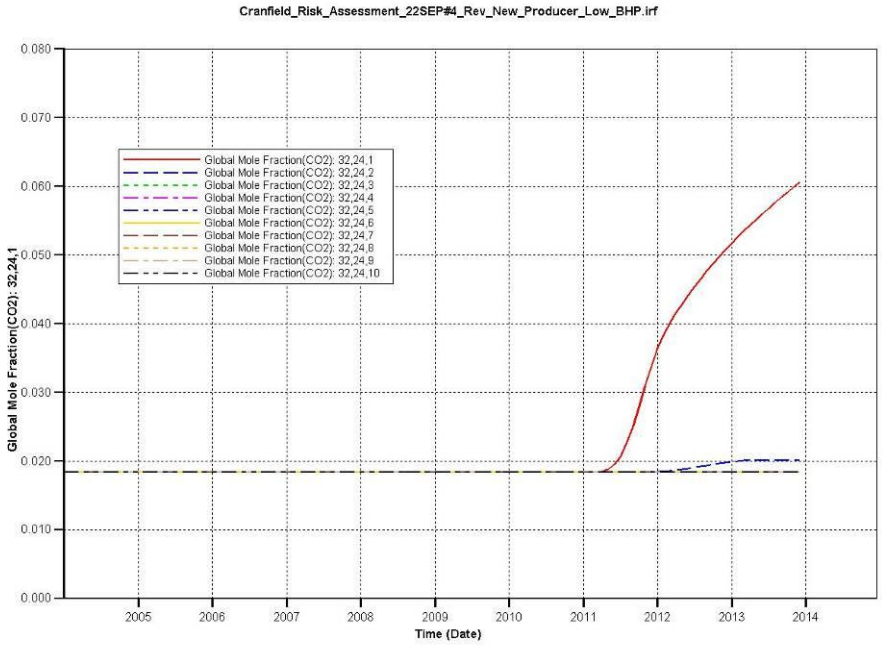

Oil mole fraction of CO_2 Real.4
Cranfield Unit 7 (40,76)

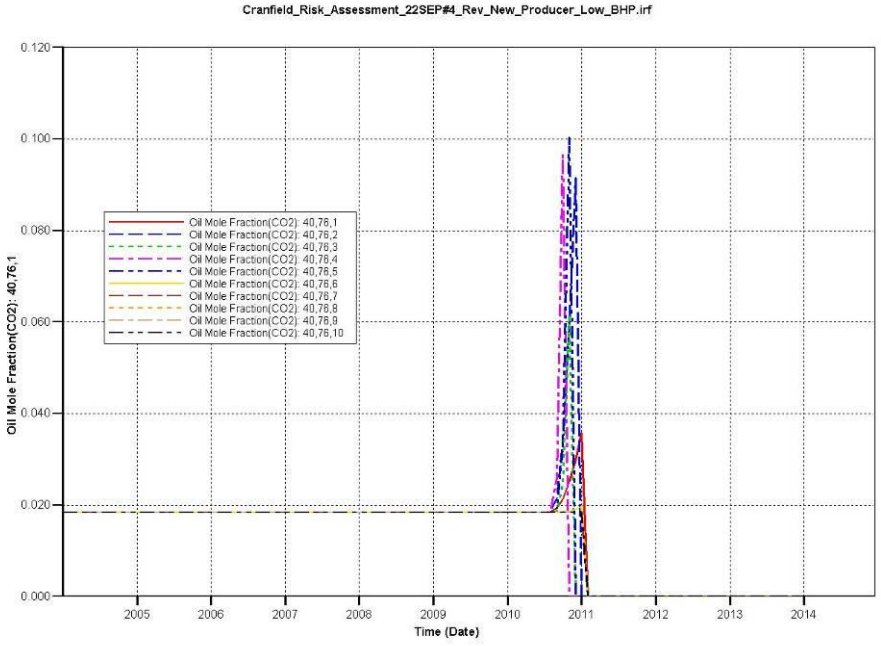

Oil mole fraction of CO_2 Real.4

Cranfield Unit 4 (26,60)

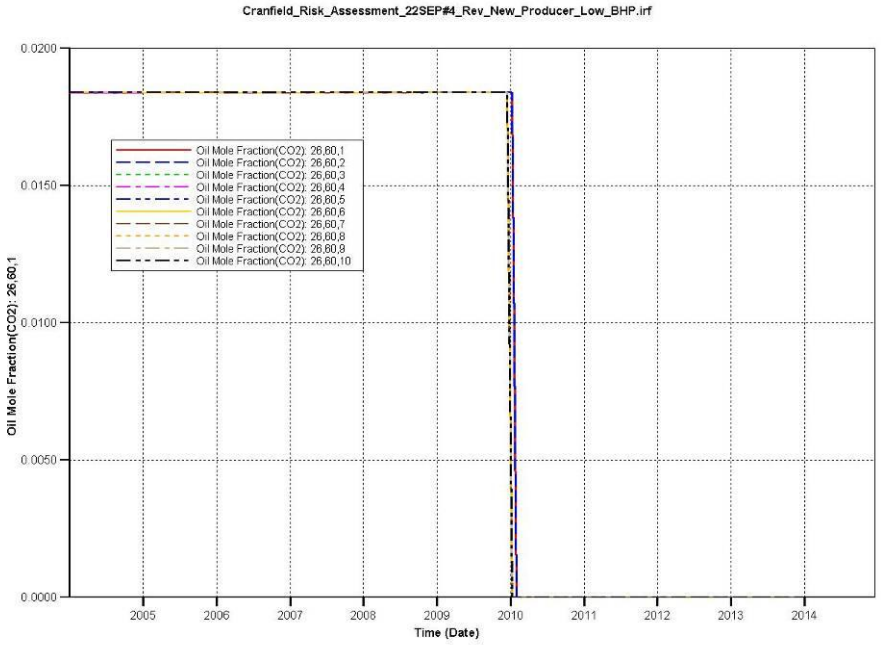

Oil mole fraction of CO_2 Real.4

Vernon Johnson 1 (22,47)

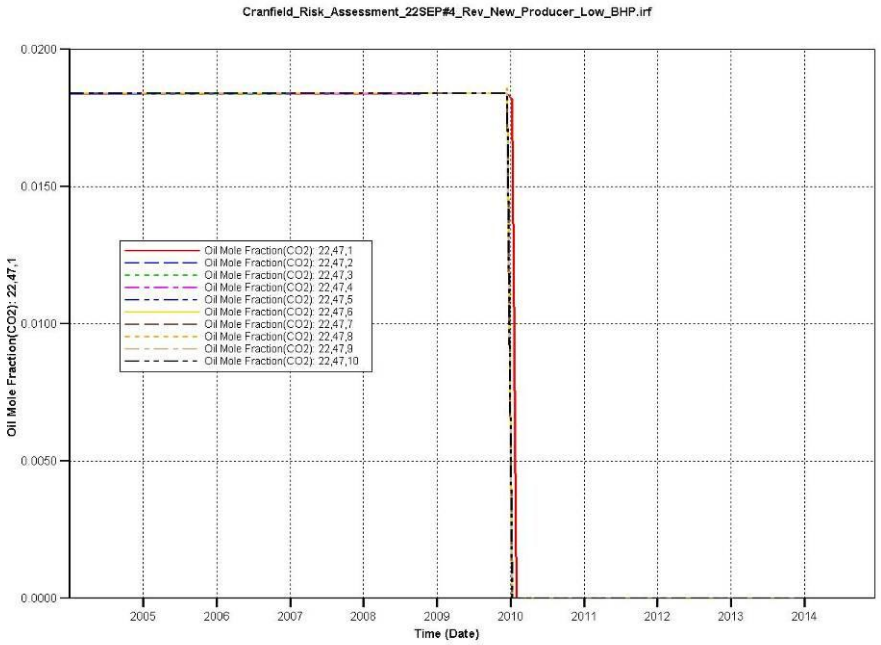

Oil mole fraction of CO_2 Real.4
Armstrong 4 (11,35)

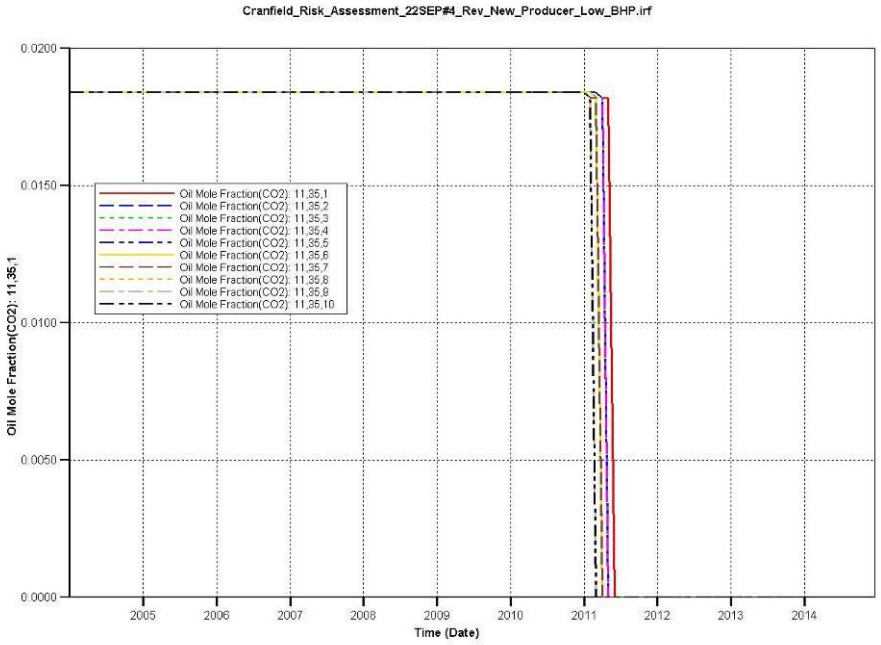

Oil mole fraction of CO_2 Real.4
Armstrong 2 (18,39)

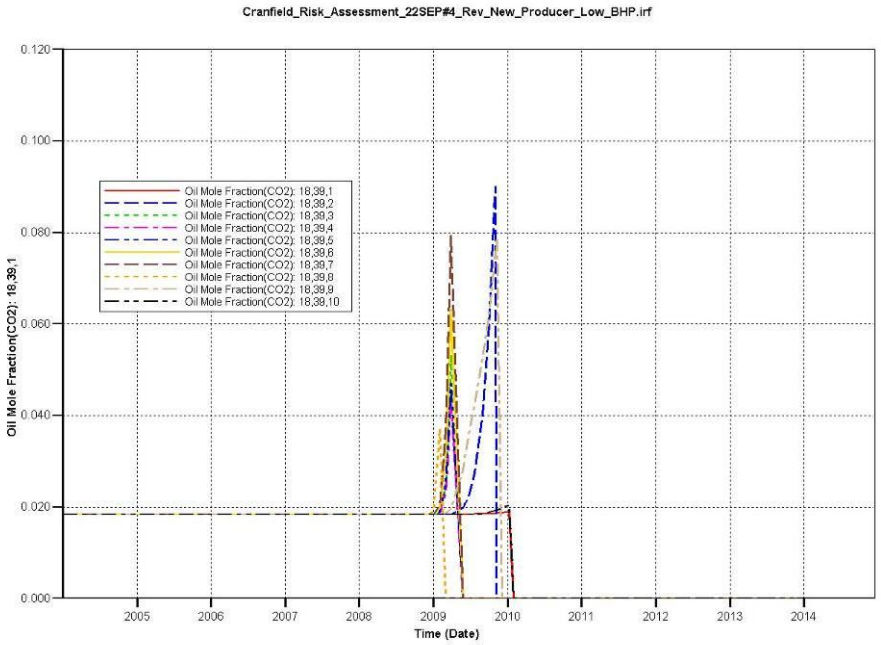

Oil mole fraction of CO_2 Real.4
R G CALCOTE 1 (27,39)

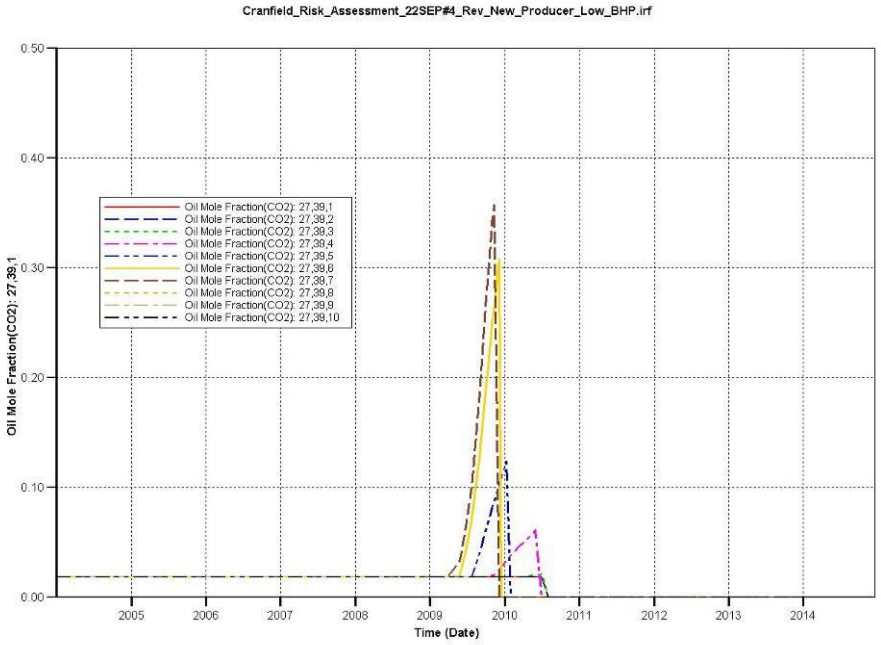

Oil mole fraction of CO_2 Real.4
H H CROSBY ETAL 1 (32,24)

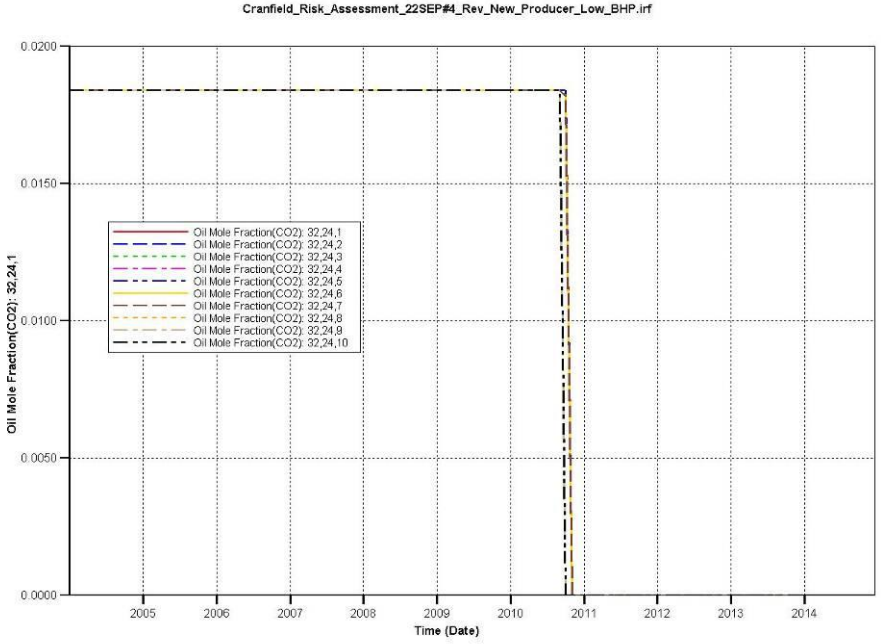

5 Realization #5 (ten cells of a vertical profile displayed on each plot)

Gas saturation Real.5
Cranfield Unit 7 (40,76)

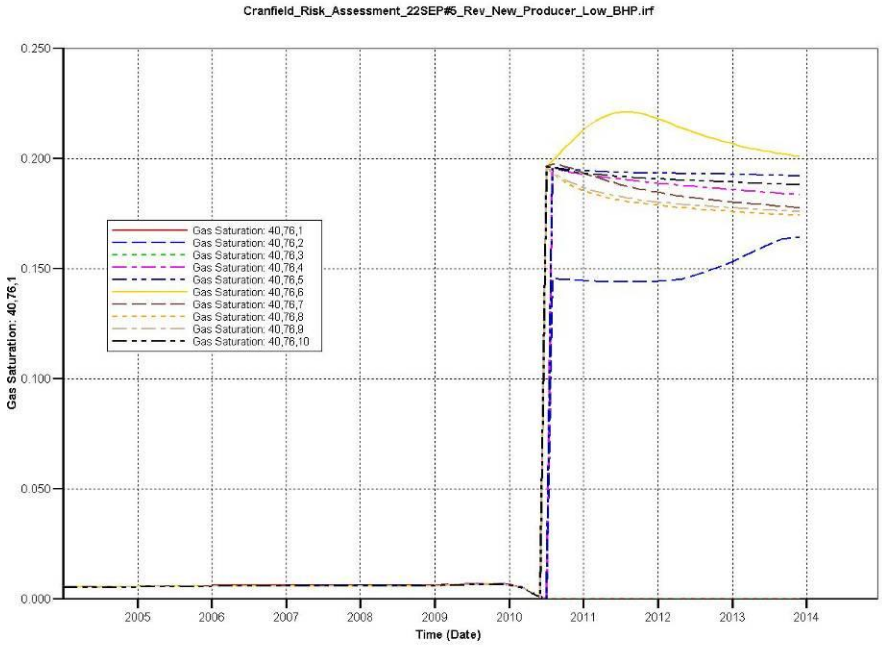

Gas saturation Real.5
Cranfield Unit 4 (26,60)

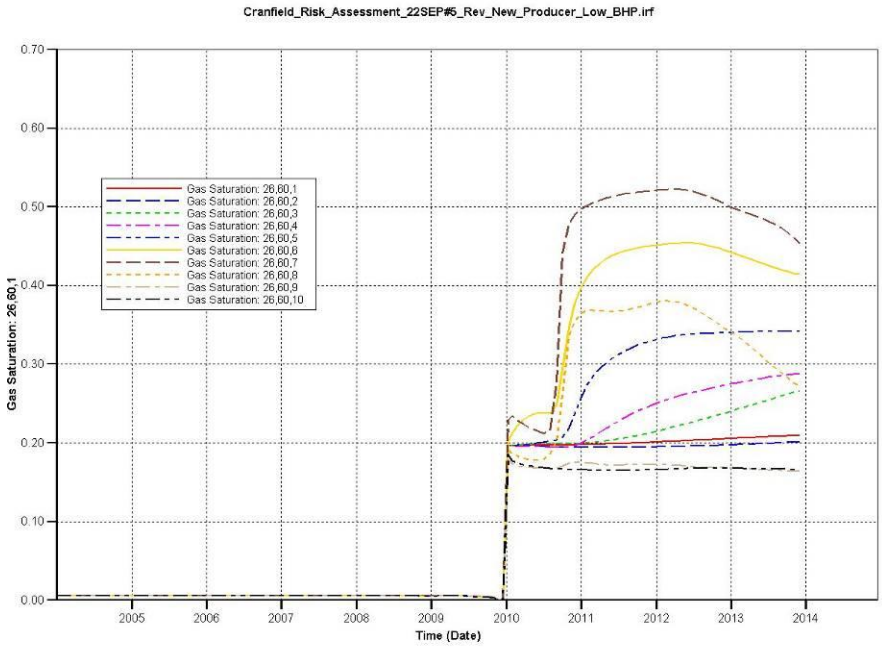

Gas saturation Real.5
Vernon Johnson 1 (22,47)

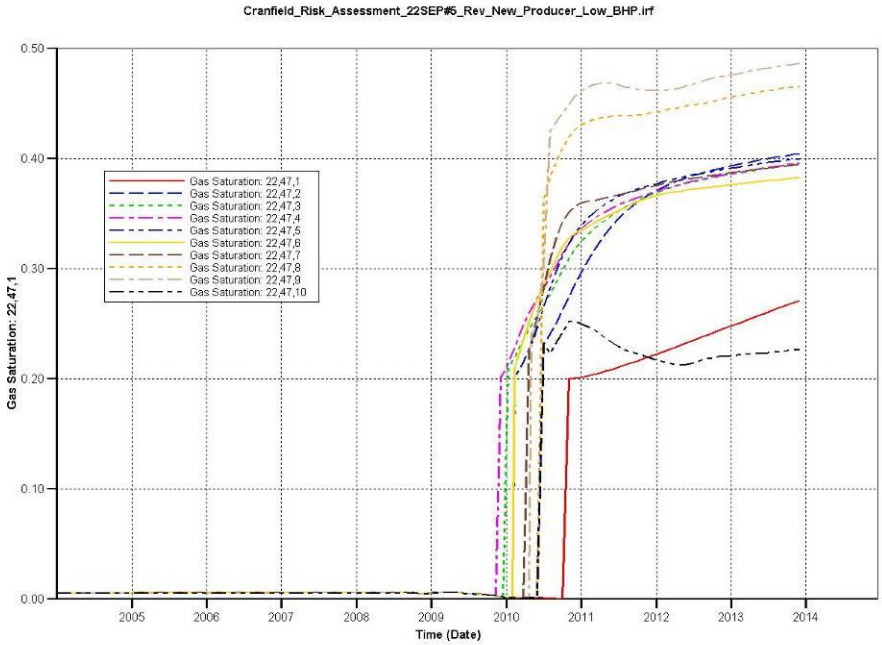

Gas saturation Real.5
Armstrong 4 (11,35)

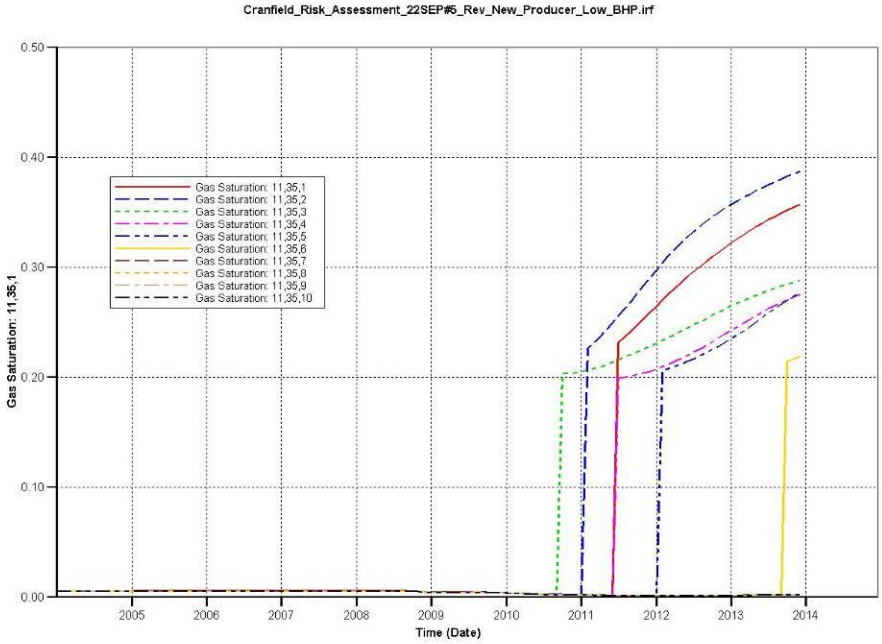

Gas saturation Real.5
Armstrong 2 (18,39)

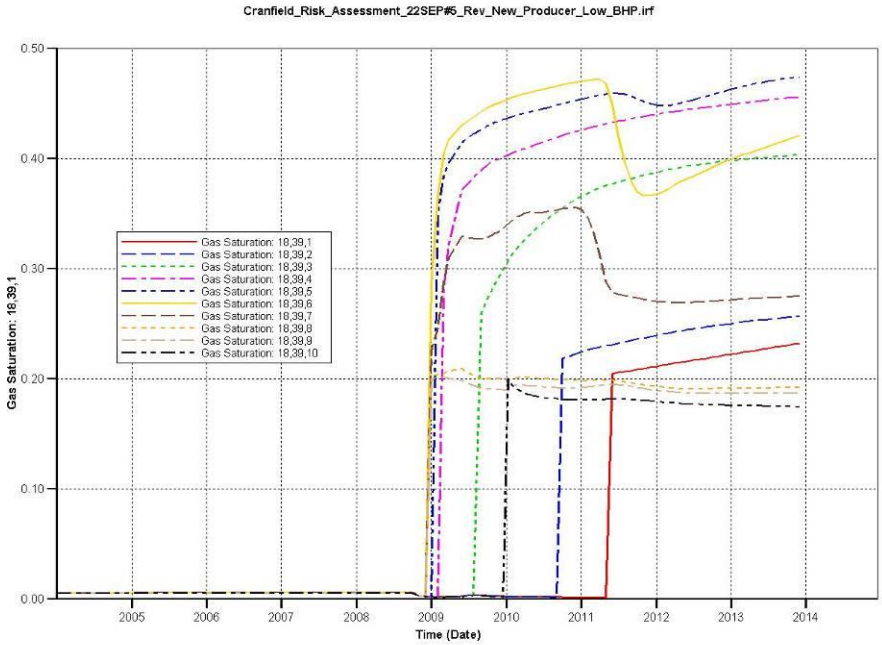

Gas saturation Real.5
R G CALCOTE 1 (27,39)

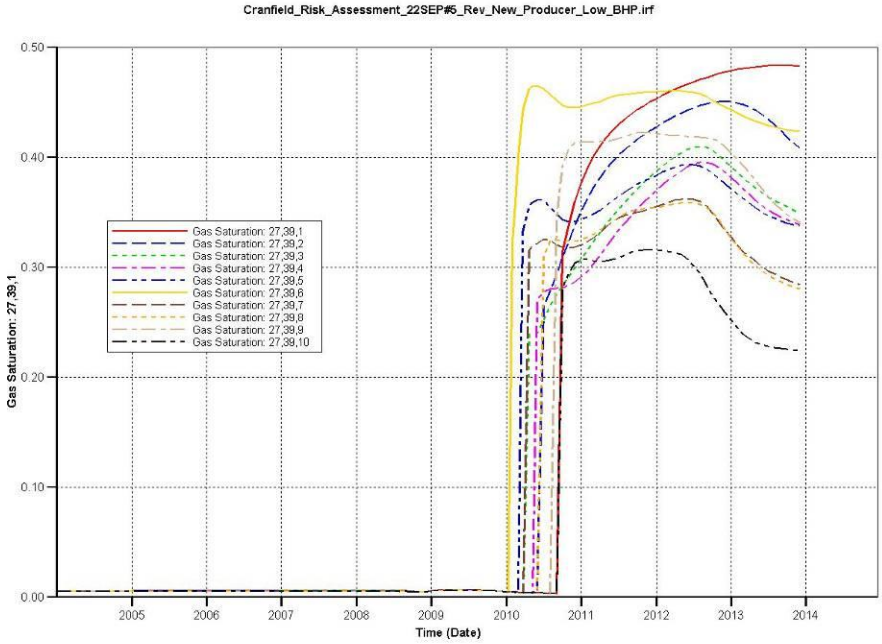

Gas saturation Real.5
H H CROSBY ETAL 1 (32,24)

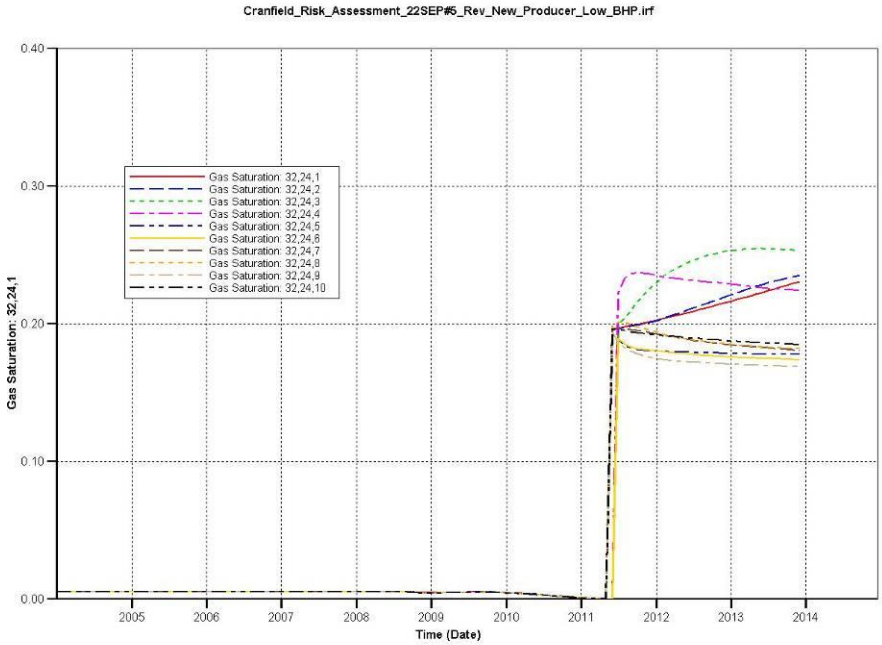

Global mole fraction of CO_2 Real.5
Cranfield Unit 7 (40,76)

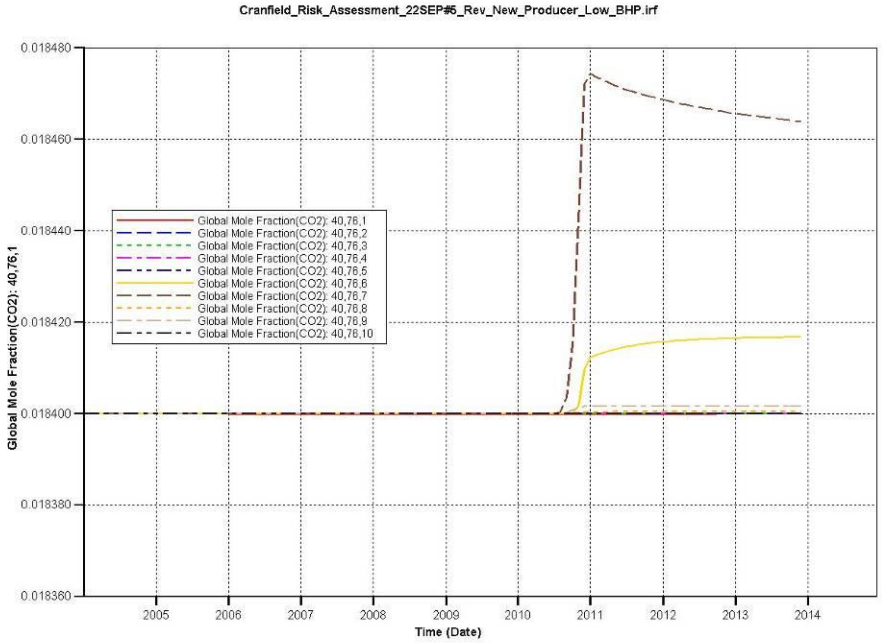

Global mole fraction of CO_2 Real.5
Cranfield Unit 4 (26,60)

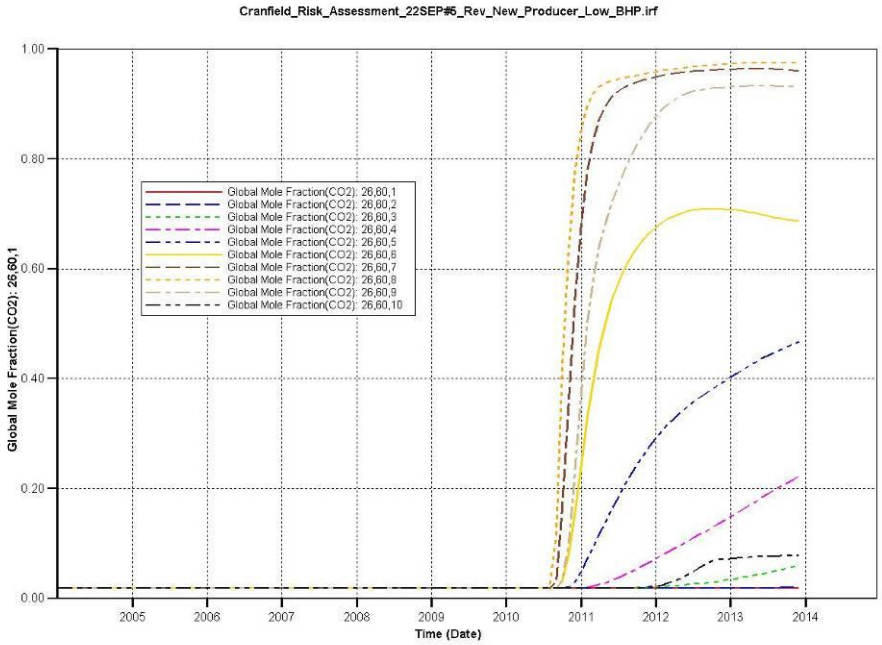

Global mole fraction of CO_2 Real.5
Vernon Johnson 1 (22,47)

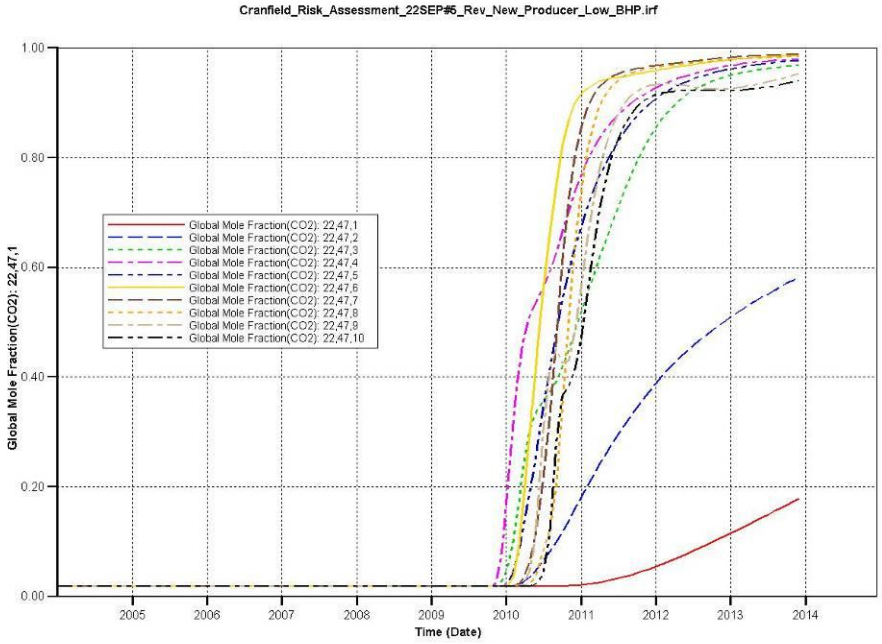

Global mole fraction of CO_2 Real.5
Armstrong 4 (11,35)

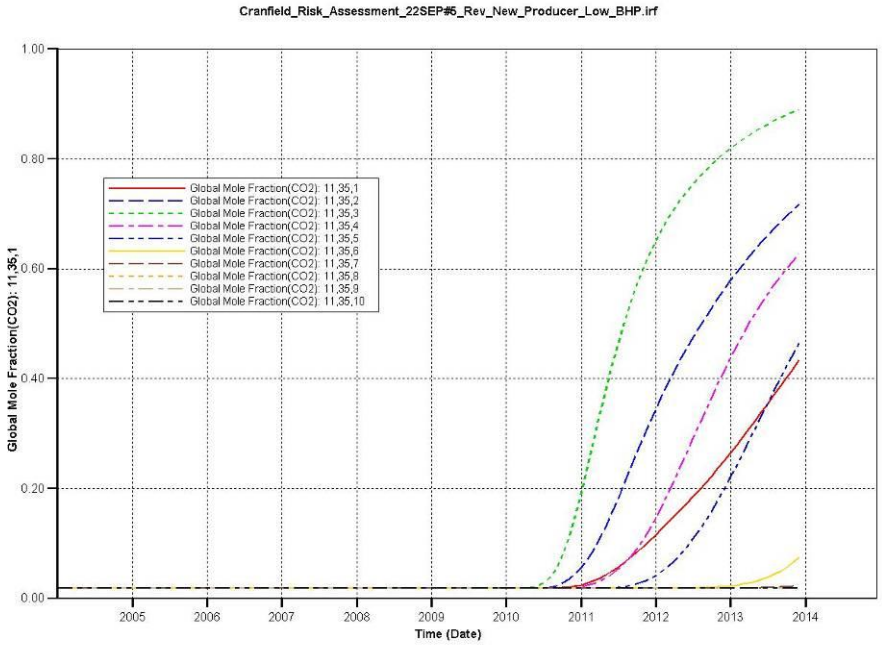

Global mole fraction of CO_2 Real.5
Armstrong 2 (18,39)

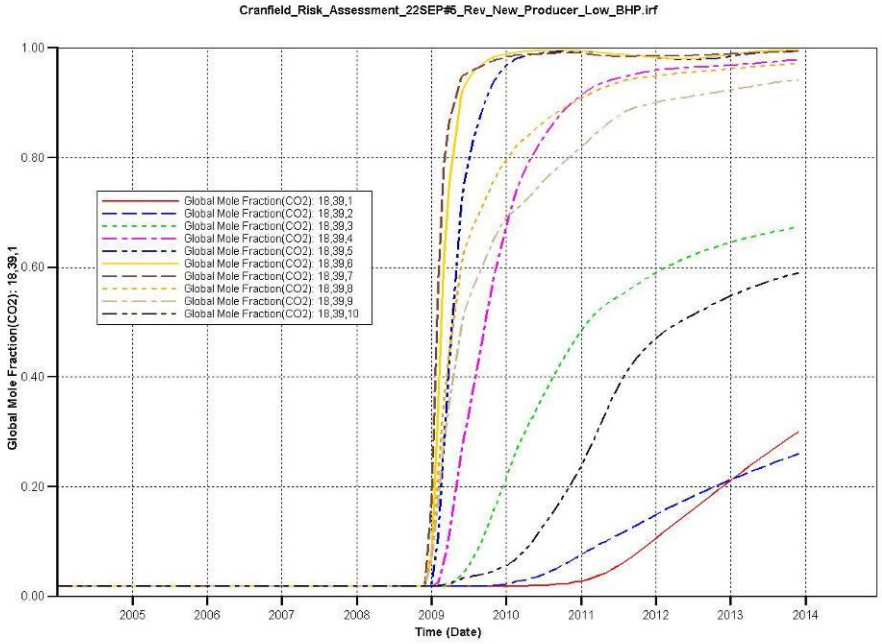

Global mole fraction of CO_2 Real.5
R G CALCOTE 1 (27,39)

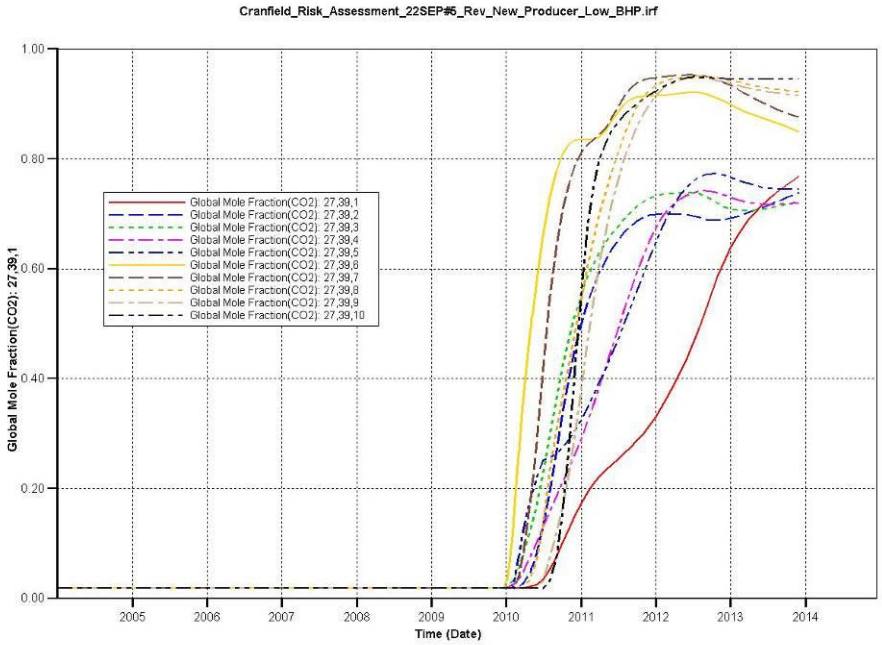

Global mole fraction of CO_2 Real.5
H H CROSBY ETAL 1 (32,24)

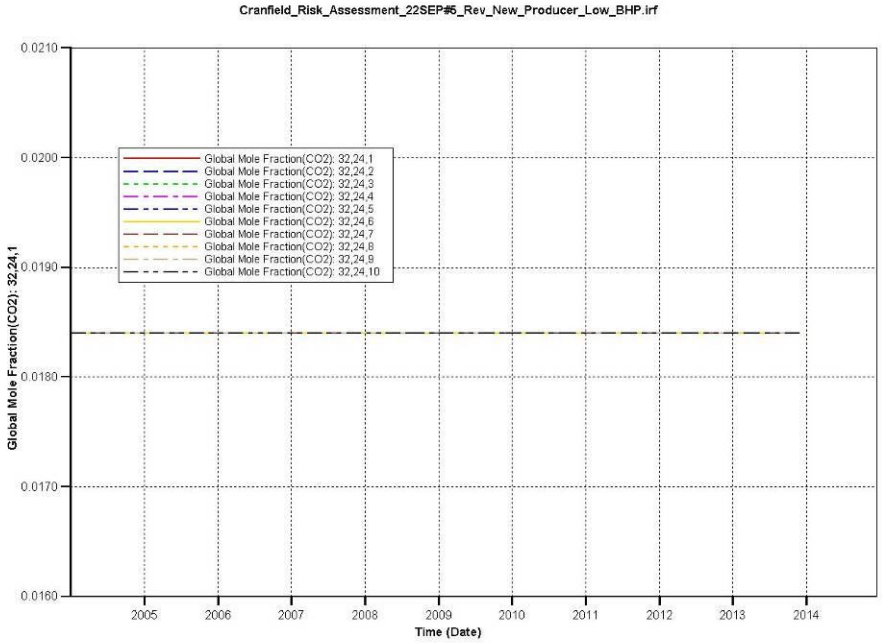

Oil mole fraction of CO_2 Real.5
Cranfield Unit 7 (40,76)

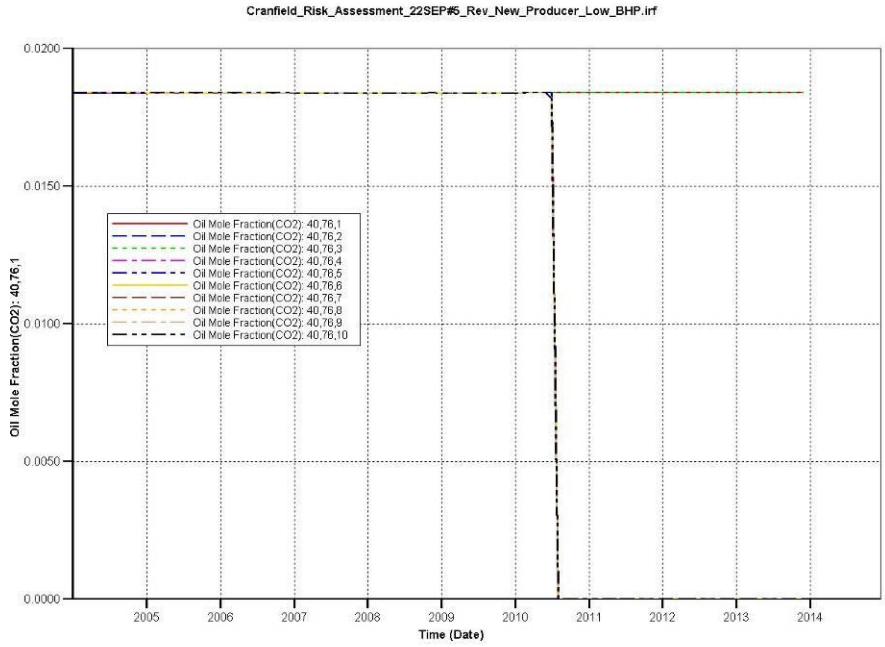

Oil mole fraction of CO_2 Real.5
Cranfield Unit 4 (26,60)

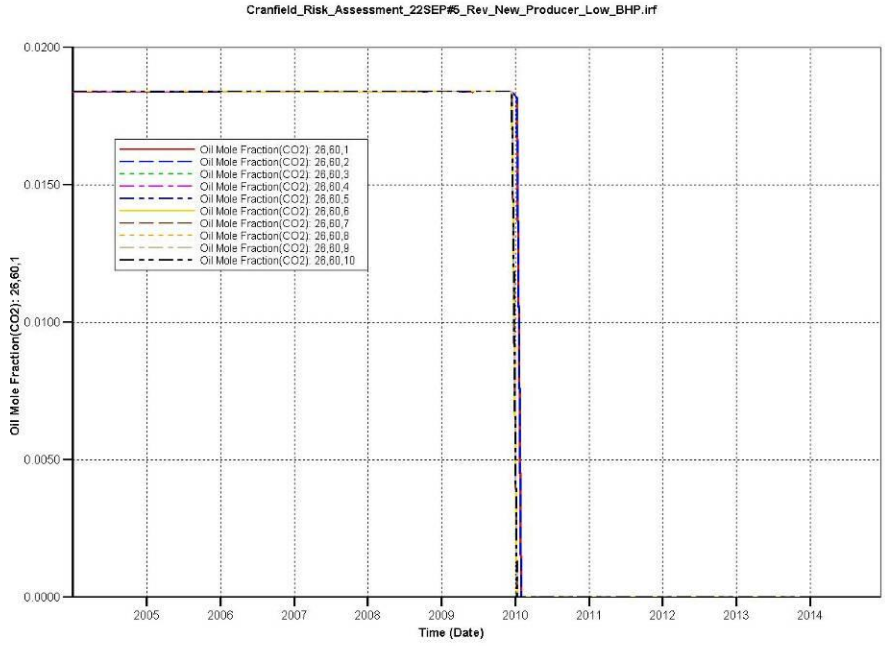

Oil mole fraction of CO_2 Real.5

Vernon Johnson 1 (22,47)

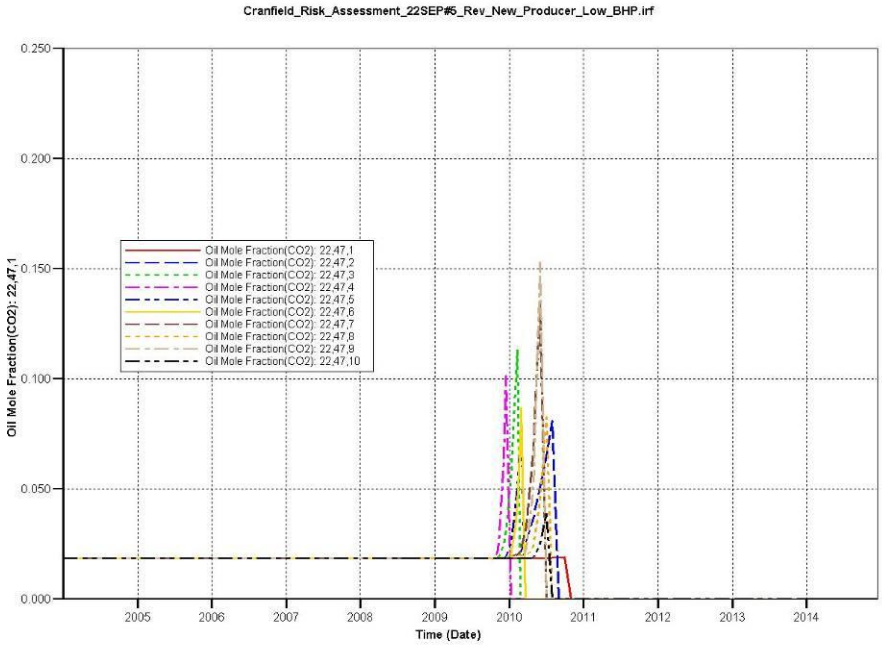

Oil mole fraction of CO_2 Real.5

Armstrong 4 (11,35)

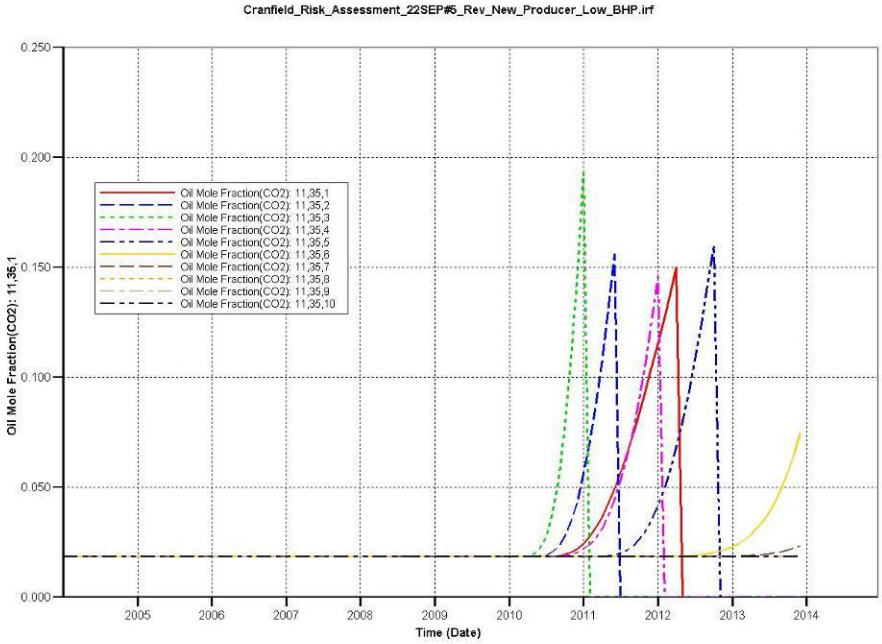

Oil mole fraction of CO_2 Real.5
Armstrong 2 (18,39)

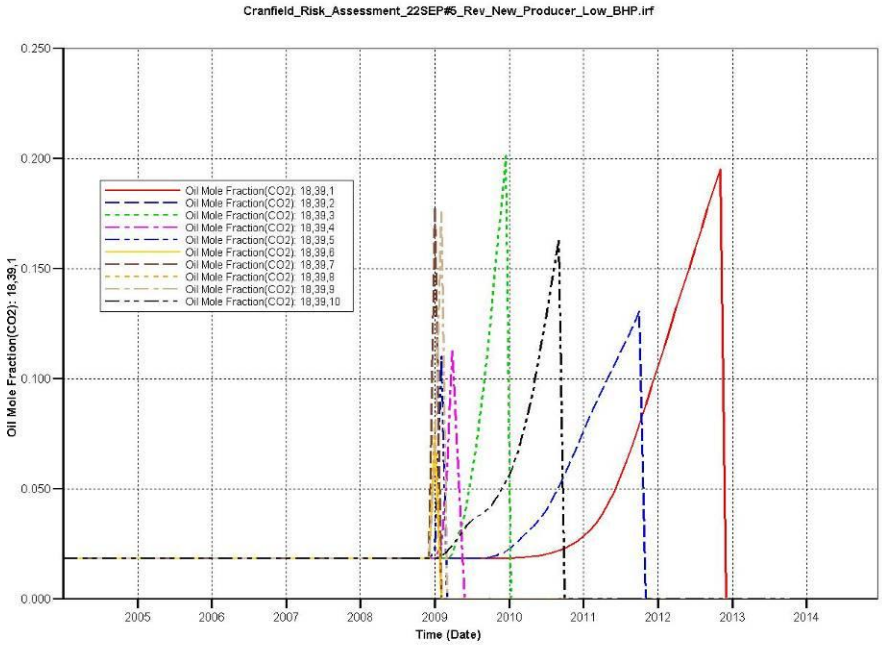

Oil mole fraction of CO_2 Real.5
R G CALCOTE 1 (27,39)

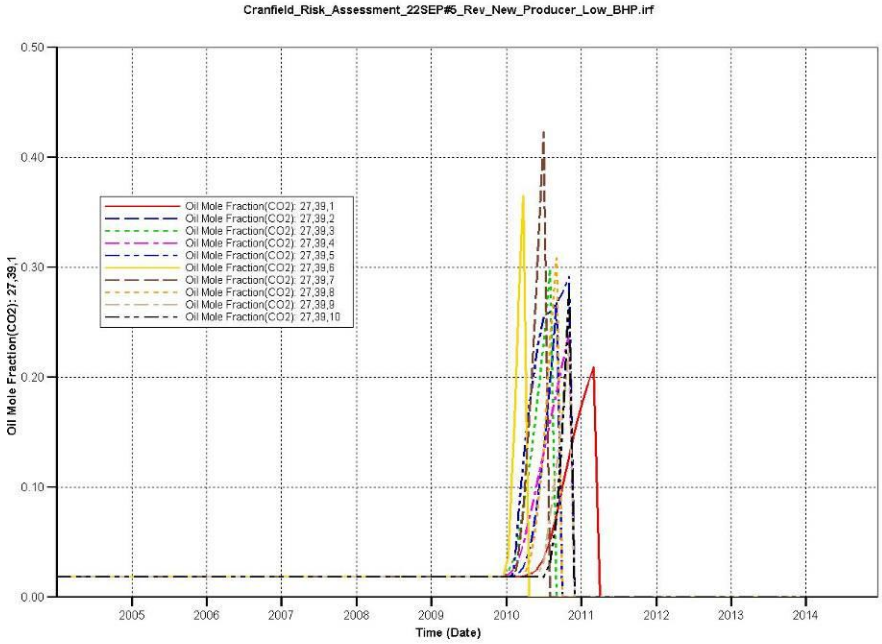

Oil mole fraction of CO_2 Real.5
H H CROSBY ETAL 1 (32,24)

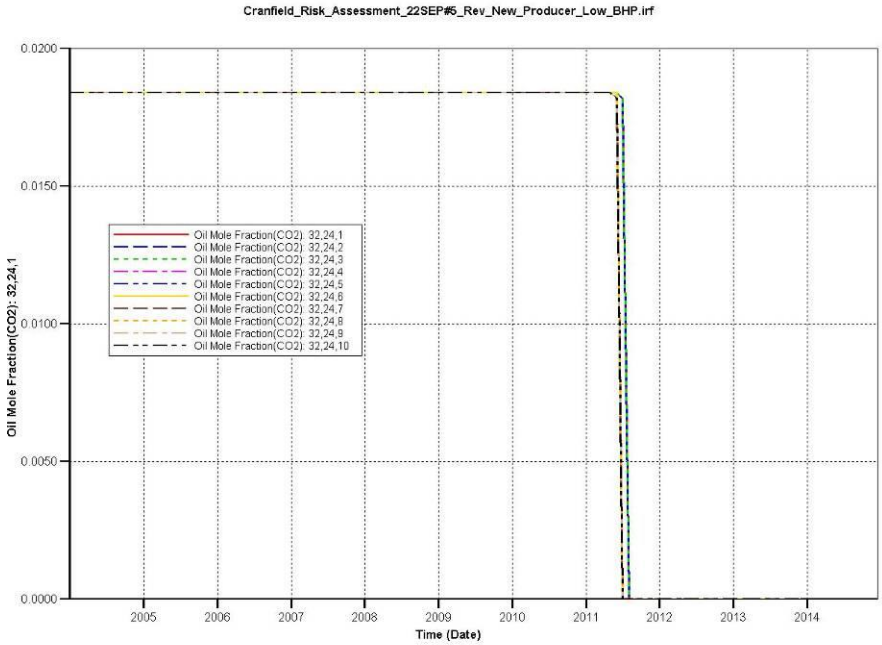

11 Appendix E: List of wells

All wells in the Tuscaloosa reservoir footprint are listed below (Courtesy of IHS). They are sorted by total depth (TD).

API	Formation at Total Depth	Total Depth (ft)	Lat.	Long.	Elev. (ft)	Cumul. Oil (bbl)	Cumul. Gas (mcf)	Cumul. Water (bbl)	Completion date
23001001500000	CANE RIVER MARL	3760	31.556527	-91.170295	392				4/11/1948
23001224090000	WILCOX	4152	31.587282	-91.169214	297	0	83704	20314	11/11/1982
23001001570000	WILCOX	4355	31.58539	-91.15875	267				8/27/1963
23001002190000	WILCOX	4373	31.555275	-91.173487	362	80385	88828	15293214	2/8/1949
23001001920001	WILCOX	4394	31.55777	-91.17629	372				1/21/1944
23001001520000	WILCOX	4406	31.57535	-91.16801	266				7/3/1946
23001217640000	WILCOX	4438	31.585093	-91.17797	231				8/27/1979
23001202400000	WILCOX	4450	31.55713	-91.17374	345				7/1/1968
23001231840000	WILCOX	4510	31.567244	-91.174223	315				5/4/1994
23001218550000	WILCOX	4524	31.560133	-91.181438	354	301392	11632	6388313	12/20/1979
23001219050000	WILCOX	4530	31.548886	-91.179173	367	25526	0	394107	4/11/1980
23001219050001	SPARTA SAND	4530	31.54888	-91.17917					11/29/2000
23001018240000	4600 FT SD	4617	31.533556	-91.215783	380				6/13/1964
23001002550000	WILCOX	5630	31.556945	-91.167836	332	265515	31554	355335	6/22/1962
23001002550001	5600 FT SD	5630	31.55694	-91.16783	377				10/20/1962
23001002200000	WILCOX	5638	31.55748	-91.171159	339	35404	3540	113902	3/5/1962
23001002210000	5520 FT SD	5690	31.554773	-91.172691	394	102187	25526	293789	5/30/1962
23001002500000	WILCOX	5690	31.554306	-91.169449	272	98730	9886	46955	5/22/1962
23001032500000	WILCOX	5700	31.552097	-91.172408	382				2/23/1962
23001002140000	WILCOX	5752	31.57449	-91.16608	250	290856	42155	1215468	4/29/1947
23001002150000	WILCOX	5762	31.57804	-91.166493	245	348990	37323	3453515	1/1/1949
23001001540000	WILCOX	5783	31.58418	-91.16557	282	161937	23957	383702	3/10/1949
23001001880000	WILCOX	5784	31.57026	-91.16421	257	80412	40281	862548	3/25/1947
23001002050000	WILCOX	5795	31.56393	-91.16678	310	152438	135234	2976802	2/23/1946
23001001550000	WILCOX	5798	31.58434	-91.16216	281				4/29/1949
23001002080000	WILCOX	5813	31.56751	-91.1662	316	75411	16784	606865	6/9/1946
23001002220000	WILCOX	5813	31.55895	-91.16926	320	856694	117855	36087577	6/13/1951
23001002070000	WILCOX	5818	31.55782	-91.17134	326				4/2/1946

API	Formation at Total Depth	Total Depth (ft)	Lat.	Long.	Elev. (ft)	Cumul. Oil (bbl)	Cumul. Gas (mcf)	Cumul. Water (bbl)	Completion date
23001002040001	WILCOX	5823	31.56063	-91.17064	335	80204	8245	461538	3/29/1962
23001002040000	WILCOX	5823	31.56063	-91.17064	335	454381	68834	2038286	1/2/1946
23001002060000	WILCOX	5825	31.56734	-91.16614	339	323127	47153	1829319	4/15/1946
23001002440000	WILCOX	5826	31.558874	-91.164024	325	127963	27751	604935	5/4/1946
23001002440001	WILCOX	5828	31.558874	-91.164024	325	83592	33392	1042251	11/1/1954
23001002440002	WILCOX	5828	31.558874	-91.164024	325	51891	5230	188044	3/26/1962
23001002520000	WILCOX	5835	31.561873	-91.163667	335	370630	59002	2116507	10/22/1948
23001002530000	WILCOX	5835	31.554618	-91.166	334				3/16/1948
23001002100000	WILCOX	5838	31.559233	-91.171272	316				7/8/1946
23001002180000	WILCOX	5845	31.56372	-91.1637	346	904354	146907	43355790	11/4/1948
23001002620000	WILCOX	5853	31.5432	-91.173905	325				8/20/1957
23001001490000	WILCOX	5857	31.58077	-91.16428	243	102717	5581	213087	5/1/1956
23001001560000	WILCOX	5859	31.58726	-91.16358	347				7/2/1949
23001002410000	WILCOX	5862	31.555559	-91.164466	362	393554	104532	1896254	9/5/1945
23001212520000	WILCOX	5868	31.57581	-91.16582	244				6/15/1976
23001002420000	WILCOX	5877	31.557625	-91.167915	377				10/15/1945
23001002420001	WILCOX	5877	31.557625	-91.167915	377	128640	15265	533437	3/6/1956
23001002420002	WILCOX	5877	31.557625	-91.167915	377	322460	56157	262007	5/13/1962
23001002400000	WILCOX	5879	31.554978	-91.168247	380	793475	150566	2693545	5/11/1945
23001002270000	WILCOX	5880	31.557707	-91.179383	330				2/14/1944
23001002630000	WILCOX	5883	31.550714	-91.175869	379	555033	96103	1709441	3/15/1944
23001033960000	WILCOX	5886	31.56002	-91.16607	386	585293	98522	3111058	11/23/1945
23001033960001	WILCOX	5886	31.56058	-91.16332					5/21/2010
23001001920000	WILCOX	5887	31.55777	-91.17629	372				1/21/1944
23001002640000	WILCOX	5888	31.548577	-91.179901	390				6/20/1945
23001002230000	WILCOX	5889	31.55608	-91.17016	377	779820	114637	28911246	5/25/1951
23001002230001	WILCOX	5889	31.55608	-91.17016	376				10/22/1987
23001002370000	WILCOX	5890	31.55315	-91.17764	386	407338	78632	3199244	2/24/1946
23001002640001	WILCOX	5890	31.548577	-91.179901	390	56461	5636	177362	5/11/1962
23001001930000	WILCOX	5894	31.554692	-91.172356	395	133599	97239	2689724	3/16/1945
23001002460000	WILCOX	5894	31.551593	-91.168093	395	274808	35058	1942341	9/5/1945
23001001930001	WILCOX	5897	31.554692	-91.172356	395	34901	3652	104270	12/16/1963

API	Formation at Total Depth	Total Depth (ft)	Lat.	Long.	Elev. (ft)	Cumul. Oil (bbl)	Cumul. Gas (mcf)	Cumul. Water (bbl)	Completion date
23001002540000	WILCOX	5908	31.551686	-91.172013	408				8/2/1945
23001002250000	WILCOX	5929	31.553362	-91.177203	389				7/23/1945
23001210550000	WILCOX	5980	31.56761	-91.162589	261				3/1/1975
23001210870000	WILCOX	6003	31.548484	-91.174631	371	83055	12	1213923	5/30/1975
23001017430000	WILCOX	6006	31.549177	-91.156242	345				3/5/1951
23001219210000	WILCOX	6007	31.55499	-91.17471	378	306708	29684	32366110	3/31/1980
23001210480000	WILCOX	6010	31.550075	-91.175153	366	205901	0	2006560	2/21/1975
23001213130000	WILCOX	6010	31.55663	-91.16907	329	214719	658	2289197	11/29/1976
23001219420000	WILCOX	6010	31.547375	-91.180407	353				5/28/1980
23001221190000	WILCOX	6010	31.555746	-91.183415	371				2/10/1981
23001226220000	WILCOX	6010	31.579149	-91.168537	259	0	1053112	8307	4/20/1984
23001211360000	WILCOX	6011	31.549515	-91.176164	381	98004	0	995190	9/22/1975
23001215700000	WILCOX	6013	31.55491	-91.16748	378				4/23/1978
23001216610000	WILCOX	6014	31.55667	-91.17642	383				10/31/1978
23001212760000	WILCOX	6019	31.547496	-91.171769	353				8/28/1976
23001216510000	WILCOX	6019	31.54077	-91.17332	304				10/30/1978
23001217210000	WILCOX	6023	31.593369	-91.180429	227				3/29/1979
23001221660000	WILCOX	6023	31.552849	-91.175631	345	73776	2028	4068590	4/17/1981
23001217290000	WILCOX	6025	31.554977	-91.164838	347				4/24/1979
23001213370000	WILCOX	6030	31.56008	-91.17771	358				12/5/1976
23001215820000	WILCOX	6031	31.57152	-91.17193	266				5/24/1978
23001215750000	WILCOX	6034	31.540764	-91.171855	341	49132	0	459808	5/5/1978
23001222540000	WILCOX	6034	31.55567	-91.17259	379	59540	0	2586119	1/29/1982
23001220760000	WILCOX	6058	31.55276	-91.18888	377				12/30/1980
23037212440000	WILCOX	6106	31.555479	-91.149673	313				8/7/1985
23001216050000	WILCOX	6110	31.586957	-91.167308	279				9/25/1978
23001204110000	WILCOX	6120	31.58599	-91.16911	293				5/7/1969
23001217070000	WILCOX	6150	31.592743	-91.166565	392				5/16/1979
23001213840000	WILCOX	6210	31.54027	-91.16883	333	275494	0	5181781	3/23/1977
23001214080000	WILCOX	6210	31.54677	-91.16092	379				4/29/1977
23037207940000	WILCOX	6210	31.548372	-91.152096	387				11/19/1977
23001214660000	WILCOX	6213	31.527138	-91.181339	259				9/13/1977

API	Formation at Total Depth	Total Depth (ft)	Lat.	Long.	Elev. (ft)	Cumul. Oil (bbl)	Cumul. Gas (mcf)	Cumul. Water (bbl)	Completion date
23001216860000	WILCOX	6220	31.562996	-91.184853	368				1/9/1979
23001222550000	WILCOX	6220	31.55832	-91.17693	379				1/2/1982
23001216360000	WILCOX	6225	31.55232	-91.17956	366				10/6/1978
23001221960000	WILCOX	6247	31.54622	-91.18612	383				8/9/1981
23001224560000	WILCOX	6270	31.542087	-91.172699	346				3/2/1983
23001032480000	WILCOX	6301	31.558729	-91.181648	324	5116	510	75957	3/23/1966
23037000630000	MINTER SAND	6305	31.543027	-91.151962	405				12/22/1964
23001003990000	5800 FT SD	6316	31.55887	-91.19112	362				1/4/1965
23001004060000	5800 FT SD	6322	31.55557	-91.15636	306				1/4/1965
23001004070000	MINTER LIGNITE	6473	31.53906	-91.18033	359				12/13/1964
23001004260000	MINTER LIGNITE	6511	31.55947	-91.1806	290				12/12/1964
23001221740000	WILCOX	6515	31.53725	-91.17043	304				5/12/1981
23001209750000	WILCOX	6805	31.55144	-91.1705	405				8/24/1974
23001209740000	WILCOX	6810	31.56217	-91.16877	397				9/4/1974
23001211160000	WILCOX	6810	31.57939	-91.16942	239				9/10/1975
23001002240000	WILCOX	7111	31.55673	-91.17084	326	498190	53222	36594086	1/17/1961
23037000420002	MASSIVE TUSCALOOSA	10042	31.53909	-91.15137	370	2221	2513	80719	11/24/1963
23001002130000	MASSIVE TUSCALOOSA	10277	31.55832	-91.17192	358	7891	4166975	31807	2/7/1947
23001002160000	LOWER CRETACEOUS	10282	31.55396	-91.17316	372	241822	29479	42282258	9/25/1947
23001002160001	LOWER TUSCALOOSA	10282	31.55396	-91.17316					5/10/2010
23001001670000	MARINE TUSCALOOSA	10285	31.57979	-91.16394	247	985934	18850768	574190	11/6/1948
23001001670001	MARINE TUSCALOOSA	10285	31.57979	-91.16394	245				8/22/1967
23001001610000	LOWER TUSCALOOSA	10294	31.55337	-91.17025	379	61374	11773	679005	5/19/1948
23001001630000	LOWER CRETACEOUS	10298	31.56772	-91.15899	285	1569	16108	130010	8/30/1948
23001002610000	LOWER TUSCALOOSA	10303	31.54864	-91.17151	400	3823	652742	33899	10/31/1946
23001001990001		10304	31.5772	-91.16985					
23001001990000	MASSIVE TUSCALOOSA	10305	31.5772	-91.16985	259	1799142	22304175	1608381	9/7/1945
23001002000000	MASSIVE TUSCALOOSA	10305	31.57823	-91.16846	244	719253	9303380	594567	1/11/1946
23001015540000	MASSIVE TUSCALOOSA	10305	31.58029	-91.15732	249	11781	5218	47033	5/5/1947
23001002030000	MASSIVE TUSCALOOSA	10307	31.57971	-91.1729	247	778387	1312746	1504918	11/8/1945
23001002110000	MASSIVE TUSCALOOSA	10307	31.58044	-91.17708	215	989600	23808518	76525	9/2/1946
23001033940000	MASSIVE TUSCALOOSA	10307	31.58127	-91.16297	246	703672	2540697	1177957	1/11/1946

API	Formation at Total Depth	Total Depth (ft)	Lat.	Long.	Elev. (ft)	Cumul. Oil (bbl)	Cumul. Gas (mcf)	Cumul. Water (bbl)	Completion date
23001001510000	MASSIVE TUSCALOOSA	10309	31.57851	-91.16338	248	1018631	10474030	1982691	5/2/1946
23001001590000	LOWER CRETACEOUS	10310	31.57406	-91.16693	258	193865	17502987	681928	3/8/1948
23001002120000	LOWER TUSCALOOSA	10310	31.57493	-91.16524	249	352128	5039775	44713	9/18/1946
23001001760000	LOWER CRETACEOUS	10314	31.58029	-91.17718	237	596629	15528528	207655	8/30/1952
23001001890000	MASSIVE TUSCALOOSA	10314	31.57598	-91.16042	254	464081	2072772	182322	1/9/1946
23001002090000	LOWER TUSCALOOSA	10314	31.57603	-91.16814	253	860206	27579792	263480	7/4/1946
23001001960000	LOWER TUSCALOOSA	10315	31.57589	-91.18094	290	1595105	29505370	2165011	7/9/1945
23001033940001	LOWER TUSCALOOSA	10316	31.58127	-91.16297		18464	0	253027	
23037000390000	MASSIVE TUSCALOOSA	10319	31.562274	-91.149318	288	438323	12231072	805004	2/17/1949
23001001980000	MASSIVE TUSCALOOSA	10323	31.57785	-91.17299	287	668001	23419831	712088	7/8/1945
23001001960001	LOWER TUSCALOOSA	10324	31.57589	-91.18094	280				10/2/2007
23001002730000	MASSIVE TUSCALOOSA	10325	31.57227	-91.18994	277				8/30/1945
23001001780000	BASAL TUSCALOOSA	10326	31.5804	-91.17296	241	88152	652832	375542	12/28/1953
23001001760001	LOWER TUSCALOOSA	10327	31.58029	-91.17718	236	25232	0	242057	10/31/2008
23001001950000	MASSIVE TUSCALOOSA	10330	31.57763	-91.1763	281	470344	3807803	13546	9/7/1945
23001002560000	MASSIVE TUSCALOOSA	10330	31.52997	-91.17404	274	378830	3395263	959668	8/30/1945
23001001730000	LOWER TUSCALOOSA	10331	31.57735	-91.18039	272	484463	12286833	379280	10/14/1951
23001018150000	MASSIVE TUSCALOOSA	10332	31.52296	-91.17951	282				4/8/1946
23001001750000	LOWER TUSCALOOSA	10333	31.53015	-91.15905	298	0	3260	7013	12/27/1949
23001002020000	MASSIVE TUSCALOOSA	10333	31.5784	-91.17965	274	867948	18980672	51241	11/18/1945
23001001740000	MASSIVE TUSCALOOSA	10334	31.57108	-91.1842	289	451886	7578902	505032	9/15/1949
23001001910000	MASSIVE TUSCALOOSA	10336	31.57328	-91.16087	276	309540	2627409	980197	7/30/1946
23001001680000	MASSIVE TUSCALOOSA	10337	31.56906	-91.18508	297	262205	14043122	102165	1/13/1949
23037000470000	LOWER TUSCALOOSA	10338	31.56374	-91.15304	276	501949	4684575	147578	9/17/1946
23001001580000	LOWER CRETACEOUS	10339	31.5646	-91.16137	280	491164	14498497	58704	3/8/1948
23001001900000	MASSIVE TUSCALOOSA	10339	31.57642	-91.15749	279	668035	6269185	708053	3/13/1946
23001002580000	MASSIVE TUSCALOOSA	10341	31.53006	-91.171	278	259458	376407	561527	11/5/1945
23001002490000	LOWER TUSCALOOSA	10342	31.56069	-91.15524	282	1196	2850410	17691	8/25/1947
23001002570000	MASSIVE TUSCALOOSA	10345	31.531445	-91.167575	275	679356	2313293	3120746	9/22/1945
23001002570001	MASSIVE TUSCALOOSA	10346	31.53144	-91.16757	275				6/24/1956
23001001650000	MASSIVE TUSCALOOSA	10348	31.53261	-91.16359	322	194558	3397315	1995294	9/25/1948
23001001620000	LOWER TUSCALOOSA	10350	31.57019	-91.15806	299	109081	1010862	17690	5/12/1948

API	Formation at Total Depth	Total Depth (ft)	Lat.	Long.	Elev. (ft)	Cumul. Oil (bbl)	Cumul. Gas (mcf)	Cumul. Water (bbl)	Completion date
23001001790000	BASAL TUSCALOOSA	10350	31.58295	-91.18152	256	136354	5124155	286402	2/22/1954
23001001720000	LOWER TUSCALOOSA	10352	31.58084	-91.18243	288	588228	16750177	108546	1/24/1952
23001032440000	LOWER TUSCALOOSA	10355	31.56932	-91.17334	280	4967	2661540	18522	1/20/1963
23001002590000	MASSIVE TUSCALOOSA	10357	31.53092	-91.16491	297	245916	396473	868675	11/13/1945
23001001940000	MASSIVE TUSCALOOSA	10358	31.57504	-91.17541	303	1035751	16291142	2922777	5/4/1945
23001017370000	LOWER CRETACEOUS	10360	31.55282	-91.15604	324	426182	8694127	771503	12/9/1946
23001001720001	LOWER TUSCALOOSA	10360	31.58084	-91.18243	290	76	0	8882	11/2/2008
23037000460000	MASSIVE TUSCALOOSA	10361	31.56591	-91.15044	301	476509	6574709	1068822	4/18/1946
23037003340000	LOWER CRETACEOUS	10361	31.55815	-91.15339	311				9/3/1946
23001001530000	LOWER TUSCALOOSA	10364	31.58319	-91.16788	266	265029	54842	1577165	11/30/1946
23001002510000	MASSIVE TUSCALOOSA	10369	31.53377	-91.17	314	585530	12706302	157074	7/19/1945
23037003390000	LOWER CRETACEOUS	10370	31.55798	-91.15258	289				10/7/1947
23001002740000	MASSIVE TUSCALOOSA	10371	31.57156	-91.19056	245				3/26/1946
23001017360000	LOWER CRETACEOUS	10373	31.53299	-91.16109	299	314914	1198805	1572076	6/9/1946
23037000410000	BASAL TUSCALOOSA	10380	31.56146	-91.14973	313	14313	85630	831271	8/5/1953
23037003330000	MASSIVE TUSCALOOSA	10380	31.55308	-91.15296	308				6/13/1946
23037003330001	TUSCALOOSA	10380	31.55308	-91.15296					6/23/1998
23037003330002	LOWER TUSCALOOSA	10380	31.55308	-91.15296	308				
23001001810000	LOWER CRETACEOUS	10382	31.54071	-91.18348	337	13553	3026137	172270	12/10/1956
23001001810001	LOWER TUSCALOOSA	10382	31.54071	-91.18348	337				9/22/1960
23001002390000	MIDWAY GROUP	10383	31.55257	-91.18148	388				10/6/1943
23001017410000	LOWER CRETACEOUS	10383	31.53525	-91.15693	322	571269	8583211	1572281	7/24/1947
23001002390001	MIDWAY GROUP	10383	31.55257	-91.18148	388				3/22/1946
23001001970000	LOWER CRETACEOUS	10384	31.53629	-91.16097	327	578902	7937745	1640908	8/24/1946
23001001970001	LOWER CRETACEOUS	10384	31.536291	-91.160976	327				12/8/1954
23001001970002	LOWER CRETACEOUS	10384	31.536291	-91.160976	327				7/26/1962
23001002450000	MASSIVE TUSCALOOSA	10385	31.5362	-91.17361	324	249551	2670014	505214	12/5/1944
23001002300000	MASSIVE TUSCALOOSA	10386	31.55472	-91.19394	310	494112	9670451	289733	6/19/1944
23001001800000	LOWER CRETACEOUS	10389	31.58264	-91.16036	266	35382	2257	66158	10/6/1954
23001001800001	LOWER CRETACEOUS	10389	31.58264	-91.16036	266				11/6/1961
23001001800002	LOWER CRETACEOUS	10389	31.58264	-91.16036					2/10/2009
23001002660000	LOWER TUSCALOOSA	10390	31.53905	-91.18475	306	660914	6811364	1111609	2/2/1945

API	Formation at Total Depth	Total Depth (ft)	Lat.	Long.	Elev. (ft)	Cumul. Oil (bbl)	Cumul. Gas (mcf)	Cumul. Water (bbl)	Completion date
23001017390000	LOWER CRETACEOUS	10390	31.54234	-91.15679	377	311585	13871271	610350	2/10/1947
23001017420000	LOWER CRETACEOUS	10391	31.53164	-91.15725	330	614127	74588	5958863	7/2/1947
23001001690000	LOWER TUSCALOOSA	10397	31.55722	-91.18156	289	87792	3282257	116485	5/25/1952
23037000450000	LOWER TUSCALOOSA	10398	31.57259	-91.144458	308				2/20/1946
23001001770000	LOWER TUSCALOOSA	10400	31.56751	-91.19022	300	205246	8809092	297504	5/2/1954
23001017380000	LOWER CRETACEOUS	10400	31.53871	-91.1573	357	470029	7497075	774520	11/26/1946
23001214910000	LOWER TUSCALOOSA	10400	31.5466	-91.16412	351	15706	333180	1538	12/29/1977
23001216000000	LOWER CRETACEOUS	10400	31.55246	-91.16441	381				11/30/1978
23001216530000	LOWER TUSCALOOSA	10400	31.54082	-91.1694	331				3/1/1979
23001017400000	LOWER CRETACEOUS	10404	31.54561	-91.157581	394	259667	1092364	1307721	4/27/1947
23001002710000	MASSIVE TUSCALOOSA	10407	31.56247	-91.19422	318	470494	10501219	1296106	9/15/1944
23001017350000	LOWER CRETACEOUS	10407	31.54013	-91.16083	373	455093	5151925	384912	11/28/1945
23037000400000	MARINE TUSCALOOSA	10408	31.546623	-91.154289	368	22614	29580	563285	11/20/1948
23001214800000	LOWER TUSCALOOSA	10410	31.533636	-91.178951	328				10/19/1977
23037000480000	MASSIVE TUSCALOOSA	10410	31.57154	-91.15269	349				6/10/1946
23037000480001		10410	31.57154	-91.15269		28	0	28951	
23001002310000	MASSIVE TUSCALOOSA	10412	31.53988	-91.1893	325	533708	3580099	2088216	8/11/1944
23037003370000	MASSIVE TUSCALOOSA	10412	31.54235	-91.15382	364				10/17/1947
23037003370001	TUSCALOOSA	10412	31.54235	-91.15382					9/8/2000
23001002650000	MASSIVE TUSCALOOSA	10413	31.545	-91.18813	378	490153	8607170	521774	8/25/1944
23001002480000	MASSIVE TUSCALOOSA	10415	31.53325	-91.17652	319	547113	9687567	719094	4/25/1945
23001002280000	LOWER CRETACEOUS	10417	31.55815	-91.19633	336	437190	9099770	138603	5/17/1944
23001002680000	MASSIVE TUSCALOOSA	10430	31.53339	-91.18018	306	623427	18269125	873030	1/23/1945
23001002470000	MASSIVE TUSCALOOSA	10430	31.53239	-91.17371	284	568237	9094388	2460531	2/18/1945
23001002720000	MASSIVE TUSCALOOSA	10433	31.56499	-91.19222	343	511874	19824415	203690	12/26/1944
23037000430000	MASSIVE TUSCALOOSA	10434	31.592333	-91.152245	300				9/14/1945
23001002290000	MASSIVE TUSCALOOSA	10443	31.54269	-91.19274	386	280347	4648960	3024125	5/9/1944
23037003350000	MASSIVE TUSCALOOSA	10448	31.54712	-91.1537	381	312988	13927953	400066	3/8/1947
23001225630000	LOWER TUSCALOOSA	10450	31.56996	-91.16892	356				11/16/1983
23001002320000	MASSIVE TUSCALOOSA	10453	31.55323	-91.19801	396	59243	68666	324597	6/24/1945
23001233910000	LOWER TUSCALOOSA	10453	31.55689	-91.16004					3/22/2010
23001001870000	MASSIVE TUSCALOOSA	10459	31.54474	-91.19554	394	45286	133364	1445018	6/27/1945

API	Formation at Total Depth	Total Depth (ft)	Lat.	Long.	Elev. (ft)	Cumul. Oil (bbl)	Cumul. Gas (mcf)	Cumul. Water (bbl)	Completion date
23037003360000	LOWER CRETACEOUS	10461	31.54147	-91.15366	391				5/18/1947
23001001860000	MASSIVE TUSCALOOSA	10467	31.54682	-91.19473	400	604990	8917971	747730	9/11/1944
23001002700000	MASSIVE TUSCALOOSA	10468	31.53049	-91.17833	307	276102	3413187	1009892	4/6/1945
23001002260000	LOWER TUSCALOOSA	10469	31.55062	-91.19711	354	748500	6709631	730425	1/24/1944
23037000420001	MASSIVE TUSCALOOSA	10470	31.539098	-91.151372	370				9/25/1953
23037003320001	LOWER TUSCALOOSA	10470	31.55194	-91.1512					6/18/2010
23001002330000	LOWER TUSCALOOSA	10473	31.53689	-91.18792	360	326480	660053	1615902	11/6/1944
23037003320000	MASSIVE TUSCALOOSA	10473	31.55194	-91.1512	390				3/25/1946
23001002670000	MASSIVE TUSCALOOSA	10475	31.53496	-91.18318	318	791274	14643610	721532	1/18/1945
23001216830000	LOWER CRETACEOUS	10500	31.53221	-91.19096	300				12/28/1978
23001224880000	WASHITA-FREDERICKSBU	10500	31.56789	-91.18356	340	3894	109376	0	7/14/1983
23001233590000	LOWER TUSCALOOSA	10500	31.58772	-91.18057					11/17/2009
23001225630001	LOWER TUSCALOOSA	10500	31.56993	-91.16882					
23001233420000	LOWER TUSCALOOSA	10500	31.57242	-91.17682					
23037000420000	MASSIVE TUSCALOOSA	10505	31.539098	-91.151372	370				2/17/1954
23001233720000	LOWER TUSCALOOSA	10510	31.57485	-91.15771		76456	0	330765	1/30/2009
23001233460000	LOWER TUSCALOOSA	10515	31.57094	-91.18195					12/6/2009
23037003300000	LOWER CRETACEOUS	10520	31.547818	-91.1491	361	193876	232850	429109	8/3/1945
23037003300001	LOWER CRETACEOUS	10520	31.54781	-91.1491	381				8/3/1945
23001002690000	MASSIVE TUSCALOOSA	10546	31.53162	-91.18333	306				5/7/1945
23001233800000	LOWER TUSCALOOSA	10551	31.58336	-91.16108		89388	0	300110	5/26/2009
23001233810000		10600	31.56286	-91.1616					
23001013950000	LOWER TUSCALOOSA	10605	31.529909	-91.193535	320	4	0	258	4/4/1962
23001234020000	LOWER TUSCALOOSA	10610	31.58001	-91.16024					
23037214880000		10700	31.56345	-91.14062					
23001233580000	LOWER TUSCALOOSA	10715	31.56085	-91.15713	290				1/10/2008
23037214960000	LOWER TUSCALOOSA	10748	31.55123	-91.14585					4/30/2010
23037214980000	LOWER TUSCALOOSA	10770	31.55107	-91.14574					4/27/2010
23001233900000	LOWER TUSCALOOSA	10780	31.57052	-91.16876					3/15/2010
23037214850000	LOWER TUSCALOOSA	10790	31.56313	-91.14074					
23037214860000	LOWER TUSCALOOSA	10790	31.56322	-91.14042					
23037214940000	LOWER TUSCALOOSA	10895	31.55145	-91.14599					6/29/2010

API	Formation at Total Depth	Total Depth (ft)	Lat.	Long.	Elev. (ft)	Cumul. Oil (bbl)	Cumul. Gas (mcf)	Cumul. Water (bbl)	Completion date
23037214890000	TUSCALOOSA	10919	31.57117	-91.1459					10/16/2009
23001233620000	LOWER TUSCALOOSA	11020	31.58796	-91.18071					3/18/2008
23001233650000	LOWER TUSCALOOSA	11073	31.57942	-91.15813					
23001233650100	FREDRICKSBRG-WASHITA	11100	0	0					
23001226220001	WASHITA-FREDERICKSBU	11214	31.579149	-91.168537	272				8/18/1998
23001232210000	HOSSTON	11215	31.56568	-91.15935					1/9/1996
23001001820000	LOWER CRETACEOUS	11278	31.53647	-91.19419	351				7/11/1961
23001034600000	11150 FT SD	11303	31.557409	-91.160162	309				1/20/1967
23001233660000	LOWER TUSCALOOSA	11667	31.57948	-91.15811					7/15/2008
23001232910000	WASHITA-FREDERICKSBU	11700	31.57316	-91.16232	285	0	400604	5720	6/27/2001
23001232910001	LOWER TUSCALOOSA	11700	31.57316	-91.16232					7/25/2005
23001231830000	FREDERICKSBURG GROU	11880	31.55645	-91.17123	353	0	2658152	14755	9/9/1994
23001002380000	PALUXY	11910	31.5686	-91.18197	327	269397	10361805	409907	6/14/1947
23001002600000	PALUXY	11982	31.53387	-91.16467	340	452303	5408030	693009	6/29/1946
23001231620000	PALUXY	12000	31.5631	-91.15965	284				10/20/1993
23001001910001	PALUXY	12115	31.57328	-91.16087	276	267418	1417730	349458	8/26/1965
23001002490001	11800 FT SD	12300	31.560695	-91.155244	282				1/7/1962
23001002340000	MASSIVE TUSCALOOSA	12400	31.53377	-91.18634	306				6/7/1945
23001002010000	PALUXY	12718	31.55722	-91.1716	355	5785	20662328	89870	6/25/1946
23001002010001	PALUXY	12718	31.55722	-91.1716	355				12/18/1948
23001032510000	SLIGO	15948	31.54411	-91.17518	337	488	810692	6808	9/15/1966
23001209890000	SALT	20190	31.54973	-91.17615	397				12/4/1975
23001209890001		20190	31.54973	-91.17615					7/27/2000
23001002360000			31.539289	-91.197041					10/5/1945
23001001780001			31.5804	-91.17296					
23001001900001			31.57642	-91.15749					
23037000460001			31.56709	-91.15084		6269	0	80437	
23001233630000			31.58694	-91.18055					
23001001580001			31.5646	-91.16137					
23001001620001			31.57019	-91.15806					
23001017410001			31.53525	-91.15693					
23001231830001			31.55645	-91.17123					

API	Formation at Total Depth	Total Depth (ft)	Lat.	Long.	Elev. (ft)	Cumul. Oil (bbl)	Cumul. Gas (mcf)	Cumul. Water (bbl)	Completion date
23037000390001			31.56084	-91.14951					
23037003360001			31.54147	-91.15366					
23037215010000			31.56324	-91.14133					